



The
University
Of
Sheffield.

Computational understanding of heterocyclisation reactions and synthesis of fluorinated isoquinolines

Giovanna Zanella

Thesis submitted for the degree of Doctor of Philosophy (PhD)

The University of Sheffield
Faculty of Science
Department of Chemistry

October 2020

Declaration

I, the author, confirm that the Thesis is my own work. I am aware of the University's Guidance on the Use of Unfair Means (www.sheffield.ac.uk/ssid/unfair-means). This work has not been previously presented for an award at this, or any other, university.

List of Publications

1. Rinaldi, A.; Langé, V.; Gómez-Bengoa, E.; Zanella, G.; Scarpi, D.; Occhiato, E. G. Synthesis of Indenes by Tandem Gold(I)-Catalysed Claisen Rearrangement/Hydroarylation Reaction of Propargyl Vinyl Ethers. *J. Org. Chem.* **2019**, *84*, 106298-6311.
2. Urruzuno, I.; Mugica, O.; Zanella, G.; Vera, S.; Gómez-Bengoa, E.; Oiarbide, M.; Palomo, C. Alfa-Branched Ketone Dienolates: Base-Catalysed Generation and Regio- and Enantioselective Addition Reactions. *Chem. Eur. J.* **2019**, *25*, 9701-9709.
3. Olaizola, O.; Iriarte, I.; Zanella, G.; Vera, S.; Gómez-Bengoa, E.; Oiarbide, M.; Palomo, C. Brønsted Base Catalysed One-Pot Synthesis of Stereodefined Six-Member Carbocycles Featuring Transient Trienolates and a Key Intramolecular 1,6-Addition. *Angew. Chem. Int. Ed.* **2019**, *58*, 14250-14254.
4. Zanella, G.; Petrović, M.; Scarpi, D.; Occhiato, E. G.; Gómez-Bengoa, E. A Combined Computational and Experimental Study on the Role of the N Atom in the Pentannulation of *N*-Heterocycles by the Tandem Gold-Catalysed [3,3]-Rearrangement/Nazarov Reaction of Propargyl Ester Derivatives. *Submitted*

List of Abbreviations

Abbreviation	Description
AO	Atomic orbital
BB	Brønsted base
BSSE	Basis Set Superposition Error
C-Au	Carbon-Gold
CBS	Complete basis set
C-C	Carbon-Carbon
cc	Correlated Consistent
C-F	Carbon-Fluorine
C-H	Carbon-Hydrogen
C-N	Carbon-Nitrogen
C-O	Carbon-Oxygen
CP	Counterpoise
DCD	Dewar–Chatt–Duncanson model
DCM	Dichloromethane
DFT	Density functional theory
DMF	Dimethylformamide
<i>dr</i>	Diastereomeric ratio
DZ	Double-zeta valence
ECP	Effective core potentials
<i>ee</i>	Enantiomeric excess
EWG	Electron withdrawing group
<i>f</i>	Fukui Nucleophilicity index
FDA	Food and Drug Administration
GGA	Generalised gradient approximation
GTO	Gaussian-type orbitals
H-bond	Hydrogen bond
HF	Hartree-Fock
HFIP	Hexafluoroisopropanol
IEFPCM	Integral equation formalism variant of PCM
IRC	Intrinsic reaction coordinate
L	Ligand
LANL	Los Alamos National Laboratory

LDA	Local density approximation
KS	Kohn-Sham
M	Metal
MM	Molecular Mechanics
MO	Molecular Orbital
NAO	Natural atomic orbital
NBO	Natural bond orbital
N-H	Nitrogen-Hydrogen
NHC	<i>N</i> -heterocyclic carbene
NHO	Natural hybrid orbital
NLMO	Natural (semi-) localised molecular orbitals
NMR	Nuclear magnetic resonance
N-N	Nitrogen-Nitrogen
P	Product
PCM	Polarised continuum model
PVE	Propargyl vinyl ether
PZ	Quintuple-zeta
QM/MM	Quantum Mechanics/Molecular Mechanics
QZ	Quadruple-zeta
SCRf	Self-Consistent Reaction Field
SDD	Stuttgart-Dresden
SIE	Self-Interaction Error
SM	Starting Materials
S _N Ar	Nucleophilic aromatic substitution
S _N V	Vinyllic nucleophilic substitution
STO	Slater-type orbitals
SVP	Split Valence Polarised
TFE	2,2,2-Trifluoroethanol
THF	Tetrahydrofuran
TON	Turnover number
TS	Transition state
TZ	Triple-zeta

Abstract

The present thesis deals with three different topics that have in common the formation of carbo- and heterocycles. As part of the CATMEC network (Catalytic Methods for Sustainable Synthesis. A Merged Experimental and Computational Approach), a multi-partner Innovative Training Network (ITN) European Joint Doctorate (EJD), the author of the thesis has carried out her work between the University of Sheffield and the Universidad del País Vasco. The whole work is organised as a synergy of experimental and computational studies to provide a deep understanding of the systems of interest. The first chapter contains an introduction about computational chemistry with a particular focus on DFT and its application. The second chapter regards asymmetric catalysis and includes two works made in collaboration with the group of Prof. Palomo at the Universidad del País Vasco. Bifunctional catalysts are employed to afford good levels of stereoselectivity in the α -functionalisation of challenging substrates, as substituted dienolates and trienolates, with olefins. Computational studies were performed mainly to rationalise the role of the catalyst. The third chapter in collaboration with the group of Prof. E. Occhiato at the Università degli Studi di Firenze presents two examples of gold catalysis applied to the [3,3]-rearrangement/Nazarov reaction of propargylic esters and the tandem Claisen rearrangement/hydroarylation reaction of propargyl vinyl ethers. The mechanisms of the reactions were studied computationally, as well as the effect of particular features in the substrates or in the catalysts. The last two chapters concern the synthesis of fluorinated isoquinolines and computational studies on particular issues encountered experimentally. The strategy employed is a two step reaction that includes a Rh-catalysed CH activation of oximes with difluoroalkenes and an electrocyclisation. The formation of an undesired side product induced us to undertake computational investigations on the electrocyclisation step.

Acknowledgements

I would like to express my sincere thanks to Professor J. Harrity and Prof. E. Gómez Bengoa for their guidance, encouragement and advice during my PhD. I would also like to thank my colleagues for the time spent together.

I gratefully acknowledge the financial support provided by the European Funding Horizon 2020-MSCA (ITN-EJD CATMEC 14/06-721223).

I also thank SGIker (UPV/EHU) for providing computational resources and all the technical staff of the Sheffield University and the University of Basque Country for their help and assistance.

I am grateful to all the people I have met during my PhD, who in different manner have left their mark in my life. I will keep you in my heart.

Il grazie piú significativo e sincero va alla mia famiglia, che c'è sempre e rappresenta per me il porto sicuro.

Grazie ai miei genitori per appoggiarmi in qualsiasi mia scelta ed adattarsi ai cambiamenti a modo loro. Grazie alla mia mamma per il sostegno e la comprensione, per le telefonate infinite e per ascoltare tutte le mie lamentele e condividere le piccole soddisfazioni.

Grazie a Lori, che mi fa sentire il suo affetto in modo alternativo, ma sempre costante. Mamma, papa, Lori, vi voglio bene.

Grazie ai miei amici di sempre, che mi fanno sentire tanto amata, distanti o vicini che siano. Sono tanto orgogliosa di voi e vi ringrazio per le telefonate, i messaggi, il sushu, le cene di ritrovo, i ricordi e le tante risate. In particolare, grazie a Alex, Sara, Erika, Ale e Alice per la vostra presenza e perle di saggezza, per gli spronamenti continui e per aver condiviso ansie e successi.

Por último, quiero agradecerle a una persona especial, que entró en mi vida trayendo mucha positividad y cada día la mejora un poco más. Gracias por tu cariño, tu energía y paciencia. Maite zaitut Xabat.

Quasi dimenticavo, grazie a me, per essere riuscita con determinazione a terminare questo percorso, nonostante le sfide e le difficoltà. Grazie per essere così emotiva, ma così testarda e combattiva.

List of Contents

Declaration	i
List of Publications	i
List of Abbreviations.....	iii
Abstract	v
Acknowledgements.....	vii
Context of the thesis	1
Chapter 1 Introduction to the computational approach	3
1.1 Density Functional Theory.....	5
1.1.1 Functionals and the Jacob's Ladder	8
1.1.2 Basis set.....	10
1.1.3 Pseudopotentials.....	13
1.2 DFT computational calculation on a system – the approach.....	14
1.2.1 Microscopic/structural model.....	14
1.2.2 The conformational complexity	14
1.2.3 The dispersion forces	14
1.2.4 Solvation correction	15
1.2.5 Charge calculation – Fukui indices	16
1.2.6 General methodology applied in the present thesis.....	18
1.3 References.....	19
Chapter 2 Asymmetric catalysis	23
2.1 Introduction	25
2.1.1 Asymmetric organocatalysis	25
2.1.2 α -functionalisation of carbonyl compounds	28
2.1.3 Action mechanisms of bifunctional catalysts.....	37
2.2 Computational studies on the reactivity of α -branched ketone dienolates: regio- and enantioselective α -additions leading to all-carbon quaternary adducts.....	42
2.2.1 Introduction.....	42
2.2.2 Abstract	51
2.2.3 Objectives.....	52
2.2.4 Experimental work	53
2.2.5 Computational work.....	56
2.2.6 Conclusion	63
2.3 Computational studies on the reactivity of transiently generated trienolates: Brønsted Base catalysed α -functionalisation and further elaboration.....	64
2.3.1 Introduction.....	64

2.3.2.	Abstract	67
2.3.3.	Objectives.....	68
2.3.4.	Experimental work	69
2.3.5.	Computational work.....	72
2.3.6.	Conclusion	81
2.4.	References.....	83
Chapter 3 Gold catalysis.....		91
3.1	Introduction	93
3.1.1	Mechanism of gold-catalysed processes.....	94
3.1.2	Description of the M– π -Bond Interaction in Alkyne Complexes.....	97
3.1.3	Tuning of gold catalysts.....	98
3.2	A combined computational and experimental study on the role of the N atom in the pentannulation of <i>N</i> -heterocycles by the tandem gold(I)-catalysed [3,3]-rearrangement/Nazarov reaction	105
3.2.1	Introduction.....	105
3.2.2	Background.....	115
3.2.3	Abstract	118
3.2.4	Objectives.....	119
3.2.5	Computational work.....	119
3.2.6	Experimental work	130
3.2.7	Conclusion	131
3.3	Computational studies on the tandem gold(I)-catalysed Claisen rearrangement/hydroarylation reaction of propargyl vinyl ethers.	133
3.3.1	Introduction.....	133
3.3.2	Abstract	140
3.3.3	Objectives.....	141
3.3.4	Experimental work	141
3.3.5	Computational work.....	143
3.3.6	Conclusion	147
3.4	References.....	148
Chapter 4 Fluorinated isoquinolines		155
4.1	Introduction	157
4.1.1	Isoquinolines	157
4.1.2	Background CH activation in presence of difluoroalkenes	169
4.1.3	Electrocyclisation.....	173
4.2	Abstract	177
4.3	Objectives.....	178

4.4	Experimental work	178
4.4.1	C-H activation	178
4.4.2	Electrocyclisation.....	184
4.5	Computational work.....	186
4.5.1	Methods	186
4.5.2	Electrocyclisation studies	186
4.6	Conclusion	192
4.7	References.....	194
Chapter 5 Experimental section		199
5.1	Materials and techniques.....	201
5.1.1	Reagents and solvents.....	201
5.1.2	General experimental.....	201
5.1.3	NMR spectra.....	201
5.1.4	Mass spectra	201
5.1.5	Infrared Spectra.....	202
5.2	Experimental procedures of Chapter 4.....	202
5.2.1	Synthesis of O-alkyl oximes	202
5.2.2	Synthesis of Hydrazones	208
5.2.3	Synthesis of difluoroalkenes	209
5.2.4	Synthesis of azatrienes through Rh-catalysed CH activation	210
5.2.5	Synthesis of fluorinated isoquinoline (12)	216

Context of the thesis

My PhD thesis is part of the network CATMEC (Catalytic Methods for Sustainable Synthesis. A Merged Experimental and Computational Approach), a multi-partner Innovative Training Network (ITN) European Joint Doctorate (EJD) in the field of sustainable chemical synthesis, catalysis, computational chemistry and bioactive molecule design. The main scientific objectives of CATMEC are to exploit novel synthetic concepts in the preparation of small molecules of high societal value and suitable computational methods for the understanding and optimisation of important catalytic processes with the ambitious goal of discovering new biologically active compounds that address current challenges in new medicines.

During my three years of PhD, based at UPV/EHU, I had the chance of working in other outstanding environments. I spent 9 months at the laboratory of Prof. J. Harrity, at the University of Sheffield, working on experimental synthesis of fluoroisoquinolines and 3 months at Evotec (UK) in the Research Informatics, computational chemistry group, where I had the opportunity to expand my computational knowledge learning suitable methods for drug design and protein modelling. The work at Evotec regarded the analysis of metal-organic systems (zinc finger domains in particular) with the density-functional based tight-binding (DFTB) method, but the work is not reported in this thesis. The title of the thesis "*Computational understanding of heterocyclisation reactions and synthesis of fluorinated isoquinolines*" aims to include on one hand the project co-supervised by Prof. Harrity, which deals with the synthesis of fluorinated isoquinolines and the computational study of the cyclisation step and on the other hand, taking advantage of the expertise in calculations, the collaborations I run, in which my only contribution was the computational approach.

The topic of density functional theory is introduced in the **first chapter**, together with the principles and methodology applied in the calculations. The following four chapters deal with the work done and are organised to include the introduction of the topic, the objectives and the discussion of the results.

Chapter 2: This chapter deals with asymmetric organocatalysis and computational calculations are employed to compare the reactivity of a series of substrates through the study of charges, nucleophilicity characters and activation energies of the potential reaction pathways. Stereochemistry issues were faced through computational studies to explain and support the experimental evidences. Hydrogen bond networks between the catalyst and the substrates, responsible of the stereochemistry, were modelled to justify the experimental outcome.

Chapter 3: The topic of this chapter is gold homogenous catalysis and computational studies were carried out to investigate the reaction mechanisms and have an insight on the reactivity of similar substrates to explain the different reaction behaviours. The influence of the catalyst ligands was also explored computationally justifying the experimental evidence.

Chapter 4: This chapter includes an experimental part, the synthesis of fluorinated isoquinolines, and a computational one, which analyses one step of the methodology

employed experimentally. Calculations were performed to define the mechanism of the formation of the desired product and of an unpredictable side product.

In the **fifth and last chapter**, the experimental part of the fourth chapter is reported, including materials and techniques, synthetic procedures and characterisation of the synthesised compounds.

Chapter 1

Introduction to the computational approach



General aspects of computational chemistry with particular focus on DFT are described. In this chapter the fundamental theories, principles and methodology of the computational approach are presented.

A deep study of an organic reaction involves the development and the understanding of the process through the combination of different laboratory techniques. In addition to the experimental and the analytic techniques, computational chemistry provides important information and it is a convenient tool for the characterisation of some properties of the system. Computational means have shown enormous progress during the last decades due to better computer performance (speed and major advances in hardware and software), more efficient algorithms and more accurate methods. Nowadays, calculations of molecular processes can be done with reasonable accuracy on a time-scale that is competitive or even faster than experiments. Mechanistic studies are commonly investigated through calculation, computational modelling and molecular simulations. For example, it is common in homogenous catalysis to find multistep complicated catalytic cycles, involving the formation and evolution of intermediate species often difficult to characterise experimentally and here computational chemistry plays an important role.¹ Indeed, this methodology has demonstrated to be a good tool for the understanding of the nature of transition states and intermediates suggested by spectroscopic and kinetic studies or simply by chemical intuition. Thanks to the combination of computation and experiment, which support each other, it is possible to shed light on complex reaction pathways, chemical reactivity, catalytic cycles and kinetic models.² Nevertheless, it is to keep in mind that it is unlikely that calculations themselves provide a correct representation of a mechanism. Indeed, experiments are essential to describe the system and the mechanism, which can be corrected by computational chemistry when some experimental data are misinterpreted.³ Using the appropriate methodology developed by theoretical chemistry and the valuable data obtained experimentally, computational chemistry can interpret the results and construct models. If the models are accurate enough, they can be used to predict new properties or reactions, facilitating the discovery of new processes in a rational manner. Several properties can be obtained through computational calculations, such as structures (expected positions of the constituent atoms), absolute and relative energies, electronic charge distributions, dipoles and higher multipole moments, vibrational frequencies or other spectroscopic quantities, substrate-enzyme interactions, collision cross sections between particles and chemical reactivity. In this thesis, I am presenting five projects involving combined and synergic experimental and computational works to gain insight into the mechanism and reactivity issues of catalytic (and not) organic reactions.

1.1 Density Functional Theory

Among the several computational tools, DFT (Density Functional Theory) method is especially convenient to use because it ensures chemical accuracy at very low computational cost.

Conventionally, computational accuracy is meant as the good performance of a specific methodology to compute specific fundamental chemical properties taking as reference experimental or highly accurate (high level) theoretical results. Generally, mainly in catalytic systems, the quality of the model used to represent the system plays a determinant role.⁴ Indeed, it must feature a good balance between theoretical approximation and chemical details.

1.1 Density Functional Theory

Classically, quantum chemistry followed the multielectronic wavefunction approach. Wavefunctions depend on $3N$ variables (where N is the number of electrons of a specific system) and N spin variables that have to be added and must satisfy the Schrödinger equation. The resolution of the Schrödinger equation is very complicated from a mathematical point of view. Therefore, the methodologies developed rely on an approximate wavefunction and try to improve it systematically. The drawback is the computational cost of these methods (Hartree-Fock derived methods) that is too high to be applied in the study of real chemical reactions, thus they are usually only applied in model systems.

A balance between accuracy and computational cost has always to be considered when starting a computational study of a system. Quantum mechanical models based on wavefunctions provide high accuracy in the description and prediction of properties of the system. High accuracy in this case requires high computational time or CPU resources, which limit the size of the sample system that can be only small and simple. On the other hand, molecular mechanical models (MM), based on classical mechanics, lack in accuracy, but are little demanding of time and CPU resources. These characteristics led to the employment of MM for rough descriptions of the properties of a system. A satisfactory answer to all these requirements is given by DFT.^{5,6}

Density functional theory uses electron density to determine the ground state electronic energy. The electron density is defined as the probability of finding one electron in an infinitesimal volume. The total electron density $\rho(r)$ depends on just three variables (x , y , z positions in space), thus results simpler than the electronic wavefunctions, which depend on $3N$ variables (x , y , z coordinates of each electron). As a consequence, the electron density was considered able to offer a more direct way to obtain the molecular energy of a system. There exists a one-to-one correspondence between the electron density of a system and the energy.

DFT was first developed in the early 20th century on the basis of the Thomas-Fermi model,^{7,8} and later formalised by the Hohenberg-Kohn theorems, which state:⁹

1) the electronic energy and any other properties of the ground state can be described as a functional of the exact electron density of the system. A mathematical *functional* relates a function to a scalar quantity. In DFT, the functionals are applied to the electron density.

2) the exact electron density of the system is the one that minimises the electronic energy of the ground state, according to the variational principle (1.1). If the true functional form is known, then the energy can be minimised by varying the electron density, in order to find the ground state electron density. Once the ground state electron density is known, all the properties can be calculated.

$$E[\rho] \geq E[\rho_{\text{exact}}] = E_{\text{min}} \quad (1.1)$$

The goal of DFT is to design functionals that correlate electron energy to electron density function. This task can be very difficult to complete, and therefore is currently not fully solved.

In 1965, Kohn and Sham¹⁰ proposed that the functional has the form

$$E[\rho]=T[\rho]+E_{en}[\rho]+J[\rho]+K[\rho] \quad (1.2)$$

Based on the classical quantum approach, the total energy functional is the sum of three terms: kinetic energy $T[\rho]$, attraction between nuclei and electrons $E_{ne}[\rho]$ and electron-electron interaction $E_{ee}[\rho]$, which can be split into the Coulomb $J[\rho]$ and exchange $K[\rho]$ contributions, implicitly including the correlation energy to all the terms (1.2). According to the Born-Oppenheimer approximation, the nuclear-nuclear repulsion is considered constant.⁵

The key element presented by Kohn and Sham for the calculation of ρ and $E[\rho]$ was the introduction of orbitals in DFT, describing a kinetic functional under the molecular orbital approximation. Since the exact density is not known, the approximate density is written using a set of auxiliary one-electron functions, the KS orbitals:

$$\rho(r) = \sum_{i=1}^N |\varphi_i^{KS}(r)|^2 \quad (1.3)$$

where $\varphi_i^{KS}(r)$ are the Kohn-Sham orbitals that can be calculated by solving the Kohn-Sham equation

$$\hat{h}^{KS}(i)\varphi_i^{KS} = \varepsilon_i^{KS}\varphi_i^{KS} \quad (1.4)$$

in which $\hat{h}^{KS}(i)$ represents the Kohn-Sham Hamiltonian and ε_i^{KS} the Kohn-Sham orbital energy.

The re-introduction of orbitals implies the increasing of the complexity from 3 to $3N$ variables, analogous to Hartree theory, but still much less complicated than post-HF (correlation) wavefunction models.

The Kohn-Sham (KS) model is based on a particular virtual reference system of non-interacting electrons with the same electron density as the real interacting electrons, moving through a local effective external potential, named the Kohn-Sham potential ($V_{eff}(r)$). There is an analogy between the KS model and the HF method. Indeed, both KS orbitals and HF MOs are separable and describe non-interacting electrons. HF uses an independent-electron wavefunction (Slater-determinant), whose electrons interact through the HF potential. Therefore, the energy functional can be written as:

$$E[\rho] = \underbrace{\frac{\hbar^2}{2m_e} \sum_{i=1}^N \int \varphi_i^*(r) \nabla^2 \varphi_i(r) dr}_{\text{Kinetic energy}} - \underbrace{\sum_{i=1}^N \int \frac{Z_i e^2}{4\pi \varepsilon_0 |R-r|} \rho(r) dr}_{\text{Nuclear-electron attraction}} + \underbrace{\frac{1}{2} \int \int \frac{\rho(r)\rho(r')e^2}{4\pi \varepsilon_0 |r-r'|} dr dr'}_{\text{Electron-electron repulsion}} + \underbrace{E_{XC}[\rho]}_{\text{Exchange-correlation}} \quad (1.5)$$

1.1 Density Functional Theory

The kinetic term is defined as the kinetic energy of noninteracting electrons whose density is the same as the density of true interacting electrons and is expressed in an equivalent way to the one used in HF theory. The second term, $E_{ne}[\rho]$, is the classical electron-nucleus attraction and the third term, $J[\rho]$, is the classical Coulomb repulsion between charges. Both terms follow the equivalent expressions of HF theory. The last term, $E_{xc}[\rho]$, is the exchange-correlation functional and takes into account all other aspects of the true system, i.e. the difference between the exact kinetic energy and the kinetic energy of non-interacting electrons, non-classical interactions between electrons. Due to the similarity with HF, it is noteworthy that for a similar computational cost as the HF method, DFT provides the exact total energy of a molecule that includes the electron correlation (advantage respect to uncorrelated HF). Nevertheless, the issue is that the exchange-correlation term is the only unknown energetic term in the KS formalism of DFT. There is no way of deriving this term, thus different functionals have been proposed, leading to the developments of several DFT methods, which differ for the approximation for the exchange-correlation functional $E_{xc}[\rho]$.

1.1.1 Functionals and the Jacob's Ladder

Perdew defined a hierarchy of approximate treatments of the exchange-correlation term, called "Jacob's Ladder" (Figure 1.1).^{11,12}

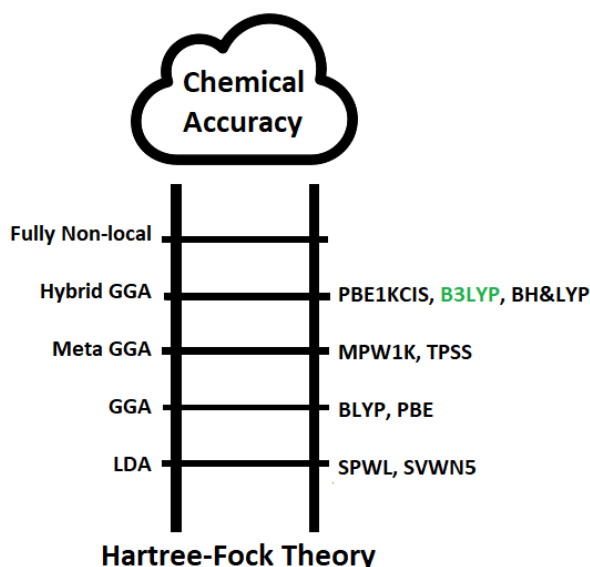


Figure 1.1 Jacob's Ladder representation.

The ladder is grounded in HF theory at the bottom and reaches the top, where the exact functional is found. Along the way, five rungs are present, each defining a set of assumptions made in creating an exchange-correlation expression. The simplest approximation for the DFT exchange-correlation energy, located at the first rung, is the so called *Local Density Approximation* (LDA), which assumes that the density can be treated locally as a uniform electron gas, or equivalently that the density is a slowly varying function. Going up, the next level of sophistication is the *Generalised Gradient Approximation* (GGA), in which the energy functional depends on the electron density

and on derivatives of the density, thus the gradient of the density at that given position. The third rung is occupied by the *meta-GGA* functional, which includes the dependence on the Laplacian of the density ($\nabla^2\rho$) or on the local Kohn-Sham orbital kinetic energy density (τ). One rung upper, the *hyper-GGA* or *hybrid functionals* include a dependence on Hartree-Fock exact exchange. Finally, the fifth rung incorporates the unoccupied Kohn-Sham orbitals in the double hybrid functionals (or *fully non-local functionals*). They improve the accuracy, but they imply nonlocality dependence for the density and higher computational cost.¹³

It is worth to say that DFT provides an exact theory with an approximate solution. Therefore, it contains errors by default. There are three main errors.

The first one is the *Self-Interaction Error* (SIE), due to the fact that $E_{xc}[\rho]$ is an approximation and to the lack of a precise way to distinguish between the correct two-body Coulomb interactions from fictitious one-electron self-interactions, since the energy is a functional of the one-electron density.^{6,14} Exchange–correlation functionals without self-interaction corrections badly describe loosely bound electrons, such as anions arising from systems with relatively low electron affinities.

The second error is the *near-degeneracy energy* (non-dynamical or static correlation) *error* that raises from the description of the wavefunction as a single determinant. The use of spin-unrestricted description, according to which α - and β -spin electron densities occupy different regions of space, is a way to deal with this error (commonly applied in the studies involving first-row transition metals complexes).

Fortunately, these two errors have opposite effects on the barriers (the first decreases while the second increases them) and they tend to substantially cancel each other. Thus, it is less convenient trying to remove just one error's sources because it could cause larger errors.¹⁵

The third error is caused by the poor description of the weak interactions due to dispersion forces (known as Van der Waals type interactions). These long-range interactions can be seen as instantaneous electron correlations when “charge fluctuations” on one region of the system induce dipole moments on the other fragment. The corresponding (pseudo)densities interact electrostatically (with exchange-type modifications at smaller distances). Conventional (hybrid) DFT functionals cannot describe these interactions that only consider electron exchange but do not employ virtual orbitals.¹⁶ The dispersion correction is an add-on term and does not alter the wavefunction or molecular properties for a specific given geometry. Nevertheless, it influences the geometry optimisation process because it contributes to the forces acting on the atoms.

In general, hybrid functionals, such as the B3LYP exchange-correlation functional, are the most common to use. Indeed, B3LYP¹⁷ has been the most popular quantum chemical method for studying mechanisms of complexes containing transition metals and it has been extensively used in this thesis. The reasons behind its popularity are related to its high accuracy demonstrated in several benchmark tests regarding energetic descriptions¹⁸ and to the low computational cost despite being a hybrid functional, which allows to treat even large models up to a few hundred atoms.

1.1.2 Basis set

Once the best functional for the system is chosen, it is necessary to define the basis set. The basis set is a set of basis functions able to describe the shape of the orbitals in terms of atomic orbital contributions. Linear combinations of these functions with angular functions describe molecular orbitals. The basis functions can be Slater Type Orbitals (STO) or Gaussian Type Orbitals (GTO) and are expressed by the following functional forms:

$$\text{STO} \quad \chi_{\zeta,n,l,m}(r, \theta, \varphi) = NY_{l,m}(\theta, \varphi)r^{n-1}e^{-\zeta r} \quad (1.6)$$

$$\text{GTO} \quad \chi_{\zeta,n,l,m}(r, \theta, \varphi) = NY_{l,m}(\theta, \varphi)r^{2n-2-l}e^{-\zeta r^2} \quad (1.7)$$

$$\chi_{\zeta,l_x,l_y,l_z}(x, y, z) = Nx^{l_x}y^{l_y}z^{l_z}e^{-\zeta r^2}$$

where N is a normalisation constant, $Y_{l,m}$ are spherical harmonic functions, ζ represents varied parameters and controls the width of the orbital and r is the radial (distance) parameter. In cartesian GTO, the sum of l_x , l_y and l_z determines the type of orbital (for example $l_x + l_y + l_z = 0$ is a s-orbital and $l_x + l_y + l_z = 1$ is a p-orbital). Due to the r^2 dependence in the exponential in GTO, STO are able to better describe the orbitals near the nucleus than GTO (GTO have a zero slope, in contrast to STO which have a “cusp”). Furthermore, their functional decay away from the nucleus is better described by STO because GTO fall off too rapidly far from the nucleus compared with STO (Figure 1.2).

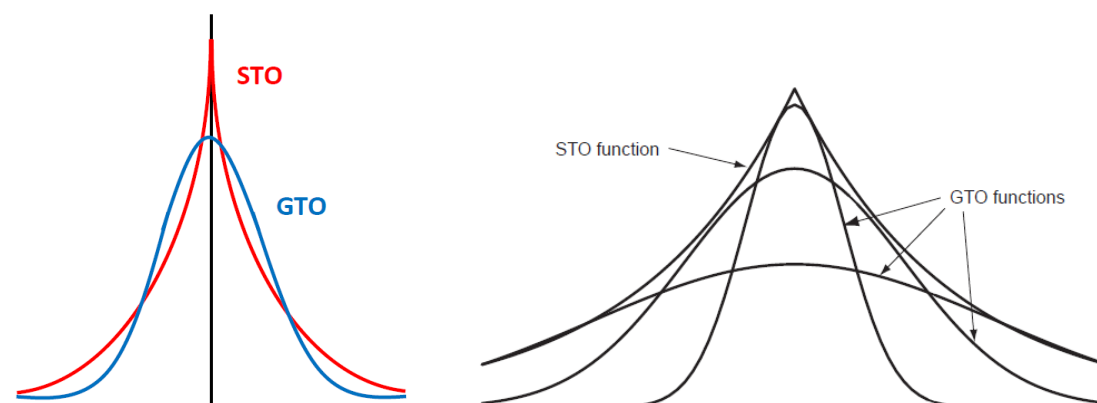


Figure 1.2 On the left, a schematic comparison of Slater-type (STO) AND Gaussian-type orbitals (GTO) and on the right, the approximation of a STO with three GTO (most of the STO is covered by the three GTO functions).⁵

More GTOs are necessary for achieving the same accuracy of STOs. Nevertheless, the integrals of a GTO function are less demanding to compute than the ones in STO. This is the reason why the construction of linear combinations of GTOs (called *primitives*) in order to mimic the STO functions results more convenient and computationally affordable. Nowadays it is the preferred method to construct a basis set.

For example, the linear combination of three GTOs can model a STO (Figure 1.2 on the right). GTOs are generally centred at the nuclei. It is important to decide the number of functions to use. The smallest number of functions possible is a *minimum basis set*.

The real molecular orbitals are better described by a basis set that contains much more basis functions (in principle, an infinite number of basis functions would be a *complete basis set*, CBS).

On the other hand, the higher is the number of functions it has, the higher the computational cost is. Thus, in the election of the basis set, a correct number of functions has to be chosen in order to achieve a balance between the accuracy and the computational cost.

Many basis set describe differently the inner core orbitals and the valence shell orbitals. Since the valence shell orbitals contribute more to the reactivity and the properties, usually they are described by more functions.

The *degree of split valence basis* is indicative of the amount of functions involved in the representation of the valence orbitals (that is the number of basis sets that describes each valence orbital compared to the minimum basis set). A double-zeta valence (DZ) basis set contains the double of functions of the minimum basis set of functions. Going up, there are the triple-zeta valence (TZ), the quadruple-zeta (QZ) and the quintuple-zeta (PZ).

In addition, basis sets can be enhanced by *polarisation* and *diffuse functions*. Polarisation functions add a basis function of higher molecular momentum to further improve the flexibility of the valence orbitals described, thus for example, if the valence electrons are p, one d function is added to let the p orbital polarised. They are denoted by a "P" after describing the type of valence split (i.e. TZP or DZP).

On the other hand, diffuse functions are basis functions with small exponents and can be added to describe more accurately the behaviour of the electrons far from the nucleus. They are needed in the presence of loosely bound electrons (for example anions, radicals or excited states) or when the property of interest is dependent on the wave function tail (for example polarisability).

Several basis sets have been developed with different purposes. They are catalogued by families of basis sets. The basis sets in each family share common features and their nomenclature. Pople style basis set (e.g. 3-21G, 6-31G, 6-311G), Ahlrichs type basis set (e.g. SVP, TZVP, Def2SVP, Def2TZVP), and Correlation consistent basis set (cc-pVDZ, cc-pVTZ, cc-pVQZ) are among the most popular.¹⁹

Pople family basis sets are named according to the notation *k-nlmG*. They are of split valence type and the *k* indicates how many primitive GTOs are used to represent the core orbitals. The *nlm* indicate how many functions the valence orbitals are split into, and the number of primitive GTOs used for their representation. Two values (*nl*) indicate a split valence, while three values (*nlm*) indicate a triple split valence. The values before the G (for Gaussian) indicate the s- and p-functions in the basis; the polarisation functions for heavy atoms (different from hydrogen) are indicated after the G by adding a "*". A second asterisk is indicative of the polarisation functions for hydrogen orbitals. The diffuse functions can also be added to heavy or hydrogen atoms by adding one or two "+", respectively. In this type of basis sets the same exponent is used for both the s- and p-functions in the valence, thus increasing the computational efficiency, but decreasing the flexibility of the basis set. Pople basis sets are considered outdated and have serious deficiencies, but they are still useful in some specific cases.²⁰

As an example, 6-311G basis set means that 6 primitives describe each basis set function associated to core electrons, the valence shell is triple split and there are 3, 1, 1 primitives for each of the valence basis functions respectively.

In this thesis the basis sets 6-31G**, 6-311+G** belonging to Pople family have been used.

Ahlrichs basis sets do not show the number of primitives in their nomenclature. From the notation it is possible to understand that SVP (*Split Valence Polarised*) is a single split only for the valence orbitals (i.e. DZVP), with polarised functions added (the “P” represents the polarised functions added by default). Then, the other basis set TZVP, QZVP corresponds to triple- and quadruple- zeta respectively. The basis sets that bear a “Def2” as a prefix are those that have been redefined and greatly improved in the last years.

In this thesis it has been used the Def2TZVPP,²¹ which corresponds to a redefined Ahlrichs basis set with triple split and two sets of polarised functions. This redefined family of basis sets is more flexible than the Pople family because they have different exponents for the s and p orbitals.

In the case of the correlation consistent basis sets, the “cc” expresses that they are *correlated consistent*, tuned towards recovering the correlation energy of the valence electrons. The basis sets are built such that functions that contribute similarly to the correlation energy are included at the same stage, independently of the function type. The level of split in the valence core is indicated by their name. For example, cc-pVDZ, cc-pVTZ, cc-pVQZ, cc-pV5Z and cc-pV6Z are correlation consistent polarised valence Double/Triple/Quadruple/ Quintuple/Sextuple Zeta (split) respectively. This kind of basis sets always has polarisation functions, decreasing the split of the functions with the degree of polarisation. For instance, for the atoms of the second period, cc-pVTZ assigns three basis functions for the 2s and 2p orbitals, two basis functions for the 3d orbitals and one basis function for the 4f orbitals. This basis was designed especially for post-HF methods, in such a way that, for example, the first d function provides a large energy lowering, but the contribution from a second d function is similar to that of the first f function. The energy lowering from a third d function is similar to that of the second f function and the first g function. These polarisation functions should, therefore, be added in the order 1d2d1f and 3d2f1g.

A Complete Basis Set, CBS, would require an infinite number of basis functions. However, it is possible to perform an extrapolation using increasing larger basis sets providing an approximate value for the CBS value. Specifically designed basis sets, named *correlation consistent basis sets*, have to be used to guarantee reliable results from CBS limit extrapolations i.e cc-pVxZ. At least three basis sets should be employed (e.g. cc-VDZ, cc-VTZ, and cc-VQZ).^{5,22} If the basis set is not complete, there is the generation of the Basis Set Superposition Error (BSSE). Some methods, such as the Counterpoise (CP) correction or the extrapolation to CBS methods,²³ have been designed to correct and compensate this error.

The selection of a basis set heavily depends on the size of the system under study, on the number of atoms and more specifically the number of electrons. Small basis sets with limited number of functions are recommended for calculations that require heavy

computing (like geometry optimisations, frequency calculation) on systems with a considerable amount of atoms (or with more than one heavy element).²⁴ On the other hand, the restrictions and lack of flexibility imposed by a small number of functions to describe the orbitals cause the formation of an implicit error into the small basis sets. Therefore, it is a common practice to perform a single point calculation with a better basis set (more flexible or complete) after the heavy calculation (i.e. optimisation) performed with a smaller one.

In all the works presented in this thesis, the optimisation is carried out using a smaller basis set, in order to gain quickly information about the system. Then, once stationary-point structures are available, single point calculations with a more robust basis set are performed to obtain more accurate properties, such as energy differences.

1.1.3 Pseudopotentials

As previously said, valence electrons are those that play a determinant role in chemical transformations of molecules. The core electrons are not involved in these processes, but affect the corresponding orbitals. To reduce the computational effort, it is possible to focus only on the valence electrons and approximate the effect of the core electrons with *pseudopotentials* or *effective core potentials* (ECPs). The ECPs could include relativistic effects that are very important in molecules with heavy elements without necessarily need to apply relativistic theory to the rest of the system. The most popular ECP types in the literature are the Stuttgart-Dresden (SDD) energy-consistent effective core potentials²⁵ and the Los Alamos National Laboratory (LANL) shape-consistent effective core potentials (e.g. LANL2DZ - valence electrons are handled with double-zeta quality).²⁶

ECP bases are useful for two main reasons, reducing computational cost in handling metal containing systems and circumventing having to describe relativistic effects in deep core electrons.

In Chapter 3 we have used SDD for gold atom for the study of gold catalysed systems.

1.2 DFT computational calculation on a system – the approach

Computational calculations are defined by the choice of the DFT method or level of theory, which includes the functional and the basis set. DFT functional and basis set are selected on the basis of the system and the properties under study, i.e. type and number of atoms and bonds. Searching in the literature pre-existing studies related to similar chemical systems could help in the choice of the most suitable method. The best solution would be performing a benchmark on your own system using different known functionals, but this requires time and resources. Many factors influence the accuracy and consistency of the study and some expedients, as seen for the basis set, need to be considered concerning the microscopic/structural model, the conformational complexity, the dispersion forces, the solvation correction and further corrections (i.e. the entropy and temperature).

1.2.1 Microscopic/structural model

Sometimes some chemical systems are difficult to represent or to model in order to perform computationally feasible calculations. A good approach is to employ a simplified model of the real reaction, which describes the important elements of the real system and can be computed with the computational power available. The design of the simplified system is the result of the personal chemical intuition, it has to contain the key variables of the systems and make chemical sense. The real system is divided into the core part, which needs to be studied in detail and the frame part, which can be omitted or simplified because it does not play a determinant role into the study.

1.2.2 The conformational complexity

Most of the times, it is quite difficult finding all the plausible conformers of a system, especially in the case of organometallic systems due to the flexibility of the metal-ligand bonds. To sort this issue out, it is possible to use programmes that systematically explore all the conformational and reactive space, but they are computationally very expensive. Another alternative is to explore manually the most relevant conformers dictated by personal intuition. It is very probable that some mechanistically important conformers are not taken in consideration, but anyway this is the most used approach.

1.2.3 The dispersion forces

Dispersion forces are poorly described by DFT methods, but they are relevant despite their weakness. The contribution of these weak interactions can be added as an extra term in any functional allowing the evaluation of the steric interactions, which can be determinant for the discrimination between enantiomers.²⁷

Grimme and coworkers developed a method to add the dispersion effect to most of the common functionals, improving the accuracy of several functionals, even if it does not reach the perfection.

On the other hand, there exist some functionals that were designed to include already the dispersion effects, such as the highly parametrised Minnesota functional family, developed by Truhlar group. The M06 family includes certain empirical parameters that are adjusted to take into account such dispersion forces. Indeed, the M06 family is constituted of four meta-hybrid GGA DFT functionals that are designed by empirically

fitting their parameters, while constrained to a uniform electron gas. The functionals developed are M06,²⁷ M06-L,²⁸ M06-2X²⁷ and M06-HF²⁹ and they differ for the amount of exact exchange. M06-L is fully local without HF exchange (thus it cannot be considered hybrid), M06 has 27% of HF exchange, M06-2X 54% and M06-HF 100%.

Among them, M06 is the most versatile. Because of its large applicability, it can be slightly worse than M06-2X for the calculation of specific properties that require high percentage of HF exchange, such as thermochemistry and kinetics.

The M06 and M06-2X functionals are used in some parts of this thesis.

1.2.4 Solvation correction

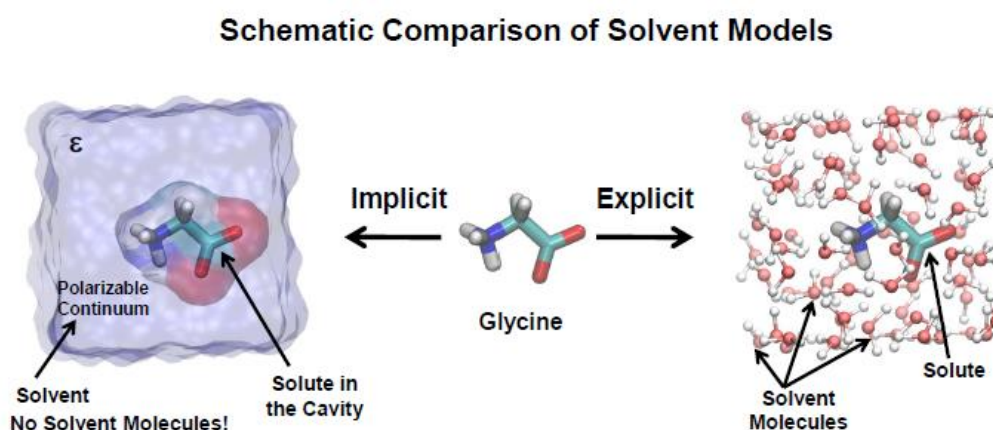


Figure 1.3 Schematic comparison of implicit and explicit solvation model.³⁰

Most of chemical reactions are carried out in the presence of a solvent, which plays an important role especially in those cases where it stabilises species in the reaction or acts as reactant. Therefore, it emerges the necessity to describe the solvent effects also in computational studies.

At the beginning computing solvated systems, in which thousands of solvent molecules surround the substrate, constituted a problem in DFT. Thus, molecules were studied in vacuum conditions or in gas phase, neglecting important information in the study.

Nowadays, there are two conventional ways to include solvent effects in electronic-structures calculations: one is by considering the individual solvent molecules explicitly with QM/MM methods (*explicit solvation model*) and another treating the solvent as a continuous medium (*continuum or implicit method*) (Figure 1.3).^{31,32} The former implies a high computational cost due to the presence of a high number of molecules. In addition, some extra errors could arise depending on how the molecules are placed around the reactant species or on the number of molecules that should be considered. The second approach treats the molecules implicitly and is the most common. Among such methods, the Self-Consistent Reaction Field (SCRF) method³³ is perhaps the most widely used. The solvent is considered as a uniform polarisable medium with a dielectric constant ϵ (or relative permittivity, ϵ_r), where the solute is placed in a suitable shaped cavity inside a dielectric medium, which electrostatically stabilises the solute. The method is iteratively repeated until the mutual polarisation between the solute and

solvent reaches the self-consistency. The free energy of solvation is calculated as the sum of different energy contributions:

$$\Delta G_{\text{solvation}} = \Delta G_{\text{cavity}} + \Delta G_{\text{dispersion}} + \Delta G_{\text{repulsion}} + \Delta G_{\text{electrostatic}} \quad (1.8)$$

where ΔG_{cavity} is the cavitation energy, that is the energy needed to create the cavity for the solute (it is a destabilising term and therefore is always positive), $\Delta G_{\text{dispersion}}$ is the dispersion energy between solute and solvent that contributes as a stabilising term, $\Delta G_{\text{repulsion}}$ is associated to the repulsive interactions between solute and solvent (it is also a destabilising term) and $\Delta G_{\text{electrostatic}}$ is related to the electrostatic interactions due to the instantaneous polarisation caused by the charge distribution of the solute molecules in the solvent, and vice versa, and is a stabilising term.

There are several SCRF methods for the calculation of solvation energies. However, only the Polarizable Continuum Model (PCM)³⁴ is used in this thesis. In PCM, the cavity is constructed as an assembly of atom-centred overlapping spheres with radius approximately 1.2 times larger than the van der Waals radius.

1.2.5 Charge calculation – Fukui indices

Calculations can be used to perform charge distribution analysis. The results can be used then to have information about the nucleophilicity and electrophilicity character of atoms in the substrates, predicting somehow the reactivity towards other reactants.

In this thesis to this purpose, we have used the *Natural Bond Orbital analysis* (NBO). Natural bond orbital (NBO) analysis is one of many available options for 'translating' computational solutions of Schrödinger wave equation into the familiar language of chemical bonding concepts.^{35,36}

The idea at the base of NBO analysis was developed by Weinhold and coworkers,^{5,37} who thought to use the one-electron density matrix to define the shape of the atomic orbitals in the molecular environment, and to derive molecular bonds from electron density between atoms.

NBO analysis is based on a method that optimally transforms a given wavefunction into localised form, corresponding to the one-centre ("lone pairs") and two-centre ("bonds") elements of the Lewis structure picture. The input atomic orbital basis set is transformed through a multistep process involving natural atomic orbitals (NAOs) and natural hybrid orbitals (NHOs) into natural bond orbitals (NBOs).

In an initial step, orbitals that are associated almost entirely with a single atom, e.g., core orbitals and lone pairs, are localised as *natural atomic orbitals* (NAOs).

Next, orbitals involving bonding (or antibonding) between pairs of atoms are localised by using only the basis set AOs of those atoms.

Finally, the remaining Rydberg-like orbitals are identified, and all orbitals are made orthogonal to one another.

The result is that, except for very small contributions from other AOs to ensure orthogonality, all NAOs and Rydberg orbitals are described using the basis-set AOs of a single atom and all NBOs are described using the basis-set AOs of two atoms. Thus, NBO analysis provides an orbital picture that is as close as possible to a classical Lewis structure for a molecule, in which two-centre bonds and lone pairs are localised.

In computational chemistry, NBO analysis is used to calculate the distribution of electron density in atoms and in bonds between atoms of a molecule in a system.

They have the "maximum-occupancy character" in localised 1-centre and 2-centre regions of the molecule. NBOs include the highest possible percentage of the electron density.

To sum up, the NBOs are one of a sequence of natural localised orbital sets that include "natural atomic orbitals" (NAO), "natural hybrid orbitals" (NHO), "natural bonding orbitals" (NBO) and "natural (semi-)localised molecular orbitals" (NLMO). These natural localised sets are intermediate between basis atomic orbitals (AO) and molecular orbitals (MO):



The concept of natural orbitals may be used for distributing electrons into atomic and molecular orbitals, and thereby deriving atomic charges and molecular bonds.

Through this localisation approach, hybridisation can also be assigned to the atomic lone pairs and to each atom's contributions to its bond orbitals. The percentage of s and p character (and d, f, etc.) is immediately evident from the coefficients of the AO basis functions from which the NAO or NBO are formed.

NBO analysis provides the charges on the single atoms of a substrate. These data can be used to calculate the Fukui indices of the atoms, which can be considered as reactivity indices; they give information about which atoms in a molecule have a larger tendency to either lose or accept an electron, or more practically which are more prone to undergo a nucleophilic or an electrophilic attack, respectively. This deals with the tendency of the molecules to become polarised in the presence of an external field or upon the change of electron density. From a mathematical point of view, Fukui functions are defined by Yang and Parr³⁸ as the functional derivative of the chemical potential respect to the external potential (the one produced by the nuclei) at a constant electron number. Since the chemical potential is defined as the derivative of the density functional respect to the electron density, Fukui functions are also defined as the derivative of the electron density respect to the number of electrons at a constant potential. Thus, it is possible to calculate how the density changes at every point when adding or removing an electron while keeping the potential constant (that is the position of the nuclei or in other words maintaining the molecular geometry).^{39,5}

$$f(r) = \frac{\partial \rho(r)}{\partial N_{elec}} \quad (1.9)$$

Fukui indices (also known as condensed-to-atoms Fukui functions) can be calculated through the finite differences method. Two finite difference versions of the function, corresponding to addition or removal of an electron are defined:

Electrophilicity of atom A in molecule M (of N electrons)

$$f_A^+ = P_A(N+1) - P_A(N) \quad (1.10)$$

Nucleophilicity of atom A in molecule M (of N electrons)

$$f_A^- = P_A(N) - P_A(N-1) \quad (1.11)$$

Radical attack susceptibility of atom A in molecule M (of N electrons)

$$f_A^0 = 1/2[P_A(N+1) - P_A(N-1)] \quad (1.12)$$

where P stands for the population of atom A in molecule M. The population analysis on the + or – system has to be performed at the same equilibrium geometry as the original molecule to avoid to lose information on the polarisation of the electron density upon the change in number of electrons.⁴⁰

These indices are very sensitive towards changes in basis sets and population analysis paradigm. Therefore, those numbers are not to be taken as absolutes, but instead as comparative parameters within the same system to have an insight on the reactivity.

In chapters 2 and 3 we have performed NBO analysis and in some cases used the results to calculate the Fukui indices.⁴¹

1.2.6 General methodology applied in the present thesis

In this thesis, all geometries were fully optimised in gas phase with a simple method (simple functional and small basis) as implemented in Gaussian 16.⁴² Once the optimised geometries are obtained, single point calculations with a better basis set are performed adding a PCM in order to consider the solvent effects.

Depending on the kind of system, different methods have been used and specified in every chapter in the section “*Methods*”. Computational chemistry in these works plays a synergistic role with experiments to provide a complete analysis of the reaction systems under study.

1.3 References

1. Maseras, F.; Lledós, A. *Computational modeling of homogeneous catalysis*; Kluwer Academic Publishers: Dordrecht, 2002.
2. a) Sperger, T.; Sanhueza, I. A.; Schoenebeck, F. *Acc. Chem. Res.* **2016**, *49*, 1311–1319; b) Cheng, G. J.; Zhang, X.; Chung, L. W.; Xu, L.; Wu, Y. D. *J. Am. Chem. Soc.* **2015**, *137*, 1706–1725; Vogiatzis, K. D.; Polynski, M. V.; Kirkland, J. K.; Townsend, J.; Hashemi, A.; Liu, C.; Pidko, E. A. *Chem. Rev.* **2019**, *119*, 2453–2523; Spivey, J. J.; Krishna, K. S.; Kumar, C. S. S. R.; Dooley, K. M.; Flake, J. C.; Haber, L. H.; Xu, Y.; Janik, M. J.; Sinnott, S. B.; Cheng, Y. T. *J. Phys. Chem. C* **2014**, *118*, 20043–20069; Medford, A. J.; Vojvodic, A.; Hummelshøj, J. S.; Voss, J.; Abild-Pedersen, F.; Studt, F.; Bligaard, T.; Nilsson, A.; Nørskov, J. K. *J. Catal.* **2015**, *328*, 36–42; Van Speybroeck, V.; Hemelsoet, K.; Joos, L.; Waroquier, M.; Bell, R. G.; Catlow, C. R. A. *Chem. Soc. Rev.* **2015**, *44*, 7044–7111; Sperger, T.; Sanhueza, I. A.; Kalvet, I.; Schoenebeck, F. *Chem. Rev.* **2015**, *115*, 9532–9586.
3. Garcia-Borràs, M.; Luis, J. M.; Swart, M.; Solà, M. *Chem. Eur. J.* **2013**, *19*, 4468–4479.
4. Harvey, J. N.; Himo, F.; Maseras, F.; Perrin, L. *ACS Catal.* **2019**, *9*, 6803–6813.
5. Jensen, F. *Introduction to computational chemistry*; John Wiley & Sons Ltd: Chichester, England, 2007.
6. Pribram-Jones, A.; Gross, D. A.; Burke, K. *Annu. Rev. Phys. Chem.* **2015**, *66*, 283–304.
7. Thomas, L. H. *Math. Proc. Cambridge Philos. Soc.* **1927**, *23*, 542–548.
8. Fermi, E. *Rend. Accad. Naz. Lincei* **1927**, *6*, 602.
9. Hohenberg, P.; Kohn, W. *Phys. Rev.* **1964**, *136*, B864–B871.
10. Kohn, W.; Sham, L. J. *Phys. Rev.* **1965**, *140*, A1133–A1138.
11. Perdew, J. P.; Schmidt, K. *Jacob's Ladder of density functional approximations for the exchange-correlation energy in Density Functional Theory and its Application to Materials* Doren, V. V.; Alsenoy, C. V.; Geerlings, P. eds., AIP-Press: Melville, 2001, 1-20.
12. Perdew, J. P.; Ruzsinszky, A.; Tao, J. J. *J. Chem. Phys.* **2005**, *123*, 62201.
13. Car, R. *Nat. Chem.* **2016**, *8*, 820–821.
14. Bao, J. L.; Gagliardi, L.; Truhlar, D. G. *J. Phys. Chem. Lett.* **2018**, *9*, 2353–2358.
15. Vydrov, O. A.; Scuseria, G. E. *J. Chem. Phys.* **2005**, *122*, 184107.
16. Grimme, S. *Wiley Interdiscip. Rev. Comput. Mol. Sci.* **2011**, *1*, 211–228.
17. a) Lee, C.; Yang, W.; Parr, R. G. *Phys. Rev. B* **1988**, *37*, 785–789; b) Becke, A. D. *J. Chem. Phys.* **1993**, *98*, 5648–5652; c) Kohn, W.; Becke, A. D.; Parr, R. G. *J. Phys. Chem.* **1996**, *100*, 12974–12980.
18. a) Koch, W.; Holthausen, M. C. *Chemist's Guide to Density Functional Theory*; Wiley-VCH Verlag GmbH: Weinheim, FRG, 2001; b) Curtiss, L. A.; Raghavachari, K.;

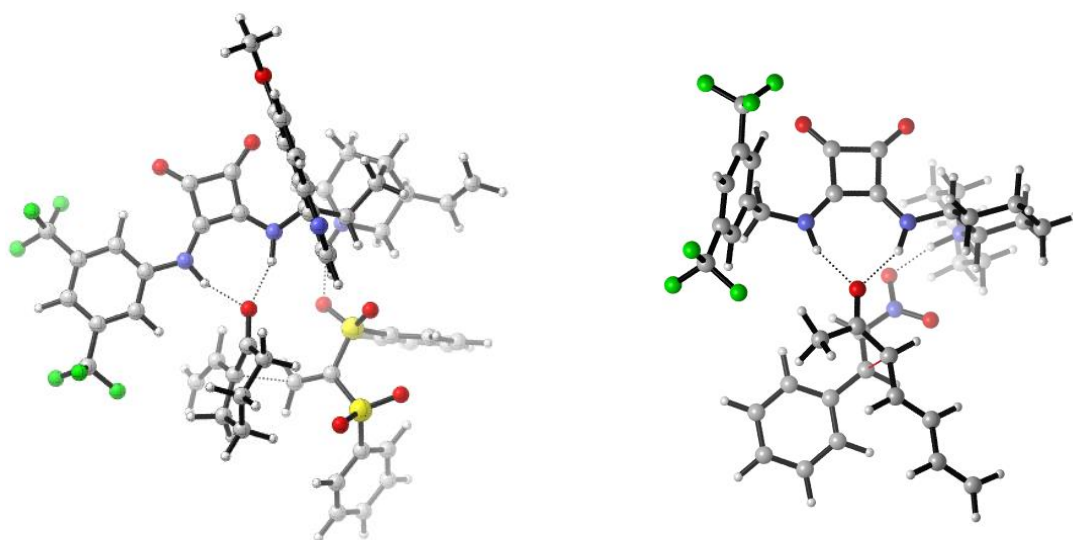
1.3 References

- Redfern, P. C.; Pople, J. A. *J. Chem. Phys.* **1997**, *106*, 1063-1079; c) Curtiss, L. A.; Raghavachari, K.; Redfern, P. C.; Pople, J. A. *J. Chem. Phys.* **2000**, *112*, 7374-7383.
19. Moran, D.; Simmonett, A. C.; Leach, F. E.; Allen, W. D.; Schleyer, P. V. R.; Schaefer, H. F. *J. Am. Chem. Soc.* **2006**, *128*, 9342-9343.
20. Varandas, A. J. C. *J. Phys. Chem. A* **2008**, *112*, 1841-1850.
21. a) Furche, F.; Ahlrichs, R. *J. Chem. Phys.* **2003**, *119*, 12753-12762; b) Weigend, F.; Ahlrichs, R. *Phys. Chem. Chem. Phys.* **2005**, *7*, 3297-3305.
22. a) Varandas, A. J. C. *J. Chem. Phys.* **2007**, *126*, 244105; b) Schwenke, D. W. *J. Chem. Phys.* **2005**, *122*, 014107.
23. Jensen, F. *J. Chem. Phys.* **2001**, *115*, 9113-9125.
24. a) Truhlar, D. G. *J. Chem. Educ.* **2019**, *96*, 1671-1675; b) Young, D. C. *Computational Chemistry: A Practical Guide for Applying Techniques to Real World Problems*; John Wiley & Sons, Inc.: New York, USA, 2001.; c) Morgante, P.; Peverati, R. *ChemRxiv* (Preprint) **2019**, DOI 10.26434/CHEMRXIV.10187756.V1.
25. a) Dolg, M.; Wedig, U.; Stoll, H.; Preuss, H. *J. Chem. Phys.* **1987**, *86*, 866; b) Andrae, D.; Haussermann, U.; Dolg, M.; Stoll, H.; Preuss, H. *Theor. Chim. Acta* **1990**, *77*, 123.
26. a) Hay, J. P.; Wadt, W. R. *J. Chem. Phys.* **1985**, *82*, 270-283; b) Wadt, W. R.; Hay, P. *J. Chem. Phys.* **1985**, *82*, 284-298; c) Hay, P. J.; Wadt, W. R. *J. Chem. Phys.* **1985**, *82*, 299-310.
27. Zhao, Y.; Truhlar, D. G. *Theor. Chem. Acc.* **2008**, *120*, 215-241.
28. Zhao, Y.; Truhlar, D. G. *J. Chem. Phys.* **2006**, *125*, 194101.
29. Zhao, Y.; Truhlar, D. G. *J. Chem. Phys. A* **2006**, *110*, 13126-13130.
30. PhD thesis of Fiser, B. *A Computational Glance at Organometallic Cyclisations and Coupling Reactions*. (UPV/EHU, 2016).
31. Tomasi, J.; Mennucci, B.; Cammi, R. *Chem. Rev.* **2005**, *105*, 2999-3093.
32. Miertus, S.; Scrocco, E.; Tomasi, J. *J. Chem. Phys.* **1981**, *55*, 117.
33. a) Young, D. *Computational Chemistry: A Practical Guide for Applying Techniques to Real World Problems*; John Wiley & Sons, Inc, 2001; b) Tomasi, J.; Persico, M. *Chem. Rev.* **1994**, *94*, 2027; c) Mennucci, B.; Cammi, R. *Continuum Solvation Models in Chemical Physics: From Theory to Applications*; Wiley: Chichester, UK, 2007.
34. a) Weinhold, F.; Landis, C. R.; Glendening, E. D. *Int. Rev. Phys. Chem.* **2016**, *35*, 399-440; b) Cossi, M.; Barone, V.; Cammi, R.; Tomasi, J. *Chem. Phys. Lett.* **1996**, *255*, 327; c) Cancés, E.; Mennucci, B.; Tomasi, J. *J. Chem. Phys.*, **1997**, *107*, 3032-3041; d) Cossi, M.; Barone, V.; Mennucci, B.; Tomasi, J. *Chem. Phys. Lett.*, **1998**, *286*, 253-260; e) Tomasi, J.; Mennucci, B.; Cancès, E. *J. Mol. Struct.: THEOCHEM*, **1999**, *464*, 211-226.
35. Reed, A. E.; Curtiss, L. A.; Weinhold, F. *Chem. Rev.* **1988**, *88*, 899.

36. Weinhold, F. J. *Comput. Chem.* **2012**, *33*, 2363–2379.
37. Cramer, K. *Essentials of Computational Chemistry - Theories and Models*; John Wiley & Sons Ltd: Chichester, England, 2004.
38. Parr, R. G.; Yang, W. *J. Am. Chem. Soc.* **1984**, *106*, 4049–4050.
39. Barroso, J. *How to calculate Fukui indices*; 2010. Available at: <https://joaquinbarroso.com/2010/07/26/how-to-calculate-fukui-indices/>.
40. Li, Y.; Evans, J. N. S. *J. Am. Chem. Soc.* **1995**, *117*, 7756–7759.
41. NBO Version 3.1, E. D. Glendening, A. E. Reed, J. E. Carpenter, and F. Weinhold.
42. Gaussian 16, Revision A.03, Frisch, M. J.; Trucks, G. W.; Schlegel, H. B.; Scuseria, G. E.; Robb, M. A.; Cheeseman, J. R.; Scalmani, G.; Barone, V.; Petersson, G. A.; Nakatsuji, H.; Li, X.; Caricato, M.; Marenich, A. V.; Bloino, J.; Janesko, B. G.; Gomperts, R.; Mennucci, B.; Hratchian, H. P.; Ortiz, J. V.; Izmaylov, A. F.; Sonnenberg, J. L.; Williams-Young, D.; Ding, F.; Lipparini, F.; Egidi, F.; Goings, J.; Peng, B.; Petrone, A.; Henderson, T.; Ranasinghe, D.; Zakrzewski, V. G.; Gao, J.; Rega, N.; Zheng, G.; Liang, W.; Hada, M.; Ehara, M.; Toyota, K.; Fukuda, R.; Hasegawa, J.; Ishida, M.; Nakajima, T.; Honda, Y.; Kitao, O.; Nakai, H.; Vreven, T.; Throssell, K.; Montgomery, J. A., Jr.; Peralta, J. E.; Ogliaro, F.; Bearpark, M. J.; Heyd, J. J.; Brothers, E. N.; Kudin, K. N.; Staroverov, V. N.; Keith, T. A.; Kobayashi, R.; Normand, J.; Raghavachari, K.; Rendell, A. P.; Burant, J. C.; Iyengar, S. S.; Tomasi, J.; Cossi, M.; Millam, J. M.; Klene, M.; Adamo, C.; Cammi, R.; Ochterski, J. W.; Martin, R. L.; Morokuma, K.; Farkas, O.; Foresman, J. B.; Fox, D. J. Gaussian, Inc., Wallingford CT, 2016.

Chapter 2

Asymmetric catalysis



In this chapter, we have studied the action of bifunctional squaramide/tertiary amine catalysts that introduce chirality into the reaction environment. A comprehensive computational study was conducted in view of the experimental results obtained in the group of Prof. Claudio Palomo at the Universidad del País Vasco. They employed bifunctional organocatalysts to develop highly site-, regio- and stereoselective methodologies. We studied the reaction mechanisms focusing on electronic properties of the substrates, selectivity aspects and interactions between the catalyst and the substrates from a computational point of view.

Based on:

Urruzuno, I.; Mugica, O.; Zanella, G.; Vera, S.; Gómez-Bengoia, E.; Oiarbide, M.; Palomo, C. *Chem. Eur. J.* **2019**, *25*, 9701-9709.

Olaizola, O.; Iriarte, I.; Zanella, G.; Vera, S.; Gómez-Bengoia, E.; Oiarbide, M.; Palomo, C. *Angew. Chem. Int. Ed.* **2019**, *58*, 14250-14254.

This chapter includes two projects based on two collaborations carried out with an experimental group. The experimental part was performed by the group of Prof. Claudio Palomo at the Universidad del País Vasco. The contribution of the author of this thesis is exclusively computational and is presented in the *computational work* sections. A general introduction about asymmetric organocatalysis is initially provided. Then, for each project, the nature of the chemistry, the aim of the work, experimental and computational procedures and results are described.

2.1 Introduction

2.1.1 Asymmetric organocatalysis

Enantiomeric pure compounds are highly required in numerous fields, as pharmaceutical and biological areas, in electronic and optical devices and in polymers,¹ making asymmetric catalysis a prominent area of investigation.

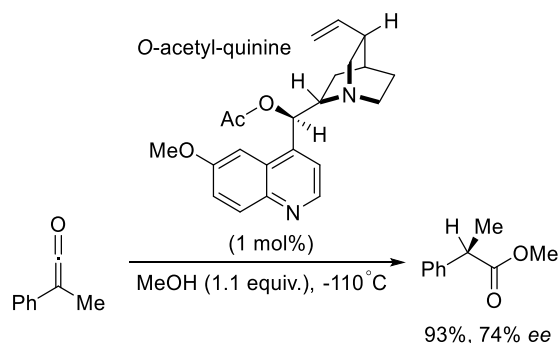
Together with transition metal catalysis and enzymatic transformations, asymmetric organocatalysis is one of the approaches used for the enantioselective synthesis of organic compounds. Organocatalysts are defined as purely low-molecular-weight organic molecules that show catalytic activity themselves.²

In the last decades, the several advantages of this metal-free approach compared to the other two catalytic areas have attracted the interest of many research groups.

First, organocatalytic methods are preferred for the preparation of those compounds that do not tolerate metal contamination, as pharmaceutical products.³ Then, it is noteworthy that organocatalysts are usually robust, inexpensive, non-toxic, often commercially available or anyway easy to synthesise. They tolerate many functional groups and allow to avoid time-consuming manipulations (protection, deprotection, ...). They can be incorporated onto a support and in this way easily recovered and recycled. Finally, they are inert to moisture and oxygen, allowing to perform reactions in mild conditions.

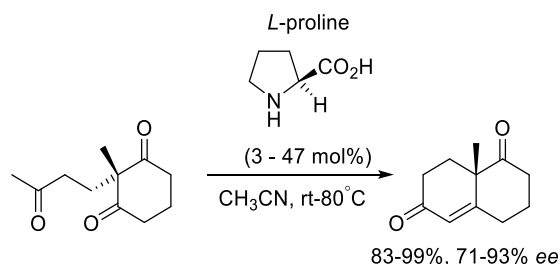
This kind of catalysis was born from the interest of employing low-molecular-weight compounds in the understanding and mimicking the catalytic activity and selectivity of enzymes. Although the name “organocatalysis” was coined only in 2000 by MacMillan,⁴ the first example of metal free enantioselective catalysis was reported in 1912 by Bredig and Fiske.⁵ They described the addition of HCN to aldehydes catalysed by natural cinchona alkaloids, which yielded the resulting cyanohydrins with *ee* <10%. Some years later, in 1960, Pracejus and co-workers succeeded to get higher *ee* up to 74% using alkaloids as catalysts in the addition of methanol to phenylmethylketene (Scheme 2.1).^{6,7}

2.1 Introduction



Scheme 2.1 Alkaloid-catalysed addition of methanol to a prochiral ketene by Pracejus *et al.*^{6,7}

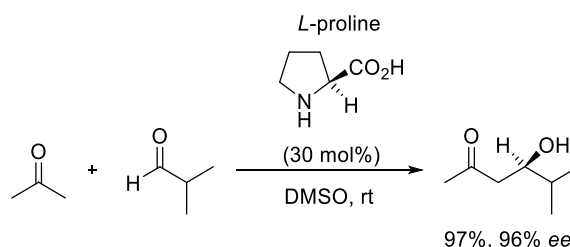
In the 1970s, the Hajos-Parrish-Eder-Sauer-Wiechert reaction was discovered and became a milestone of the asymmetric organocatalysis. It employed proline as catalyst in the intramolecular asymmetric aldol cyclodehydration to get the unsaturated Wieland-Miescher ketone, important intermediate for the synthesis of steroids and other enantiomerically pure molecules (Scheme 2.2).^{8,9}



Scheme 2.2 The Hajos-Parrish-Eder-Sauer-Wiechert reaction.^{8,9}

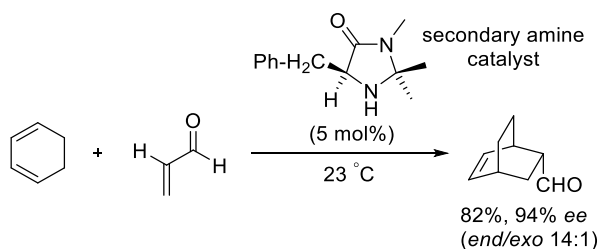
Until 2000, the field remained quite unexplored, only a few examples of satisfactory *ee* asymmetric catalysis were reported. From that year, the work of scientists as List and MacMillan triggered the exponential growth of the asymmetric catalysis field.

List focused on the study of the catalytic potential of proline in asymmetric intermolecular aldol reactions.^{10,11} His group found out that acetone can react with numerous aldehydes to give the corresponding aldols in good up to excellent yield with high enantioselectivities (*ee* up to 96%) (Scheme 2.3).



Scheme 2.3 Proline-catalysed intermolecular aldol reaction by List *et al.*^{10,11}

Simultaneously, MacMillan group reported an asymmetric Diels-Alder reaction of α,β -unsaturated aldehydes that was catalysed by a phenylalanine-derived secondary amine, giving the products in enantiomeric purity up to 94% (Scheme 2.4).⁴

Scheme 2.4 Secondary amine-catalysed Diels-Alder reaction by MacMillan *et al.*⁴

Nowadays, asymmetric organocatalysis has been deeply explored and applied to numerous transformations providing high enantioselectivity, i.e. iminium-, enamine- and phosphoramidate- catalysed cycloadditions, Michael additions, aldol reactions, nucleophilic substitutions, chiral ureas and thioureas catalysed addition of nucleophiles to aldehydes and imines.

The presence of the organocatalyst causes the formation of an asymmetric environment that is determinant for the introduction of the chirality into the product. The catalyst can activate the nucleophile or the electrophile or both in case of bifunctional catalysis. Depending on its structure, it is possible to define two “modes of action”, the covalent and the non-covalent one. The former works through the formation of covalent bonds between the catalyst and the substrate, increasing the interaction between the substrate and the reagent in the reaction (aminocatalysts and carbenes belong to this category). The non-covalent mode is based on the activation of the substrate *via* hydrogen bonds (thioureas, squaramides and phosphoric acids) or ionic interactions (chiral bases as cinchona alkaloids and phase-transfer catalysis) (Figure 2.1).

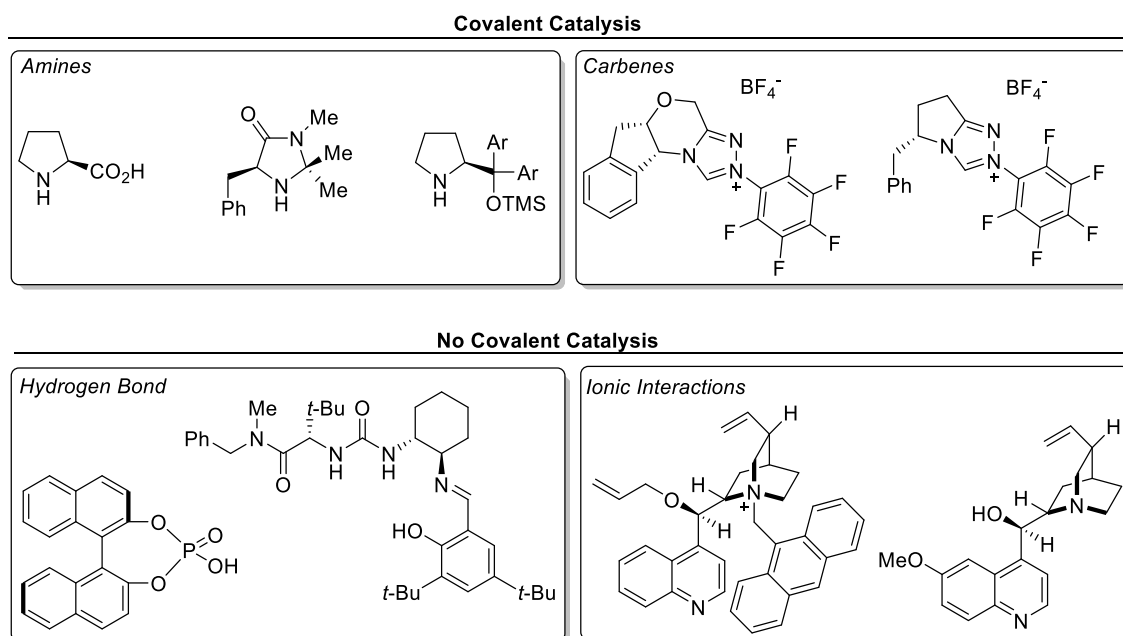


Figure 2.1 Activation modes in organocatalysis.

The field of asymmetric organocatalysis started with the research on aminocatalysts¹² and carbenes¹³ working through covalent interactions with the substrates, before many other small molecules started to play an important role.¹⁴ The covalent catalysis remains

nowadays an efficient tool for the asymmetric synthesis of natural compounds but, inspired by enzymes and catalysed natural processes, the main focus has shifted towards catalytic processes that employ small organic molecules able of binding and activating substrates *via* non-covalent interactions.

Non-covalent interactions include hydrogen bonds, electrostatic interactions, π - π , cation- π , hydrophobic and Van der Waals forces. They all have some common features even if in a different degree: they are weaker than covalent bonds, less directional and less distance dependent and more entropy dependent. Due to their “flexibility”, structural reorganisations can occur without energetically changing largely the binding interactions. It could appear counterintuitive that this kind of interactions can afford the conformational constraint required for high stereoselection, unless a cooperative model takes place. Indeed, if multiple noncovalent interactions operate in concert, it is possible to obtain high levels of stereoselectivity in the reaction.¹⁵ The network of interactions allows to locate accurately the substrates in space.

In the past 20 years hydrogen-bond promoted asymmetric organocatalysis has been deeply explored and many works related to this topic have been reported.^{16,17} The catalysts contain H-bond donor (as thiourea, squaramide, acylamide units) and H-bond acceptor (as tertiary amino groups) structural fragments. Among all the catalysts developed, those based on chiral ureas, thioureas, diols, phosphoric acid cores and then squaramides dominated the field of hydrogen bonding.

In this chapter, all the concepts mentioned so far are going to be examined in depth focusing on the asymmetric α -functionalisation of ketones.

2.1.2 α -functionalisation of carbonyl compounds

Many natural products and biologically active compounds contain carbonyl groups with an adjacent stereocentre (Figure 2.2)¹⁸ and new methods for accessing these moieties in high selectivity are in continuous development.

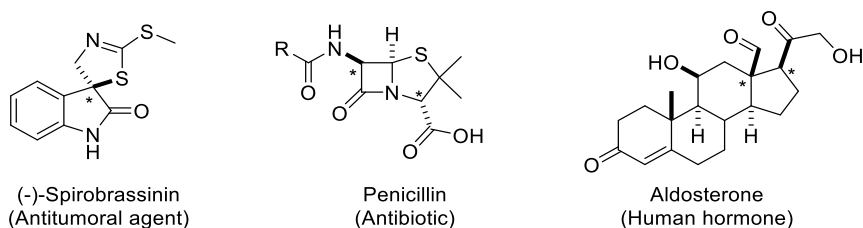
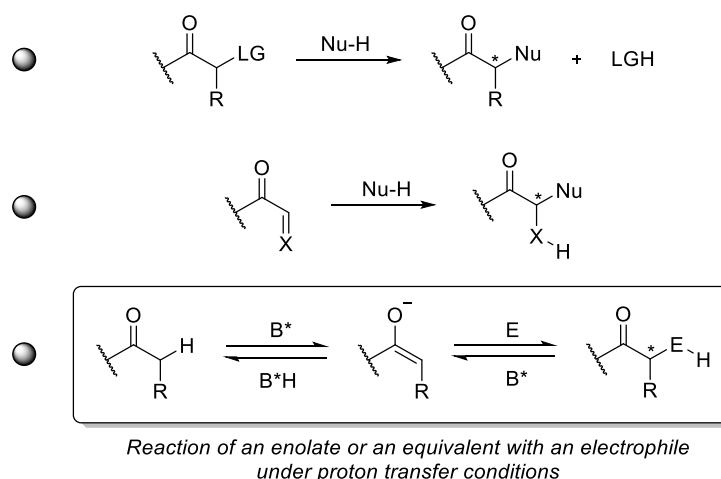


Figure 2.2 Some examples of biologically active compounds and natural products containing carbonyl groups with an adjacent stereocentre.

There are three main approaches for the stereoselective formation of stereogenic centres in the α -position of a carbonyl compound (Scheme 2.5) and in this thesis only the third one, the reaction of an enolate or its equivalent with an electrophile under proton transfer conditions is addressed.



Scheme 2.5 Approches for the stereoselective formation of stereogenic centres at the α -position of a carbonyl compound.

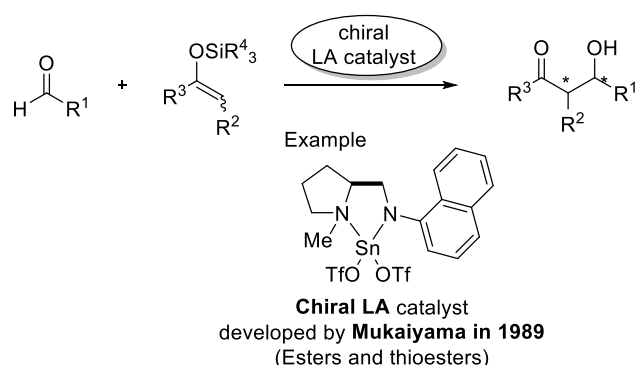
This strategy is quite versatile because enolates can be generated through different procedures and have high nucleophilic character, thus they react with a wide range of electrophiles. Moreover, if the nucleophile and electrophile are prostereogenic, the product ends up containing two contiguous stereocentres.¹⁹

The stereoselective control at the α -stereocentre can be performed through two approaches, using covalently bound chiral auxiliaries or catalytic methods.

Chiral auxiliaries transfer the chiral information bonding covalently to the substrate, they are very effective but need to be used in stoichiometric amounts and require additional steps for the attachment to and detachment from the substrate.

In terms of atom economy, the catalytic methods are more convenient and guarantee high chemo-, regio-, and stereoselectivity even using substoichiometric amounts of chiral promoter.

Inside the field of catalysis, we can distinguish two methods, the directed and the direct. The directed approach consists in the employment of preformed enolates in combination with a chiral Lewis acid catalyst, a representative example is the Mukaiyama aldol reaction (Scheme 2.6).²⁰



Scheme 2.6 Mukaiyama aldol reaction.

This method gives high stereocontrol but requires the previous preparation of the enolate through a stoichiometric synthetic procedure.

On the other hand, the direct methods appear to be more practical and attractive; they consist in the use of a substoichiometric chiral inductor in the reaction of unmodified carbonyl compounds with an electrophile.

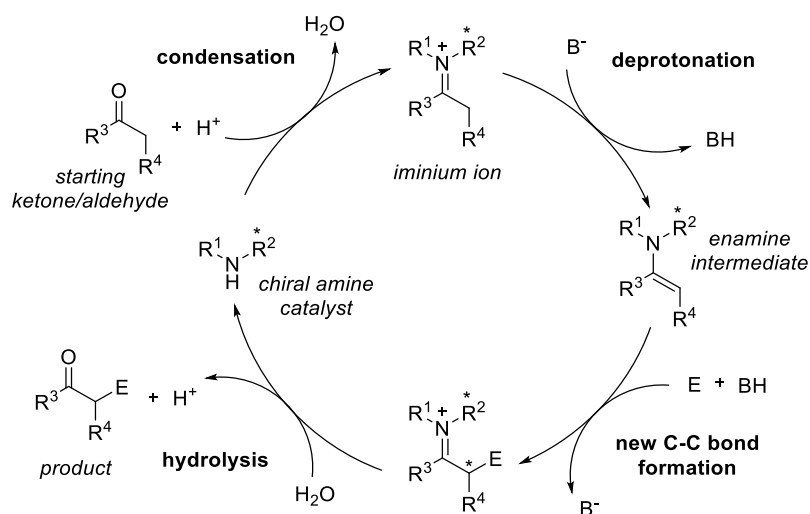
The chiral inductor can be a metal-based catalyst²¹ or an organocatalyst.

Considering that metal based methods rely on the use of toxic metals of limited availability and most of the times require inert conditions, the chapter focuses on organocatalysed α -functionalisation of carbonyl compounds.

There are two ways to activate the enolisable carbonyl substrate: *via* enamine formation (covalent aminocatalysis) or *via* enolisation (H-bond Brønsted base catalysis).

2.1.2.1 Organocatalysed α -functionalisation of carbonyl compounds via enamine formation

The main concept of aminocatalysis is the formation of an enamine intermediate through the condensation of a ketone or an aldehyde with a chiral primary or secondary amine catalyst. The formation of the enamine intermediate by deprotonation of the iminium ion is the rate-determining step and it is helped by protic additives and polar solvents in speeding up the deprotonation and stabilising the charges. Enamines have enhanced nucleophilicity and react with many electrophiles, forming new C-C bonds enantioselectively. Then, to collect the α -substituted carbonyl compound and recover the catalyst for the next cycle, the adduct is subjected to acid hydrolysis (Scheme 2.7).²²



Scheme 2.7 Catalytic cycle for enamine mediated processes.²²

The stereochemistry of the newly formed α -substituted carbonyl compounds can be explained through two different models (Figure 2.3). In the H-bond mediated model, the H-bond donor group of the catalyst addresses the electrophile to one of the two diastereotopic faces of the enamine, while in the steric-controlled model the bulky substituents of the catalyst shield one face forcing the electrophile to interact with the enamine from the opposite side.

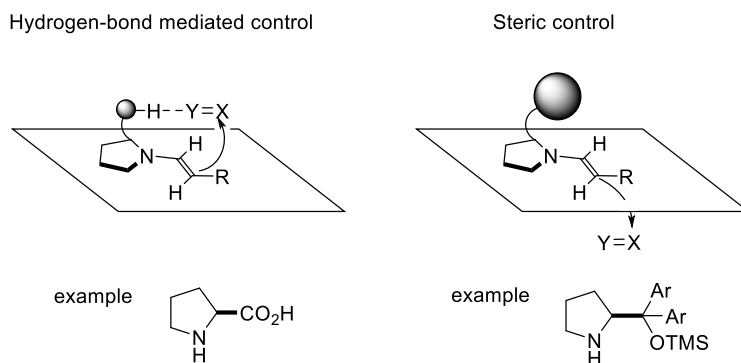
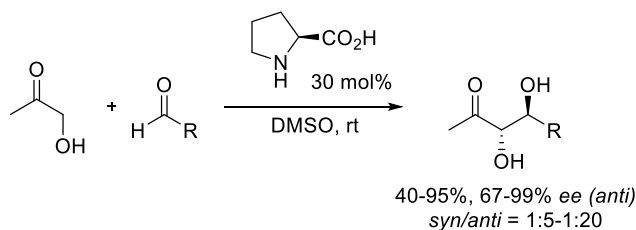


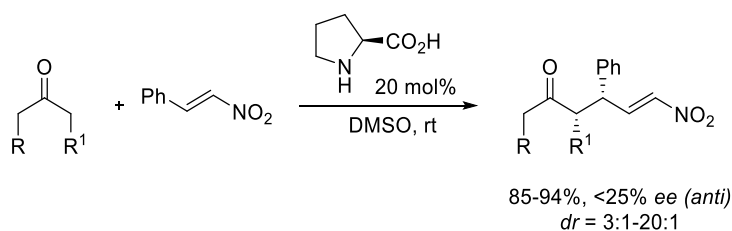
Figure 2.3 Two models to control the stereochemistry of newly formed α -substituted carbonyl compounds

Proline was the first amine involved in an enamine mediated organocatalysed transformation. In 2000, List and Barbas reported an asymmetric intermolecular aldol reaction in presence of proline as catalyst and launched the new field of aminocatalysis (Scheme 2.3).¹¹ Proline resulted to be a useful molecule to generate carbonyl compounds with α -stereogenic centres, as demonstrated by the enamine mediated aldol reaction developed by Notz and List (Scheme 2.8).²³ They used α -hydroxyacetone as donor compound and aromatic or α -branched aldehydes as acceptor components and obtained anti-aldol products with excellent enantioselectivity, even if with variable yields and diastereoselectivities.



Scheme 2.8 Proline-catalysed aldol reaction by Notz and List.²³

In 2001, List reported the first proline-catalysed Michael reaction yielding products with stereogenic centre in C_{α} even if with low levels of enantioselectivity (Scheme 2.9).²⁴



Scheme 2.9 Proline-catalysed Michael reaction by List *et al.*²⁴

During the years, proline-catalysed asymmetric transformations of ketones and aldehydes have been largely investigated and many valid procedure were disclosed.²⁵ Inspired by proline potential, new and more efficient catalysts were developed modifying its structure; for instance, the substitution of the carboxylic acid moiety with other functional group led to catalysts with better solubility in organic solvents, improved reactivity and stereocontrol (Figure 2.4).²⁶

2.1 Introduction

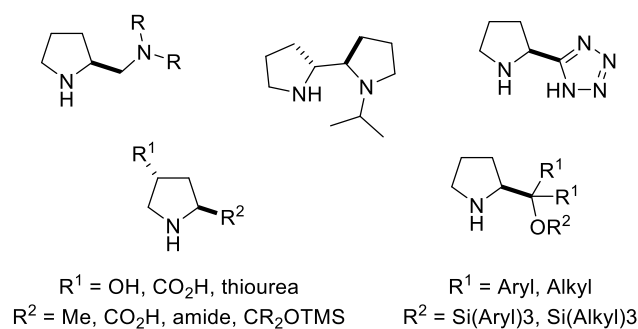
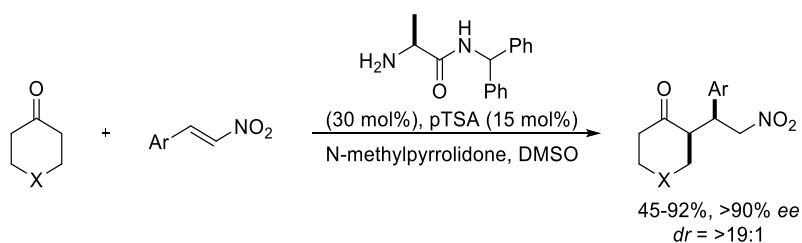


Figure 2.4 Proline-based catalysts.

Even though secondary enamines are known to be better stabilised than their primary counterparts, also chiral primary amine-base organocatalysis was found to be successful, mainly in asymmetric reactions involving ketones as donors.²⁷ In 2006, Córdova *et al.* used a primary amine catalyst derived from L-alanine to perform the Michael addition of cyclic ketones to aromatic nitroalkenes (Scheme 2.10).²⁸

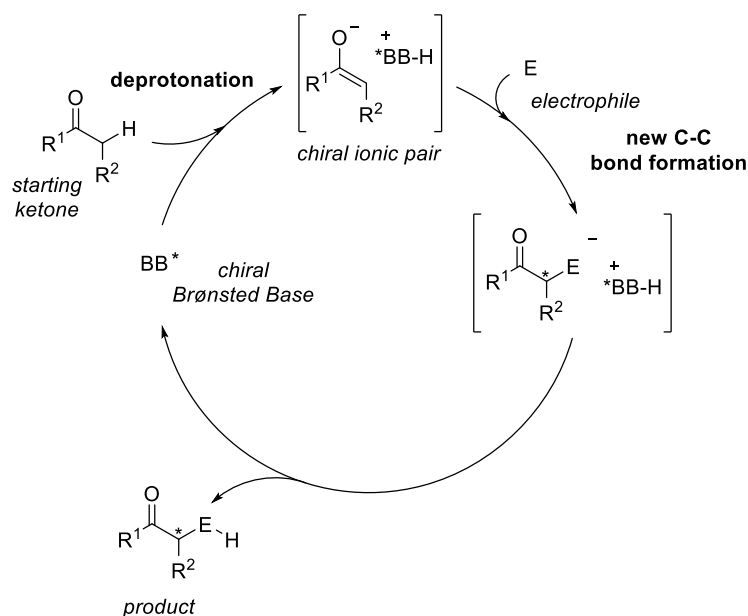


Scheme 2.10 Primary amine-catalysed Michael addition by Córdova *et al.*²⁸

The enamine mediated asymmetric organocatalysis revealed to be an efficient strategy for the α -functionalisation of carbonyl compounds and numerous examples have been reported in the literature. Nevertheless, many limitations regarding substrate scope, regio- and stereocontrol are still present. Indeed, the procedures reported so far involve only aldehydes and symmetric ketones as donors. Sterically hindered ketones show low tendency to form enamines and still remain challenging substrates, together with unsymmetrical ketones that are problematic due to the difficult regiocontrol.

2.1.2.2 Organocatalysed α -functionalisation of carbonyl compounds via enolisation

Carbonyl compounds can be activated through α -deprotonation by action of a base to give the corresponding enolate. The favourite substrates for Brønsted base catalysis are enolisable carbonyl compounds with relatively small pK_a values (10-17).²⁹ A general catalytic cycle for Brønsted Base catalysed reactions is shown in Scheme 2.11. The process starts with the deprotonation of the pronucleophile by the basic catalyst forming a chiral ionic pair, key step for the non covalent chirality transfer; next, the enolate reacts with an electrophile in an enantioselective manner allowing the regeneration of the free base that can re-enter in the catalytic cycle.



Scheme 2.11 General catalytic cycle for Brønsted Base-catalysed reactions.

Due to the nondirectional nature of electrostatic interactions in ion-pairs, it looks convenient to combine the chiral basic scaffold with an H-bond donor unit in a unique catalyst capable of anchoring nucleophile and electrophile in the transition state. This kind of catalysts is called *bifunctional Brønsted base/H-bond donor catalysts* and demonstrates to be more active because of the higher degree of stereochemical order achieved (Figure 2.5). The H-bond unit is essential to keep in place a substrate, while the chiral scaffold activates and directs the reaction partner in the proximity for the reaction. The chiral pocket that is formed induces the enantioselectivity.

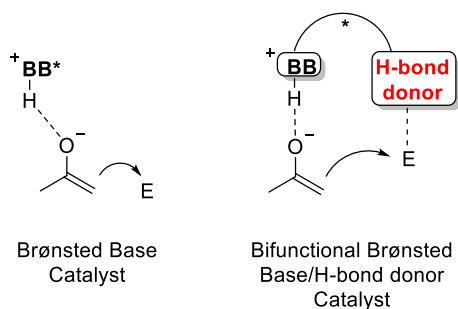


Figure 2.5 Transition states in Brønsted base catalysis and bifunctional Brønsted base/H-bond donor catalysis.

Tertiary amines, guanidines, amidines and imidazoles are the most common groups that constitute the BB moiety. The first examples of bifunctional BB catalysts applied to the α -functionalisation of easily enolisable carbonyl compounds were cinchona alkaloids derivatives (Figure 2.6).³⁰

2.1 Introduction

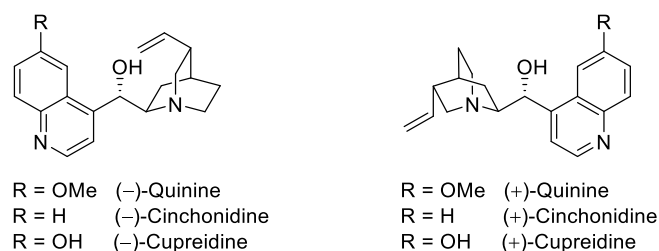


Figure 2.6 Cinchona alkaloids derivatives.

Further improvements in the design of bifunctional BB catalysts were obtained employing readily available chiral amines and efficient H-bond donor groups, such as urea, thiourea, sulphonamide or squaramide (Figure 2.7).

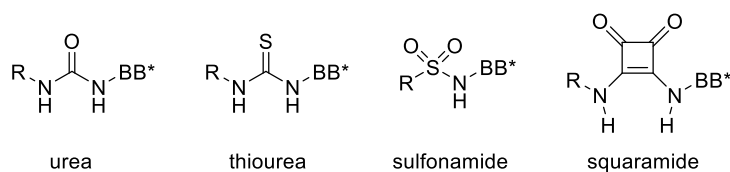
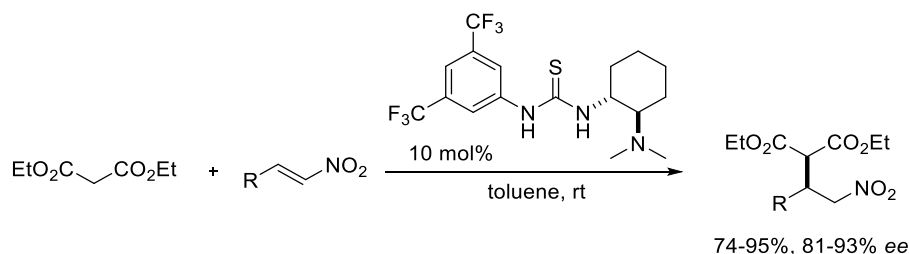


Figure 2.7 Examples of H-bond donor groups.

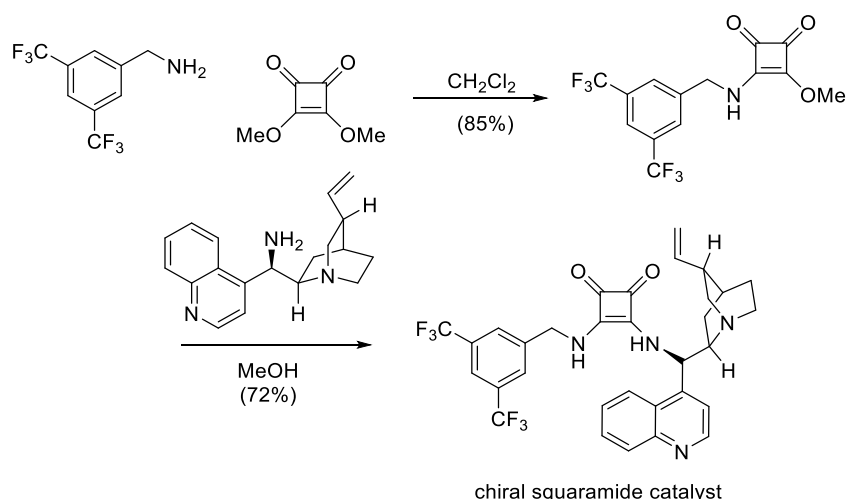
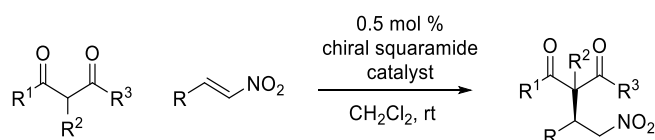
In 2003, Takemoto *et al.* reported the first chiral thiourea-tertiary amine bifunctional catalyst applied in the Michael reaction of malonates to nitroalkenes yielding high levels of enantioselectivity (Scheme 2.12).³¹ For this reaction, also the urea/thiourea-substituted cinchona alkaloids catalysts developed by Connon³² and Dixon³³ showed good performance. In the following years, this type of bifunctional catalysts has been employed in the α -functionalisation of some carbonyl compounds.



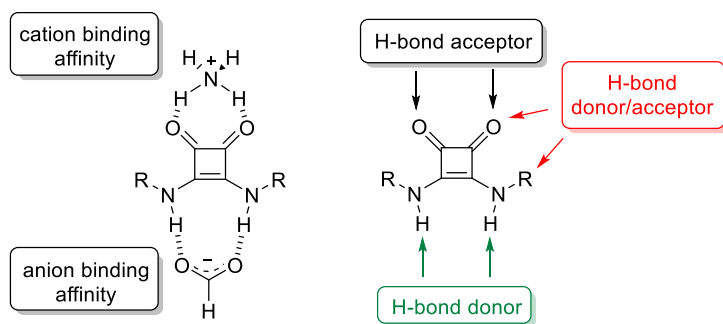
Scheme 2.12 Thiourea-tertiary amine bifunctional catalysed Michael reaction of malonates to nitroalkenes by Takemoto *et al.*³¹

Encouraged by the great advances achieved with thiourea compounds,³⁴ Rawal group reported in 2008 “a new family of H-bond catalysts based on the squaramide catalophore”.³⁵ Their work described the synthesis (Scheme 2.13) of a suitable chiral squaramide derived from cinchona alkaloids and its application as H-bond donor catalyst in the catalysed conjugate addition of 1,3-dicarbonyl compounds to nitroalkenes with excellent yields and enantioselectivity (Scheme 2.14).

The use of squaramides instead of thioureas results to be superior in terms of activity and requires low catalyst loads (as low as 0.1 mol%). The faster turnover is a result of the greater spacing between N-H groups enhancing the fitting of the reagent, together with the rigidity of the binding unit, N-H acidity and directional H-bonds.

Scheme 2.13 Synthesis of a chiral squaramide catalyst by Rawal *et al.*³⁵Scheme 2.14 Squaramide catalyzed conjugate addition of 1,3-dicarbonyl compounds to nitroalkenes by Rawal *et al.*³⁵

Originally, squaramides were exclusively used as artificial anion receptors in molecular recognition but nowadays they play an important role in the field of asymmetric catalysis^{36–39} as bifunctional hydrogen-bond catalysts in many important enantioselective organic reactions.^{35,40–45} Their action mode is very similar to thioureas, but they bear some unique skills that differ from thioureas and make them so attractive. The first difference is the duality in ion- and H-bonding. Squaramides show not only anion-binding affinity, as thioureas, but also cation-binding affinity due to the “increase of the aromatic character” in the four-membered ring upon complexation,⁴⁶ participating in ditopic binding. Concerning the H-bond network, squaramides bear three hydrogen-bond patterns: one constituted of two hydrogen-bond donors (N-H), the second of two acceptors (C=O) and the third of one donor and one acceptor. The duality offers more possibilities in binding and allows to develop a broader substrate scope (Figure 2.8).

Figure 2.8 Duality in ditopic- and hydrogen-bonding of squaramides.³⁶

The second difference concerns the rigidity. Squaramides have a rigid planar square-shaped structure: they are constituted of a cyclobutenedione ring containing two coplanar carbonyls and two N-H that are almost coplanar. This arrangement is stabilised by the nitrogens that are essentially sp^2 -hybridised, making the lone pairs available for conjugation from N(p-orbital) into the π -system orthogonal to the plane, thus restricting the rotation of C-N bonds (Figure 2.9).³⁹ The higher delocalisation of N lone pair through the cyclobutenedione system makes the squaramide system more rigid than thioureas. As a consequence of its vinylogous amide nature, the N-H acidity of a squaramide is higher as compared to that of an urea/thiourea (0.1-2 pKa gap units)⁴⁷ providing a polarised nitrogen moiety. Different rigidity and acidity of squaramides account for unique binding properties and higher reactivity, enhancing the catalytic activity.

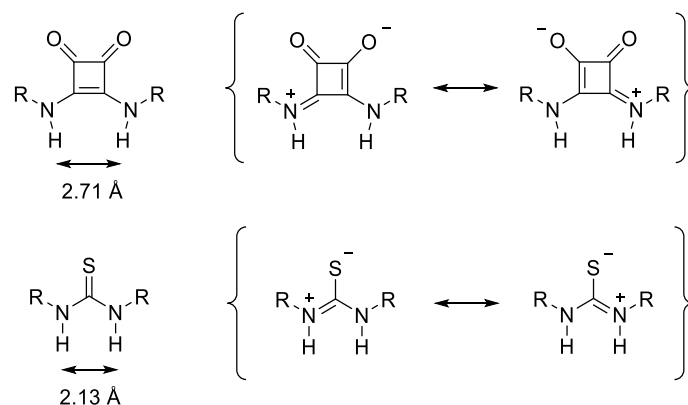


Figure 2.9 Structural differences between squaramides and thioureas.

Squaramide moiety has been found to form stronger hydrogen bonds with the substrates bearing nitro, carbonyl, imino, nitrile groups (complexes 1-2 orders of magnitude more stable) (Figure 2.10).

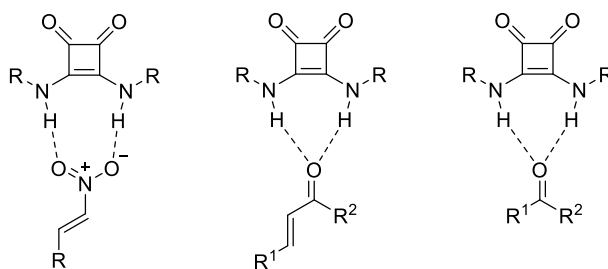


Figure 2.10 Activation of different substrates by squaramides.

The following difference is structural and deals with the relative distance and spacing between the N-H groups. From the calculations of Takemoto⁴⁸ and Rawal³⁵ groups, in *N,N'*-dimethylthiourea (one-carbon link) the two H atoms are positioned 2.13 Å apart, increasing in *N,N'*-dimethylsquaramide to 2.73 Å. Moreover, the cyclobutenedione scaffold of squaramides induces a convergent orientation of the N-H groups giving different specific binding properties, influencing the stereocontrol (Figure 2.9 and 2.11).

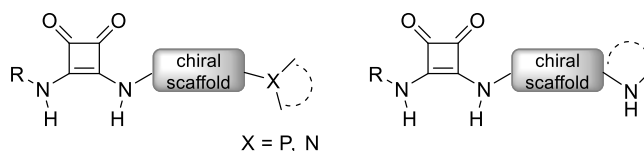


Figure 2.11 General structures of squaramide asymmetric organocatalysts.

Eventually, an additional advantage of this kind of catalysts lies in the simple and modular preparation that offers the possibility of synthesising a large range of catalysts (as shown in Scheme 2.13). It is a two steps synthesis from easily available starting materials involving a first substitution reaction of dimethyl squarate, followed by another substitution reaction with a chiral primary amine.

After the pioneering work of Rawal, many new squaramide catalysts were developed and applied in different reactions.^{36,37} They were proven to be efficient in many domino and tandem processes allowing the synthesis of complex molecules.³⁸

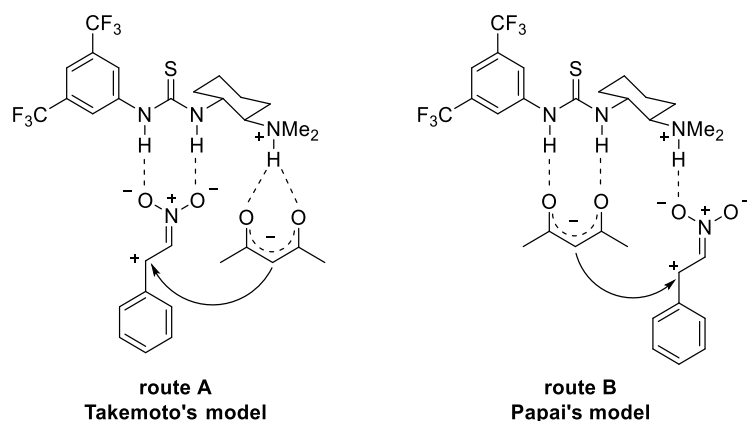
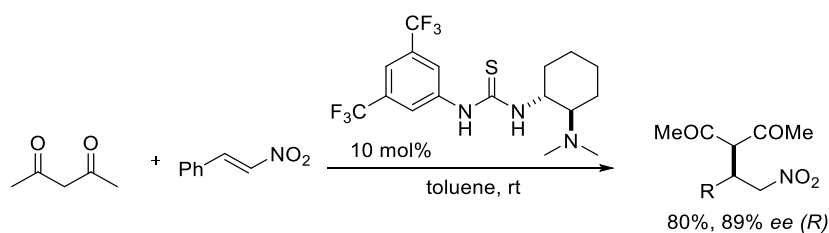
BB catalysis works for the α -functionalisation of many enolisable carbonyl compounds, but it has many limitations. In particular, it is restricted to reactions involving easily enolisable nucleophiles typically bearing an EWG at the α -position. Indeed, to ensure a reversible proton transfer compatible with the BB catalytic cycle, weak bases must be used (pK_a values of conjugated acid: 9-14) and the presence of an EWG group at the α -carbon makes the pronucleophile acidic enough to be enolised. Ketones may present two flanks for enolisation and so two reactive sites; for this reason, symmetrical ketones or ketones with an EWG are employed. In the case of conjugated dienolates, the regioselectivity represents another challenging issue, as the γ -position is the preferred one.

2.1.3 Action mechanisms of bifunctional catalysts

Bifunctional catalysts are known to be very efficient due to their ability of activating simultaneously both nucleophile and electrophile.

Takemoto group was the first to propose a reaction mechanism for the thiourea-catalysed Michael reaction they developed (Scheme 2.12).³¹ After deprotonation of the acidic proton of the 1,3-carbonyl by the tertiary amine group, the nitroolefin is activated by the thiourea scaffold through two hydrogen bonds (it is known that nitrocompounds are keen to form H-bonds with urea and thiourea)⁴⁹ and then the two substrates can react *via* the formation of a ternary H-bonded complex giving the product in the only R configuration (Scheme 2.15, route A).

Taking into account that both the nitroolefin and the enol can form two hydrogen bonds with the thiourea moiety of the catalyst, Pápai and co-workers decided to carry out a theoretical analysis on the Takemoto reaction to understand the catalyst's structure-activity relationship, how the catalyst interacts with the substrates and influences the formation of the new C-C bond. They came out with another model that differs from Takemoto's one for the activation mode of the nitroolefin.⁵⁰ Indeed, the electrophile is activated through the interaction with the protonated amino group of the catalyst, while the thiourea, as an efficient anion receptor, interacts with the deprotonated nucleophile (Scheme 2.15, route B).

Scheme 2.15 Two alternative reaction routes for the Michael addition catalysed by bifunctional catalyst.⁵¹

Scheme 2.16 Takemoto reaction (as in Scheme 2.12) considered in the theoretical analysis by Pápai.

For their analysis, they took in consideration the reaction in Scheme 2.16. Firstly, they computed the two possible complexes, the one with the thiourea coordinated to the nitroolefin and the other with the thiourea coordinated to the enolate (Figure 2.12). They demonstrated that there is not preference for the formation of one or the other adduct, as the difference in binding energy is only 0.3 kcal/mol (thiourea/nitroolefin 7.6 kcal/mol and thiourea/enolate 7.3 kcal/mol).

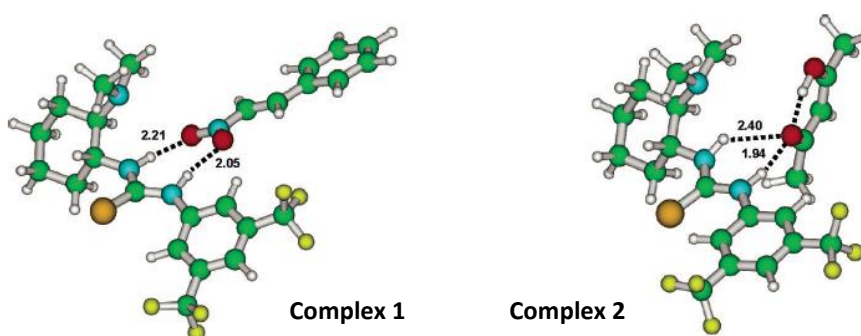


Figure 2.12 Optimised structures of the most stable catalyst-substrate adducts. H-Bond distances in angstroms.

Then, starting from **complex 2**, they computed and demonstrated that a proton transfer from the coordinated enol to the amine group of the catalyst can easily occur, as the energy barrier for the process is relatively low, 6.6 kcal/mol, and the resulting ion pair (**2'**) is predicted to be only 2.2 kcal/mol less stable than **2** (Figure 2.13). The enolate anion in complex **2'** is stabilised by N–H···O bonds involving the protonated amine moiety and one of the N–H groups of the thiourea. Another form of the ion pair is complex **2''**, the enolate is tilted from its original position to maximise the number of N–

H \cdots O bonds and all three N–H units take part in the H-bond. This intermediate is predicted to be 2.0 kcal/mol less stable than **2'** (Figure 2.13).

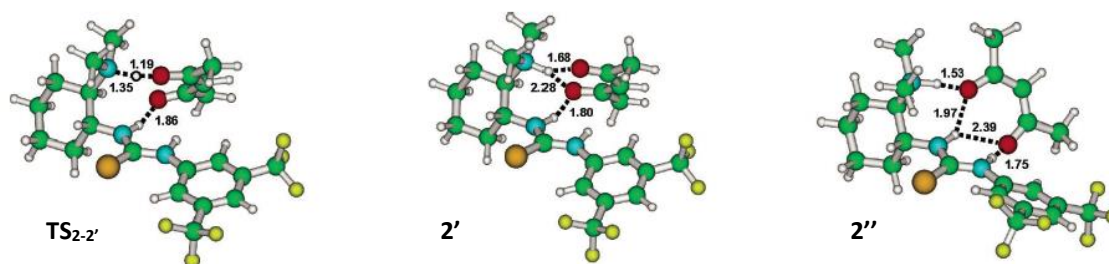


Figure 2.13 Optimised structures of stationary points located for the protonation process between catalyst and nucleophile

It is interesting to compare the two energetic profiles of the Michael reaction (Figure 2.16): in both pathways, the C–C bond formation is the rate determining step and at first sight the difference of the two energy barriers could be determinant for the election of the mechanistic pathway. Takemoto's route (A in red) has an activation energy of 11.6 kcal/mol and Pápai's route (B in blue) of 11.8 kcal/mol (calculated as difference between the TSs and the intermediates **3** and **5** respectively). Actually, since the steps that precede the C–C bond formation are kinetically mobile and thermodynamically reversible, the preference of one pathway to the other is determined by the relative energies of the two transition states **TS**₃₋₄ and **TS**₅₋₆.

As a consequence, the Pápai's route results to be the predominant one for this reaction because its TS is more stable of 2.7 kcal/mol than Takemoto's one (difference in energy between **TS**₃₋₄ and **TS**₅₋₆).

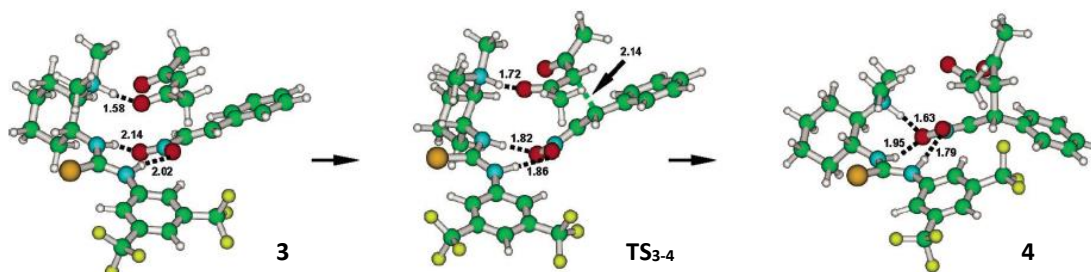


Figure 2.14 Optimised structures and selected geometric parameters of the stationary points located on route A.

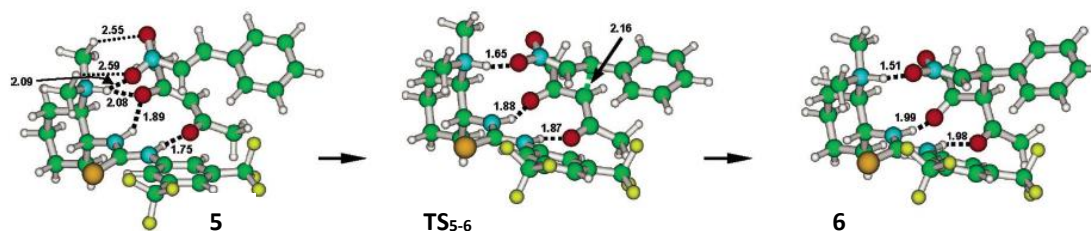


Figure 2.15 Optimised structures and selected geometric parameters of the stationary points located on route B.

2.1 Introduction

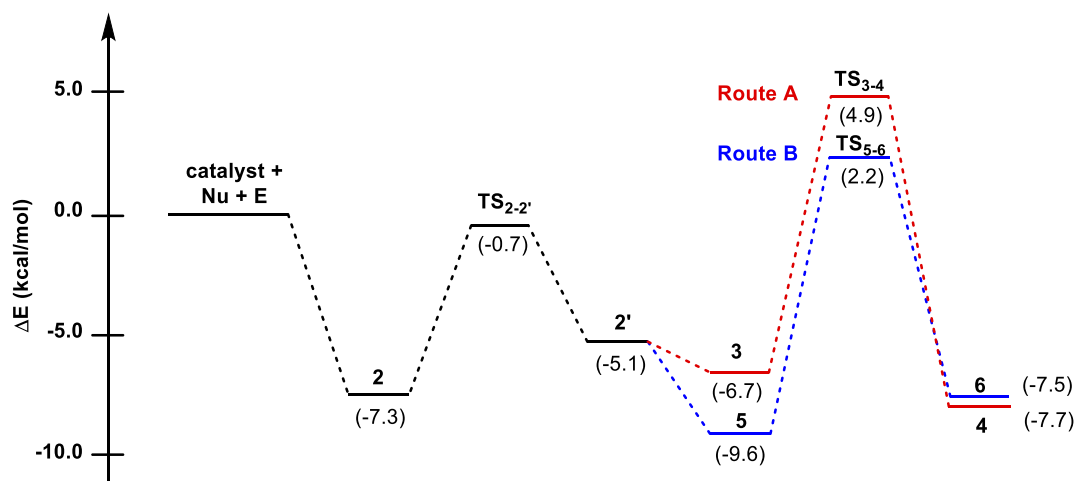


Figure 2.16 Energy profile of the C-C bond formation pathways corresponding to the formation of the (*R*) configuration of products as obtained from gas-phase calculations.

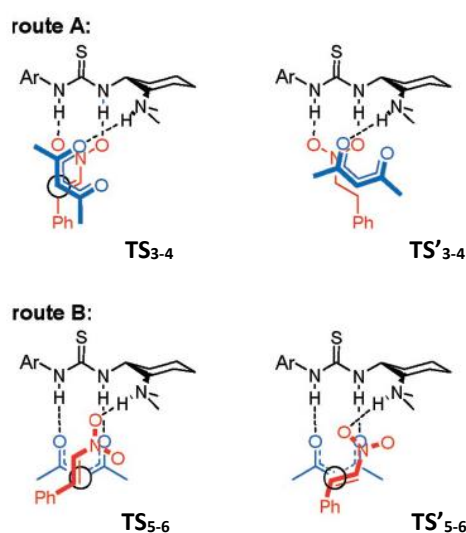


Figure 2.17 Transition States leading to the *R* and *S* isomers of Michael products on the two alternative routes.

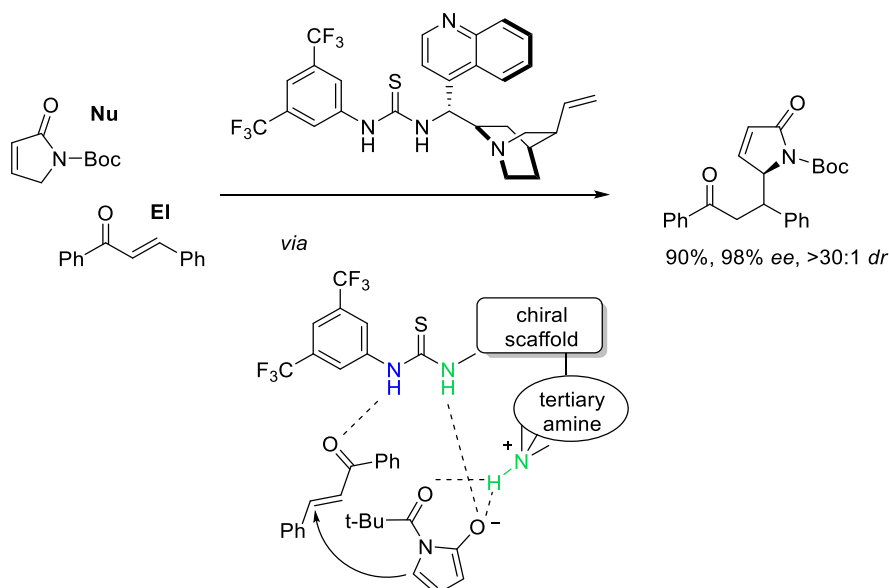
The C-C bond formation is the enantio determining step, as the enantioselectivity depends on the attacking face of the electrophile. In both routes the TS that leads to the *R* conformer is more stable than the one leading to the *S* (2.6 kcal/mol more stable in Takemoto's route and 2.4 kcal/mol in the Pápai's route). These energy differences correspond to high enantioselectivities (98% *ee* for Takemoto's and 97% *ee* for Pápai's) in perfect agreement with the *ee* values obtained experimentally (89% *ee*). The explanation stays on the special arrangement of the substrates: in the transition states affording the *R*-product (**TS₃₋₄**, **TS₅₋₆**), the substrates are aligned in a staggered conformation along the forming C–C bond, minimising steric intermolecular interactions. In the transition states leading to the *S*-product (**TS'₃₋₄**, **TS'₅₋₆**), this favourable orientation is not affordable because the electrophilic carbon atom of the nitroolefin is displaced from its ideal position when its attacking face is switched (Figure 2.17). C–C bond formation can only take place with a compromise of either the hydrogen

bond catalyst–substrate interactions, or the staggered geometry of the reacting molecules.

To conclude, both reaction pathways account for the observed enantioselectivity. It is reasonable because enantioselectivity is governed by the H-bonded network built by the three acidic N-H groups of the catalyst that drives the preferential orientation of the approaching substrates.

Even though these models have been proposed for thiourea-based bifunctional catalysed reactions, it has been demonstrated that they can be applied also to squaramide catalysed ones. In particular, it has been found that the Pápai-type model is the most plausible mechanism, which accounts well for the observed stereoselectivity.⁵² In literature, Takemoto and Pápai models are the two most commonly accepted modes of activation, both of them supported by additional theoretical and experimental studies.⁵³

Recently, a third pathway was suggested by Wang and co-workers, who performed DFT calculations on the vinylogous Michael addition of α,β -unsaturated butyrolactam to chalcone catalysed by a bifunctional cinchona alkaloid thiourea organocatalyst. They proposed that the electrophile is activated by the distal acidic NH of thiourea, while the deprotonated nucleophile forms two H-bonds with the protonated amine and the other available NH group of thiourea (Scheme 2.17).⁵⁴ Unfortunately, DFT calculations on squaramide-catalysed Michael reactions identified this pathway as not eligible for this kind of transformations.⁵²



Scheme 2.17 Vinylogous Michael addition of α,β -unsaturated butyrolactam to chalcone catalysed by bifunctional cinchona alkaloid thiourea organocatalyst that follows the mechanism by Wang.

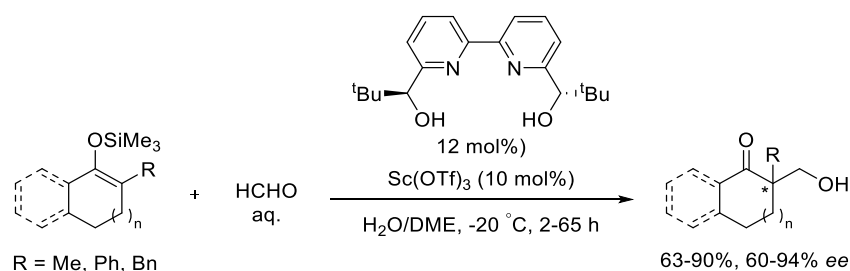
2.2. Computational studies on the reactivity of α -branched ketone dienolates: regio- and enantioselective α -additions leading to all-carbon quaternary adducts.

2.2.1. Introduction

In the previous chapter, we have envisioned many strategies of direct asymmetric α -functionalisation of enolisable ketones and it appears clear that, due to the several limitations regarding the substrate activation and the enantiocontrol, this reactivity still constitutes a challenging field. This situation is more complicated in the case of non-symmetrical unactivated ketones with two sites for deprotonation. Two regioisomeric enolates may be formed leading to competitive reaction pathways and therefore product mixtures.⁵⁵

Cyclic ketones belong to this class of compounds and their fragment bearing a quaternary α -stereocentre is common in numerous natural products and bioactive substances (for example in alkaloids). As a result, the interest in the synthesis of these units in an enantioselective manner using catalytic direct approaches from readily accessible starting materials is high.⁵⁶

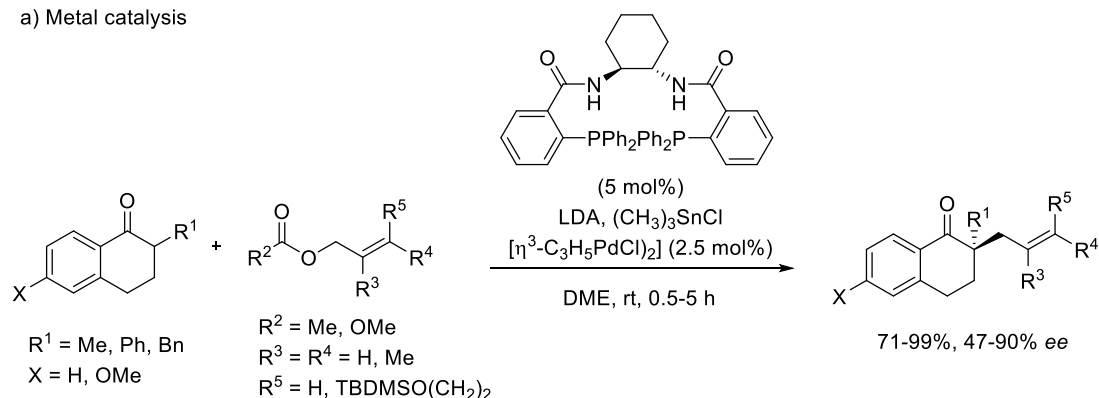
Several attempts of catalytic enantioselective C-alkylation of unactivated ketone precursors have been described. Some strategies are based on the use of either chiral auxiliaries or preformed enolates and equivalents, as the catalytic asymmetric α -functionalisation of silyl enolates with a chiral scandium complex (Scheme 2.18).⁵⁷



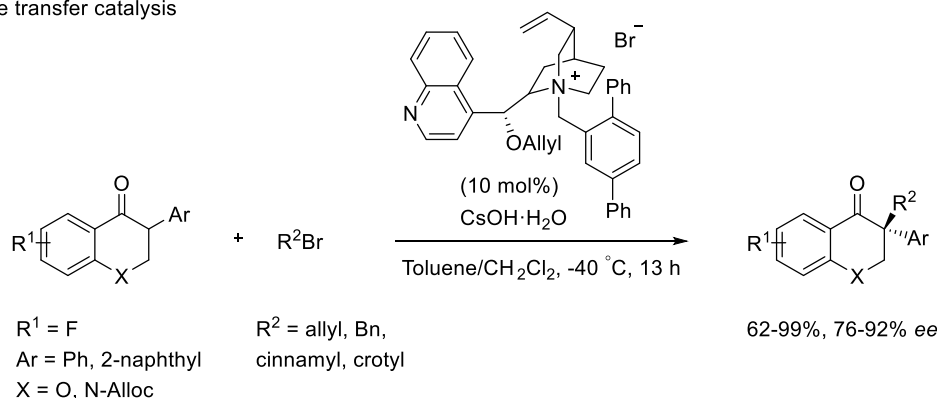
Scheme 2.18 Hydroxymethylation of silyl enolates using a chiral scandium complex by Kobayashi *et al.*

Alternatively, metal (mainly Pd and Ir)⁵⁸ (Scheme 2.19a) and phase transfer catalysis⁵⁹ (Scheme 2.19b) demonstrated to be useful approaches for the asymmetric allylic/benzylic α -alkylations of α -substituted (mainly benzo-fused or $C\alpha'$ -protected) cyclic ketones, even if quite inefficient for other type of alkylating processes.

a) Metal catalysis



b) Phase transfer catalysis



Scheme 2.19 a) Example of metal catalysis, Pd catalysed asymmetric alkylation of α -tetralones by Schroeder *et al.*⁶⁰ b) Example of phase transfer catalysis, alkylation of substituted isoflavones catalysed by a cinchonidinium bromide phase-transfer catalyst by Scheidt *et al.*⁵⁹

These methods do not represent a general solution, as some require stoichiometric (strong) base, the use of α' -blocked starting ketones to avoid the regioselectivity problem or preinstalled allyl esters and carbonates.

On the other hand, enamine activation and Brønsted acid activation strategies have enabled to further advance the field by using Michael acceptors as the alkylating reagent while securing regioselectivity through exclusive formation of the “thermodynamic” enamine or enol intermediate.

These approaches suffer of limited substrate scope as enamine formation from the cycloalkanones with α -sidechains bigger than methyl or ethyl hardly occurs due to the steric hindrance (Figure 2.18a),⁶¹ while extension of the Brønsted acid activation strategy to reactions with common Michael acceptors (π -deficient olefins) other than allenamides⁶² or sterically undemanding enones (e.g. enals, acrylates, or simple enones)⁶³ appears troublesome (Figure 2.18b). Furthermore, no other α -branched cycloalkanones except cyclopentanones and cyclohexanones have been explored.

2.2. Computational studies on the reactivity of α -branched ketone dienolates

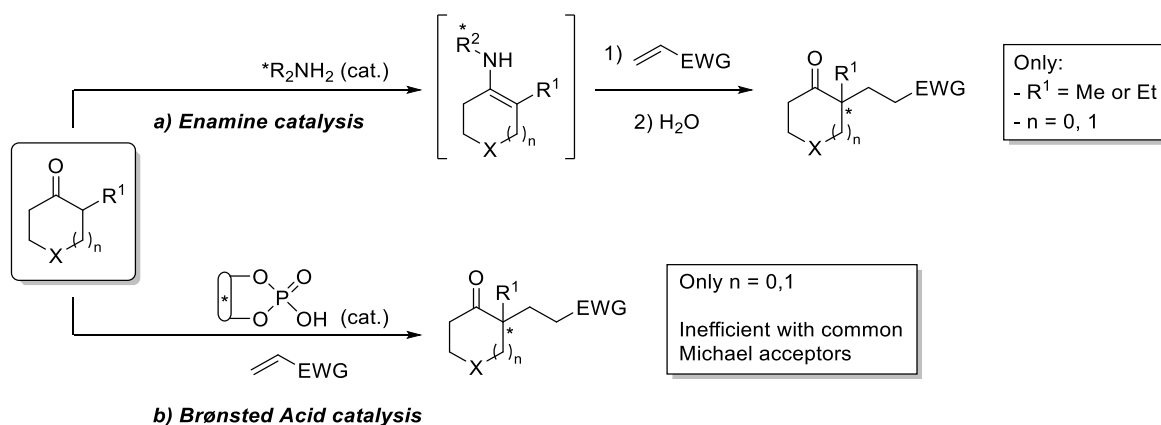
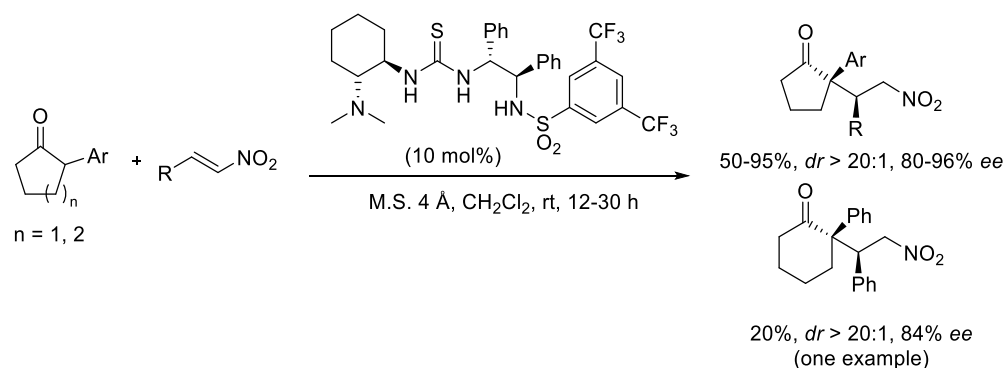


Figure 2.18 α -functionalisation of α -branched cycloalkanones via a) enamine and b) Brønsted acid catalysis.

Bifunctional Brønsted base/H-bond catalysis represents another approach to promote enantioselective additions of α -branched cyclic ketones, although the majority of the examples reported so far deals with active ketones bearing an electron-withdrawing group (EWG = carbonyl, nitrile, sulfonyl, nitro) at the $C\alpha$.⁶⁴

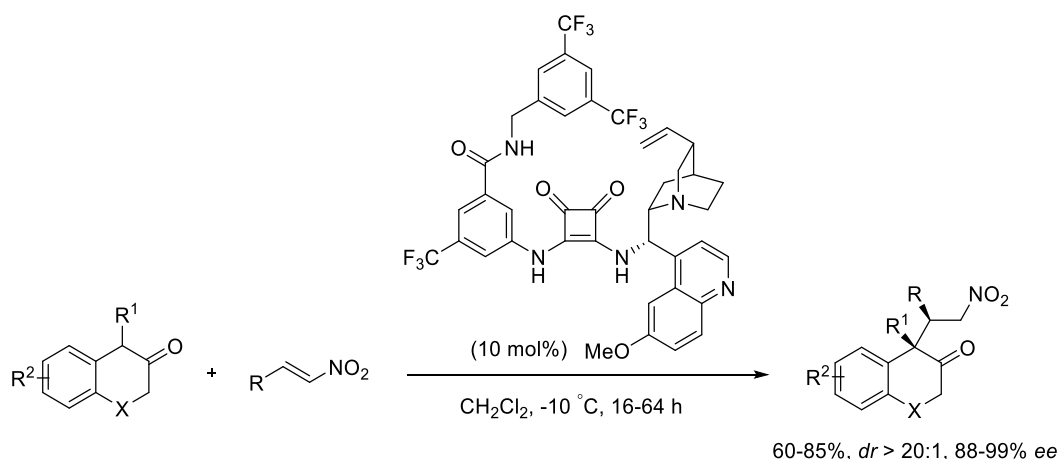
Two exceptions to this behaviour were reported and constitute unique examples of a Brønsted base catalysed enantioselective α -functionalisation of unactivated nonsymmetrical ketones leading to α -quaternary adducts.

In 2010, Wang group documented good yields and stereoselectivities for the addition reaction of α -aryl cyclopentanones to nitroolefins; however, attempts to expand the method to the important cyclohexanone analogs provided the α -quaternary product in a poor 20% isolated yield and 84% *ee* at best (reaction run at 50 °C) (Scheme 2.20).⁶⁵



Scheme 2.20 Michael reaction of α -aryl cycloalkanones catalysed by a Brønsted base/H-bond catalyst by Wang *et al.*

In 2017, Palomo group reported a regio-, diastereo-, and enantioselective BB-catalysed α -alkylation of α -substituted β -tetralones with nitroolefins; instead, α -tetralones showed to be unreactive materials under same conditions (Scheme 2.21).⁶⁶



Scheme 2.21 Brønsted base/H-bond-catalysed α -alkylation of α -substituted β -tetralones with nitroolefins by Palomo *et al.*

The main issues regarding the development of a direct regio- and enantioselective C-C bond forming reaction at C_{α} position of α -branched ketones under proton transfer conditions are the relatively high pK_a value of the ketone substrate (pK_a range of 19–24, while the functional pK_a activation barrier for common Brønsted base catalysts lies within pK_a 13-16) and the steric constraints set by the carbonyl α -substituent, which makes difficult the proton abstraction and decreases the nucleophilicity.

A possible solution for the high pK_a value of the ketone could be a slight variation on the substrate, in particular the insertion of an alkenyl group at the α -position of the carbonyl function, giving a α -alkenyl cycloalkanone. Apart from providing synthetic versatility (availability of a strategically positioned C=C double bond) to the resulting adducts, it allows to have charge delocalisation during the enolisation, increasing the α -CH acidity. In this way, also a weak base catalyst could trigger the reaction while securing regioselective α - vs α' -enolisation. The drawback of this kind of substrates is the ambiguous α - vs γ -reactivity of the transiently formed vinylogous enolate, which has to be controlled by the Brønsted base catalyst, besides the stereoselectivity in the generation of the quaternary stereogenic centre (Figure 2.19).

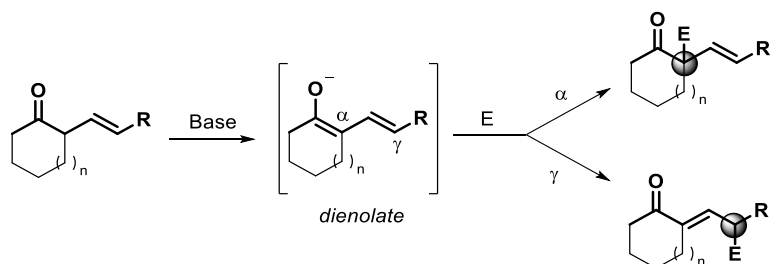


Figure 2.19 Enolisation of α -alkenyl cycloalkanones and the issue of α vs γ reaction selectivity.

The great majority of catalytic methods involving dienolates or equivalent intermediates deal with α -unsubstituted ones and proceed mainly through the γ carbon (vinylogous reactivity, Figure 2.20).⁶⁷ The γ -attack pathway appears to be kinetically favourable because no disruption of the π -conjugation along the reaction coordinate occurs.

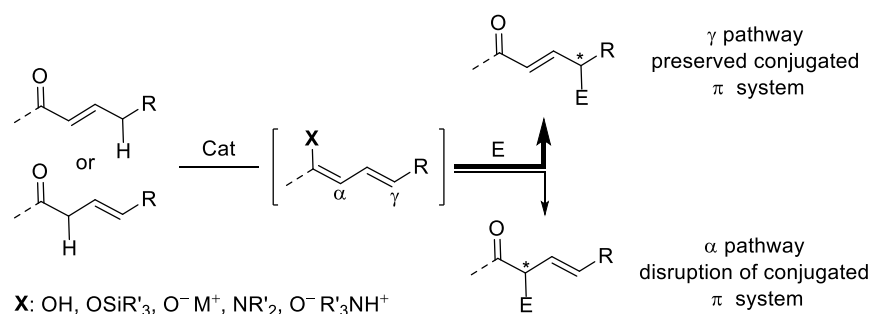
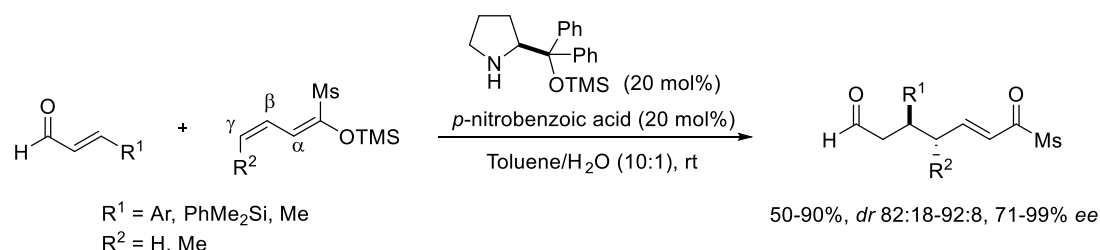


Figure 2.20 Divergent reaction pathways of dienolates and equivalents.

Some of these methods are the catalyst-promoted addition reactions of preformed silyl dienol ethers (X: OSiR'₃)⁶⁸ as well as direct approaches based on metallic catalysis (X: O⁻M⁺),⁶⁹ dienamine activation (X: NR'₂)⁷⁰ and Brønsted acid⁷¹ and base catalysed⁷² activations.

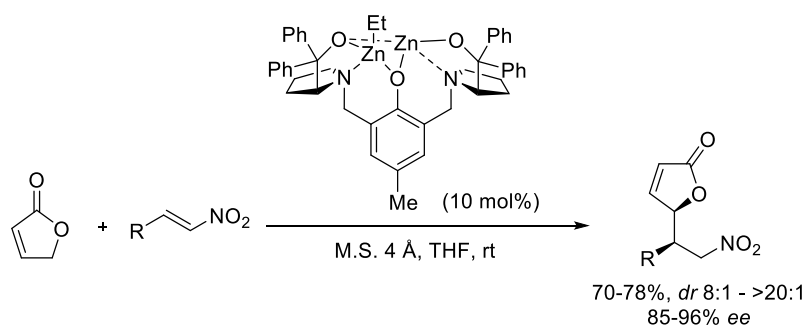
The methods employing preformed silyl dienol ethers (X: OSiR'₃) were applied mainly in the vinylogous Mukaiyama aldol reaction, but also a few examples regarding the Mukaiyama-Michael reaction were reported. In 2012, Schneider and co-workers developed the first catalytic, enantioselective vinylogous Mukaiyama-Michael reaction of acyclic dienol silyl ethers with α,β -unsaturated aldehydes, which are activated *via* iminium ion, obtaining valuable chiral 1,7-dioxo compounds in a γ -site selective process (Scheme 2.22).⁷³



Scheme 2.22 Catalytic enantioselective Michael reaction with linear preformed dienolates by Schneider *et al.*

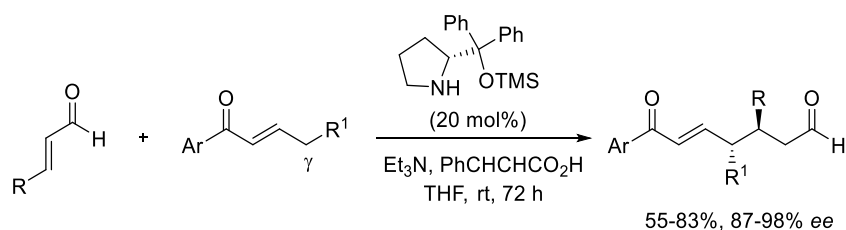
In the category of methods to perform direct addition of unmodified carbonyl compounds to different electrophiles through dienolate or equivalent intermediates, it is possible to distinguish several approaches.

One is based on metallic catalysis, in which the reactions proceed through a transiently generated metal enolate intermediate (X: O⁻M⁺) to obtain γ -functionalised products. Applications to Michael, Mannich, aldol and allylation reactions are found in the literature. One significant example is the synthesis of γ -substituted butenolides by direct asymmetric Michael addition of 2(5*H*)-furanone to nitroalkenes catalysed by a dinuclear zinc catalyst developed by Trost.⁷⁴



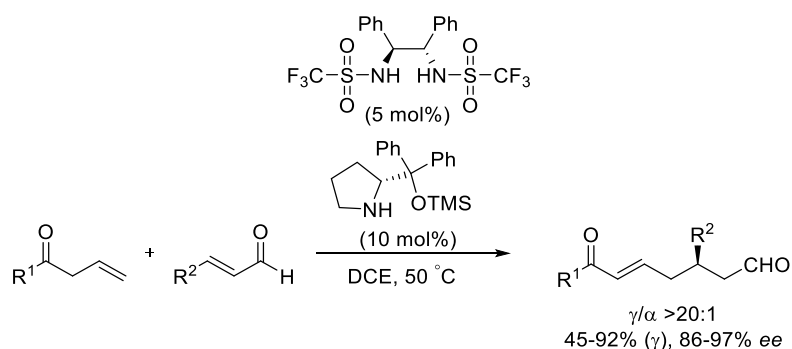
Scheme 2.23 Asymmetric Michael addition of 2(5H)-furanone to nitroalkenes catalysed by a dinuclear zinc catalyst developed by Trost.

Organocatalytic methods are also suitable for the γ -functionalisation of unsaturated carbonyl compounds. A powerful tool is the dienamine-mediated activation ($X: NR'_2$). Brenner-Moyer and co-workers reported a direct diastereo- and enantioselective vinylogous Michael addition of linear enones with and without γ -substitution.⁷⁵



Scheme 2.24 Direct diastereo- and enantioselective vinylogous Michael addition of linear enones by Brenner-Moyer *et al.*

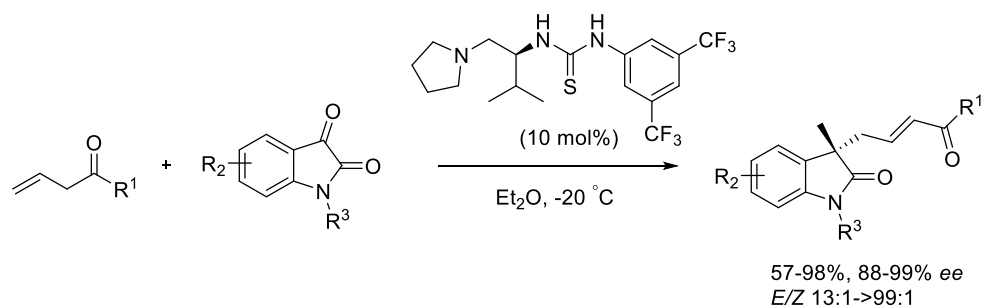
Finally unsaturated ketones, subjected to Brønsted acid or Brønsted base catalysis, generate dienols and dienolates respectively, which can react with suitable acceptors to afford the corresponding γ -addition adducts. An example of Brønsted acid catalysed reaction is the direct vinylogous Michael addition of unmodified linear β,γ -unsaturated ketones to α,β -unsaturated aldehydes by Xu and co-workers. The α,β -unsaturated aldehyde is activated *via* iminium ion and the co-catalyst activates the dienolate and shields the α -carbon, obtaining the γ -adduct exclusively in good yields and excellent enantioselectivity.⁷⁶



Scheme 2.25 Direct vinylogous Michael addition of unmodified linear β,γ -unsaturated ketones to α,β -unsaturated aldehydes by Xu *et al.*

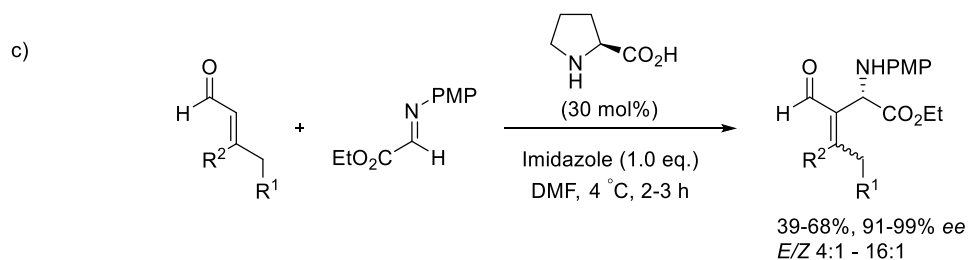
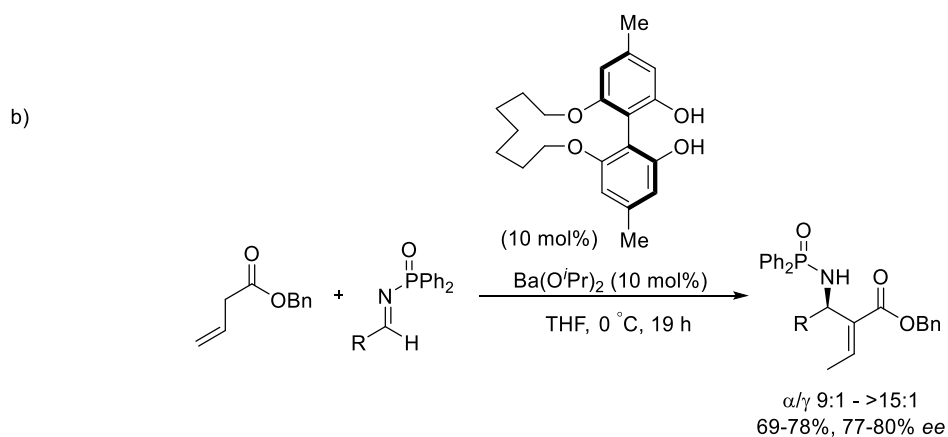
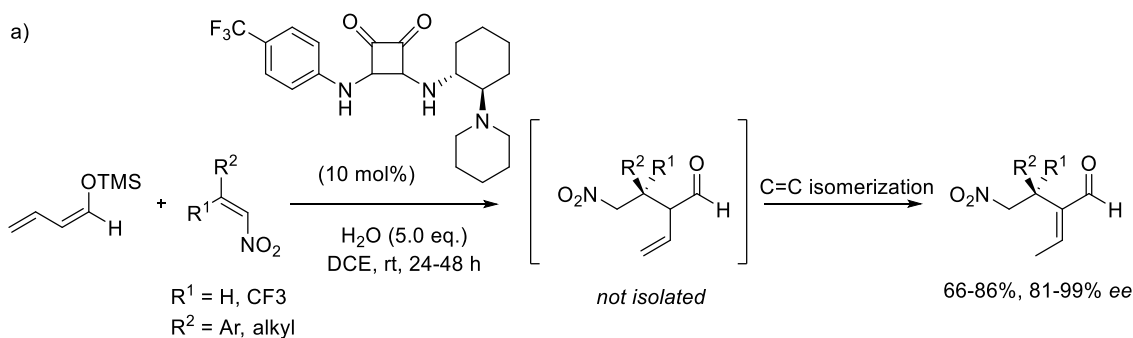
Jiang group, instead, described an interesting example of Brønsted base catalysis, a direct asymmetric vinylogous aldol reaction of allyl ketones with isatins catalysed by a

readily prepared L-valine-derived bifunctional tertiary amine/thiourea catalyst to provide 3-hydroxy-2-oxindole derivatives.⁷⁷



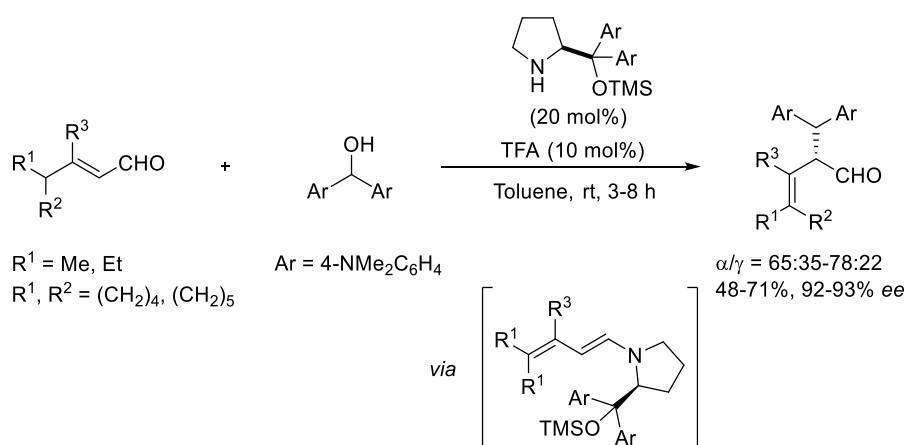
Scheme 2.26 Direct asymmetric vinylogous aldol reaction of allyl ketones with isatins catalysed by a readily prepared L-valine-derived bifunctional tertiary amine/thiourea catalyst by Jiang *et al.*

In contrast with the mainstream γ -selectivity, a few examples of methods that proceed through α -carbon have been reported, although with important limitations.



Scheme 2.27 α -addition examples of dienolates or equivalents leading to MBH-type adducts.

An α -addition of preformed aldehyde-derived silyl enol ethers to nitroalkenes (Scheme 2.27 a)⁷⁸ and to imines⁷⁹ in the presence of tertiary amine catalysts was reported by Alemán and co-workers. The concomitant isomerisation of the double bond to yield Morita-Baylis-Hillman-type or Rauhut-Currier adducts avoids the formation of a stereocentre at $C\alpha$. Similar examples of α -addition were described earlier by Shibasaki (Scheme 2.27 b)⁸⁰ and Barbas III (Scheme 2.27 c)⁸¹ using other activation pathways. Other Brønsted base catalysed α -functionalisations of transiently generated dienolates have been developed only for specific substrates, such as α -styryl acetates in the work of Zhao group⁸² or α -angelica lactones in the case of Johnson.⁸³ Other strategies to favour the α -additions deal with substrates with strong steric bias, as reported by Christmann group, who found that γ,γ -disubstituted enals react through the α -carbon atom of the dienamine intermediate because of the steric hindrance at the γ -carbon (Scheme 2.28).⁸⁴



Scheme 2.28 α -addition of γ,γ -disubstituted enals to stabilised carbocations as electrophiles *via* activation as dienamine intermediates by Christmann *et al.*

α -Addition of linear enones to different electrophiles promoted by iminium activation was performed, featuring poor enantioselectivity or providing racemic products.⁷⁵ It is noteworthy that none of these α -selective methods has demonstrated to be efficient in the enantioselective generation of α -quaternary ketone products. Indeed, this process would necessarily involve α -substituted dienolates or equivalents as intermediates (Figure 2.21). To this purpose, it is necessary to have a strong control over the E/Z enolate geometry and the face selectivity, while retaining α -reactivity despite the steric hindrance at $C\alpha$.

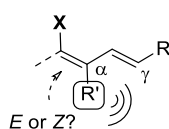
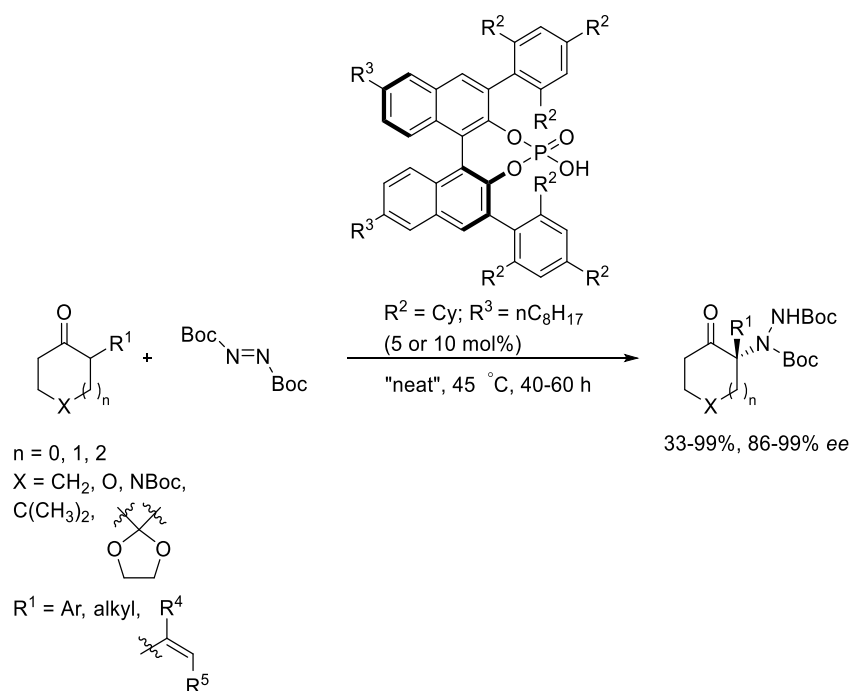


Figure 2.21 Challenging issues involving the reactivity of α -branched dienolates.

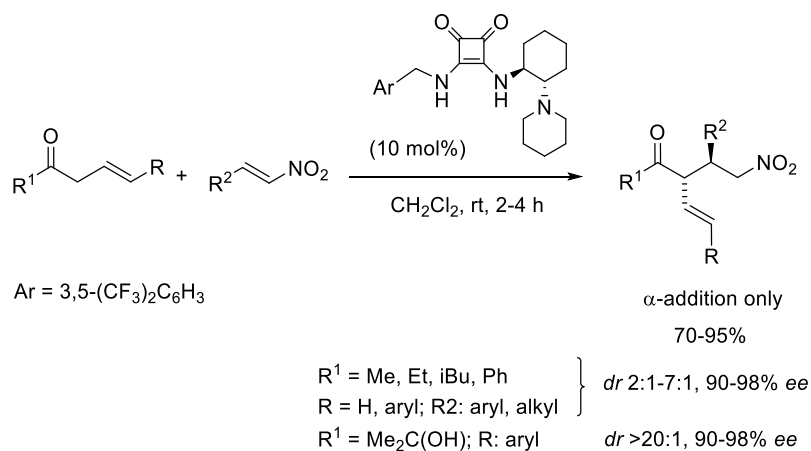
This issue has been faced by Toste group through Brønsted acid catalysis. They found that α -branched unactivated cyclic ketones smoothly undergo direct asymmetric amination catalysed by a chiral phosphoric acid to generate *N*-containing

tetrasubstituted carbon stereocentres (Scheme 2.29), but they do not work properly in the case of Michael addition to conjugated olefins, with the only exception of allenamides.⁸⁵



Scheme 2.29 Direct asymmetric amination catalysed by a chiral phosphoric acid to generate *N*-containing tetrasubstituted carbon stereocentres by Toste *et al.*

Quite recently Palomo group has reported the first direct Michael reaction of β,γ -unsaturated alkyl ketones with nitroolefins to afford exclusively α -addition products under bifunctional Brønsted base/H-bond catalysis with high diastereo- and enantioselectivity (Scheme 2.30).⁸⁶ The idea of expanding this reactivity pattern to α -branched ketone dienolates would allow to obtain valuable α -quaternary ketone adducts.



Scheme 2.30 First direct Michael reaction of β,γ -unsaturated alkyl ketones with nitroolefins to afford exclusively α -addition products under bifunctional Brønsted base/H-bond catalysis by Palomo *et al.*

2.2.2. Abstract

Taking in mind that chiral Brønsted base/H-bonding catalysts are able to promote the smooth addition of β,γ -unsaturated alkyl ketones to nitroolefins to yield the α -addition products exclusively and with very high stereoselectivity (Scheme 2.30), Palomo group thought to expand the strategy also to the challenging α -branched ketone dienolates leading to ketone products with an all-carbon quaternary α -stereocentre.

Observing the working model **A** (Figure 2.22) for the unsubstituted dienolates, in which the catalyst acts in a bifunctional manner such that tight control over the reactants approaching trajectory could be accomplished, the extrapolation to α -branched ketone dienolates looks conceivable ($R' \neq H$). However, some issues emerge and need to be overcome: the reaction stereocontrol, the ill-defined *E/Z* enolate generation, the reactivity and site-selectivity, due to the steric hindrance at the nucleophilic α -carbon influencing the enolate generation and the subsequent approaching of the electrophilic reagent.

Not surprisingly, initial attempts for the reaction between nitrostyrene and α -branched ketones ($R' = \text{CH}_3$) resulted completely unfruitful. The low reactivity of the sterically congested α -substituted dienolate could be alleviated if a sterically undemanding Michael acceptor, as 1,1-bis(phenylsulfonyl)ethylene was employed, yielding α -quaternary homoallylic ketones, although in variable yields and selectivity. Since the attenuated reactivity and the difficulties in controlling the enantioface selectivity still persisted, it was needed to slightly change the ketone substrate, thus cyclic ketones in which the double bond is tethered at the $C\alpha$ -position of the carbonyl function were adopted.

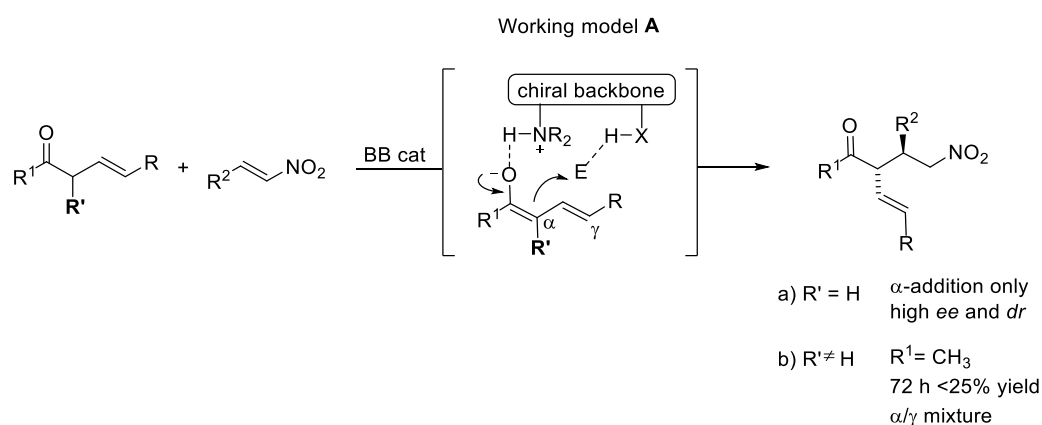


Figure 2.22 Impact of α -substitution on the reactivity of transiently formed acyclic ketone dienolates.

The dienolates from cyclic ketones might behave superior based on: (i) the higher nucleophilicity of cyclic systems as compared with the more flexible, open-chain counterparts;⁸⁷ (ii) a more rigidified transition state and consequent more efficient chirality transfer; (iii) the problem of enolate geometry (*E/Z* uncertainty) gets cancelled. They performed the reaction between α -styryl cyclohexanone and bis(phenylsulfonyl)ethylene yielding α -quaternary cycloalkanone adducts in high site-, regio- and stereoselectivity. They demonstrated that α -alkenyl cycloalkanones are a class of nonsymmetrical unactivated ketones susceptible for smooth and regioselective

activation by tertiary amine/H-bond bifunctional catalysts. The efficiency of the methodology is independent of the ring size of the cycloalkanone substrate or its substitution pattern, while the easy further elaboration of the alkenyl moiety in adducts provide synthetic versatility.

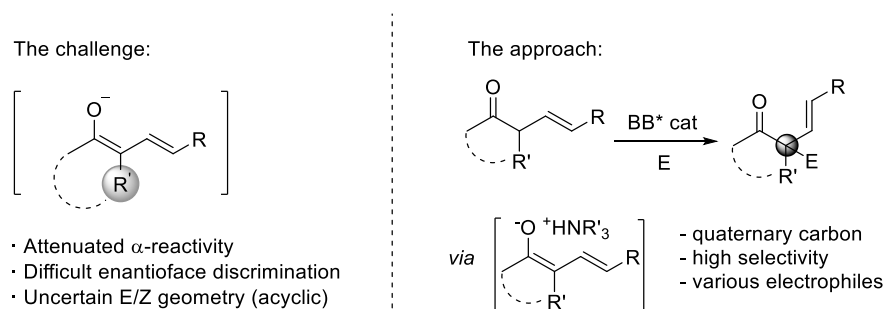


Figure 2.23 α -substituted dienolates issues and the approach based on BB catalysis.

Theoretical analysis of the unique reactivity of these transiently generated cyclic dienolates vs the acyclic counterparts was performed and their electronic properties and energies were computed. The α - vs γ - reactivity of the substrates was studied computationally and a rationale for the stereoselectivity was provided.

2.2.3. Objectives

As explained before, the substrates of this work are challenging, many issues emerged and simplifications in substrates were needed. The first experiments were thought on simple linear α -branched ketones, later replaced by cyclic substrates, to sort the problems out leading to the products bearing a α -stereocentre. Since the choice of the substrate came out to be key, a theoretical analysis on different classes of substrates was carried out to help in understanding the reactivity of the different nucleophilic systems. The substrates considered are a linear α -branched dienolate, the cyclic counterpart, a α -substituted five-membered ring enolate and a α -substituted six-membered ring enolate.

First, their charge distribution and Fukui nucleophilicity indices were calculated and then a more comprehensive analysis was completed, calculating the energies for the reaction of each enolate system with a bis-sulfone in presence of a model achiral squaramide-tertiary amine catalyst **C0** (see Figure 2.25). The results obtained from this analysis were determinant for the choice of the substrate to use in the experiments.

In a second moment, we decided to compute the whole energy pathways of the same reactions also in presence of a realistic catalyst, as **C7** (see Table 2.1).

Then, we tackled the issue of the α - vs γ - reactivity of substrates bearing the dienolate unit and we computed the two routes in presence of a model catalyst **C0** and we provided a rationale for the preference of the α - vs the γ -addition pathways.

Finally, after the experimental optimisation of the reaction between the cyclic ketone and bis-sulfone, we performed DFT calculations to elucidate the origin of the stereoselectivity and the nature of the H-bond network between the substrates and the catalyst during the transition state for the model reaction between the vinyl

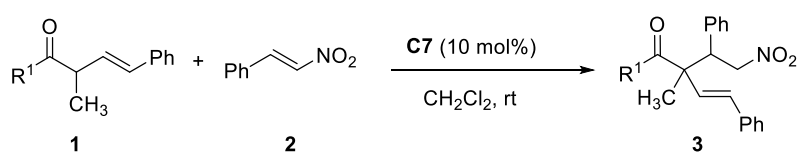
cyclohexanone enolate **III**, vinyl bis-sulfone **4** and either catalyst **C7** (R=Ar^F: 3,5-(CF₃)₂C₆H₃) or **C8** (R: ^tBu).

2.2.4. Experimental work

The experimental work was carried out by Dr. Iñaki Urruzuno, Dr. Odei Mugica and Dr. Silvia Vera of the group of Prof. Palomo, who provided us with the data we needed to perform our computational investigation.

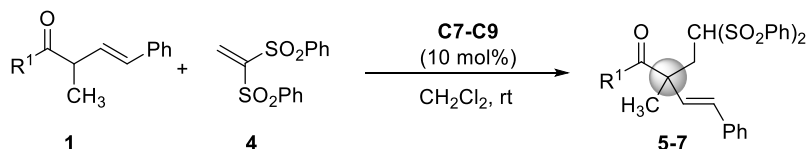
Their studies started with the reaction between the α -branched ketones **1** and nitrostyrene **2** using bifunctional catalyst **C7** (for the structure see Table 2.1) resulting in the recovery of unreacted enone (R¹ = Ph) or very low conversions to product **3** (R¹ = Me, <25% conversion after 72 h) as a mixture of α/γ isomers (Scheme 2.31).

a) Reactivity of linear α -branched ketones with nitrostyrene under BB catalysis



R¹: Me 72 h, <25% yield, α/γ mixture
R¹: Ph No reaction

b) Reactivity of linear α -branched ketones with bis-sulfone under BB catalysis



- a R¹: CH₃
b R¹: CH₃CH₂
c R¹: Ph

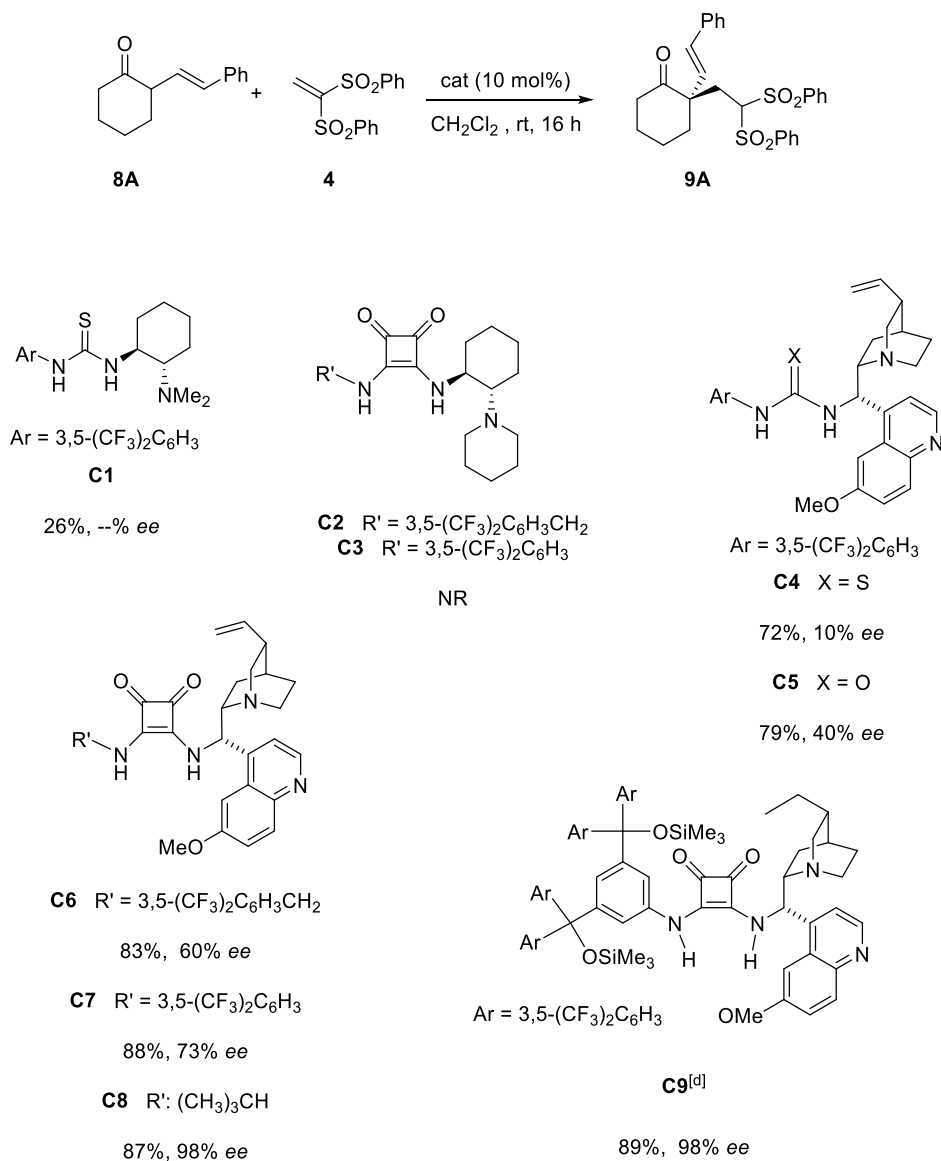
R ¹ :			
	5	6	7
with C7 :	39% y (63% ee)		
with C8 :	38% y (61% ee)	-- (--)	-- (--)
with C9 :	72% y (79% ee)	29% y (58% ee)	14% conv.

Scheme 2.31 Reactivity of linear α -branched ketones with a) nitrostyrene and b) bis-sulfone as electrophile under BB catalysis.

In view of the poor results, they reasoned that the low reactivity of the sterically congested α -substituted dienolate might be alleviated if a highly reactive and sterically less demanding Michael acceptor as 1,1-bis(phenylsulfonyl)ethylene **4** is used. Furthermore, this kind of acceptors, besides being highly reactive in Michael reactions, have synthetic utility as masked alkane surrogates.⁸⁸ As the results in Scheme 2.31b show, α -branched ketones **1** reacted with **4** in the presence of **C7**,⁸⁹ **C8**⁹⁰ or **C9**⁹¹ (for the structures see Table 2.1) to afford adducts **5–7** from reaction at the α -site exclusively, although in variable yields and enantioselectivity. These results, even if promising, highlighted the poor reactivity, the difficult control of the enantioface selectivity and the high dependence to the side-chain substitution. Supported by computational predictions (in the following section), they decided to use α -substituted cycloalkanones instead of the linear counterparts. The reaction between α -styryl cyclohexanone **8A** and

bis(phenylsulfonyl)ethylene **4** was studied in the presence of different chiral bifunctional catalysts (Table 2.1).

Table 2.1 Catalyst screening for the reaction of cyclohexanone **8A** with vinyl sulfone **4** to give **9A**.^a

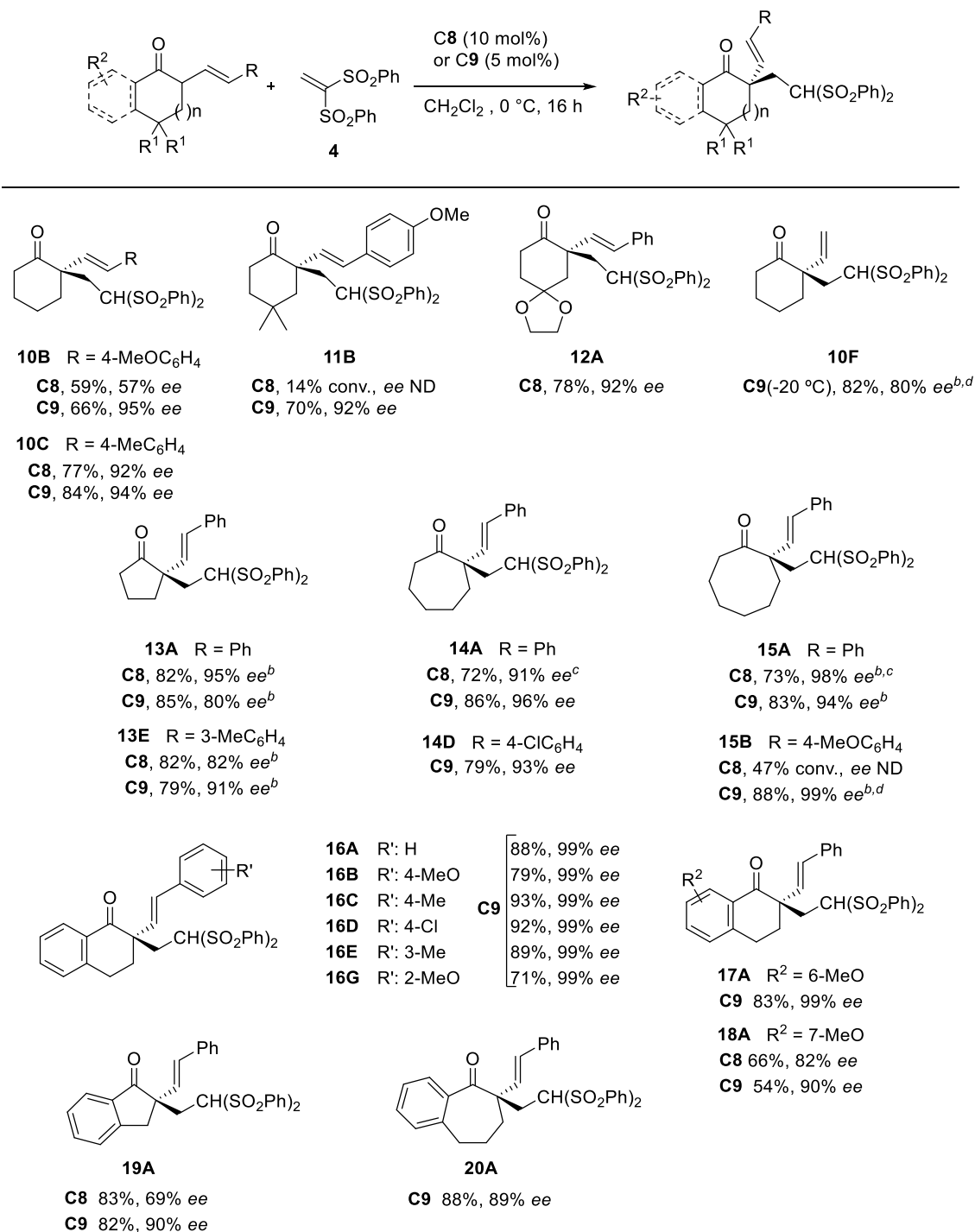


^aReactions carried out at 0.15 mmol scale, using 2 equiv. of vinyl disulfone and 10 mol% catalyst in 0.3 mL CH₂Cl₂ at room temperature. ^bYield after chromatography. ^cee determined by chiral HPLC. ^d Reaction run at 0 °C.

The reaction proceeded with low yield using Takemoto catalyst **C1**³¹ and did not proceed at all with Rawal's squaramides **C2** and **C3**.⁴⁰ Improvements in the yield could be obtained with the more active quinine-derived thioureas **C4** and urea **C5**,⁹² although with poor enantioselectivity. **C6** was the same catalyst effective in the α -functionalisation of α -unsubstituted dienolates with nitroolefins,⁸⁶ but in this case it allowed the reaction to proceed but with a modest 60% ee. **C7** showed a little improvement in stereoselectivity, but the desired results were obtained with catalyst **C8**, a sterically congested catalyst developed by Connon,⁹⁰ that allowed to get 98% ee

and good yields. A similar result was provided using **C9**, performing the reaction at lower temperature (0°C). **C8** and **C9** were selected as the best catalysts to carry out the substrate scope of alkenyl cycloalkanones (Table 2.2).

Table 2.2 Scope of the reaction of α -alkenyl cycloalkanones with bis-sulfone **4** catalysed by **C8/C9**.^a



^aReactions carried out at 0.15 mmol scale, using 10 mol% catalyst **C8** or 5 mol% catalyst **C9** in 0.3 mL of CH_2Cl_2 unless otherwise stated. Yield of isolated product after chromatography. *Ee* determined by chiral HPLC. No product from γ -addition was detected by ¹H NMR ($C\alpha/C\gamma > 95:5$). ^bReaction carried out in toluene at rt. ^cWith 3 equivalents of **4** and 48 h reaction. ^d10mol% of catalyst loading. ND= not determined.

The strategy works pretty well for 4-substituted cyclohexanones to give for example **11B** and **12A** in satisfactory yield and stereoselectivity and it was also suitable for the exceptional case of **10F**, although with low *ee*. The method turned out to be equally effective with cycloalkanones of varying ring size: cyclopentanones **13A** and **13E** with acceptable *ee*, cycloheptanones **14A** and **14D** with high *ee* and cyclooctanones **15A** and **15B** with high *ee* only in toluene. Benzo-fused cycloalkanones were also excellent substrates for this catalytic reaction affording the equivalent adducts (**16-20**) in good yields and high enantioselectivity regardless the nature of the substituents at both the aromatic ring and the olefin. Allyl cyclic alkanones under Brønsted base/H-bonding strategy resulted to be active in the reaction with other carbon electrophiles, as β -substituted nitroolefins and paraformaldehyde with high stereoselectivity. This behaviour is in contrast with the poor reactivity of the parent open chair α -branched allyl ketones. In the case of nitroolefins, a minor amount (<5%) of γ -addition was observed.

2.2.5. Computational work

2.2.5.1. Methods

All structures were initially optimised using density functional theory (DFT) with B3LYP and the 6-31G(d,p) basis set as implemented in Gaussian 16. Final energies were calculated at M06/def2tzvpp level of theory, in a solvent model (IEFPCM, solvent=dichloromethane). The stationary points were characterised by frequency calculations in order to verify that they have the right number of imaginary frequencies. The calculation of the atomic charges was carried out through Natural Bond Orbital analysis. For additional information, see Chapter 1.

2.2.5.2. Preliminary studies

Aware of the poor reactivity of non-symmetrical unactivated ketones, Palomo group focused on studying potential substrates to understand the changes needed to allow the α -functionalisation to occur yielding adducts bearing quaternary centres. For an initial assessment of the reactivity associated with these nucleophilic systems, we determined some electronic parameters, as charge distribution and Fukui nucleophilicity index (*f*) at the α -carbon on the model linear **I** and cyclic enolates **II-IV**, with the hope that the results could shed some light on their relative reactivity. The idea was to compare the linear α -substituted dienolate with the cyclic counterpart and other cyclic substrates (five and six membered rings) that bear a phenyl group in $C\alpha$, able as the allyl group to delocalise the charge and thus increase the CH acidity (Figure 2.24). Surprisingly, the differences in negative charge at that specific carbon is negligible in the four substrates, ranging from -0.35 to -0.36 e. Similarly, the Fukui indices are not informative, showing indistinguishable values for all substrates. These data are not in agreement with the observed initial experimental data, which instead highlight considerable difference in reactivity between the linear and cyclic substrates. Accordingly, it appears that purely intrinsic electronic properties might not be enlightening in dictating these reactivity trends and the role of the bifunctional catalyst

as well as structural factors (steric hindrance, enolate rigidity) or α -CH acidity might also be considered.

	I	II	III	IV
charge C_{α}	-0.33 e	-0.31 e	-0.34 e	-0.30 e
f^{\ddagger}	-0.34	-0.35	-0.35	-0.36

Figure 2.24 Charge distribution and Fukui nucleophilicity index (f^{\ddagger}) at the α -carbon on the model linear **I** and cyclic enolates **II-IV**.

For a more comprehensive analysis, the reactions between ketones **I-IV** and bis-sulphone **4** were computed in the presence of a model achiral squaramide-tertiary amine catalyst **C0**, which is not influenced by the steric constraints of catalysts **C1-C9** (Figure 2.25). Gratifyingly, the computed activation energies gave us useful information, identifying a significant difference between the most reactive species **III** and the other substrates. This evidence was taken in consideration for the choice of the cyclic substrate **III** in the experiments. Indeed, an activation energy of 20.8 kcal/mol was computed for **III**, which is affordable at room temperature. In contrast, the activation barriers for the reaction involving the acyclic species **I** and the phenyl derivative **II** and **IV** are ca. 24 kcal/mol, predicting a much more sluggish reactivity of these substrates, as found for example for **I** in initial experimental attempts (Scheme 2.31). Based on these results, it is possible to confirm that cyclic substrate **III** is more convenient than the linear counterpart. The superiority of the cyclic substrate is more related to structural aspects than to the electronic nature (against the nucleophilicity enhancement of cyclic vs acyclic carbanions proposed by Cunningham).⁸⁷ Indeed, the more rigidified transition state of cyclic substrate contributes to a more efficient chirality transfer and the issue of enolate geometry (E/Z uncertainty) is eliminated.

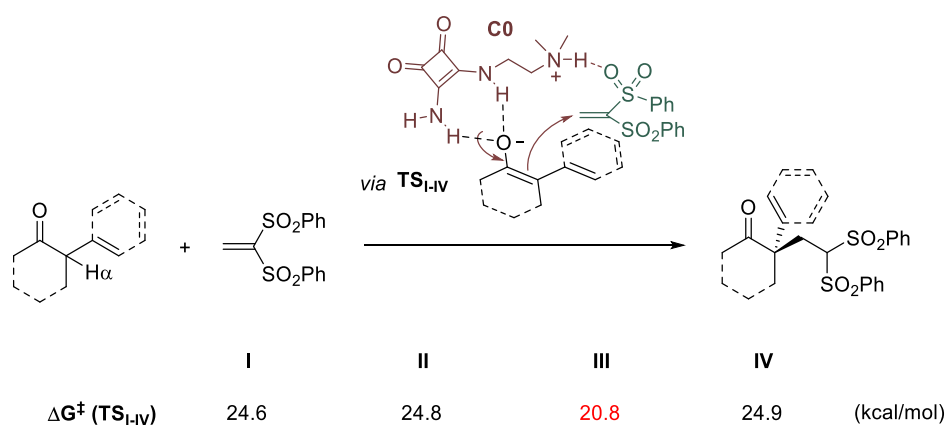


Figure 2.25 Energy barriers for the reactions between ketones **I-IV** and bis-sulphone **4** in the presence of a model achiral squaramide-tertiary amine catalyst **C0**.

Confident with these promising results in hand, we thought to examine in depth every step of the pathway, in presence of a more elaborated catalyst, as **C7**. The reaction between the ketones **I-IV** and bis-sulfone **4** is a Michael addition catalysed by a

bifunctional Brønsted base/H-bond donor squaramide. We computed the simple mechanism for all the four substrates to compare their behaviour.

The first step is the abstraction of the acid H α by the tertiary amino group of the catalyst, leading to the corresponding enolate and the catalyst in the protonated form. Next, the nucleophilic attack of the enolate to the bis-sulfone occurs, facilitated by the catalyst, which addresses the two substrates and locates them in the best orientation for the reaction. In this step, the catalyst plays its role of stereocontrol.

While the difference between the energy barriers of the reactions computed using the model **C0** (Figure 2.25) clearly identifies substrate **III** as the best candidate for this kind of synthetic strategy, when the reactions are computed using a more complicated catalyst, as **C7**, the values of activation energies for the nucleophilic attack could be misleading and a deeper analysis is required (Figure 2.26).

At first glance, it appears that a first discriminatory element could be the activation energy for the deprotonation step. The cyclic dienolate **III** is formed more easily than the others by a difference of ~1-5 kcal/mol. The highest barrier is the one of compound **IV**, probably due to the steric hindrance of the substituent in C α . Compound **II**, although featuring a phenyl group at C α , does not show high energy barrier for the first step, probably because the five-membered ring, being more planar, fits better in the catalyst pocket and makes the access at C α easier.

The intermediates are the complexes catalyst-enolate and in all the cases they are quite unstable, being located at energy levels higher than 10 kcal/mol. The intermediate from the reaction of **III** is the most stable, at an energy value of 11.5 kcal/mol, ~3-5 kcal/mol lower than the other intermediates. This result is meaningful because it implies that the intermediate for the case **III** is present in higher concentration than for the other cases, in which the intermediates, being less stable, are more prone to suffer the reversible reaction. The concentration of the intermediate may influence the speed of the following reaction that is the rate-determining step, affecting the overall reaction rate. From the energy barrier values and the high energy of the intermediates, it emerges that the first step is more favoured for compound **III** than for the others.

Concerning the second step, the nucleophilic attack of the enolate to the sulfone, cases **II** and **III** undergo this reaction overcoming a smaller barrier than **I** and **IV**. The explanation of the higher barrier for **I** could be the flexibility of the linear substrate that is more difficult to be taken in place through H-bond interactions; for **IV**, instead, the phenyl substituent also in this step plays a shielding action for the new C-C bond formation at C α . Compound **II** has the advantage of being smaller than **IV** and having a tighter ring that addresses the substituent to a convenient position allowing the C α attack.

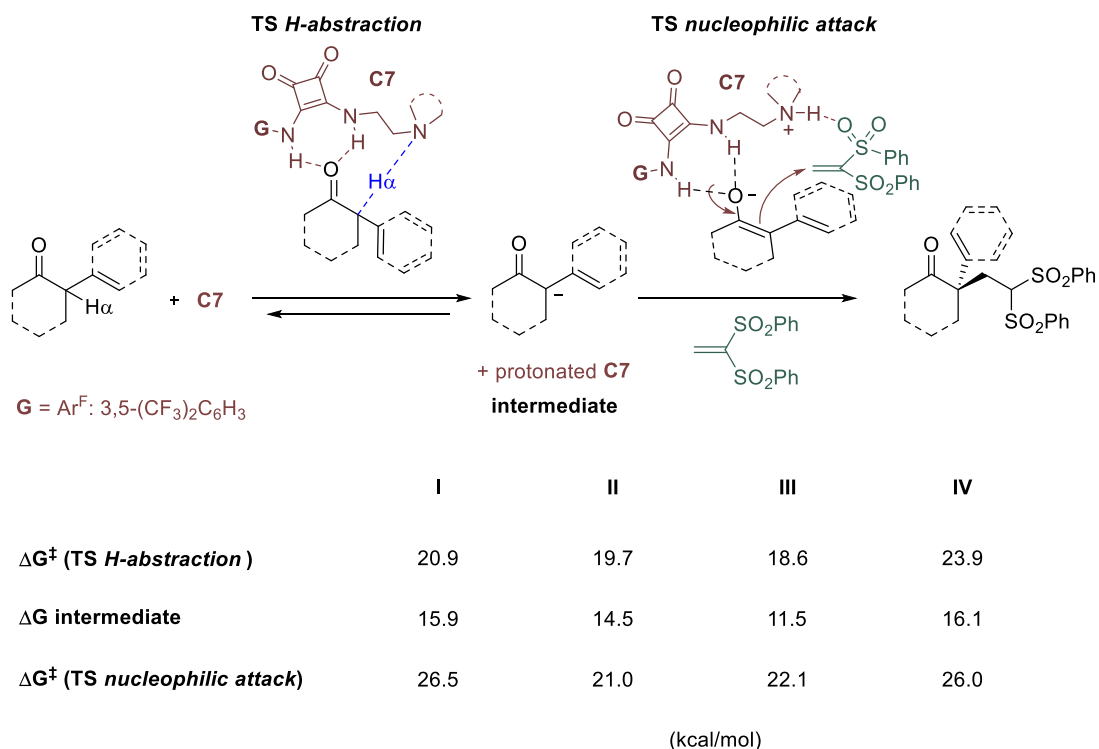


Figure 2.26 Energies for the reaction of ketones I-IV with bis-sulfone in presence of **C7**. All the energies are Gibbs Energies in kcal/mol.

To sum up, the results obtained in the computational analysis are in perfect agreement with the experimental evidence. The analysis carried out using the model catalyst **C0** influenced the choice of the substrate **III** for the development of the catalytic strategy. A more exhaustive analysis using the realistic catalyst **C7** added more information. Substrates **I** and **IV** should be excluded because their energetic profiles show high barriers for both steps of the reaction. The data are in agreement with the experimental results. Substrate **I** resulted to have very poor reactivity and stereocontrol. Substrate **IV** was subjected to the same reaction and did not show any reactivity (unpublished results).

The computational results identified **II** and **III** as potential candidates. Initially, Palomo group did not try any experiment with **II**, probably thinking to postpone this work for future studies. However, the work of Wang and co-workers⁶⁵ demonstrated that α -aryl cyclohexanones are suitable substrates for the asymmetric Michael addition with nitroolefins in the presence of bifunctional amine-thiourea leading to molecules bearing tertiary and quaternary stereocentres. The more challenging α -phenyl cyclohexanones were also investigated affording the desired product in very low yield (20%) even if with moderate enantiocontrol (*ee* 84%), when harsher conditions were applied ($T = 50^\circ\text{C}$) (Scheme 2.20). The studies of Wang group support the potential of α -substituted cyclohexanones emerged by our computational investigation.

The different behaviour of **II** observed with **C0** and **C7** makes us believe that the reactivity of this kind of substrate could be catalyst-dependent.

The reactivity of compound **III** is confirmed by calculations: both the α -deprotonation and the nucleophilic attack are feasible steps at the reaction conditions. This kind of

substrate resulted to be more reactive than the acyclic counterpart in this catalytic strategy because it has a lower energy barrier to overcome to get the desired product and the intermediate between one step and the other is located at lower energy influencing the efficiency of the second step.

2.2.5.3. α vs γ

To the best of our knowledge, no mechanistic investigation on the α/γ reactivity of ketone dienolates have been reported so far. Zanardi and co-workers performed a DFT analysis in support of the vinylogous reactivity of α -branched dienolates from alkylidene 2-oxindoles against nitroolefins affording γ -adducts exclusively.⁸⁷ In our case, α -substituted cyclic dienolates reacting with bis-sulfone yielded exclusively the α -adducts, with no evidence of γ -functionalisation products. Taking into consideration the linear dienolate **I** and its cyclic counterpart **III**, we computed their reactions with bis-sulfone in presence of the model catalyst **C0** undergoing the α - and γ -pathways. We found that for both substrates the α -addition is the preferred route. Indeed, for the linear dienolate the energy barrier for the α -adduct is 2.8 kcal/mol lower than the one for the γ -adduct. In the case of the cyclic substrate, the experimental evidence is totally supported by the computational results, because the difference in energy between the two routes is of 6.1 kcal/mol, a value that clearly highlights the preference of one pathway to the other (Figure 2.27).

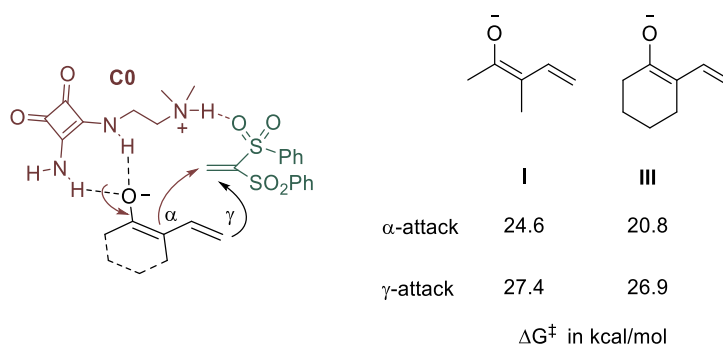


Figure 2.27 α - vs γ -reactivity of linear and cyclic α -substituted dienolates in presence of a model catalyst **C0**.

2.2.5.4. Stereoselectivity and H-bond network

The strategy reported by the group of Palomo provides the desired products in high stereoselectivity. The bifunctional Brønsted base/H-bond donor squaramide catalyst plays a determinant role in the stereocontrol of the reaction. We performed a computational analysis on the most favourable arrangement of the substrates and the catalyst during the transition state. DFT calculations were performed for the model reaction between the vinyl cyclohexanone enolate **III**, vinyl bis-sulfone **4** and either catalyst **C7** (**G**=Ar^F: 3,5-(CF₃)₂C₆H₃) or **C8** (**G**: ^tBu). The choice of the catalysts is dictated by practical considerations. Experimentally, they both give moderate (**C7**) or excellent (**C8**) enantioselectivity results, while keeping reasonable level of simplicity. They differ for the **G** substituent bound to a N atom of the squaramide unit; in **C7** the aromatic ring increases the rigidity of the structure, while **C8** bears the bulky ^tBu. We did not consider

other catalysts, as **C9**, which although performing in an excellent manner, have many groups free to rotate that would affect the calculations, in terms of convergence.

In this kind of bifunctional Brønsted base/H-bonding catalysis, the located TS structures show well defined H-bond networks that strongly bias the spatial arrangement of reactants, determining the stereochemical reaction outcome.

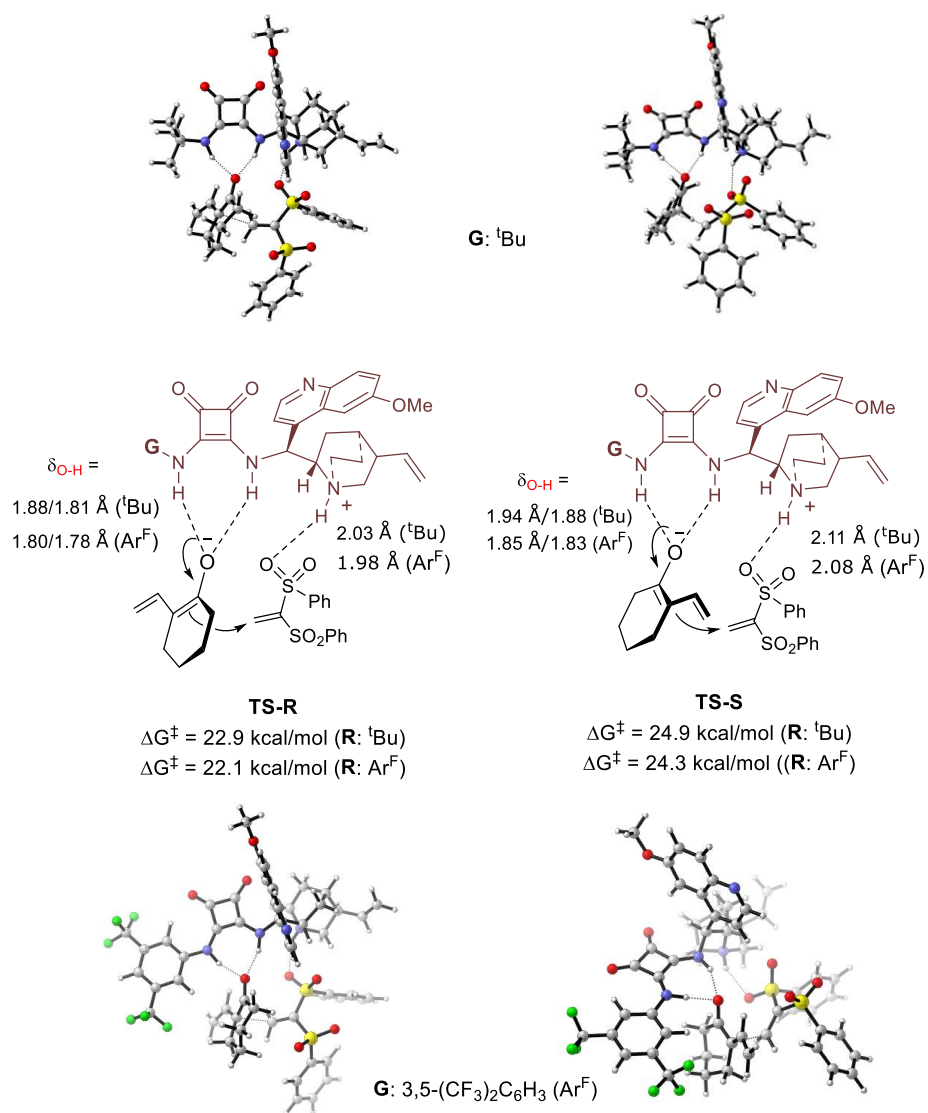
Takemoto and Pápai models are the most accepted in literature to define the H-bonding arrangements in bifunctional catalysis where proton transfer occurs (Chapter 2.1.3). We tried to compute the TSs for the two models, but it was possible to identify the two Pápai-type TSs exclusively, namely **TS-R**, leading to the R-configured product, and **TS-S**, leading to the S enantiomer, for each catalyst (Scheme 2.32). In these TSs the squaramide interacts with the enolate through the NH groups, while the protonated tertiary amine takes in place the sulfone, interacting with one of the oxygen atoms.

In spite of serious efforts, the alternative Takemoto-type activation mode TSs, with the sulfone oxygens hydrogen-bonded to the squaramide NH groups, could not be found, probably due to the low H-bond acceptor character and high steric hindrance of the sulfone group.

The energy values obtained are in agreement with the experimental observations; when catalyst **C7** is used, transition state **TS-R** presents the lowest activation energy, 22.1 kcal/mol, in comparison with 24.3 kcal/mol predicted for **TS-S**, while slightly higher values of 22.9 and 24.9 kcal/mol respectively, were obtained with catalyst **C8**. The lower barrier of **TS-R** can be associated to the stronger H-bonds (shorter XH---Y bonds) found for the interaction between oxanion **III** and the two squaramide NH moieties (1.80 and 1.78 Å for catalyst **C7**), in comparison to the values measured in **TS-S** (1.85 and 1.83 Å). Analogue trend in the presence of catalyst **C8**: 1.88 and 1.81 Å in **TS-R** against 1.94 and 1.88 Å in **TS-S**. Similarly, the weak interaction between one oxygen of the bis-sulfone group and the protonated amine group is weaker in **TS-S** vs **TS-R** (2.08 and 1.98 Å bond distances, respectively in **C7**; 2.11 and 2.03 Å, respectively, in **C8**). Comparing the behaviour of the two catalysts in the **TS-R**, it appears that in **C8** the H-bonds between dienolate oxygen and squaramide NH groups are slightly longer (1.88/1.81 Å vs 1.80/1.78 Å) indicating a worse accommodation of the large ^tBu group.

Based on these calculations, it seems that an optimally congested microenvironment is formed around the protonated catalyst **C7** for best fitting of both reactants through an efficient H-bond network.

2.2. Computational studies on the reactivity of α -branched ketone dienolates



Scheme 2.32 TS structures and selected parameters for the model reaction between α -branched dienolate **III** and bis(phenylsulfonyl)ethane.

2.2.6. Conclusion

This work has demonstrated that Brønsted base/H-bonding catalysis is a useful tool to perform Michael addition of challenging substrates, as unactivated α -substituted dienolates, affording adducts possessing an all-carbon quaternary centre. Cyclic skeleton in the ketone substrates turned out to be essential to allow the reaction to proceed and solve those issues that make α -substituted dienolates so challenging. Through a computational analysis, we found out that the difference in reactivity is not dependent on electronic properties. Indeed, it could not be confirmed that cyclic systems have higher nucleophilicity, as reported by Cunningham,⁹³ because charges and Fukui indices of the cyclic substrate and the acyclic counterpart are almost identical. Instead, we saw that structural factors are the most influential ones: the more rigidified transition state helps the efficient chirality transfer and the elimination of the E/Z uncertainty. The activation barrier found for the reaction of cyclic ketones computed with a model catalyst **C0** is lower than the one of the linear counterpart and it is feasible at the reaction conditions. The computational analysis carried out using a realistic catalyst as **C7** confirmed that the cyclic dienolate is a valid substrate and behaves better than the acyclic counterpart. The whole reaction pathway was considered and it emerged that for the cyclic dienolate the α -deprotonation occurs easily leading to a relatively stable intermediate that proceeds to the second step of the reaction with a feasible energy barrier, according to the room temperature reaction conditions. The energetic profile of the reaction of the cyclic dienolate is comparable with the one of the α -phenyl cyclopentanone, revealing the potential of this kind of substrate for future studies. This substrate was not investigated in the experimental part because the preliminary computational results with the model catalyst **C0** identified the cyclic dienolate as the best candidate for the development of the strategy. The reactivity of α -phenyl cyclopentanones is probably catalyst-dependent and deserves a deeper insight. The theoretical studies carried out on the dienolate systems are able to solve the ambiguity of α/γ selectivity and to rationalise the experimental evidence of exclusive formation of α -product. These results are in contrast with the majority of the methods that proceed instead mainly through the γ -carbon and this reactivity has been justified in some cases theoretically by DFT calculations.^{77,65} It is possible to understand that the reaction pathway of dienolate systems depends on the role of the catalyst as well as on the character of the reactants.

The action of the bifunctional catalyst is determinant for the stereoselectivity outcome. The computational results confirmed that the *R*-conformer is the preferred one, as found experimentally. Pápai model appears to describe properly and coherently our system. The NH groups of the squaramide interact with the oxygen of the dienolate, while the protonated tertiary amine group keeps in place the bis-sulfone H-binding one of the oxygen. The steric hindrance of the catalyst contributes to create the optimal microenvironment for best fitting the substrates through a H-bond network. The analysis was performed using two different catalysts. They had in common the same binding units, but they differ for the lateral substituent. We could observe the same trend in energies and in the H-bonding network, favouring the *R*-conformer.

2.3. Computational studies on the reactivity of transiently generated trienolates: Brønsted Base catalysed α -functionalisation and further elaboration.

2.3.1. Introduction

Trienolates and trienamines are substrates with structural similarities. While trienamines are known to be suitable substrates for Diels-Alder reactions, the chemistry and reactivity of trienolates are still poorly explored.

2.3.1.1. Trienamine mediated catalysis

As seen before, enamine mediated catalysis represents a useful method to perform C-C bond forming reactions starting from carbonyl compounds as pro-nucleophiles. Since 2000, the HOMO raising strategy has advanced from *enamines* to *dienamines*, and to higher level of *trienamines/cross-trienamines* (Figure 2.28). This approach allows to functionalise carbonyl compounds at more remote carbons as the γ - and ϵ -carbons.

In this section, we are going to limit the explanation to trienamines as objects of interest in our work.

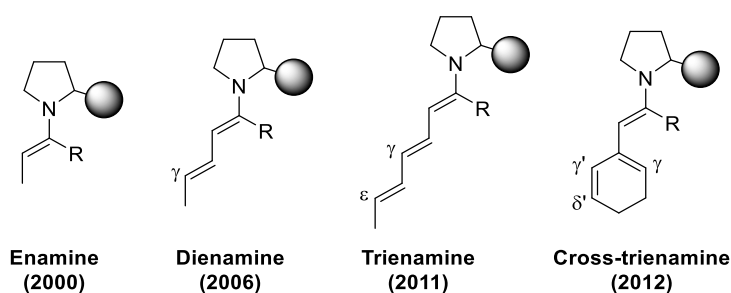
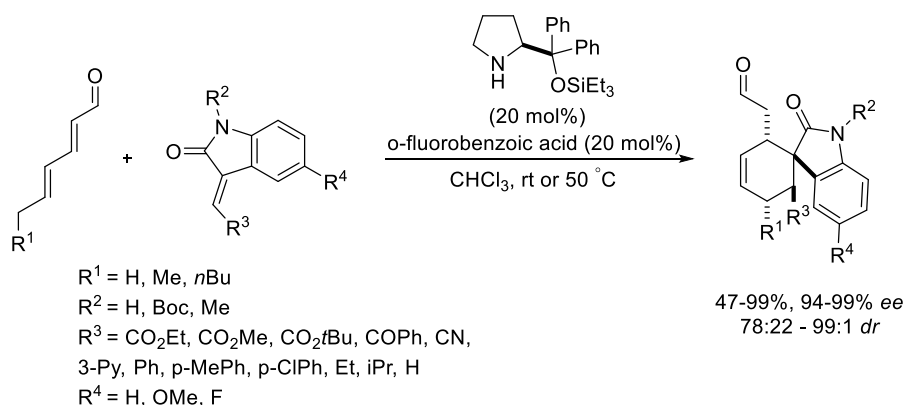


Figure 2.28 Advances in amine catalysis through HOMO-raising activation strategy.

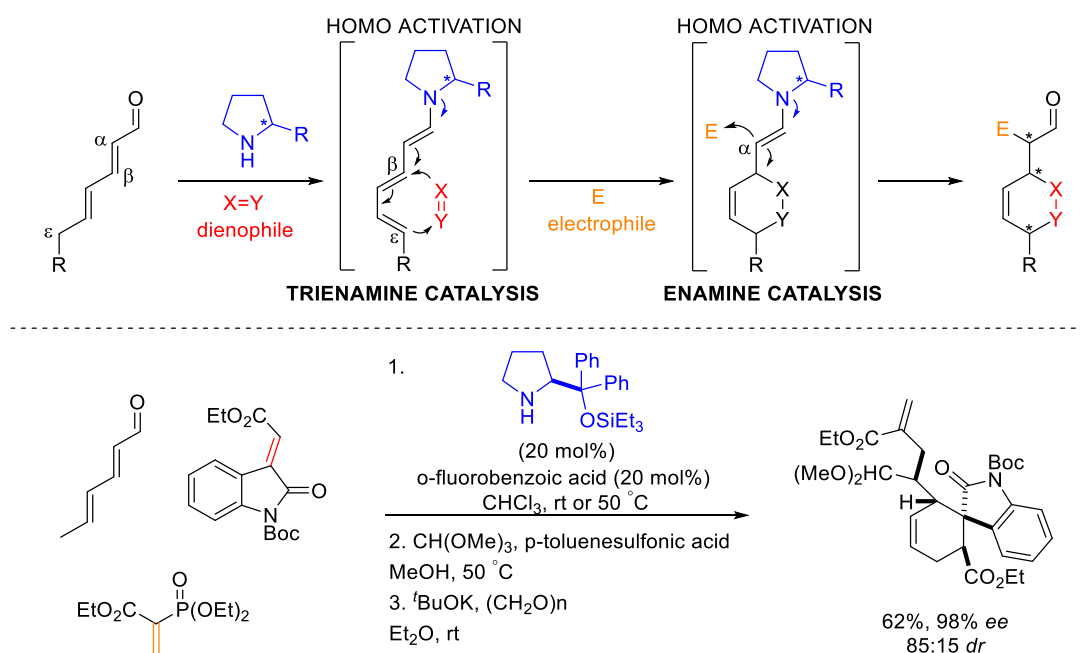
In 2011, the first trienamine catalysed Diels-Alder reaction between 2,4-dienals and electron deficient dienophiles, with ϵ -site-selectivity and high stereoselectivity was reported by Chen and Jørgensen (Scheme 2.33).⁹⁴



Scheme 2.33 First trienamine mediated catalytic Diels Alder by Chen and Jørgensen.⁹⁴

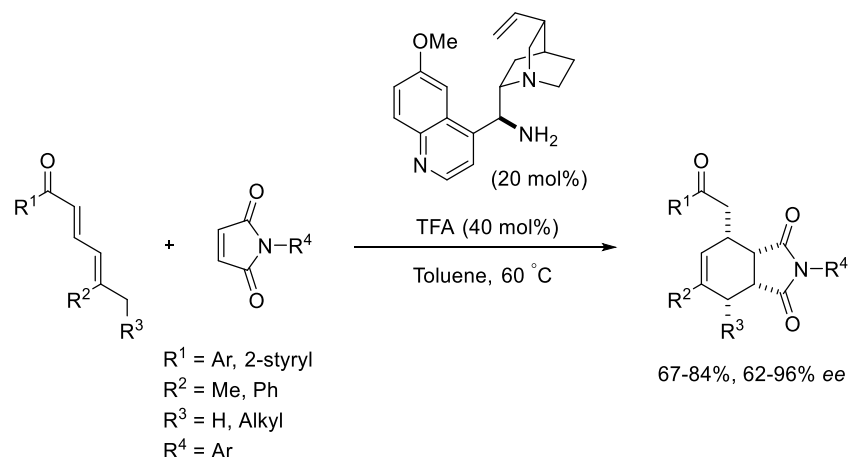
Since organocatalysis was proven to be a highly powerful tool in promoting enantioselective tandem reactions for the construction of complex molecules in a single manual operation, Chen and Jørgensen extended the applicability of trienamine catalysis to this

purpose, taking in consideration that the α -position of the aldehydes is available to react following an enamine pathway. They proposed that the organocatalyst could promote a double HOMO-activation of 2,4-dienals leading to a sequential and cycle specific trienamine and enamine tandem reaction (Scheme 2.34).



Scheme 2.34 Sequential and cycle specific trienamine and enamine tandem reaction by Chen and Jørgensen.

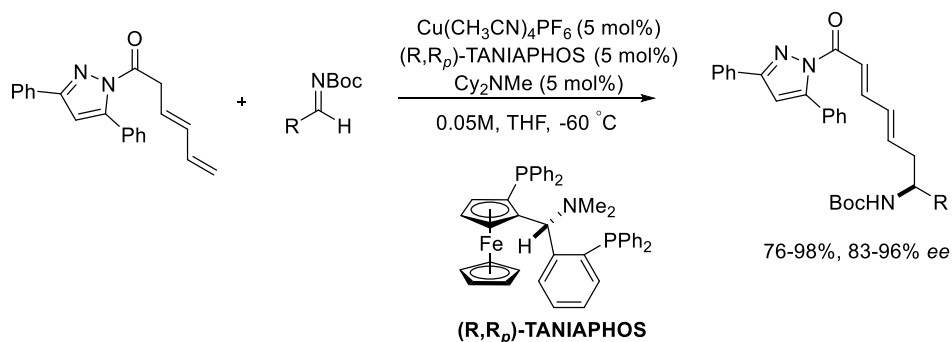
In the same year, Chen group expanded the scope of trienamine catalysis for asymmetric Diels-Alder reactions with nitroalkenes as dienophiles.⁹⁵ They found that 2,4-dienals need electron-donating alkyl substituents at C4 and C5 positions for the raising of the HOMO energy level of the trienamine intermediates and for the Diels-Alder reaction to occur. Chen and co-workers also developed a highly selective asymmetric Diels-Alder reaction of substituted 2,4-dienones as precursors for trienamine catalysis.⁹⁶ The trienamine intermediate is formed by condensation between α' -nonenolisable 2,4-dienones and cinchona alkaloid derived primary amine catalyst and δ,δ -disubstituted 2,4-dienones had to be used in order to avoid the 2,4-dienones acting as dienes in a noncatalysed cycloaddition reaction (Scheme 2.35).

Scheme 2.35 Trienamine mediated catalytic Diels Alder of 2,4-dienones by Chen *et al.*

2.3.1.2. Trienolate mediated catalysis

The limit of enamine mediated catalysis is its limitation to enolisable aldehydes and ketones. Even if the enolate chemistry is still less explored than that of the enamines, it is noteworthy that enolate strategy is quite versatile because it can be applied to other enolisable substrates such as carboxylic acid derivatives or non-carbonyl compounds. Enolate-based transformations are at the base of synthetic organic chemistry. Dienolates, owing an extra conjugated double bond, have larger reactivity because they can react with electrophiles from the α - or γ - position. The majority of the examples of reactions with dienolates proceeds through the γ -carbon.⁹⁷ Only a few examples of α -functionalisation have been reported by Shibasaki⁹⁸, Zhao⁸², Alemán^{78,79,99} and Palomo.⁸⁶

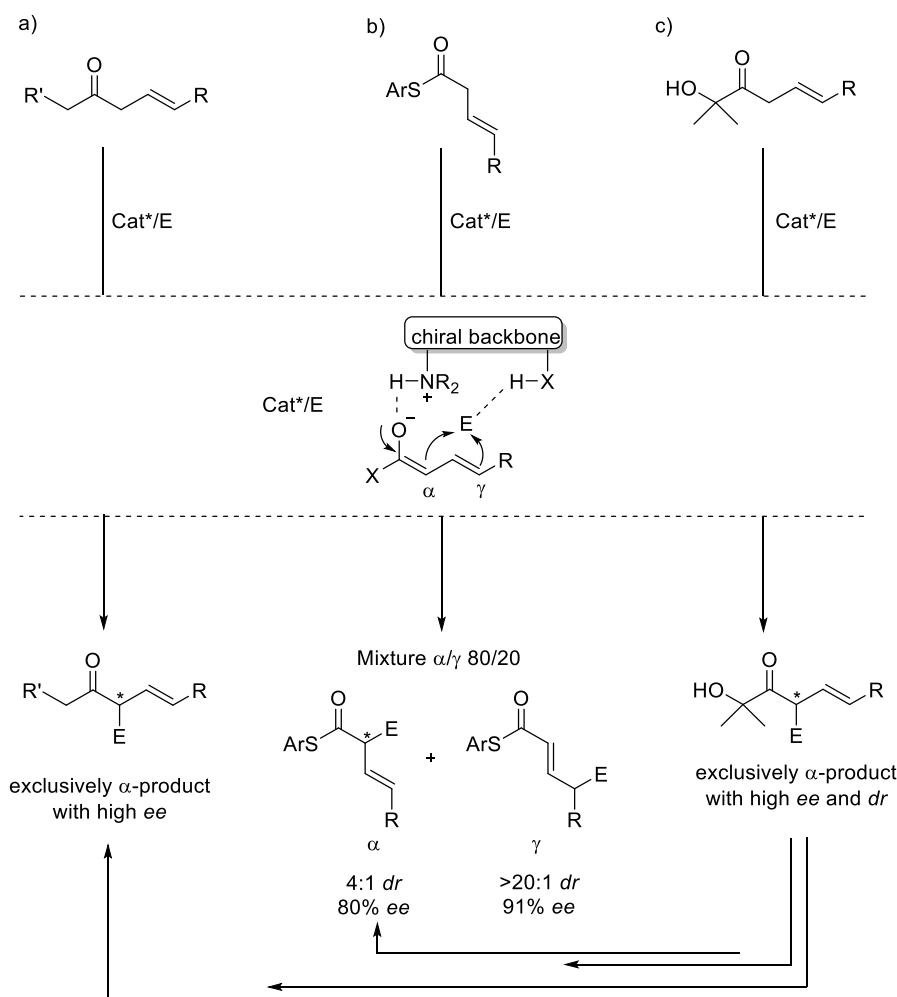
Adding another conjugated double bond to dienolates leads to the formation of trienolates. The chemistry involving this kind of compounds remains underdeveloped. A lithium trienolate formed from sorbic acid was reported to react with enones to give a mixture of regioisomeric products depending on the substituents of the acceptor.^{100,101} In 2017, Yin and co-workers reported the first catalytic and asymmetric direct functionalisation of transiently generated trienolates: an ϵ -selective catalytic asymmetric bisvinylogous Mannich reaction catalysed by a copper(I) complex (Scheme 2.36).¹⁰²

Scheme 2.36 ϵ -Selective catalytic asymmetric bisvinylogous Mannich reaction catalysed by a copper(I) complex by Yin *et al.*

2.3.2. Abstract

The group of Palomo is highly interested in studying new methodologies for the organocatalysed functionalisation of carbonyl compounds.

In 2017, they demonstrated that tertiary amine/squaramide bifunctional catalysts are capable of promoting the addition of β,γ -unsaturated ketones with nitroolefins exclusively in α with good enantio- and diastereocontrol. β,γ -Unsaturated thioesters, under similar catalytic conditions, gave instead a mixture of α - and γ -addition products. Instead, α -addition products were obtained if using β',γ' -unsaturated ketols as equivalents of β,γ -unsaturated esters (Scheme 2.37).⁸⁶

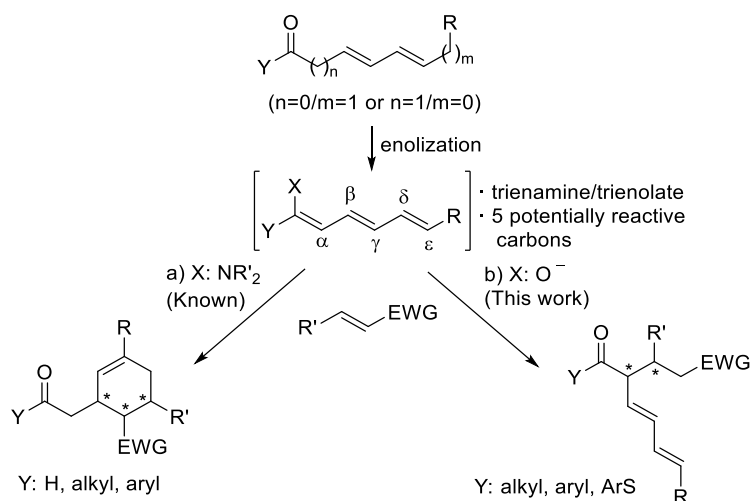


Scheme 2.37 BB/H-bond donor catalysed addition of β,γ -unsaturated substrates with nitroolefins by Palomo *et al.*

Tertiary amine/squaramide bifunctional catalysts demonstrated to be good tools to induce α -addition selectively. Intrigued by the fact that no catalytic and asymmetric direct functionalisation of trienolates is reported, Dr. Igor Iriarte and Dr. Olatz Olaizola started working in expanding the applicability of the strategy and they focused on the study of the reactivity of trienolates with nitroolefins, under bifunctional Brønsted base/H-bond donor catalysis.

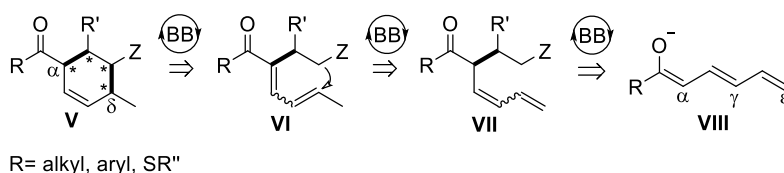
We performed some calculations of the nucleophilicity of the substrates that encouraged the group to undertake the experimental study. The reactions resulted to

be completely regioselective and the nucleophilic attack of the transiently generated trienolates proceeded through the C α exclusively. This reactivity is divergent from that shown by trienamine intermediates transiently generated in aminocatalytic reactions, which instead follow a Diels-Alder reaction pathway (Scheme 2.38).



Scheme 2.38 Difference in reactivity between trienamines and trienolates.

Interestingly, the trienolates were found to be precursors of an unprecedented one-pot catalytic, enantio- and diastereoselective synthesis of stereodefined six-member carbocycles featuring i) a highly enantioselective α -addition of transiently generated trienolates to nitroolefins; ii) a catalytic intramolecular 1,6-addition with high stereocontrol and iii) two intermediate isomerisations promoted by Brønsted base catalysts (Scheme 2.39).



Scheme 2.39 Retrosynthetic pathway of the one-pot catalytic, enantio- and diastereoselective synthesis of stereodefined six-member carbocycles.

2.3.3. Objectives

Being trienolates challenging substrates, we thought that a computational analysis could help in driving some choices in the experimental work. Furthermore, we wanted to provide a rationale for the divergent reactivity of trienolates and trienamines at comparison.

In the first part of our computational studies, we focused on computing electronic properties, as charges and nucleophilicity indices, of different substrates: trienoates (in the alkoxy and salt forms) and trienamine with the purpose of getting preliminary data about the reactivity of these poorly explored substrates. Then, to examine in depth the potential divergent reactivity of the substrates, both Michael addition and Diels Alder mechanisms were computed for trienolates and model trienamine systems reacting with a nitroolefin.

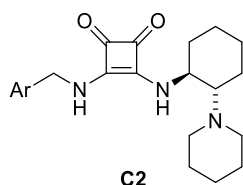
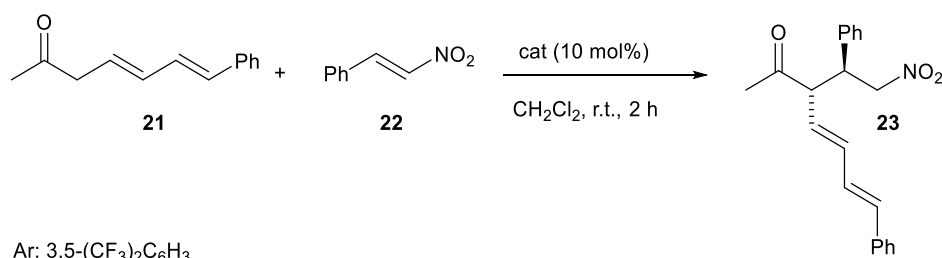
In the second part, after having confirmed trienolates to be suitable for α -functionalisation, we focused on studying the mechanism of the bifunctional BB catalysed Michael addition, studying the interaction between the catalyst and the substrates to justify the enantioselectivity found experimentally.¹⁰³

In the third part, we focused on the intramolecular 1,6-addition, final step of the one-pot six-member carbocycles synthesis, and explained the stereoselectivity observed in the final products.

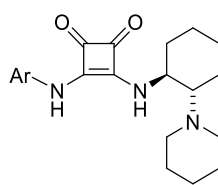
2.3.4. Experimental work

The experimental work was carried out by Dr. Igor Iriarte and Dr. Olatz Olaizola of the group of Prof. Palomo, who provided us with the data we needed to perform our computational investigation.

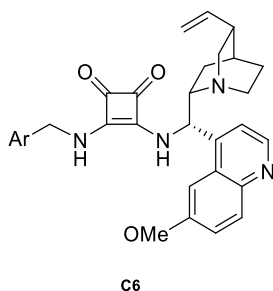
After the work of dienolates,⁸⁶ Palomo group expanded the area of organocatalysed functionalisation of carbonyl compounds focusing on transiently generated trienolates. The experimental study started by evaluating several available bifunctional Brønsted base catalysts for the reaction between doubly unsaturated methyl ketone **21** and (*E*)-nitrostyrene **22**. Products derived by the attack at C α of the ketone were obtained exclusively, although with variable diastereo- and enantioselectivities. The catalyst **C2** in Table 2.3 showed the best performance with increased selectivity lowering the temperature to -10°C. With these conditions in hand, a series of doubly unsaturated enolisable ketones were subjected to the reaction with nitroalkenes.

Table 2.3 Catalyst screening for the addition of **21** to **22** leading to **23**.^a

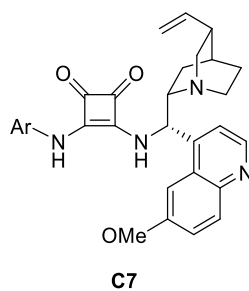
75%, dr 5.7:1, 99% ee
 70%, dr 4:1, 99% ee (toluene, r.t.)
 83%, dr 11.5:1, 98% ee (toluene, -10 °C, 24 h)



81%, dr 1.2:1, 77% ee



76%, dr 3:1, 82% ee



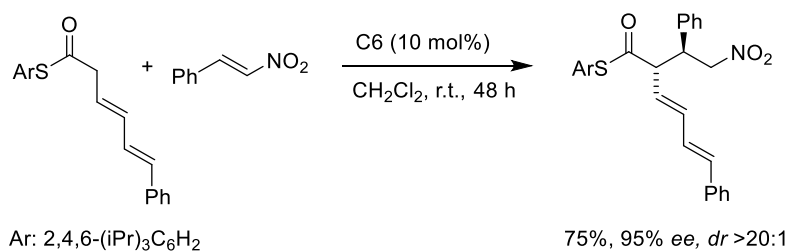
70%, dr 1.6:1, 90% ee

^aReactions carried out on 0.2 mmol scale, with **21** (1.5 equiv.) and catalyst (10 mol%) in CH₂Cl₂. Diastereomeric ratio and *ee* values determined by HPLC analysis on a chiral stationary phase. The *ee* values of the major diastereomers are given.

Various alkenes were suitable, electron rich (4-MeOC₆H₄ and 3-MeOC₆H₄) and poor (4-ClOC₆H₄) β-aryl substituents as well as β-alkyl (CH₃(CH₂)₂ and *i*Bu) substituents were tolerated.

Regarding the ketones, phenyl and tolyl ketones worked uniformly well and aliphatic groups attached at the distal carbon were tolerated too. Finally, high yields and selectivities were achieved with the corresponding ethyl, phenethyl and cyclohexyl ketones, which afforded the α-addition products exclusively, without detecting any α'-addition side product formation.

While thioesters are unable to be activated *via* enamine mediated catalysis, screening experiments carried out with several β,γ- and δ,ε-doubly unsaturated aryl thioesters provided evidence for the formation of the α-addition adducts exclusively. The stereoselectivity could be optimised by varying the thioester aryl group, with the 2,4,6-triisopropylphenyl group resulting the best. For the reaction in Scheme 2.40, it was found that the cinchona-derived catalyst **C6** was a more efficient chiral inductor, affording product in 95% *ee*, instead of 85% *ee* with **C2**. Substrate scope was explored and revealed the suitability of various β-aryl-substituted (4-MeOC₆H₄, 3-MeOC₆H₄, 4-ClC₆H₄, 3-ClC₆H₄, 2-ClC₆H₄) nitroalkenes and di-unsaturated thioester combinations.



Scheme 2.40 BB/H-bond donor catalysed addition of β,γ - and δ,ϵ -doubly unsaturated aryl thioesters to nitroolefin.

Further investigations on the applicability of the resulting α -functionalised products were carried out.

Surprisingly Palomo and co-workers found out that the adducts obtained in the trienolate mediated Michael reaction could potentially be precursors of cyclohexenes upon base-catalysed isomerisation of the double bonds and subsequent intramolecular 1,6-addition (Figure 2.29). They developed a one-pot catalytic, enantio- and diastereoselective synthesis of stereodefined six-member carbocycles using only Brønsted base catalysts as the only promoters. The unprecedented intramolecular 1,6-addition step makes the strategy very innovative and it encouraged them to expand the scope.

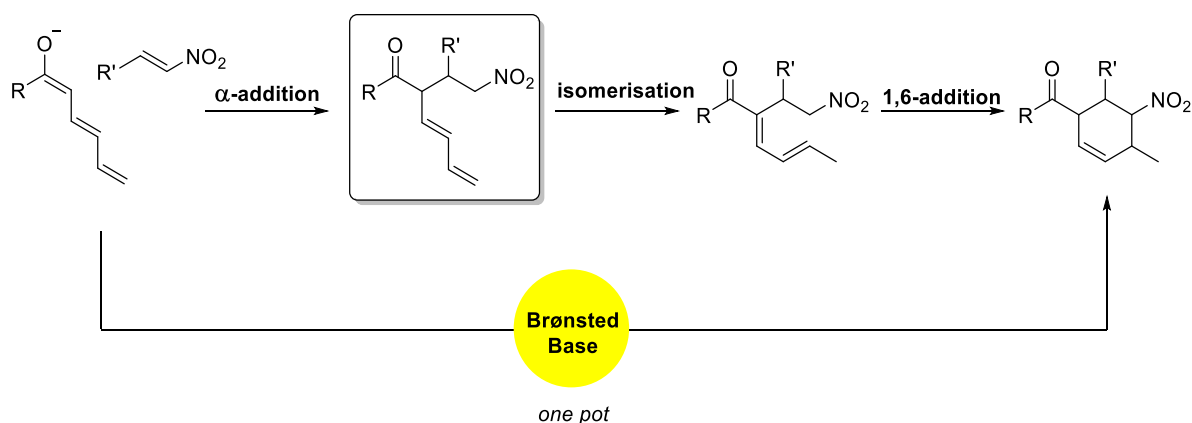
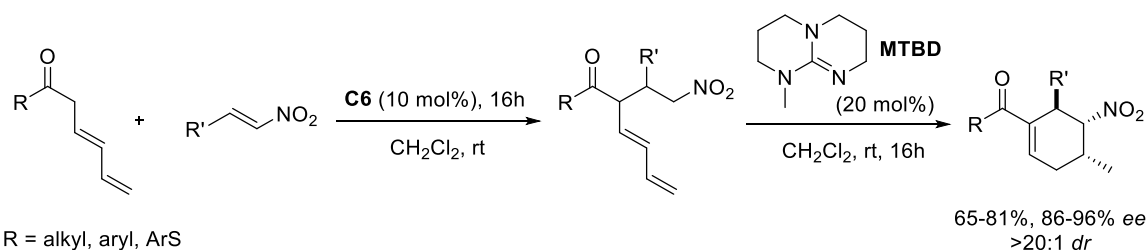


Figure 2.29 One-pot catalytic, enantio- and diastereoselective synthesis of stereodefined six-member carbocycles.

After the evaluation of several bases, they observed that catalysts **C2-C3-C6-C7** promoted the α -selective functionalisation of unsaturated ketones with nitroolefins in 16h at room temperature. Next, MTBD was added to the reaction mixture to promote the isomerisation of the adduct to obtain the final cyclohexene as an essentially single diastereomer. The enantioselectivity of the process was strongly dependent on the catalyst and catalyst **C6** emerged to be the one giving the best performance (75%, >20:1 *dr*, 90% *ee*). Using substrates bearing aliphatic R groups of different length did not affect the regio- and stereochemical outcome of the reaction and branched chains were tolerated too. As in the α -functionalisation step, chloro- and methoxy- substituted nitrostyrenes were suitable substrates for the one-pot strategy.

The Brønsted base-catalysed one-pot access to cyclohexene systems *via in situ* generated trienolates is not limited to doubly unsaturated alkyl ketones, but also

suitable to other unsaturated carbonyl compounds, as thioesters and aryl ketones under similar conditions, affording cyclohexenes in very good yields and enantioselectivity, and essentially as a single diastereomer (Scheme 2.41).



Scheme 2.41 Suitability of the Brønsted base-catalysed one pot strategy to various unsaturated carbonyl compounds.

2.3.5. Computational work

2.3.5.1. Methods

All structures were initially optimised using density functional theory (DFT) with B3LYP and the 6-31G(d,p) basis set as implemented in Gaussian 16. Final energies were calculated at M06-2X/def2tzvpp level of theory, in a solvent model (IEFPCM, solvent=dichloromethane). The stationary points were characterised by frequency calculations in order to verify that they have the right number of imaginary frequencies. The calculation of the atomic charges and Fukui indices was carried out through Natural Bond Orbital analysis. For additional information, see Chapter 1.

2.3.5.2. Trienamines vs trienolates

To help Palomo group to have some preliminary data regarding the reactivity of trienolates before starting to investigate them experimentally, we decided to compute some electronic properties of different trienolates **IX**, **X**, **XI** and the corresponding trienamine **XII**. We hypothesised that the reactivity of these compounds could be related to their nucleophilicity at the different C atoms. We computed the charge distribution and calculated the Fukui nucleophilicity indices (f^-) for the significant carbon atoms. The data in Figure 2.30 show that in trienolates (in the alkoxy and salt forms), the most negative Fukui index corresponds to the α -carbon with values between -0.23 and -0.28. The indices at the C_γ are lower by 0.02-0.03 units (more positive) and the values at C_ϵ differ for 0.02-0.03 units from the C_γ ones (in the alkoxy forms, more in the salts). The trend observed suggests a decreasing nucleophilicity in the order $C_\alpha > C_\gamma > C_\epsilon$. This result supports a α -selectivity preference for trienolates. The highest nucleophilicity index for the C_α of trienolate **I** compared to the others could be explained by the absence of heteroatoms as substituents at the carbonyl that could interfere with the charge distribution along the trienolate skeleton.

The nucleophilicity profile is different in the case of trienamine **XII**, for which the γ -carbon has the highest calculated electronic charge, with a Fukui index of -0.20. The nucleophilicity indices at the other C atoms are smaller by 0.02 units. This result is in agreement with the γ - and γ,ϵ -reactivities observed experimentally for trienamines.

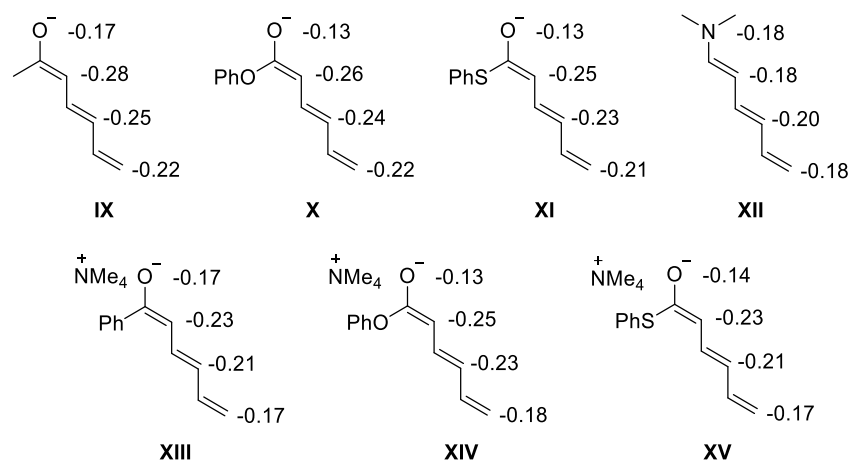


Figure 2.30 Fukui indices of relevant trienolates (alkoxy or ammonium salt form) and trienamine.

Trienolates and enamines have structural analogies and they both are potential starting materials for Diels Alder reaction and Michael addition. The mechanisms of the reactions of an unsaturated alkyl ketone and a model unsaturated alkyl trienamine compound with a nitroolefin are investigated computationally. The energies of the molecules, orbitals energies and atoms charges were computed in order to define the mechanism, Fukui indices and nucleophilicity/electrophilicity characters.

In this first part, the catalyst was not considered because our interest was focused on the reactivity of the free substrates.

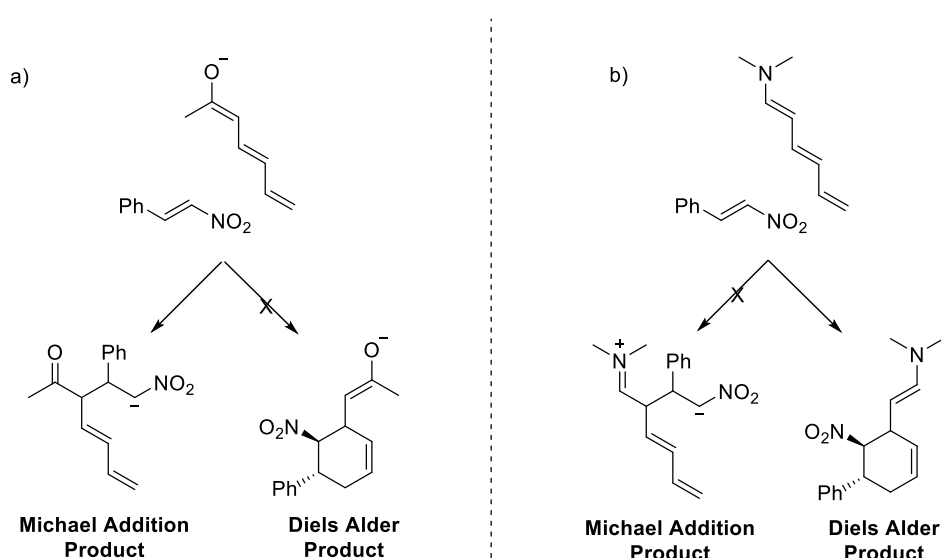
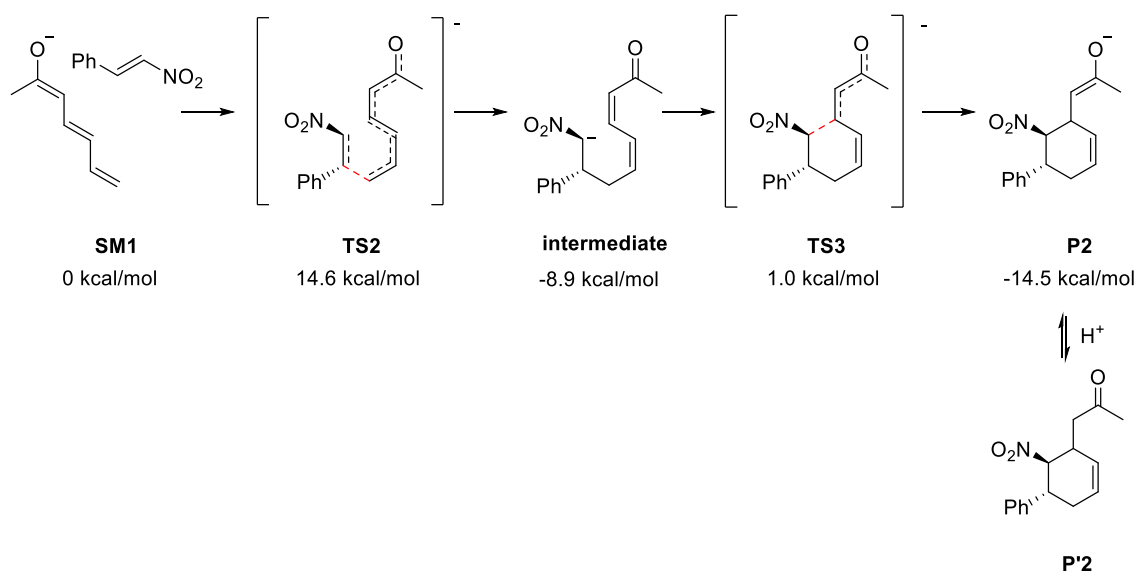


Figure 2.31 Potential reactivity of a) trienolates and b) trienamines with nitroolefins.

Experimentally, Palomo and co-workers performed the reaction in Figure 2.31a obtaining only the Michael addition product, as expected from the charge distribution depicted in Figure 2.30. We computed the energies of starting materials, transition states and products for both the potential reactions to evaluate the energetics of the two pathways.

In Scheme 2.42, the Michael addition mechanism is represented. All the energies are calculated considering the sum of the energies of the enolate and the nitroolefin as the



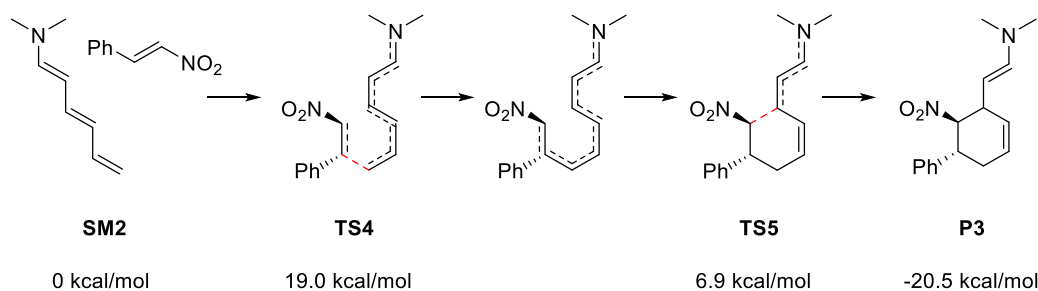
Scheme 2.43 Mechanism of Diels Alder reaction of trienolate and nitroolefin. The energies are Gibbs Energies in kcal/mol.

Summing up, the Michael reaction is the preferred pathway for trienolates reacting with nitroolefins, as predicted from the Fukui index values. The C_{α} is the most nucleophilic and has high tendency to react with the electrophile. The energy barrier is very low, 4.3 kcal/mol, allowing to perform this reaction at mild conditions. The Diels Alder reaction is a potential pathway for this kind of substrates because the energy barrier of 14.6 kcal/mol would be accessible at the working conditions, but since it is much higher than the one of the Michael addition, it does not occur.

The same calculations were performed on the reactions in Figure 2.31b, in which we considered a model trienamine compound and nitrostyrene as starting materials. Experimentally, trienamines are known to undergo preferentially the Diels-Alder reaction but, for the sake of computational cost, the chosen model substrate does not contain a sterically hindered amine, so it would not be surprising to get similar energy values for the Diels Alder and Michael addition routes.

First, we computed energy values of the starting materials, transition states and product for the Diels Alder reaction. The mechanism resulted to be stepwise, as in the case of trienolate substrates (Scheme 2.44). The first C-C bond formation is the rate-determining step (**TS4**), with an activation energy of 19.0 kcal/mol. The activation energy is coherent with the experimental conditions; indeed, the reactions are carried out at 55-60°C. The formation of the second C-C bond occurs immediately after the formation of the first one, demonstrated by the impossibility to locate the intermediate between one step and the other. The reaction is exergonic and leads to the formation of the cyclic product.

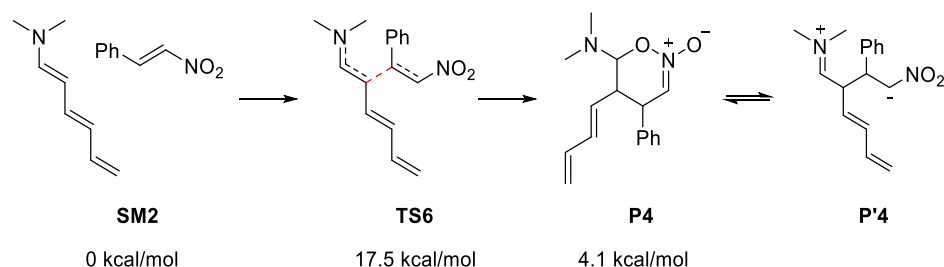
2.3. Computational studies on the reactivity of transiently generated trienolates



Scheme 2.44 Mechanism of Diels Alder reaction of trienamine and nitroolefin. The energies are Gibbs Energies in kcal/mol.

Finally, the Michael addition between the model trienamine and nitrostyrene was computed, and the energetic pathway is represented in Scheme 2.45. The mechanism is single-step with an activation barrier of 17.5 kcal/mol.

We did not succeed to optimise the expected Michael addition product **P'4**, probably because of its instability due to the high charge separation in the molecule. Instead, we obtained the optimised structure of product **P4**, which is in equilibrium with the expected **P'4**. In this case, the reaction is endergonic, the reaction is not favoured thermodynamically because of the formation of a high charge separation during the process that persists in product **P4**, making it less stable than the reagents.



Scheme 2.45 Mechanism of Michael addition of trienamine to nitroolefin. The energies are Gibbs Energies in kcal/mol.

In the case of trienamines, the computed activation energies of Diels-Alder and Michael addition are very similar ($\Delta\Delta G^\ddagger = 1.5$ kcal/mol) and they are not indicative of the preferred reactivity of these substrates. The first noteworthy observation is that the model trienamine is lacking the usual steric hindrance around the amine that would make the C α hardly accessible. Further calculations would be needed to evaluate the importance of the substituents at the N atom.

Since the reason that differentiates the reaction routes is not kinetic, it is reasonable considering the thermodynamics. While the Diels-Alder reaction leads to a stable cyclic product through an exergonic pathway, the Michael addition results to be endergonic leading to the formation of an unstable product owing a high charge separation.

Also thioesters were tested as suitable substrates for this kind of reactivity and showed the same charge distribution trend as the unsaturated ketones (Figure 2.30). As explained in the introduction, the bifunctional catalyst is capable of positioning the

substrates at a suitable distance to undergo the preferred reaction. In the case of trienolates, C_α , C_γ and C_ϵ are all accessible sites (Figure 2.32). Without considering the catalyst, we calculated the energy barriers for the addition reactions from the three available sites of thioester **XI** to the nitroolefin. Also with these substrates, the reaction at the C_α is the preferred one, with the lowest energy barrier, at least 2 kcal/mol lower than the other two routes, in accordance with the calculated Fukui indices. The energy barriers found for the functionalisation reactions in C_α , C_γ and C_ϵ justify the experimental evidence of α -functionalisation product exclusively.

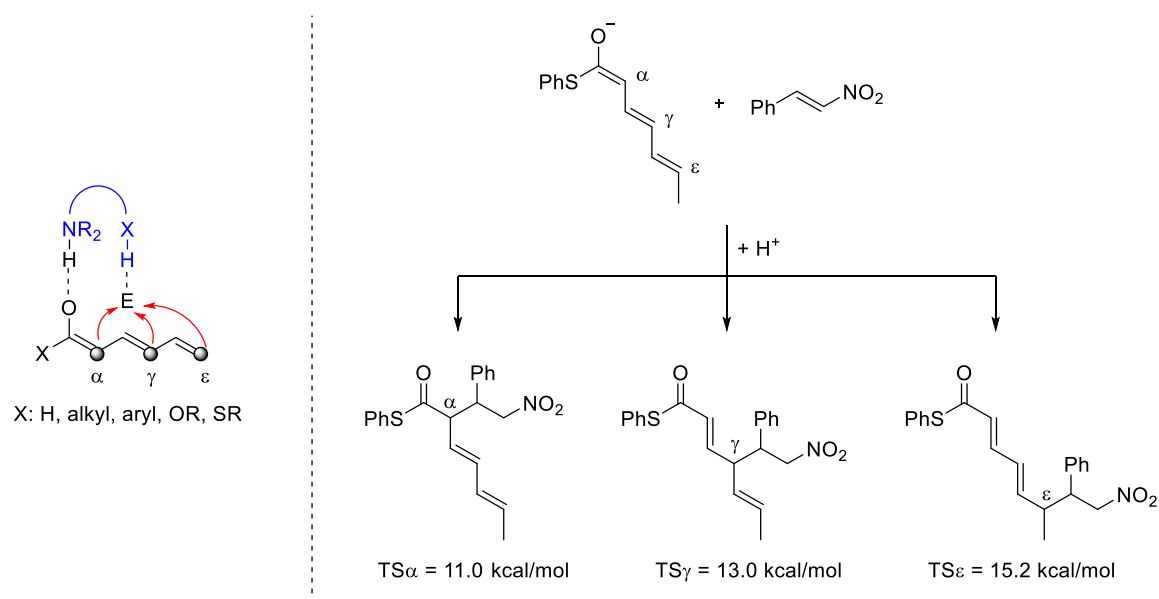


Figure 2.32 Generic bifunctional activation model involving trienolates (on the left); activation energies of the transition states of the reaction of nitrostyrene with thioester enolate **XI** through C_α , C_γ and C_ϵ , respectively (on the right).

2.3.5.3. Action of the bifunctional catalyst and stereocontrol

The squaramide/H-bond donor bifunctional catalyst plays high stereocontrol on the reaction. A computational analysis was carried out to investigate how the substrates interact with the chiral catalyst during the stereo-determining C-C bond forming step. The possible transition state energies and geometries were calculated for the reaction between trienolate **IX** and nitrostyrene in the presence of catalyst **C2**, selected as model reaction. Among all the catalysts examined, given that experimentally all four chiral catalysts **C2-C3-C6-C7** induced the same sense of enantioselectivity, **C2** was selected for this study due to its computational simplicity and reliability. It features comparatively less conformational complications than **C6**.

Each of the reactants orientations leading to the four possible stereoisomers were investigated considering the two most commonly accepted modes of activation, Takemoto and Pápai models (Figure 2.33). Following Pápai-type activation mode (**TS7-TS10**) the enolate substrate interacts with squaramide moiety of the catalyst *via* two H-bonds. The nitroalkene instead is stabilised by a H-bond by the protonated ammonium group. Among the calculated transition states within this model, **TS7** has the lowest activation barrier, thus correctly predicting major formation of *S,S*-adduct. On the other hand, Takemoto-type transition states (**TS11-TS12**) showed activation energies higher

than the corresponding Pápai type TSs, and very poor stereoselectivity, thus allowing us to sum up that the observed stereochemistry is best described by a Pápai-type activation mode. Not all the Takemoto-type TSs leading to the four stereoisomers could be found due to convergence problems. This supports the fact that Pápai model is the most suitable for this kind of reaction because allows to locate all the TSs and compare the energies between them.

Considering that Pápai model is the one activating the substrates in this Michael addition, we could focus only on the **TS7-TS10** and compare their energies to get some details related to experimental *ee* and *dr* values.

TS7 and **TS9** are the transition states that lead to two enantiomers, *S,S* configuration and *R,R* configuration. The difference in energy between them is 2.8 kcal/mol and taking into account that "at 298 K, every error of ca. 1.4 kcal/in predicted relative energies between two TS structures will change the ratios of predicted products by an order of magnitude",¹⁰⁵ it is possible to conclude that the results we got are in perfect agreement with the experimental results (86-96% *ee*).

TS8 and **TS10** are the transition states that lead to diastereoisomers of the *S,S*-product (deriving from **TS7**). They differ from **TS7** by 1.1 kcal/mol and 3.9 kcal/mol respectively. These values of energy justify the experimental *dr* values obtained.

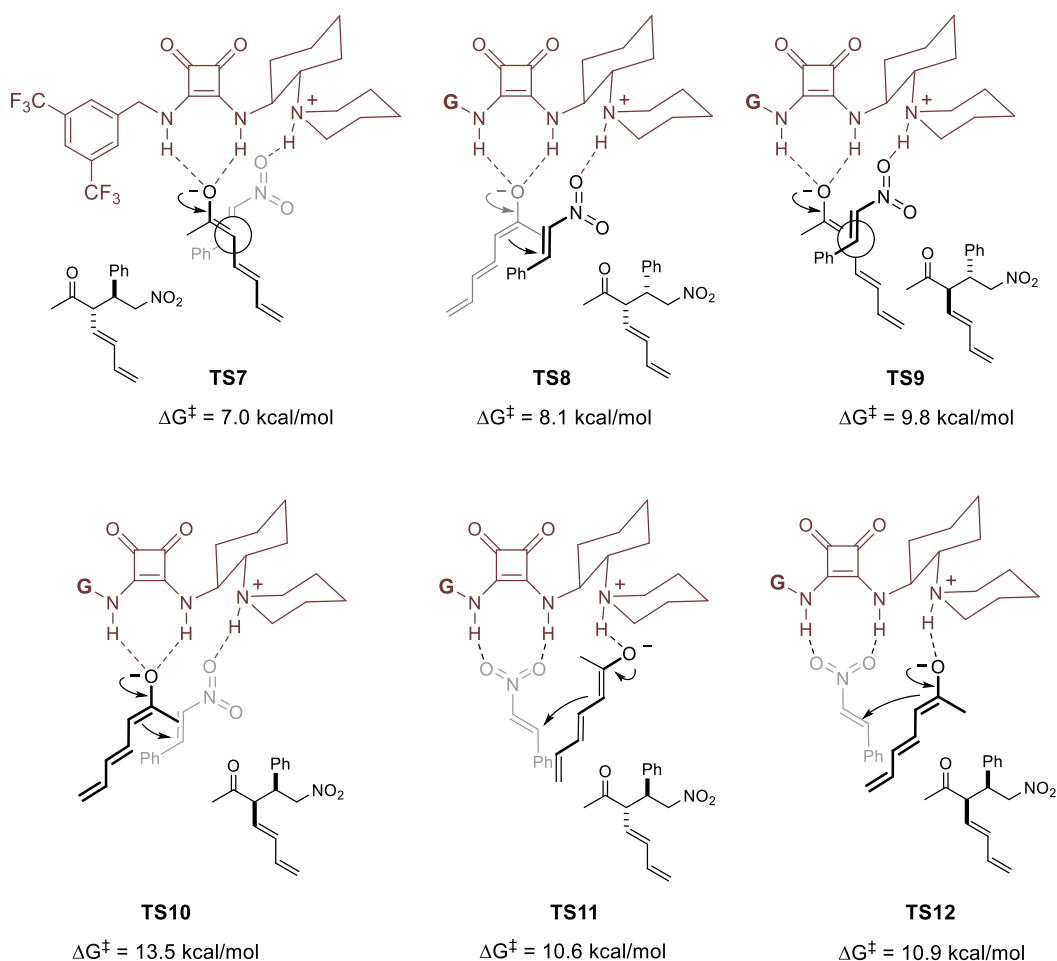


Figure 2.33 Geometries and Gibbs energies of the located TS for the catalysed reaction.

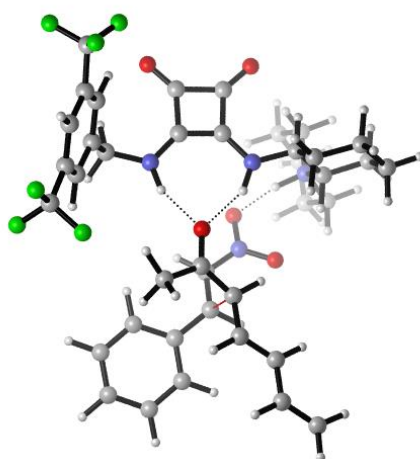
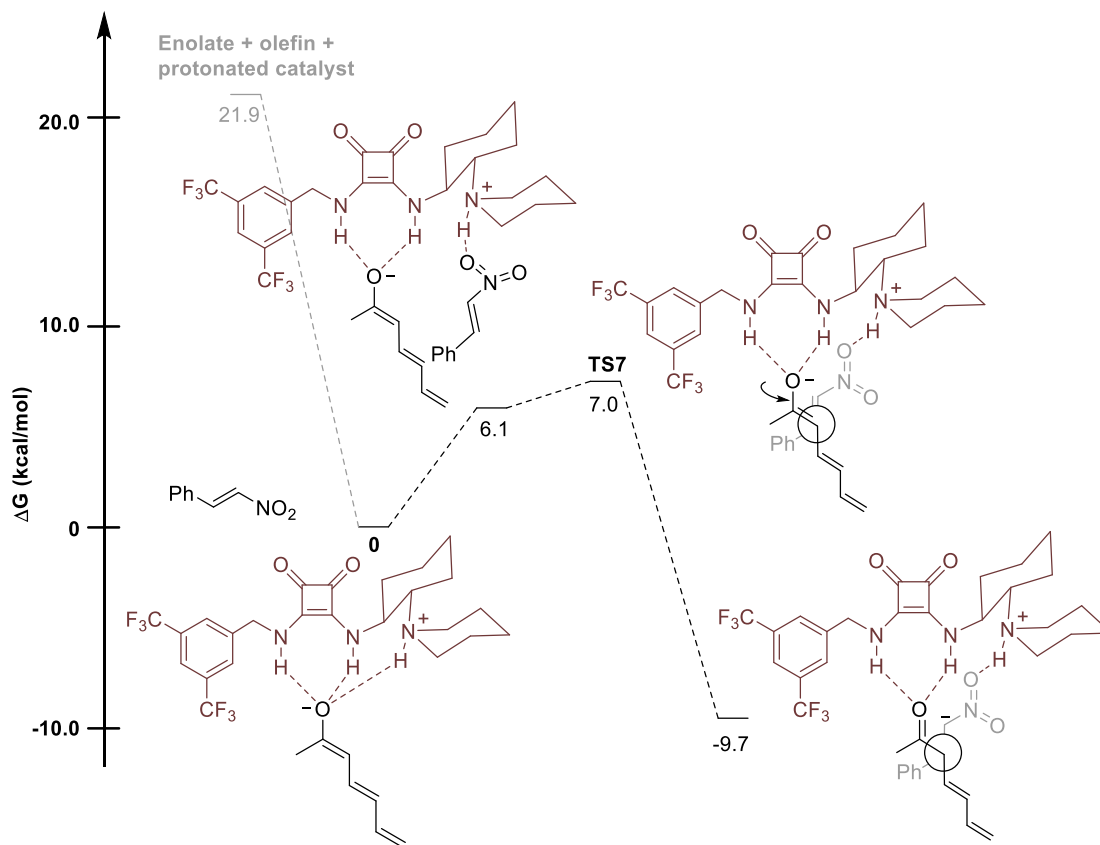


Figure 2.34 Optimised structure of **TS7**, the most stable TS leading to *S,S*-conformer.

The energetic profile of **C2**-catalysed Michael addition of trienolate **IX** and nitrostyrene leading to *S,S*-conformer product is reported in Scheme 2.46.



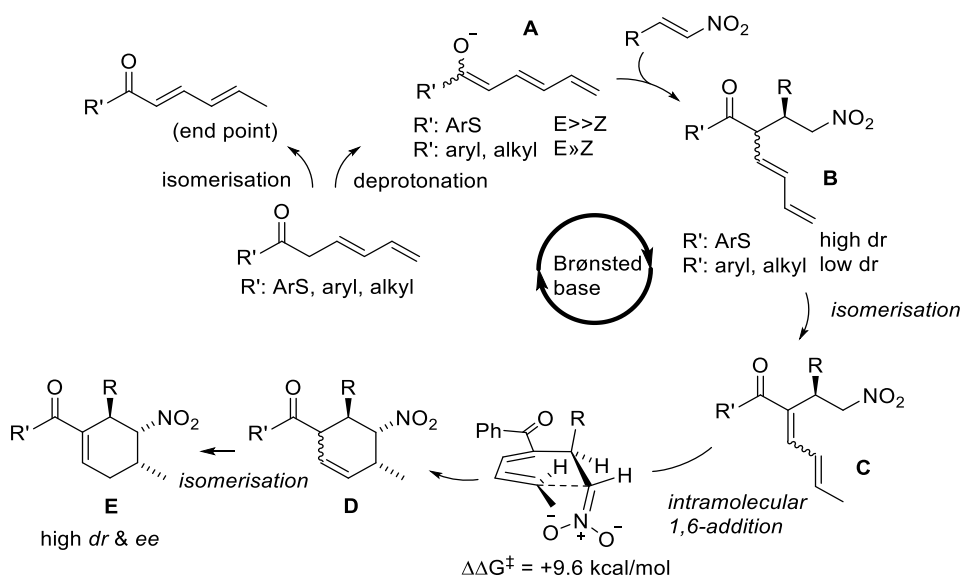
Scheme 2.46 Energetic profile of **C2**-catalysed Michael addition of trienolate **IX** and nitrostyrene. The energies are Gibbs energies in kcal/mol.

The sum of the energies of the trienolate, the nitroolefin and the protonated catalyst is quite high and cannot be taken as reference point for the energetic profile in Scheme 2.46. Instead, it is evident that the coordination of the enolate by the catalyst lowers down significantly the energy of the starting materials. The sum of the energy of nitroolefin and the complex trienolate-catalyst was taken as reference point ($\Delta G = 0$

kcal/mol). When the nitroalkene enters to take part in the coordination, an intermediate is formed with higher energy (6.1 kcal/mol). Following Pápai's model, the squaramide keeps in place the enolate, while the protonated amine coordinates the alkene. Once the substrates are set and oriented in the favourable arrangement, the C-C bond formation can occur. Among the TSs computed (Figure 2.33), **TS7**, the most stable one, is represented in Scheme 2.46, which leads to the formation of the *S,S*-conformer after overcoming an energy barrier of 7.0 kcal/mol, in agreement with the experimental results. The reaction is exergonic.

2.3.5.4. One pot cyclohexenes synthesis – intramolecular 1,6-addition

As described above, α -functionalisation products have been found to be valuable precursors for the synthesis of stereodefined six-member carbocycles, with Brønsted base catalysis as the unified mode of activation. To rationalise the experimental observations, Palomo and co-workers proposed the mechanism outlined in Scheme 2.47.



Scheme 2.47 Plausible pathway of the one-pot reactions sequence.

First, the tertiary amine unit of the catalyst deprotonates the unsaturated ketone/thioester to render trienolate intermediate **A**, which reacts with the alkene at the α preferentially. At this point, an isomerisation of the double bond occurs to give the conjugated dienone/dienoate **C**. This substrate is able to cyclise through a base-promoted intramolecular 1,6-addition (**D**). Finally, the α,β -conjugation is re-established after isomerisation of the double bond. While the asymmetric catalyst is essential for the stereocontrol in the α -functionalisation step, the last steps (from **B** to **E**) proceed only in presence of a stronger base, as MTBD, which catalyses the isomerisations.

The stereochemistry of the carbocyclisation process resulted to be substrate-controlled, depending on the approach of dienone and nitronate and not on the chiral catalyst. Experimentally, they obtained high values of enantiomeric excess and diastereomeric ratios. To get further insights about the factors that govern the high stereocontrol of the process, the energies of the TS for the carbocyclisation step in its four possible nitronate-

dienone face combinations, *ReRe*, *SiRe*, *ReSi* and *SiSi* were calculated (Figure 2.35). The energy values of the four TSs highlight that the energy barrier for the *Re,Re* approach is 9.6 kcal/mol, at least ~2 kcal/mol lower than all the other possibilities. This result is in perfect agreement with the stereoinduction observed in all the final products, with one only exception (when R = *n*Pr). After a second isomerisation, the final product **E** results stable due to the re-established conjugation.

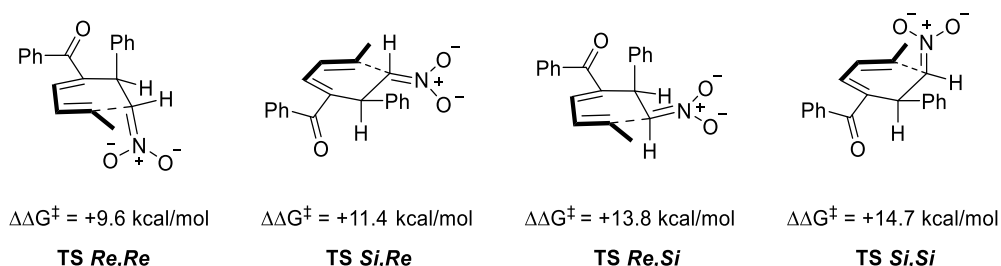


Figure 2.35 Study of the activation energies of the transition states for the carbocyclisation reaction (from deprotonated **A**)

The observed stereochemistry of the reaction is explained by the higher stability of **TS *Re,Re*** compared to the other isomers. Furthermore, we analysed the thermodynamics stability of the product **E**, taking as example the cycloadduct in Figure 2.36, and we calculated the energy of the four possible diastereoisomers. The isomer isolated experimentally is not the one that was located at the lowest energy, meaning that the last step of the reaction occurs under kinetic control and thermodynamics is not determining the stereochemistry of the cyclic product.

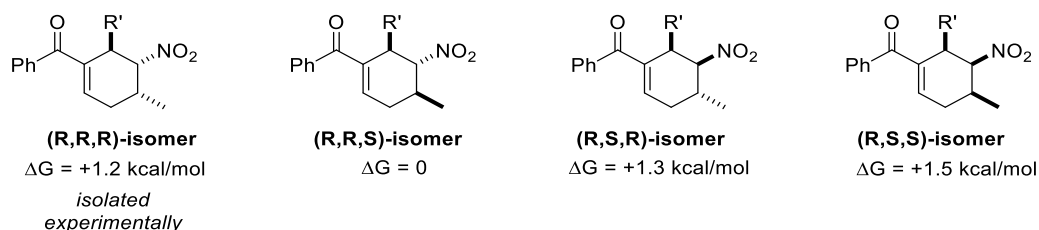


Figure 2.36 Study of the relative stability of cycloadduct **E** and its three diastereomers.

2.3.6. Conclusion

Under BB catalysis, trienolates have been found to react with nitroolefins at the C_α exclusively leading to α -functionalised products in high yields and stereoselectivity. Trienolates follow the same behaviour of dienolate substrates⁸⁶ but react completely differently from trienamines, with which they share structural analogies. Our computational analysis demonstrates that this divergence arises from electronic factors. The charge distribution in the two substrates highlights that the most nucleophilic atom in trienolates is the C_α , while in trienamines is the C_γ , in agreement with the respective reactivities. The energy barrier for the Michael addition reaction of trienolate to nitrostyrene was found to be lower than the one for the Diels Alder reaction between the same reactants. Also thioesters show to be suitable substrates for Michael addition and feature analogous charge distribution to the unsaturated ketones. Their tendency to react through the C_α was demonstrated by simple calculations of the activation

energies of the α -, γ - and ϵ -attack to nitrostyrene. It emerged that the α -attack proceeds with the smallest energy barrier.

This computational analysis provided an interesting rationale to the stereoselectivity observed experimentally. The pathway for the formation of the experimental isomer resulted to be the least energetic one and the energies of the other stereoisomers justify the values of *ee* and *dr*. The H-bond network that best describes our reaction system follows the Pápai-type model, in which the NH groups of the squaramides interact with the trienolate and the protonated tertiary amine binds the nitro group of the olefin.

Moreover, trienolates have been found to be useful substrates to synthesise more complex molecules with high stereocontrol. Indeed, through a one-pot sequence it was possible to synthesise stereodefined six-member carbocycles, with Brønsted base catalysis as the unique mode of activation. The stereochemistry of the carbocyclisation was investigated computationally, considering that the process is substrate-controlled. The stereocontrol depends on the approach of dienone and nitronate and not on the chiral catalyst. The energy barrier for the *Re,Re* approach that leads to the observed product was found to be the lowest and differs from the other cases by values of energies that explain the experimental stereoselectivities.

2.4. References

1. Pellissier, H. *Recent Developments in Asymmetric Organocatalysis*; RSC Publishing: Cambridge, 2010.
2. Berkessel, A.; Gröger, H. *Asymmetric Organocatalysis*; Wiley Online Library, 2005.
3. Alemán, J.; Cabrera, S. *Chem. Soc. Rev.* **2013**, *42*, 774–793.
4. Ahrendt, K. A.; Borths, C. J.; MacMillan, D. W. C. *J. Am. Chem. Soc.* **2000**, *122*, 4243–4244.
5. Breiding, G.; Fiske, P. S. *Biochem. Z.* **1912**, *46*, 7–23.
6. Pracejus, H. *Justus Liebigs Ann. Chem.* **1960**, *634*, 9–22.
7. Pracejus, H.; Mätje, H. *J. Prakt. Chem./Chem.-Ztg.* **1964**, *24*, 195–205.
8. Hajos, Z. G.; Parrish, D. R. *J. Org. Chem.* **1974**, *39*, 1615–1621.
9. Eder, U.; Sauer, G.; Wiechert, R. *Angew. Chem., Int. Ed. Engl.* **1971**, *10*, 496–497.
10. List, B. *Tetrahedron* **2002**, *58*, 5573–5590.
11. List, B.; Lerner, R. A.; Barbas, C. F. *J. Am. Chem. Soc.* **2000**, *122*, 2395–2396.
12. Nielsen, M.; Worgull, D.; Zweifel, T.; Gschwend, B.; Bertelsena, S.; Jørgensen, K. A. *Chem. Commun.* **2011**, *47*, 632–649.
13. Grossmann, A.; Enders, D. *Angew. Chem. Int. Ed.* **2012**, *51*, 314–325.
14. Abbasov, M. E.; Romo, D. *Nat. Prod. Rep.* **2014**, *31*, 1318–1327.
15. Knowles, R. R.; Jacobsen, E. N. *PNAS* **2010**, *107*, 20678–20685.
16. Doyle, A. G.; Jacobsen, E. N. *Chem. Rev.* **2007**, *107*, 5713–5743.
17. Dalko, P. I. *Enantioselective Organocatalysis*; Wiley-VCH: Weinheim, 2007.
18. a) Jaisser, F.; Farman, N. *Pharmacol. Rev.* **2016**, *68*, 49–75; b) Liu, L.; Zhang, S. L.; Xue, F.; Lou, G. S.; Zhang, H. Y.; Ma, S.C.; Duan, W.; Wang, W. *Chem. Eur. J.* **2011**, *17*, 7791–7795; c) Colloway, J.; Couch, A.; Foster, F.; Hunter, W.; Knight, V.; White, A. C. *Antibiotics Annu.* **1955**, *3*, 490–501.
19. a) Spino, C. *Org. Prep. Proced. Int.* **2003**, *35*, 1–120; b) Carruthers, W.; Coldham, I. *Modern Methods of Organic Synthesis*; Ed. Cambridge University Press: Cambridge, 2004; c) Carey, F.A.; Sundberg, R. J. *Advanced Organic Chemistry*; Ed. Springer: Heidelberg, 2007, vol. B; d) Knochel, P.; Molander, G. A. *Comprehensive Organic Synthesis II*; Ed. Elsevier: Amsterdam, 2014, vol. 1.
20. a) Mukaiyama, T.; Narasaka, K.; Banno, K. *Chem. Lett.* **1973**, *2*, 1011–1014; b) Mukaiyama, T.; Banno, K.; Narasaka, K. *J. Am. Chem. Soc.* **1974**, *96*, 7503–7509; c) Kobayashi, S.; Sano, T.; Mukaiyama, T. *Chem. Lett.* **1989**, 1319–1322; d) Kobayashi, S.; Mukaiyama, T. *Chem. Lett.* **1989**, 297–300.
21. a) Ikariya, T.; Murata, K.; Noyori, R. *Org. Biomol. Chem.* **2006**, *4*, 393–406; b) Shibasaki, M.; Kanai, M.; Matsunaga, S. *Acc. Chem. Res.* **2009**, *42*, 1117–1127; c) Ito, J.; Nishiyama, H. *Bifunctional Molecular Catalysis. Topics in Organometallic Chemistry*, vol. 37, Ed. Springer: Berlin 2011.

2.4 References

22. Ojima, I. *Catalytic Asymmetric Synthesis*, 3rd ed., John Wiley & Sons: New York, 2010.
23. Notz, W.; List, B. *J. Am. Chem. Soc.* **2000**, *122*, 7386–7387.
24. List, B.; Pojarliev, P.; Castello, C. *Org. Lett.* **2001**, *3*, 573–575.
25. Mukherjee, S.; Yang, J. W.; Hoffmann, S.; List, B. *Chem. Rev.* **2007**, *107*, 5471–5569.
26. Liu, J.; Lei, W. *Synthesis* **2017**, *49*, 960–972.
27. Xu, L. W.; Luo, J.; Lu, Y. *Chem. Commun.* **2009**, 1807–1821.
28. Xu, Y.; Córdova, A. *Chem. Commun.* **2006**, 460–462.
29. Palomo, C.; Oiarbide, M.; López, R. *Chem. Soc. Rev.* **2009**, *38*, 632–653.
30. a) Marcelli, T.; Van Maarseveen, J. H.; Hiemstra, H. *Angew. Chem. Int. Ed.* **2006**, *45*, 7496–7504; b) Marcelli, T.; Hiemstra, H. *Synthesis* **2010**, 1229–1279; c) Yeboah, E. M. O.; Yeboah, S. O.; Singh, G. S. *Tetrahedron.* **2011**, 1725–1762; d) Bryant, L. A.; Fanelli, R.; Cobb, A. J. A. *Beilstein J. Org. Chem.* **2016**, *12*, 429–443.
31. Okino, T.; Hoashi, Y.; Takemoto, Y. *J. Am. Chem. Soc.* **2003**, *125*, 12672–12673.
32. McCooey, S. H.; Connon, S. J. *Angew. Chem. Int. Ed.* **2005**, *44*, 6367–6370.
33. Ye, J.; Dixon, D. J.; Hynes, P. S. *Chem. Commun.* **2005**, 4481–4483.
34. Connon, S. J. *Chem. Eur. J.* **2006**, *12*, 5418–5427.
35. Malerich, J. P.; Hagihara, K.; Rawal, V. H. *J. Am. Chem. Soc.* **2008**, *130*, 14416–14417.
36. Alemán, J.; Parra, A.; Jiang, H.; Jørgensen, K. A. *Chem. Eur. J.* **2011**, *17*, 6890–6899.
37. Zhao, B. L.; Li, J. H.; Du, D. M. *Chem. Rec.* **2017**, *17*, 994–1018.
38. Chauhan, P.; Mahajan, S.; Kaya, U.; Hack, D.; Enders, D. *Adv. Synth. Catal.* **2015**, *357*, 253–281.
39. Ian Storer, R.; Aciro, C.; Jones, L. H. *Chem. Soc. Rev.* **2011**, *40*, 2330–2346.
40. Zhu, Y.; Malerich, J. P.; Rawal, V. H. *Angew. Chem. Int. Ed.* **2010**, *49*, 153–156.
41. Qian, Y.; Ma, G.; Lv, A.; Zhu, H.-L.; Zhao, J.; Rawal, V. H. *Chem. Commun.* **2010**, *46*, 3004–3006.
42. Konishi, H.; Lam, T. Y.; Malerich, J. P.; Rawal, V. H. *Org. Lett.* **2010**, *12*, 2028–2031.
43. Lee, J.-W.; Ryu, T.-H.; Oh, J.-S.; Bae, H.-Y.; Janga, H.-B.; Song, C.-E. *Chem. Commun.* **2009**, 7224–7226.
44. Xu, D. Q.; Wang, Y.-F.; Zhang, W.; Luo, S.-P.; Zhong, A.-G.; Xia, A.-B.; Xu, Z.-Y. *Chem. Eur. J.* **2010**, *16*, 4177–4180.
45. Dai, L.; Wang, S. X.; Chen, F. E. *Adv. Synth. Catal.* **2010**, *352*, 2137–2141.
46. Quiñonero, D.; Prohens, R.; Garau, C.; Frontera, A.; Ballester, P.; Costa, A.; Deyà, P. M. *Chem. Phys. Lett.* **2002**, *351*, 115–120.
47. Ni, X.; Li, X.; Wang, Z.; Cheng, J. P. *Org. Lett.* **2014**, *16*, 1786–1789.

48. a) Okino, T.; Hoashi, Y.; Furukawa, T.; Xu, X.; Takemoto, Y. *J. Am. Chem. Soc.* **2005**, *127*, 119–125; b) Okino, T.; Hoashi, Y.; Takemoto, Y. *J. Am. Chem. Soc.* **2003**, *125*, 12672–12673.
49. a) Kelly, T. R.; Kim, M. H. *J. Am. Chem. Soc.* **1994**, *116*, 7072–7080; b) Linton, B. R.; Goodman M. S.; Hamilton, A. D. *Chem. Eur. J.* **2000**, *6*, 2449–2455; c) Bu, J.; Lilienthal, N.D.; Woods, J. E.; Nohrden, C. E.; Hoang, K. P. T.; Truong, D.; Smith, D. K. *J. Am. Chem. Soc.*, **2005**, *127*, 6423–6429.
50. Hamza, A.; Schubert, G.; Soós, T.; Pápai, I. *J. Am. Chem. Soc.* **2006**, *128*, 13151–13160.
51. List, B. *Topics in Current Chemistry: Asymmetric Organocatalysis*; vol. 291, Springer: Berlin, 2009.
52. Kótai, B.; Kardos, G.; Hamza, A.; Farkas, V.; Pápai, I.; Soós, T. *Chem. Eur. J.* **2014**, *20*, 5631–5639.
53. For works supporting Takemoto's model: a) Zuend, S. J.; Jacobsen, E. N. *J. Am. Chem. Soc.* **2007**, *129*, 15872; b) Hammar, P.; Marcelli, T.; Hiemstra, H.; Himo, F. *Adv. Synth. Catal.* **2007**, *349*, 2537; c) Zuend, S. J.; Jacobsen, E. N. *J. Am. Chem. Soc.* **2009**, *131*, 15358. For works supporting Pápai's model: a) Almasi, D.; Alonso, D. A.; Gómez-Bengoa, E.; Nájera, C. *J. Org. Chem.* **2009**, *74*, 6163; b) Tan, B.; Lu, Y.; Zeng, X.; Chua, P. J.; Zhong, G. *Org. Lett.* **2010**, *12*, 2682; c) Han, X.; Lee, R.; Chen, T.; Luo, J.; Lu, Y.; Huang, K. W. *Sci. Rep.* **2013**, *3*, 2557; d) Azuma, T.; Kobayashi, Y.; Sakata, K.; Sasamori, T.; Tokitoh, N.; Takemoto, Y. *J. Org. Chem.* **2014**, *79*, 1805.
54. Zhu, J. L.; Zhang, Y.; Liu, C.; Zheng, A. M.; Wang, W. *J. Org. Chem.* **2012**, *77*, 9813–9825.
55. Cano, R.; Zakarian, A.; McGlacken, G. P. *Angew. Chem. Int. Ed.* **2017**, *56*, 9278–9290.
56. a) Hong, A. Y.; Stoltz, B. M. *Eur. J. Org. Chem.* **2013**, 2745–2759; b) Das, J. P.; Marek, I. *Chem. Commun.* **2011**, *47*, 4593–4623; c) Bella, M.; Casper, T. *Synthesis* **2009**, 1583–1614; d) Cozzi, P. G.; Hilgraf, R.; Zimmerman, N. *Eur. J. Org. Chem.* **2007**, 5969–1614; e) Trost, B. M.; Jiang, C. *Synthesis* **2006**, 369–396; f) Christoffers, J.; Baro, A. *Quaternary Stereocentres*; Wiley-VCH: Weinheim, 2005; g) Douglas, C. J.; Overman, L. E. *Proc. Nat. Acad. Sci.* **2004**, *101*, 5363–5367.
57. Ishikawa, S.; Hamada, T.; Manabe, K.; Kobayashi, S. *J. Am. Chem. Soc.* **2004**, *126*, 12236–12237.
58. a) Trost, B. M.; Lee, C. *Catalytic Asymmetric Synthesis*, 2nd ed.; Wiley-VCH: New York, 2000; b) Pfaltz, A.; Lautens, M. *Comprehensive Asymmetric Catalysis*, Springer: New York, 1999; c) Mohr, J. T.; Stoltz, B. M. *Chem. Asian J.* **2007**, *2*, 1476–1491; d) Trost, B. M. *Tetrahedron* **2015**, *71*, 5708–5733.
59. a) Nibbs, A. E.; Baize, A.-L.; Herter, R. M.; Scheidt, K. A. *Org. Lett.* **2009**, *11*, 4010–4013; b) Kano, T.; Hayashi, Y.; Maruoka, K. *J. Am. Chem. Soc.* **2013**, *135*, 7134–7137; c) Teng, B.; Chen, W.; Dong, S.; Kee, C. W.; Gandamana, D. A.; Zong, L.; Tan, C.-H. *J. Am. Chem. Soc.* **2016**, *138*, 9935–9940.

60. Trost, B. M.; Schroeder, G. M. *J. Am. Chem. Soc.* **1999**, *121*, 6759–6760.
61. a) Kang, J. Y.; Carter, R. G. *Org. Lett.* **2012**, *14*, 3178–3181; b) Kang, J. Y.; Johnston, R. C.; Snyder, K. M.; Cheong, P. H.-Y.; Carter, R. G. *J. Org. Chem.* **2016**, *81*, 3629–3637; c) Horinouchi, R.; Kamei, K.; Watanabe, R.; Hieda, N.; Tatsumi, N.; Nakano, K.; Ichikawa, Y.; Kotsuki, H. *Eur. J. Org. Chem.* **2015**, 4457–4463.
62. Yang, X.; Toste, F. D. *Chem. Sci.* **2016**, *7*, 2653–2656.
63. Felker, I.; Pupo, G.; Kraft, P.; List, B. *Angew. Chem. Int. Ed.* **2015**, *54*, 1960–1964.
64. Das, J. P.; Marek, I. *Chem. Commun.* **2011**, *47*, 4593–4623; Reviews: (a) Hong, A.Y.; Stoltz, B. M. *Eur. J. Org. Chem.* **2013**, 2745–2759; (b) Das, J. P.; Marek, I. *Chem. Commun.* **2011**, *47*, 4593–4623; (c) Bella, M.; Casper, T. *Synthesis* **2009**, 1583–1614; (d) Cozzi, P. G.; Hilgraf, R.; Zimmerman, N. *Eur. J. Org. Chem.* **2007**, 5969–1614; (e) Trost, B. M.; Jiang, C. *Synthesis* **2006**, 369–396; (f) Christoffers, J.; Baro, A. *Quaternary Stereocentres*; Wiley-VCH: Weinheim, 2005; (g) Douglas, C. J.; Overman, L. E. *Proc. Nat. Acad. Sci.* **2004**, *101*, 5363–5367; (h) Quasdorf, K. W.; Overman, L. E. *Nature* **2014**, *516*, 181–191; (i) Ling, T.; Rivas, F. *Tetrahedron* **2016**, *72*, 6729–6777; (j) Liu, Y.; Han, S.-J.; Liu, W.-B.; Stoltz, B. M. *Acc. Chem. Res.* **2015**, *48*, 740–751. Selected reviews on Michael additions: (a) Vicario, J. L., Badía, D.; Carrillo, L.; Reyes, E. *Organocatalytic Enantioselective Conjugate Addition Reactions: A Powerful Tool for the Stereocontrolled Synthesis of Complex Molecules*; RSC Publishing: Cambridge, 2010; (b) Tsogoeva, S. B. *Eur. J. Org. Chem.* **2007**, 1701–1716; (c) Almasi, D.; Alonso, D. A.; Najera, C. *Tetrahedron: Asymmetry* **2007**, *18*, 299–365; (d) Reyes, E.; Uria, U.; Vicario, J. L.; Carrillo, L. *The Catalytic Enantioselective Michael Reaction*, *Org. React.* **2016**, *90*, 1–898.
65. Dong, X.-Q.; Teng, H.-L.; Tong, M.-C.; Huang, H.; Tao, H.-Y.; Wang, C.-J. *Chem. Commun.* **2010**, *46*, 6840–6842.
66. Urruzuno, I.; Mugica, O.; Oiarbide, M.; Palomo, C. *Angew. Chem. Int. Ed.* **2017**, *56*, 2059–2063.
67. a) Schneider, C.; Abels, F. *Org. Biomol. Chem.* **2014**, *12*, 3531–3543; b) Casiraghi, G.; Battistini, L.; Curti, C.; Rassu, G.; Zanardi, F. *Chem. Rev.* **2011**, *111*, 3076–3154; c) Yin, Y.; Jiang, Z. *ChemCatChem* **2017**, *9*, 4306–4318.
68. Reviews: a) Denmark, S. E.; Heemstra, J. R.; Beutner, G. L. *Angew. Chem. Int. Ed.* **2005**, *44*, 4682–4698; b) Pansare, S. V.; Paul, E. K. *Chem. Eur. J.* **2011**, *17*, 8770–8779. For selected examples: c) Denmark, S. E.; Beutner, G. L. *J. Am. Chem. Soc.* **2003**, *125*, 7800–7801; d) Ratjen, L.; García-García, P.; Lay, F.; Beck, M. E.; List, B. *Angew. Chem. Int. Ed.* **2011**, *50*, 754–758; e) Gupta, V.; Sudhir, S.; Mandal, T.; Schneider, C. *Angew. Chem. Int. Ed.* **2012**, *51*, 12609–12612; f) Basu, S.; Gupta, V.; Nickel, J.; Schneider, C. *Org. Lett.* **2014**, *16*, 274–277.
69. Selected examples: a) Trost, B. M.; Hitce, J. *J. Am. Chem. Soc.* **2009**, *131*, 4572–4573; b) Yamaguchi, A.; Matsunaga, S.; Shibasaki, M. *Org. Lett.* **2008**, *10*, 2319–2322; c) Yin, L.; Takada, H.; Kumagai, N.; Shibasaki, M. *Angew. Chem. Int. Ed.* **2013**, *52*, 7310–7313; d) Shepherd, N. E.; Tanabe, H.; Xu, Y.; Matsunaga, S.; Shibasaki, M. *J. Am. Chem. Soc.*; **2010**, *132*, 3666–3667; e) Xiao, X.; Mei, H.; Chen, Q.; Zhao, X.;

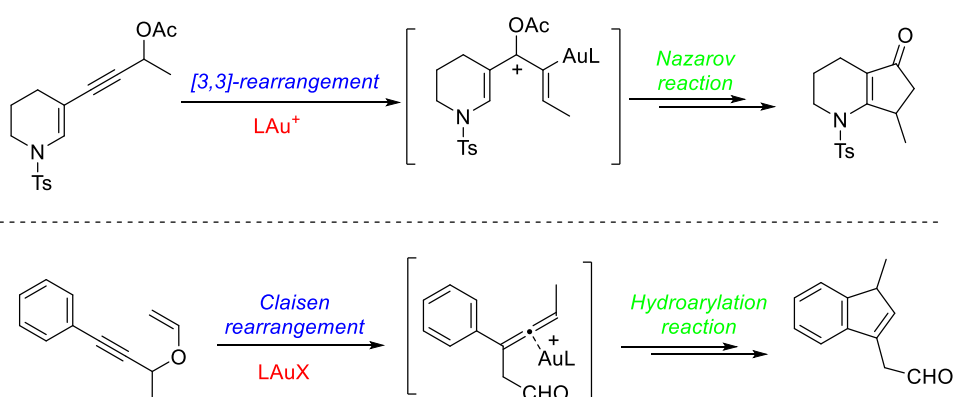
- Lin, L.; Liu, X.; Feng, X. *Chem. Commun.* **2015**, *51*, 580-583; f) Yang, D.; Wang, L.; Han, F.; Zhao, D.; Zhang, B.; Wang, R. *Angew. Chem. Int. Ed.* **2013**, *52*, 6739-6742; g) Yang, D.; Wang, L.; Han, F.; Zhao, D.; Wang, R. *Chem. Eur. J.* **2014**, *20*, 8584-8588; h) Zhang, H.-J.; Shi, C.-Y.; Zhong, F.; Yin, L. *J. Am. Chem. Soc.* **2017**, *139*, 2196-2199.
70. Reviews: a) Jurberg, I. D.; Chatterjee, I.; Tannerta, R.; Melchiorre, P. *Chem. Commun.* **2013**, *49*, 4869-4883; b) Marcos, V.; Alemán, J. *Chem. Soc. Rev.* **2016**, *45*, 6812-6832. Selected examples: (c) Bencivenni, G.; Galzerano, P.; Mazzanti, A.; Bartoli, G.; Melchiorre, P. *Proc. Natl. Acad. Sci. USA* **2010**, *107*, 20642-20647 (correction *PNAS*, **2013**, *110*, 4852-4853); d) Zhan, V.; He, Q.; Yuan, X.; Chen, Y.-C. *Org. Lett.* **2014**, *16*, 6000-6003; e) Guo, Q.; Fraboni, A. J.; Brenner-Moyer, S. E. *Org. Lett.* **2016**, *18*, 2628-2631; f) Shi, M.-L.; Zhan, G.; Zhou, S.-L.; Du, W.; Chen, Y.-C. *Org. Lett.* **2016**, *18*, 6480-6483.
71. a) Gu, Y.; Wang, Y.; Yu, T.-Y.; Liang, Y.-M.; Xu, P.-F. *Angew. Chem. Int. Ed.* **2014**, *53*, 14128-14131; b) Li, X.; Lu, M.; Dong, Y.; Wu, W.; Qian, Q.; Ye, J.; Dixon, D. J. *Nat. Commun.* **2014**, *5*, 4479.
72. a) Zhu, B.; Zhang, W.; Lee, R.; Han, Z.; Yang, W.; Tan, D.; Huang, K.-W.; Jiang, Z. *Angew. Chem. Int. Ed.* **2013**, *52*, 6666-6670; b) Li, T.-Z.; Jiang, Y.; Guan, Y.-Q.; Sha, F.; Wu, X.-Y. *Chem. Commun.* **2014**, *50*, 10790-10792; c) Poulsen, T. B.; Bell, M.; Jørgensen, K. A. *Org. Biomol. Chem.* **2006**, *4*, 63-70; d) Curti, C.; Rassu, G.; Zambrano, V.; Pinna, L.; Pelosi, G.; Sartori, A.; Battistini, L.; Zanardi, F.; Casiraghi, G. *Angew. Chem. Int. Ed.* **2012**, *51*, 6200-6204; e) Wang, J.; Chen, J.; Kee, C. W.; Tan, C.-H. *Angew. Chem. Int. Ed.* **2012**, *51*, 2382-2386; f) Xie, J.-K.; Wang, Y.; Lin, J.-B.; Ren, X.-R.; Xu, P.-F. *Chem. Eur. J.* **2017**, *23*, 6752-6756; g) Deepake, S. K.; Lanjewar, A. B.; Thatikonda, T.; Gonnade, R. G.; Das, U. *ChemistrySelect* **2018**, *3*, 8189-8192; h) Bai, X.; Zeng, G.; Shao, T.; Jiang, Z. *Angew. Chem. Int. Ed.* **2017**, *56*, 3684-3688.
73. Gupta, V.; Sudhir, S. V.; Mandal, T.; Schneider, C. *Angew. Chem. Int. Ed.* **2012**, *51*, 12609-12612.
74. Trost, B. M.; Hitce, J. *J. Am. Chem. Soc.* **2009**, *131*, 4572-4573.
75. Guo, Q.; Fraboni, A. J.; Brenner-Moyer, S. E. *Org. Lett.* **2016**, *18*, 2628-2631.
76. Gu, Y.; Wang, Y.; Yu, T.-Y.; Liang, Y.-M.; Xu, P.-F. *Angew. Chem.* **2014**, *126*, 14352-14355.
77. Zhu, B.; Zhang, W.; Lee, R.; Han, Z.; Yang, W.; Tan, D.; Huang, K.-W.; Jiang, Z. *Angew. Chem. Int. Ed.* **2013**, *52*, 6666-6670.
78. Frias, M.; Mas-Ballesté, R.; Arias, S.; Alvarado, C.; Alemán, J. *J. Am. Chem. Soc.* **2017**, *139*, 672-679.
79. Frías, M.; Carrasco, A. C.; Fraile, A.; Alemán, J. *Chem. Eur. J.* **2018**, *24*, 3117-3121.
80. Yamaguchi, A.; Aoyama, N.; Matsunaga, S.; Shibasaki, M. *Org. Lett.* **2007**, *9*, 3387-3390.
81. Utsumi, N.; Zhang, H.; Tanaka, F.; Barbas, C. F. I. *Angew. Chem. Int. Ed.* **2007**, *46*,

- 1878–1880.
82. Guang, J.; Rout, S.; Bihani, M.; Larson, A. J.; Arman H. D.; Zhao, J. C.-G. *Org. Lett.* **2016**, *18*, 2648–2651.
83. Griswold, J. A.; Horwitz, M. A.; Leiva, L. V.; Johnson, J. S. *J. Org. Chem.* **2017**, *82*, 2276–2280.
84. Stiller, J. Marqués-Lopéz, E.; Herrera, R.; Fröhlich, R.; Strohmam, C.; Christmann, M. *Org. Lett.* **2011**, *13*, 70–73.
85. Yang, X.; Toste, F. D. *J. Am. Chem. Soc.* **2015**, *137*, 3205–3208.
86. Iriarte, I.; OLaizola, O.; Vera, S.; Gamboa, I.; Oiarbide, M.; Palomo, C. *Angew. Chem. Int. Ed.* **2017**, *56*, 8860–8864.
87. Kündig, E. P.; Cunningham, A. F. *Tetrahedron* **1988**, *44*, 6855–6860.
88. Reviews on sulfones: a) Simpkins, N. S. *Tetrahedron* **1990**, *46*, 6951–6984; b) Simpkins, N. S. *Sulphones in Organic Synthesis*; Pergamon Press: Oxford, 1991; (c) Alba, A.-N. R.; Companyó, X.; Ríos, R. *Chem. Soc. Rev.* **2010**, *39*, 2018–2033; (d) Nielsen, M.; Jacobsen, C. B.; Holub, N.; Paixao, M. W.; Jørgensen, K. A. *Angew. Chem. Int. Ed.* **2010**, *49*, 2668–2679; (e) Zhu, Q.; Lu, Y. *Aust. J. Chem.* **2009**, *62*, 951–955.
89. a) Yang, W.; Du, D. M. *Org. Lett.* **2010**, *12*, 5450–5453; b) Dai, L.; Wang, S.-X.; Chen, F.-E. *Adv. Synth. Catal.* **2010**, *352*, 2137–2141.
90. Manoni, F.; Connon, S. J. *Angew. Chem. Int. Ed.* **2014**, *53*, 2628–2632.
91. Odriozola, A.; Oiarbide, M. & Palomo, C. *Chem. - A Eur. J.* **2017**, *23*, 12758–12762.
92. a) McCooey, S. H.; Connon, S. J. *Angew. Chem. Int. Ed.* **2005**, *44*, 6367–6370; b) Ye, J.; Dixon, D. J.; Hynes, P. S. *Chem. Commun.* **2005**, 4481–4483; c) Vakulya, B.; Varga, S.; Csámpai, A.; Soós, T. *Org. Lett.* **2005**, *7*, 1967–1969; d) Li, B.-J.; Jiang, L.; Liu, M.; Chen, Y.-C.; Ding, L.-S.; Wu, Y. *Synlett*, **2005**, 603–606.
93. Curti, C.; Battistini, L.; Sartori, A.; Rassu, G.; Pelosi, G.; Lombardo, M.; Zanardi, F. *Adv. Synth. Catal.* **2018**, *360*, 711–721.
94. Jia, Z.-J.; Jiang, H.; Li, J.-L.; Gschwend, B.; Li, Q.-Z.; Yin, X.; Grouleff, J.; Chen, Y.-C.; Jørgensen, K. A. *J. Am. Chem. Soc.* **2011**, *133*, 5053–5061.
95. Jia, Z. J.; Zhou, Q.; Zhou, Q. Q.; Chen, P. Q.; Chen, Y. C. *Angew. Chem. Int. Ed.* **2011**, *50*, 8638–8641.
96. Xiong, X.-F.; Zhou, Q.; Gu, J.; Dong, L.; Liu, T.-Y.; Chen, Y. C. *Angew. Chem. Int. Ed.* **2012**, *51*, 4401–4404.
97. Casiraghi, G.; Battistini, L.; Curti, C.; Rassu, G.; Zanardi, F. *Chem. Rev.* **2011**, *111*, 3076–3154.
98. Yamaguchi, A.; Aoyama, N.; Matsunaga, S.; Shibasaki, M. *Org. Lett.* **2007**, *9*, 3387–3390.
99. Laina-Martín, V.; del Río-Rodríguez, R.; Díaz-Tendero, S.; Fernández-Salas, J. A.; Alemán, J. *Chem. Commun.* **2018**, *54*, 13941–13944.

100. Ballester, A.; Costa, A.; García-Raso, A.; Gómez-Solivellas, A.; Mestres, R. *Tetrahedron* **1985**, *26*, 3625–3628.
101. Ballester, A.; Costa, A.; García-Raso, A.; Mestres, R. *J. Chem. Soc. Perkin Trans. I* **1988**, 2797–2803.
102. Zhang, H. J.; Shi, C. Y.; Zhong, F.; Yin, L. *J. Am. Chem. Soc.* **2017**, *139*, 2196–2199.
103. Olaizola, O.; Iriarte, I.; Zanella, G.; Gómez-Bengoña, E.; Ganboa, I.; Oiarbide, M.; Palomo, C. *Angew. Chem. Int. Ed.* **2019**, *58*, 14250–14254.
104. Su, Z.; Kim, C. K. *Org. Biomol. Chem.* **2015**, *13*, 6313–6324.
105. Cramer, C. J. *Essentials of Computational Chemistry, Theories and Models*, 2nd ed.; John Wiley & Sons: Chichester, UK; Hoboken, USA, 2004.

Chapter 3

Gold catalysis



In this chapter, we have envisioned the potential of gold catalysis applied to sequences of reactions, which lead to the formation of cyclic compounds.

A comprehensive computational study was conducted in view of the experimental results obtained in the group of Prof. Ernesto Occhiato at the Università degli Studi di Firenze (Italy). They developed a tandem gold(I)-catalysed [3,3]-rearrangement/Nazarov reaction for the pentannulation of *N*-heterocycles and a tandem gold(I)-catalysed Claisen rearrangement/hydroarylation reaction of propargyl vinyl ethers for the synthesis of indenenes. We studied the reaction mechanisms, the reactivity of the substrates and the effect of the catalyst ligands on the reaction.

Based on:

Rinaldi, A.; Langé, V.; Gómez-Bengoa, E.; Zanella, G.; Scarpi, D.; Occhiato, E. G. *J. Org. Chem.* **2019**, *84*, 106298-6311.

Zanella, G.; Petrović, M.; Scarpi, D.; Occhiato, E. G.; Gómez-Bengoa, E. A Combined Computational and Experimental Study on the Role of the N Atom in the Pentannulation of *N*-Heterocycles by the Tandem Gold-Catalysed [3,3]-Rearrangement/Nazarov Reaction of Propargyl Ester Derivatives. *Submitted*

This chapter includes two projects based on two collaborations carried out with an experimental group. The experimental part was performed by the group of Prof. Ernesto Occhiato at the Università degli Studi di Firenze. The contribution of the author of this thesis is exclusively computational and is presented in the *computational work* section. A general introduction about gold catalysis is initially provided. Then, for each project, the nature of the chemistry, the aim of the work, experimental and computational procedures and results are described.

3.1 Introduction

For a long time, gold was chemically neglected and considered erroneously an inert element. Only in 1986, Ito and Hayashi described the first application of gold(I) in homogeneous catalysis, a gold(I) catalysed asymmetric aldol reaction.¹ More than one decade later, a “gold rush” in synthesis started with the publication of the works of Fukuda,² Teles³ and Tanaka⁴ on the homogeneous gold-catalysed addition of water and alcohol to alkynes. Hashmi and co-workers contributed in expanding the interest in gold catalysis showing the catalytic reactivity of AuCl₃ on cycloisomerisation reactions of alkyne-based compounds leading to furans and arenes.^{5,6}

Nowadays, gold is one of the most used metals in organometallic catalysis, as revealed by the high number of publications on gold catalysis. Gold-based complexes are highly sought after catalysts due to their attractive features, as functional group and oxygen tolerance, robustness, fine-tunability, large availability in the market and applicability to asymmetric synthesis. Most importantly, gold has peculiar π -affinity and is able to activate C-C π -bonds towards nucleophilic attack also under exceptionally mild conditions, showing similar or superior reactivity to other late transition metals such as platinum, palladium, and mercury.⁷ In particular, cationic species are the most powerful catalysts for the electrophilic activation of alkynes towards a variety of nucleophiles, requiring little catalytic amounts.^{8,9,10,11} This phenomenon can be attributed to the lower LUMO and poor back-donation of the cationic gold species.^{12,13}

A broad range of gold-catalysed versatile synthetic tools have been developed for the construction of C-C or carbon-heteroatom bonds.¹⁴

On the other hand, the use of gold catalysts shows also some weak points. First, they are not suitable in fields such as medicinal chemistry and material synthesis due to the low turnover number observed in gold-catalysed reactions; gold is a precious metal and it is difficult to recycle after each reaction, becoming problematic for large scale synthesis.

Gold is an element of group 11 of the periodic table and behaves as a soft carbophilic Lewis acid due to relativistic effects.^{12,15}

The term ‘*aurophilicity*’ was introduced in 1989 *to describe phenomena in the structural chemistry of gold which could not be readily rationalised by conventional concepts of chemical bonding*.^{16,17} Structurally, Au(I) predominantly forms linear two-coordinate complexes, although higher coordination numbers have also been found.¹⁸ Gold does not undergo spontaneous oxidative addition nor β -hydride elimination. Gold is the most electronegative element among the transition metals due to relativistic effects,^{12,19–21} which induce a more significant contraction of the 6s orbital (further enhanced by the

lanthanide contraction) and expansion of 5d orbitals with decreased electron–electron repulsion (Figure 3.1 top).^{15,22} The result is that 5d electrons are too low in energy to experience a significant backbonding to anti-bonding orbitals but not to empty nonbonding orbitals. This effect alters the electron density around the metal centre, which increases its π -acidity (empty 6s orbital) and π -backbonding (occupied 5d orbitals) ability in the Dewar–Chatt–Duncanson model.^{10,12,23}

In the case of gold(I)-carbenes $[L-Au=CR_2]^+$, a three-centre four-electron σ -bond is proposed together with an orthogonal weak π -backbonding from the metal to both the ligand and the substrate (Figure 3.1 bottom).²⁴ Due to this phenomenon, ligand-supported cationic gold(I) acts as an electrophilic soft π -Lewis acid capable of activating C–C multiple bonds (alkynes, allenes and alkenes) for nucleophilic attack to form new C–C, C–O, C–N and other bonds. Thus, the limited back-donation increases the electrophilicity of the coordinated substrate.

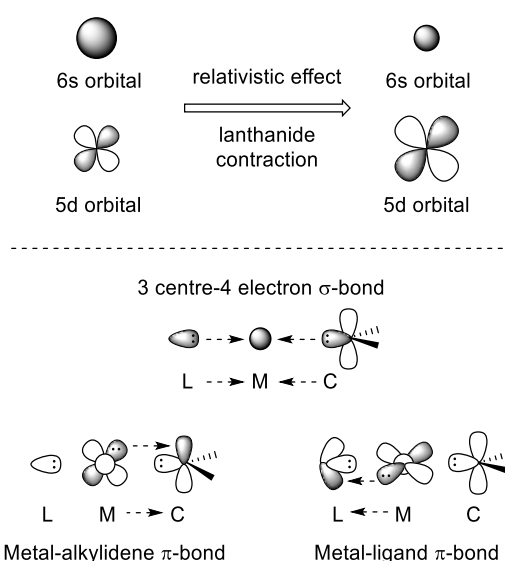


Figure 3.1 Top) effects of relativistic effect and lanthanide contraction on outer-shell orbitals of gold; bottom) Ligand-metal-substrate orbital interactions in gold carbenes $[L-Au=CR_2]^+$.

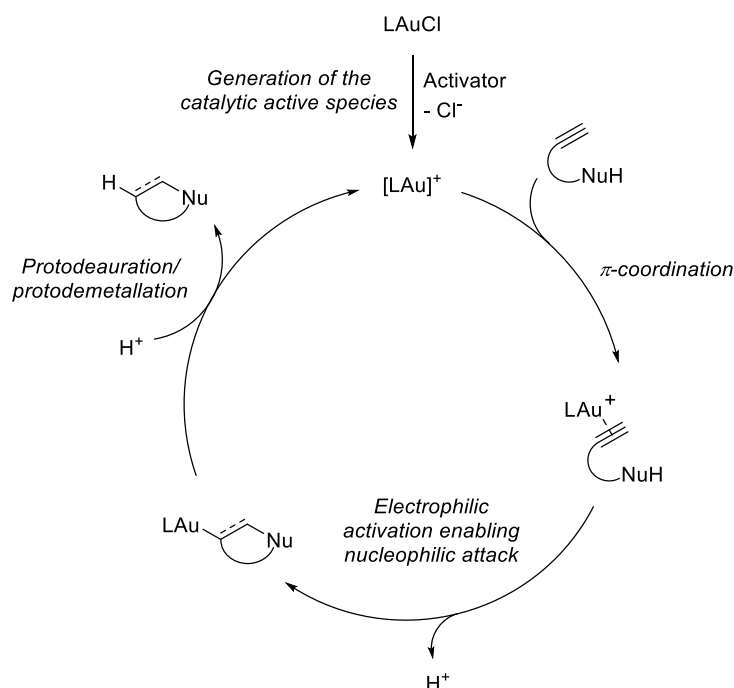
The most typical gold-catalysed transformations can be categorised in: nucleophilic functionalisation reactions on C–C multiple bonds, cycloisomerisation reactions, cycloadditions, sigmatropic rearrangements of polyunsaturated substrates and cross-coupling reactions using external strong oxidants to facilitate redox reactions on the gold centre.

The reactivity of the gold catalysts is highly influenced by the electronic nature of the ligands and the counterions.

3.1.1 Mechanism of gold-catalysed processes

The accepted mechanism for gold-catalysed processes includes the following basic reaction steps (Scheme 3.1). First, there is the generation of the catalytically active cationic species from an inactive gold chloride precursor. Once generated, this species activates the C–C multiple bond of alkynes (or equivalents) towards intra- or intermolecular nucleophilic attack leading to a cationic gold(I) vinyl (if starting from allenes or alkynes) or gold(I) alkyl intermediate (if starting from an alkene), which is

converted to a neutral intermediate through proton loss. The proton reenters in the protoauration step when intermediary Au–C σ -bond is cleaved, yielding the final product and regenerating the catalytically active cationic gold species.



Scheme 3.1 Proposed gold(I) catalytic cycle.

Gold complexes are usually poorly reactive in their precatalytic state and they need to be transformed *in situ*, for example by abstraction of one ligand, generally a chloride group [LAuCl]. Silver salts bearing a weakly coordinating anion have demonstrated to be effective agents for this purpose.²⁵

The species [AuL]⁺ are known as “*naked gold complexes*” and have not been proven to be stable and isolable, although are often suggested in mechanistic proposals.

Complexes in the form [LAuL']X or [LAuX] bearing weakly coordinating neutral (L') or anionic ligand (X⁻) are the most convenient catalysts for the activation of alkynes. These complexes can enter catalytic cycles by ligand exchange with the unsaturated substrate following associative mechanisms.²⁶

Gold(I) forms stable linear two-coordinate π -complexes with alkenes, 1,3-dienes, allenes and substituted alkynes.

Generally, in the case of an internal alkyne gold(I) complex, the coordination is almost symmetrical η^2 -type, as in the complex in Figure 3.2,²⁷ where the triple bond length is almost identical to that of a free alkyne, even if there is a significant bending back of the alkyl substituents (for further explanation see section 3.1.2 “*Description of the M– π -Bond Interaction in Alkyne Complexes*”).

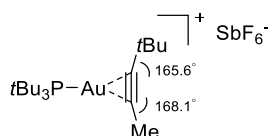
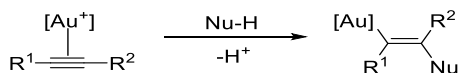


Figure 3.2 Structure of the η^2 -alkyne Au(I) complex.

3.1 Introduction

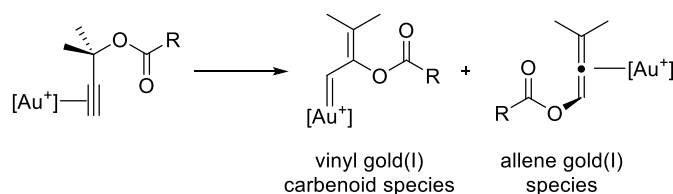
After the activation *via* π -coordination, the unsaturated substrate is deprived of electron density to the extent that it is susceptible to an outer-sphere attack by a nucleophile giving a *trans*-alkenyl species (Scheme 3.2).²⁸ The outer-sphere mechanism is the most widely accepted, even if there are a few exceptions.



Scheme 3.2 Nucleophilic attack to a Au(I) π -activated alkyne.

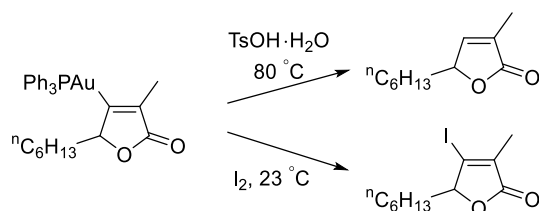
A wide range of carbon- and hetero-nucleophiles such as arenes, heteroarenes, alcohols, amines, imines, sulfoxides, *N*-oxides and thiols have been found to be suitable nucleophiles in inter- or intramolecular processes.

An example of our interest is the intramolecular nucleophilic addition when the nucleophile is located at the propargylic position.²⁹ Propargylic carboxylates resulted to undergo 1,2- or 1,3-acyloxy migrations leading to the formation of vinyl gold(I)carbenoid species or allene gold(I) complexes, in rapid equilibrium between them (Scheme 3.3).^{30,31} The direct 1,3-shift could be substituted by an energetically more favoured double 1,2-shift, which also leads to the allene gold(I) complex.



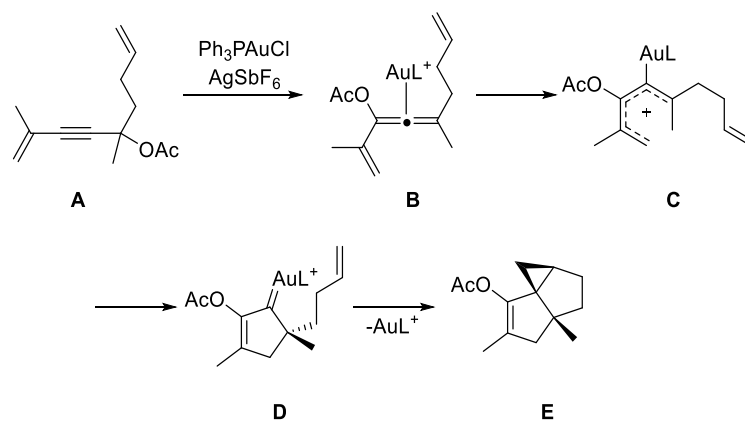
Scheme 3.3 Key intermediates in the propargylic migrations.

After the unsaturated substrate activation and the nucleophilic attack, the intermediate can evolve through many different pathways leading to a variety of complex products. The simplest route for the alkenyl gold(I) intermediate is its reaction with an electrophile, commonly by protodeauration regenerating the active catalyst (Scheme 3.4).^{32,33} Similarly, reaction with iodine and related electrophiles leads to the corresponding halo-derivatives.^{32,34}



Scheme 3.4 Electrophilic attack to an alkenyl gold(I) complex.

In alternative, the alkenyl gold(I) intermediate can participate in multistep processes. A significant example is the gold(I)-catalysed 1,3-propargylic acetate migration of substrates such as **A** leading to intermediate **B** that undergoes Nazarov-type electrocycloisatation through **C** generating gold(I) carbene **D** (Scheme 3.5).³⁵ An intramolecular cyclopropanation can take place forming tricyclic structure **E**.

Scheme 3.5 Nazarov-type cyclisation of substrate **A**.

3.1.2 Description of the M– π -Bond Interaction in Alkyne Complexes

The bonding situation in gold complexes is normally described through the Dewar–Chatt–Duncanson model (DCD),^{36,37} according to which the bonding with alkenes or alkynes is built by a synergistic combination of σ -donor and π -acceptor interactions between the metal template and the alkene or alkyne π -system.

Taking as a reference example the interaction of a gold atom with an alkyne, four main contributions to the bonding can be identified, as depicted in Figure 3.3 in order of their usual relative strengths. The first is a σ ligand-metal donation in the plane ($M \leftarrow L$; π -system of the ligand with an empty $d\sigma$ -orbital on the metal), followed by π back-donation from the metal (filled metal $d\pi$ -orbital) to the antibonding π^* -orbital of the alkyne (LUMO), also in the plane ($M \rightarrow L$). The next interaction is the π donation from the perpendicular π -orbital in the alkyne to the metal ($M \leftarrow L$) and the last and the smallest is the δ back-donation from the occupied d orbital of the metal to the empty out-of-plane π^* -orbital of the alkyne ($M \rightarrow L$).¹⁵

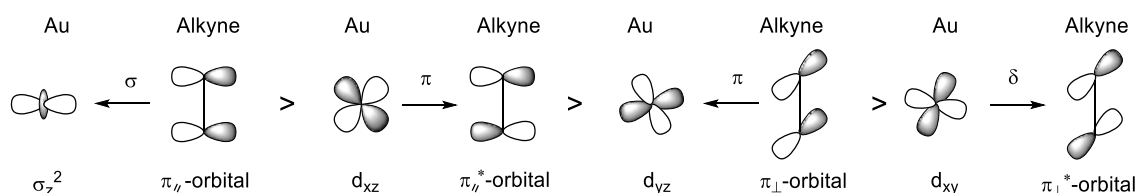


Figure 3.3 Scheme of the Au(I)-alkyne bonding interactions described by the Dewar-Chatt-Duncanson model.

The formation of the complex alters the structures of the metal fragment and of the ligand. The DCD model predicts a lengthening of the C–C multiple bond. The M-alkyne σ -bond depletes the $C\equiv C$ bond by transferring part of these electrons to the metal and thus slightly weakens and lengthens it. However, the back donation from the metal is the major factor in lengthening the $C\equiv C$ bond. Indeed, through back donation, the π^* -orbital of the $C\equiv C$ group is filled and the order of the alkyne C–C lowers. A partial bending of alkynes or pyramidalisation in the case of alkenes occurs, causing a distortion from the geometry of the unbound ligand, visible by NMR.³⁸

3.1.3 Tuning of gold catalysts

Gold catalysts (LAuX or LAuX₃) can be finely tuned through modifications of three aspects: the nature of the organic ligand (L), the oxidation state of gold and the nature of the anion (X).

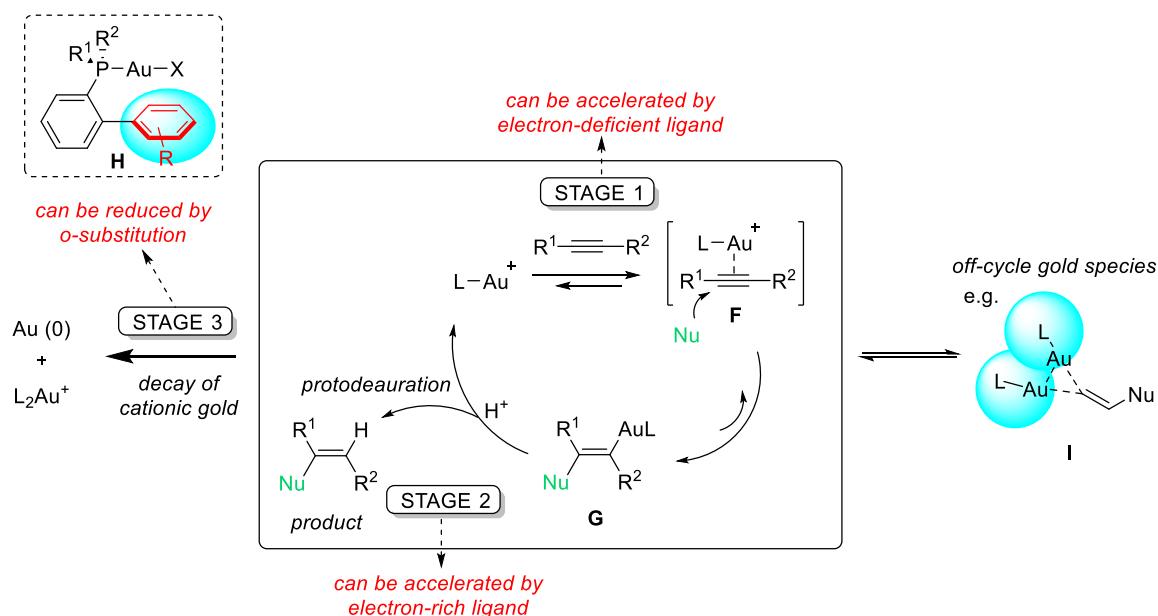
3.1.3.1 Ligand effect

In catalysis, ligands are crucial and play a major role in the tuning of the reactivity of transition metal catalysts. Thus, it is reasonable that in the last years an increased effort has been focused on rationally understanding ligand effects in gold catalysis and designing ligands to enlarge the efficiency (TON).¹⁵ Chiral ligands for enantioselective gold catalysis have been investigated, too.

The reactivity of gold(I) complexes in the activation of alkynes, alkenes, and allenes can be modulated through the sterical or electronical tuning of their ligand depending properties.

In 2012, Hammond and Xu carried out a study of ligand effects in gold catalysis.³³ It is possible to simplify the gold-catalysis cycle in three main stages (Scheme 3.6): i) the nucleophilic attack to the [L–Au]⁺-activated alkyne (or alkene) forming a trans-alkenyl gold complex (intermediate **G**) (or an alkyl gold complex in the case of alkenes), ii) the reaction of complex **G** with an electrophile (E⁺), usually a proton, yielding the final product *via* protodeauration, together with the regeneration of the cationic gold species and finally iii) the decay or deactivation of the gold catalyst.³⁹ In some gold-catalysed reactions, the formation of off-cycle gold species such as bis-Au-vinyl species **I** was observed.⁴⁰ The decay of cationic gold catalysts and the off-cycle gold species reduce the turnover of product formation.

Working on the electronic properties of the ligands, it is possible to accelerate or slow down one step or the other. Hammond and Xu found that electron-poor ligands (e.g. (*p*-CF₃C₆H₄)₃P) accelerate the electrophilic activation of the alkyne/alkene and the corresponding nucleophilic attack (stage 1). This effect may be because phosphine ligands are electron-poor ligands and do not donate to the gold centre, which remains electron-poor and pulls electron density from the alkyne/alkene to make it more electrophilic. The stage 2 (protodeauration) instead is affected by the ligands in the opposite fashion: electron-rich ligands accelerate this step because they donate electronic density to the gold metal centre turning the vinyl gold complex **G** more reactive towards an electrophile (H⁺). Concerning the stage 3 (decay of the gold catalyst), it was found that an *ortho*-substitution in the phosphine ligand greatly enhances the stability of the cationic gold (as in the *o*-biphenyl motif in **H**, Scheme 3.6) because of steric effects. The *ortho*-substituted phenyl ring very close to the gold centre may protect it from decay. Indeed, Echavarren and co-workers succeeded in obtaining crystal structures of these kind of complexes and it resulted that the average distance between an *ortho* phenyl ring and the gold centre is short around 2–3 Å.⁴¹



Scheme 3.6 Gold catalytic cycle in three main steps.

In general, complexes containing more donating ligands as *N*-heterocyclic carbenes are less electrophilic than those with phosphine ligands. Complexes with less donating phosphine ligands and related species are the most electrophilic catalysts (Figure 3.4).⁴²

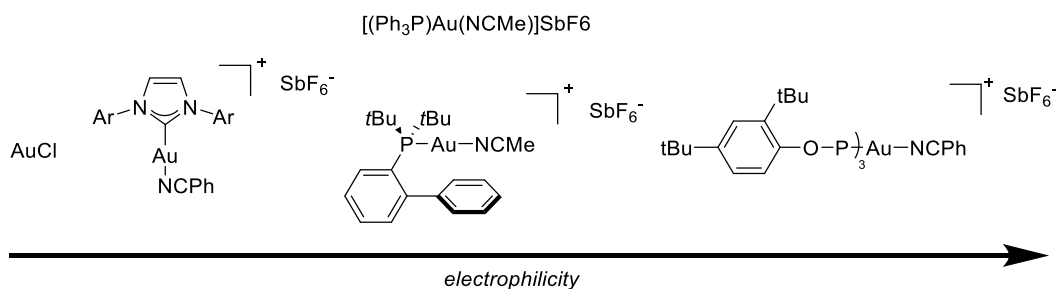


Figure 3.4 Increase in electrophilicity with decreasing donating ligand ability in gold(I) complexes.

In gold-catalysed reactions, the turnover limiting stage can be the nucleophilic addition to alkyne/allene/alkene (stage 1) (type I reactions) or the regeneration of cationic gold catalyst (e.g., protodeauration) (stage 2) (type II reactions).

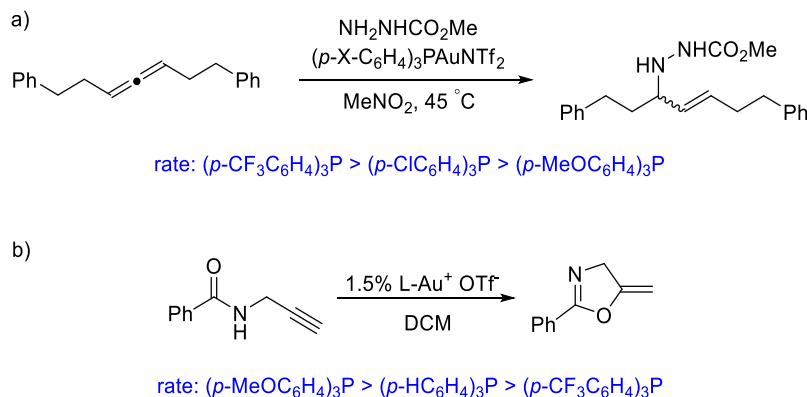
For the design of proper catalysts for the reactions, it is essential to identify the turnover limiting step of the reaction, in order to act on and improve it.

Type I reactions are sped up by electron-poor ligands. This class of reactions happens when the nucleophile is relatively weak (electron-poor amines and amides) or the substrate is a less reactive allene or alkene. The hydroamination of allenes can be classified as type I (Scheme 3.7a).⁴³

On the other hand, type II reactions (majority of gold-catalysed reactions) are sped up by electron-rich ligands. Strong nucleophiles and relatively reactive alkynes as substrates are usually involved. A typical example is the cyclisation of propargyl amide (Scheme 3.7b).³³ Electron-rich carbene-based ligands (e.g. *N*-heterocyclic carbenes) have been used extensively in gold catalysis because of their unique electronic and steric features.⁴⁴

3.1 Introduction

In reactions, in which the decay of the cationic gold is significant, it is appropriate adding special steric handles to the ligands, able to embed or surround the cationic gold centre. This feature may also limit the formation of off-cycle gold species such as the bis-Au-vinyl species (**I** in Scheme 3.6). *Ortho*-substituted phenyls in phosphine ligands are good candidates.



Scheme 3.7 Typical type I and type II gold-catalysed reactions.

3.1.3.2 Counterion effect

In gold catalysis, the effects of ligands have been deeply investigated and only in the recent years the effects of counterion have been taken in consideration in gold-catalysed reactions,⁴⁵ although their influence can be also more pronounced than the corresponding ligand effect.^{46,47} Some examples are the seminal contributions of Maier and co-workers on the gold(I)-catalysed hydroalkoxylation of alkynes,⁴⁸ Echavarren and co-workers on gold(I)-catalysed intermolecular cycloadditions⁴⁹ and Bandini, Macchioni and co-workers on gold-catalysed dearomatisation of indoles with allenamides.⁵⁰ In these works, the authors have reported the observed trends for the studied reactions, analysing the influence of the counterion in every step of the cycle depending on its coordinating ability, basicity and geometry.

An alternative interesting work was reported by Hammond and co-workers, who introduced a method to predict the counterion anion effect by a gold affinity index and a hydrogen bonding basicity index (Figure 3.5).⁵¹

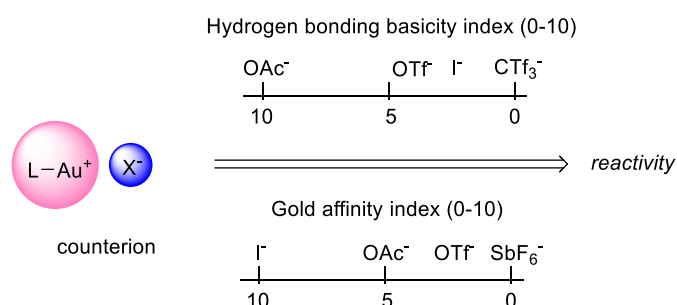


Figure 3.5 Representation of counterion hydrogen bonding basicity and gold affinity influence on the reactivity.

Simplifying, a cationic metal-catalysed reaction can be represented as a system, in which a cationic metal (M^+) interacts with the reactants (RC^1 , RC^2 , etc.) leading to the intermediate or the product through the formation of a transition state (**ts1**) (Figure 3.6

a). In most theoretical treatments of cationic gold catalysis, cationic gold is treated as “free” ion (M^+ in Figure 3.6a). Nevertheless, in low dielectric constant solvents, the cationic metal is not a free ion, but exists as ion pair ($M^+ X^-$), that interacts with RC^1 and RC^2 to produce **ts2** through a charge separation M^+ and X^- (Figure 3.6 b). Compared to the reaction of “free” M^+ , an addition energy has to be considered to overcome the coulombic attraction ($\Delta G^\ddagger_{ts2} > \Delta G^\ddagger_{ts1}$). Considering that the counterion does not influence the structures of the transition states (Figure 3.6 b), the difference in ΔG^\ddagger between **ts1** and **ts2** can be attributed to the affinity between M^+ and X^- .

In general, a catalyst that contains a weakly coordinating counterion (low affinity between M^+ and X^-) exhibits high reactivity. However, when there is a long-range electrostatic attraction interaction between the counterion (X^-) and an active proton (e.g. $O-H^{\delta+}$, $N-H^{\delta+}$) on the corresponding transition structure (**ts3**) (Figure 3.6 c), the counterion may impact for example the proton-transfer process *via* proton shuttling.⁵² This long-range interaction between an active proton and the counterion can be classified as a hydrogen bonding interaction, thus the impact of the counterion to the proton transfer could be quantified by its hydrogen bonding basicity (higher hydrogen bonding basicity, higher impact).

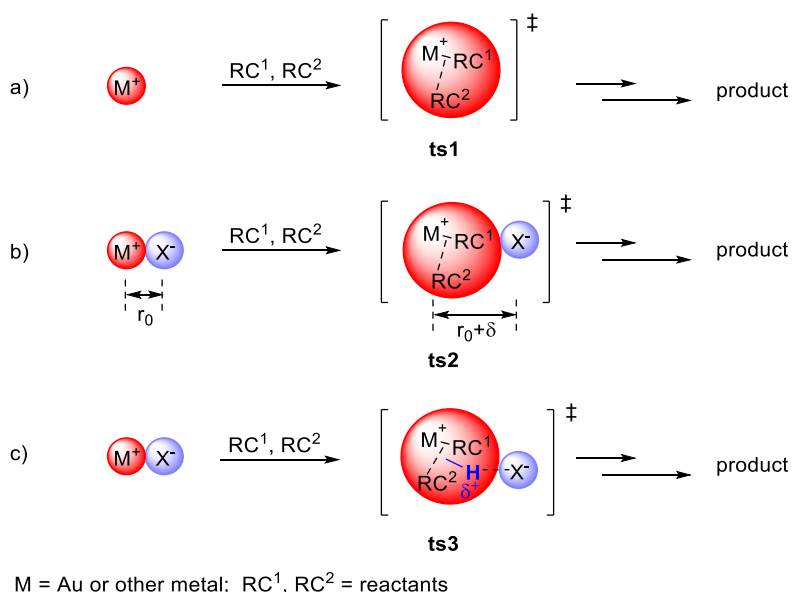


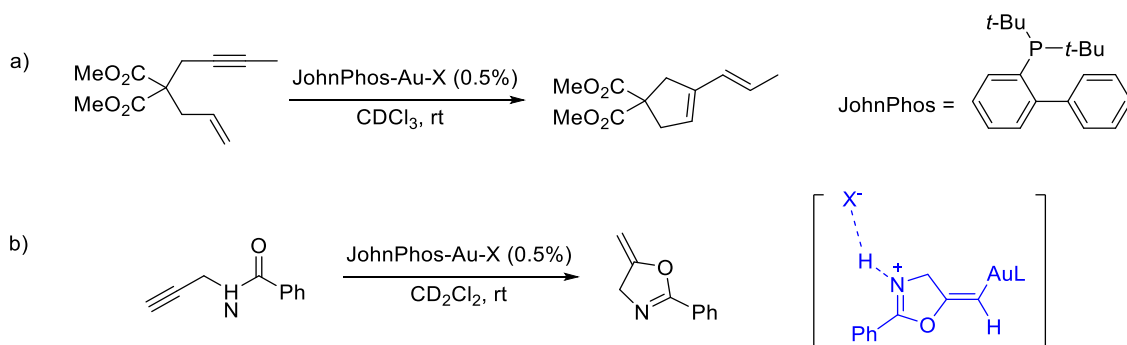
Figure 3.6 Simplified representation of cationic metal-catalysed reactions.

Hammond and co-workers did not observe correlation between hydrogen bonding basicity and Brønsted basicity of counterions, thus a strong hydrogen bonding acceptor is not necessarily a strong Brønsted base. Hydrogen bonding basicity and gold affinity indices of counterions are independent features.

Regarding the gold affinity of counterions, it depends on the size and charge distribution of the counterion, in particular large, negatively charged and highly delocalised counterions have smaller affinity towards cationic gold (e.g., SbF_6^- , CTf_3^-). Counterions, as AcO^- , relatively small and with more localised charge, form strong interactions with the cationic gold metal centre, reason why they are rarely used in gold catalysis.

3.1 Introduction

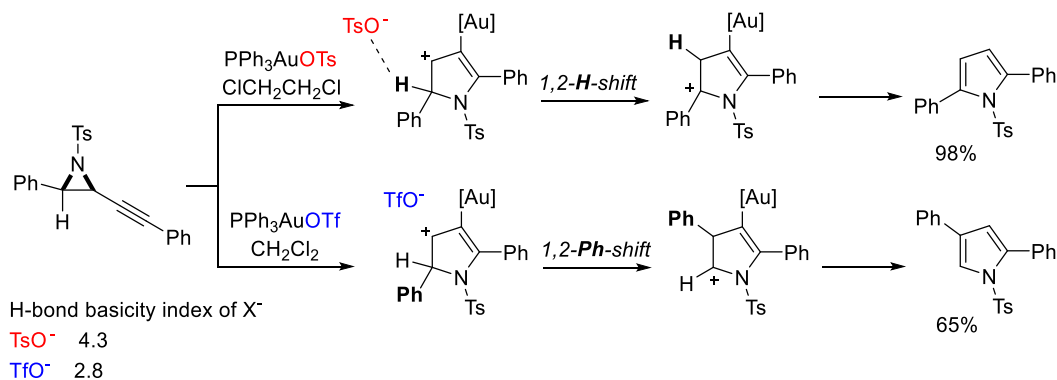
Table 3.1 Counterion effects on the kinetics.



X ⁻	H-bonding basicity index	Gold affinity index	Relative initial rate Reaction A	Relative initial rate Reaction B
OAc ⁻	1.0	6.1	0.0	0.0
OTf ⁻	3.4	2.4	1.0	5.1
BF ₄ ⁻	5.2	0.5	7.1	1.8
SbF ₆ ⁻	2.8	0	21	1.0
CTf ₃ ⁻	0	0.2	32	1.0

The efficiency of Hammond indices is visible in the selected examples reported in Table 3.1. In the case of cycloisomerisation of 1,6-enyne,⁵³ where no active proton is involved (Table 3.1 a), catalysts with counterions with low gold affinity (e.g. SbF₆⁻) show faster kinetics. For reactions, as the cyclisation of propargyl amide,⁵⁴ where there is an active proton involved (Table 3.1 b), counterions with high hydrogen bonding basicity (e.g., TfO⁻) affect more the reaction assisting the proton transfer and speeding it up. Catalysts bearing a counterion with very high gold affinity (e.g. AcO⁻) acted as inhibitor in both types of reactions.

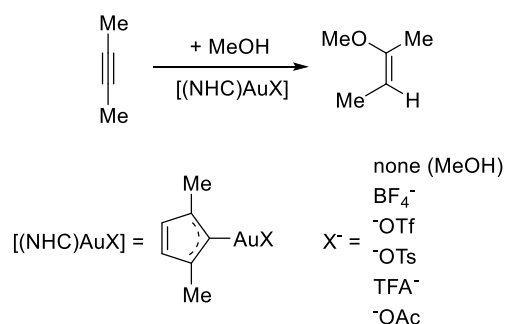
The regioselectivity can also be explained by hydrogen bonding and gold affinity parameters. In the synthesis of disubstituted pyrrole (Scheme 3.8),⁵⁵ the use of a gold catalyst with TsO⁻ as counterion promotes a 1,2-Hydrogen shift (or proton shuttling) product, while a gold catalyst with TfO⁻ (less hydrogen bonding basicity) promotes a 1,2-phenyl shift product.



Scheme 3.8 Effects of the counterion on regioselectivity.

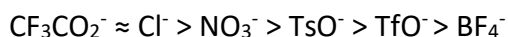
Among all the worth mentioning publications, Ciancaleoni, Zuccaccia and co-workers in 2014 examined the counter anion impact in the NHC gold(I)-catalysed alkoxylation of

alkynes by DFT calculations. They demonstrated that the coordinating ability, basicity and geometry of the counter anion influence all the steps of the reaction mechanism: pre-equilibrium, nucleophilic addition and protodeauration. In detail, in the nucleophilic attack step, the anion acts in three ways (i) as a template, holding the methanol in place for the outer-sphere attack; (ii) as a hydrogen-bond acceptor, enhancing the nucleophilicity of the attacking methanol; (iii) as catalyst deactivator, by its strong coordinating and/or basicity, preventing the alkyne coordination or forming free alkoxide, respectively. In the protodeauration step, the anion acts as a proton shuttle. It was demonstrated that a balance between the hydrogen-bond acceptor and the coordinating powers ensures the best efficiency of L–Au–X catalysed alkyne alkoxylation reactions.⁵⁶



Scheme 3.9 Study of counterion effect on NHC gold(I)-catalysed alkoxylation of alkynes by Ciancaleoni *et al.*

Before Hammond, other groups tried to quantify the metal-anion coordination ability for particular cases. For example, Ujaque and co-workers investigated the coordinating attitude of several monoanionic species towards phosphine-based gold(I) complexes on the base of the dissociation energy of several PPh_3AuX complexes into the corresponding cationic $[\text{PPh}_3\text{Au}^+] + \text{X}^-$ (DCE),^{48,57} providing the trend:



Zhdanko and Maier instead reported an affinity scale in solution for a number of mononuclear $[\text{LAu}(\text{NCMe})]^+$ versus a range of anions and neutral species via ^1H and ^{31}P NMR spectroscopy.⁴⁹

In the scientific community it is generally accepted that i) weakly coordinating anions (i.e., SbF_6^- , $\text{}^-\text{OTf}$, BArF_4^- , BF_4^-) increase the electrophilicity of the gold centres with consequent stronger metal– π system interactions,⁵⁸ ii) better coordinating anions can positively affect late-stage catalytic events, such as sequestering the metal centre from the catalyst resting state or favoring the frequently occurring protodeauration stage addition, iii) basic anions (i.e., benzoates, tosylate, and acetates) create hydrogen-bond interactions, guaranteeing optimal structural geometries or influencing multiple chemo-, regio- or stereoselective channels.

Through tuning the counterion, controlling the stereochemistry of the reaction becomes feasible. There are cases in which gold complexes featuring chiral anions (commonly binol-based phosphates) have been used as the only source of stereochemical

3.1 Introduction

information (Figure 3.7 left),⁵⁹ but in others the use of achiral counterions was enough to control both the kinetics and the stereochemistry of the process, because of steric reasons (Figure 3.7 right).⁶⁰

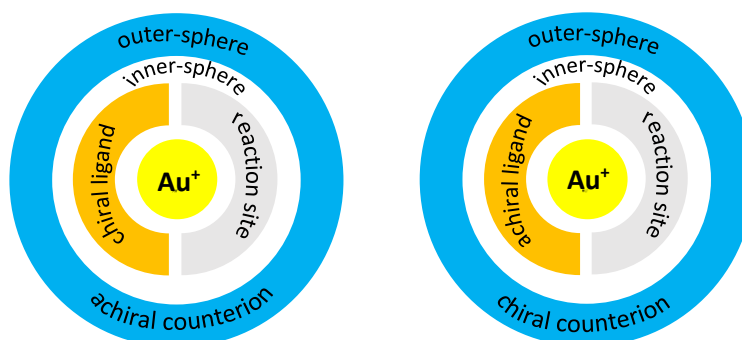


Figure 3.7 Schematic representation of the chiral ligand-based (left) and chiral counterion-based (right) approaches in asymmetric gold catalysis.

In a general perspective, the main roles of the gold counterion have been identified in modulating (i) the kinetics of the process depending on the coordinating properties; (ii) the real structure of the catalytically active species (i.e. formation of clusters, dimers); (iii) the chemo-, regio-, and stereoselectivity of the processes through the formation of optimal interactions.

3.2 A combined computational and experimental study on the role of the N atom in the pentannulation of *N*-heterocycles by the tandem gold(I)-catalysed [3,3]-rearrangement/Nazarov reaction

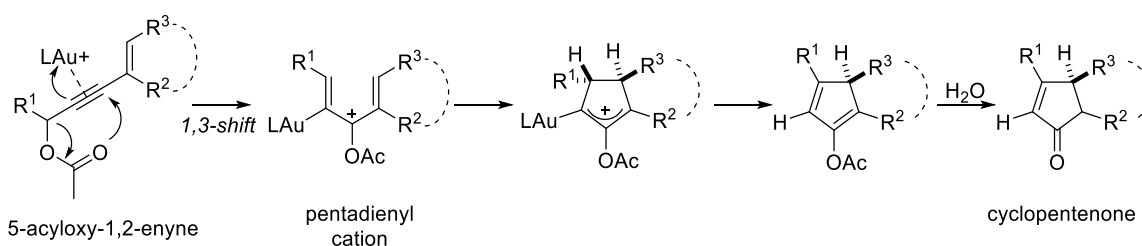
3.2.1 Introduction

2-Cyclopentenones belong to the class of cyclic enones and they participate in many areas of organic chemistry. Indeed, they are useful benchmark substrates for numerous chemical transformations. Moreover, the 2-cyclopentenone molecular scaffold is present in many natural product structures, thus methodologies for its synthesis are worth to investigate.

There are several convenient approaches available to synthesise this class of compounds⁶¹ and among them, one of the most important methods for the preparation of 2-cyclopentenones is the Nazarov cyclisation, reported for the first time in 1941.⁶² The Nazarov reaction ranks as one of the most important and versatile strategies since the requisite 4π electron pentadienyl cation can be generated from classical dienones and also from a steadily increasing variety of unconventional substrates or processes,^{63,64} including gold-catalysed transformations.⁶⁵

Suitably assembled propargylic esters are particularly useful as substrates for the Nazarov reaction, since the transition metal-catalysed migration of the carboxylic group to any of the two unsaturated positions leads to competent pentadienyl cations.

A general pathway for the synthesis of cyclopentenones starting from a propargylic ester derivative is represented in Scheme 3.10. 5-Acyloxy-1,3-enynes undergo, under mild conditions, a gold(I)-catalysed [3,3]-rearrangement yielding pentadienyl cations, which are suitable for Nazarov cyclisation and after protodeauration lead to acetyloxy-substituted cyclopentadiene products. A final hydrolysis (*in situ* or after work-up) provides the cyclopentenones. When the enyne double bond is embedded in a ring, it is possible to obtain cyclopenta-fused carbocycles.

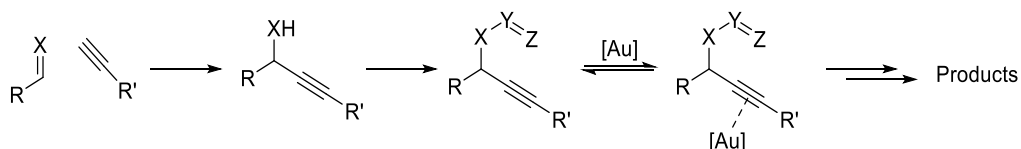


Scheme 3.10 General sequence of gold(I)-catalysed [3,3]-rearrangement/Nazarov reaction for the synthesis of cyclopentenones.

3.2.1.1 Propargylic esters

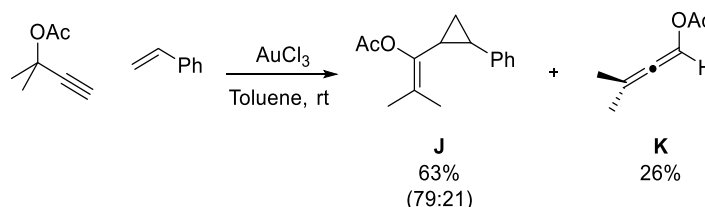
Among all the substrates involved in gold catalysed transformations, propargylic alcohol derivatives have received increasing attention. This interest is mainly due to the fact that they are easily accessible starting materials *via* standard synthetic manipulations from readily available aldehydes, ketones and alkynes. Changing the fragments attached to the heteroatom at the propargylic position (X in Scheme 3.11) widens the chemistry of these substrates.

3.2 Tandem gold(I)-catalysed [3,3]-rearrangement/Nazarov reaction



Scheme 3.11 Propargylic alcohol derivatives under gold catalysis.

In particular, propargylic ester building blocks have attracted the synthetic community since the late 1950s, before the advent of gold catalysis. Indeed, in 1959 Saucy, Marbet and co-workers reported the rearrangement of acetates of tertiary ethynylcarbinols to allenic acetates in the presence of acetic acid and a silver or copper catalyst,^{66,67} which later became one of the most emblematic gold-catalysed transformations. Only in 2003 Miki, Ohe and Uemura described the Au(III)-catalysed reaction of propargyl acetate with styrene yielding the desired cyclopropane **J** and 26% of the allenyl ester **K** (Scheme 3.12).⁶⁸



Scheme 3.12 Results of Miki, Ohe and Uemura.

Products **J** and **K** are the results of two different pathways. Many studies were published adopting either one of these two distinct mechanistic routes. Mechanistic aspects that determine the outcome of these transformations are still under debate. Indeed, there are many factors that influence the reactivity of each substrate, as the substitution at the alkyne (terminal *versus* internal), the electronic nature of the substituents directly attached to the propargylic ester, the nature of the migrating group, the Lewis acidity of the catalysts or the presence of Lewis basic or nucleophilic sites within the starting materials. Every subtle difference can heavily affect the outcome of each reaction.

The accepted scenario is the following: after coordination with the carbophilic gold catalyst,^{12,19} the alkyne undergoes a cyclisation-induced⁶⁹ nucleophilic attack by the carbonyl oxygen in the ester unit. Depending on the exact structure of the substrate and the reaction conditions, it can produce a 1,2-acyloxy migration ([2,3]-rearrangement of the ester) giving a Au-carbene (Scheme 3.13, route A) or a 1,3-acyloxy migration ([3,3]-rearrangement of the ester) giving a Au-allene (Scheme 3.13, route B).

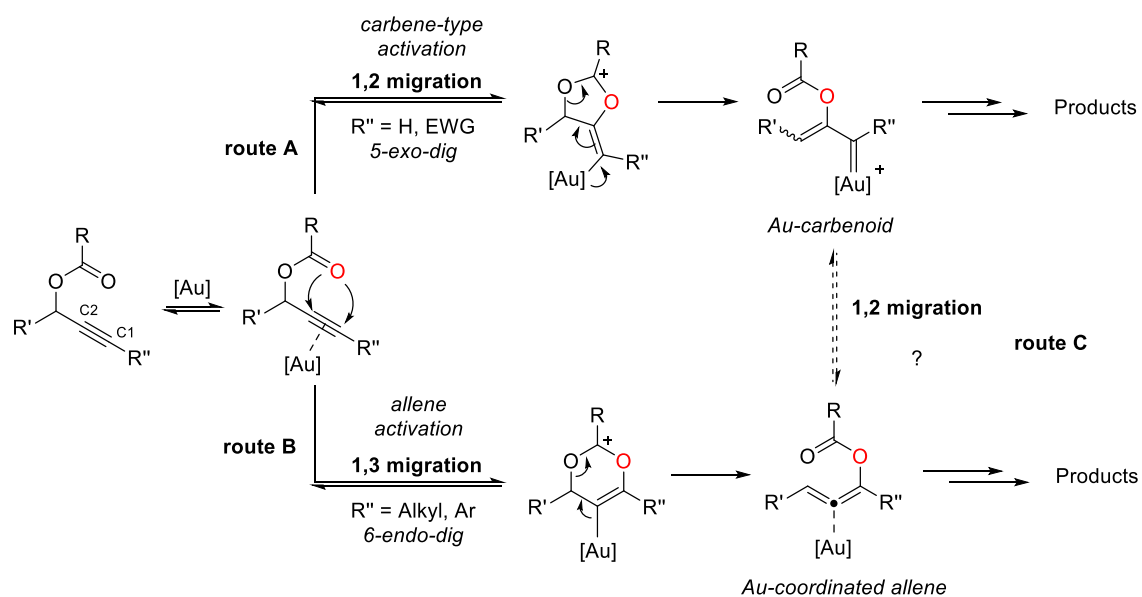
Synthetic and theoretical reports proved that the [2,3]-rearrangement leads to gold carbenoid intermediates that then react in an intra- or intermolecular fashion to produce also complex carbocyclic structures. Carbenoids are described as “intermediates which exhibit reactions qualitatively similar to those of carbenes without necessarily being free divalent carbon species”.⁷⁰ Based on experimental and theoretical reports, this behaviour results plausible and related to the relativistic expansion of the 5d orbitals of gold.⁷¹ As a result of this expansion, electrons in these orbitals can be delocalised into carbon-based orbitals.

Concerning the gold-catalysed [3,3]-rearrangements, the mechanism is still under debate, but studies generally postulate a stepwise process through two low-energy activation steps,^{30,72} which results in the formation of gold(I)-coordinated allenes (Scheme 3.13, route B). They found that the electron-donating abilities of the allene substituents determine the η^1 - or η^2 -allene character of Au(I)-coordinated allenes, influencing their reactivity.⁷³ Another hypothesis is that the formation of the gold-coordinated allene might be the result of a second 1,2-acyloxy migration through a gold carbenoid (route C in Scheme 3.13), not confirmed by synthetic evidence. Both rearrangement mechanisms are competitive processes and probably operate in most of the systems studied.⁷⁴ The electrophilicity of C1 and C2 might be the key factor for the predominance of one pathway over the other. As a result, internal and electronically unbiased propargyl esters preferentially give [3,3]-rearrangement-derived products, while terminal alkynes and internal alkynes substituted with electron-withdrawing groups typically follow the [2,3]-pathway. This “rule of thumb” is supported by the work of Soriano and Marco-Contelles, who demonstrated that substitution patterns dictate formation of vinyl gold *versus* gold carbenoid species.^{75,76}

From their studies, it emerges that: i) substitution at the acetylenic position strongly influences the electronic properties of the activated alkyne, enhancing the electrophilicity of the acetylenic atom and thus the 1,3-acyloxy shift; ii) steric repulsion between the acetylenic substituent and the gold atom makes that the latter is pushed out, increasing the metal–C1 distance (to reduce the steric hindrance) and decreasing metal–C2 distance, thus reversing the polarisation of the gold-coordinated alkyne and increasing the electrophilicity at C1.

Other groups investigated this reactivity and found some exceptions. For example, Echavarren and co-workers reported examples of [3,3]-rearrangements of terminal alkynes.⁷⁷ In addition, Zhang and co-workers reported the gold-catalysed reaction of electronically unbiased internal alkynes affording (1Z,3E)-2-pivaloxy-1,3-dienes through a 1,2-acyloxy migration.⁷⁸ Later, Nevado group observed a Au-catalysed tandem 1,2-/1,2-bis(acetoxy) rearrangement of 1,4-bis(propargyl acetates) resulting in the formation of 2,3-bis(acetoxy)-1,3-dienes.⁷⁹

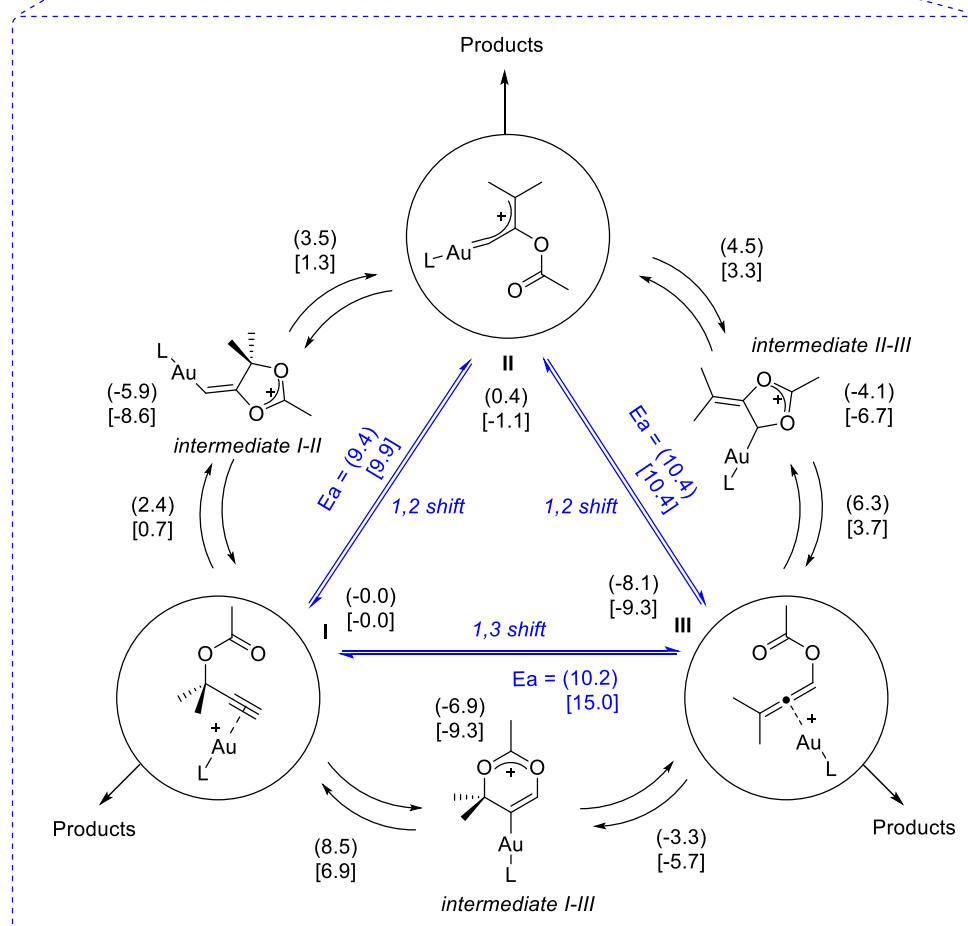
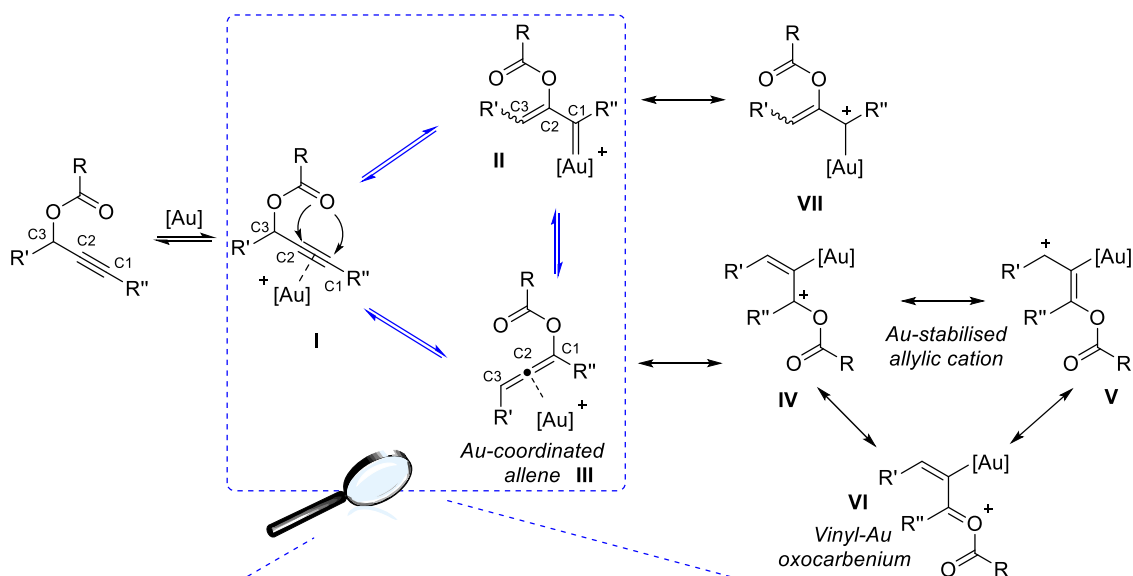
3.2 Tandem gold(I)-catalysed [3,3]-rearrangement/Nazarov reaction



Scheme 3.13 General reactivity patterns for propargyl esters.

A worth mentioning work about the reactivity of propargylic esters is the one of Cavallo and co-workers, who in 2008 reported a DFT study regarding the reversibility of the [2,3]-rearrangement and [3,3]-rearrangement of esters.³⁰ They suggested that, under typical conditions, the starting Au-coordinated propargylic esters, the gold-carbenoids and the gold-coordinated allenes could interconvert easily forming a “golden carousel” (Scheme 3.14, top). Then, several factors could dictate which intermediate is favoured and which type of product is formed.

They calculated the energy barriers of the reactions of interconversion from one to the other (forward and backward) and it resulted that all the energy values obtained are accessible at the reaction conditions and do not differ significantly between them. This evidence leads to the conclusion that the three species are in fast equilibrium and that the final direction of the equilibrium system depends on the energy barriers associated with reactions involving intermediates I, II and III and leading to products irreversibly (Scheme 3.14). It is noteworthy that the reactivity of these intermediates depends on other functional groups (typically, C-C double bonds and heteronucleophiles) on the substrate, on the nature of the ligand and on the reaction conditions too. Simple modifications of the propargylic, acetylenic, and/or acyl substituents, as well as the nature of the migrating function, result in astonishingly diverse product patterns.

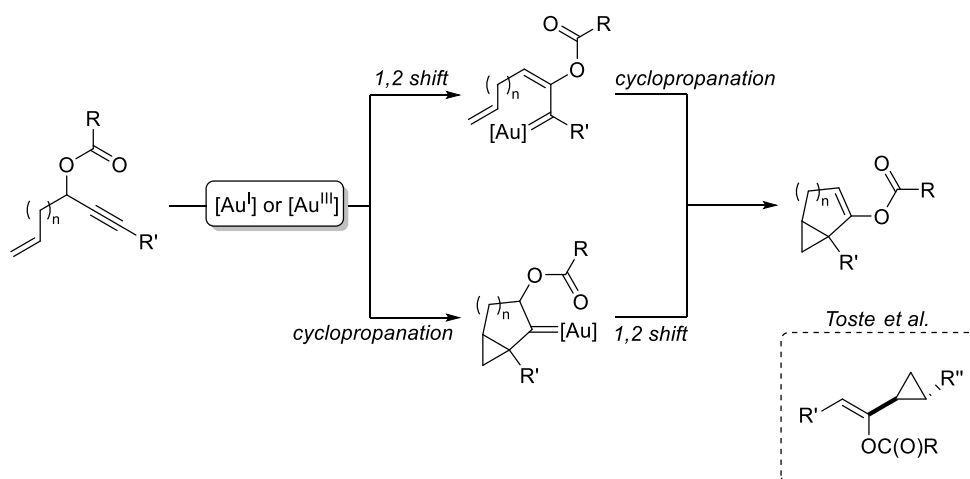


Scheme 3.14 On the top, key intermediates along the catalytic cycle of propargylic ester in equilibrium; on the bottom, a look into the equilibrium cycle thermodynamics, computed by Cavallo and co-workers. Energies in kcal/mol (in round/square brackets for $L=Me$ and PMe_3 , respectively) are calculated relative to **I**. Numbers close to the arrows represent the energies of the transition states associated with that reaction step.

The reversibility of the [3,3]-rearrangement and the [2,3]-rearrangement was demonstrated later by Toste group using a stereochemically defined starting material⁷³ and by the group of Nolan.⁸⁰

Examples of [2,3]-rearrangement

An interesting example of 1,2 acyl shift is the early work by the group of Fürstner, who showed that cationic gold(I) could catalyse the synthesis of bicyclo[(n+2).1.0] compounds (Scheme 3.15).⁸¹

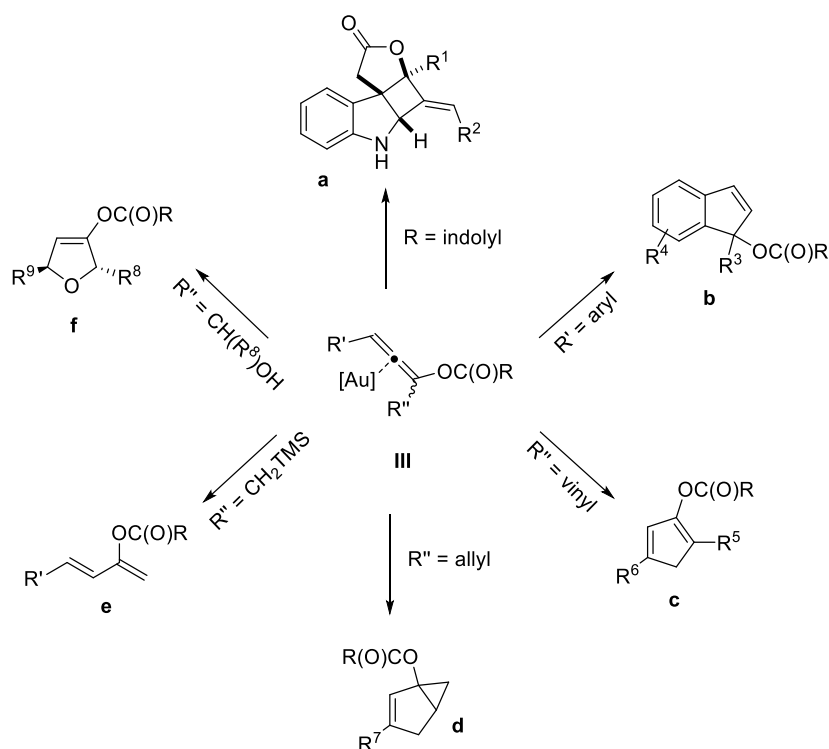


Scheme 3.15 Au-catalysed tandem 1,2-shift/cyclopropanation.

The cyclopropanated product features the stereogenic information contained in the propargylic position. Thus, a “cyclopropanation then migration” mechanism was assumed. In sharp contrast, the study of the intermolecular version, affording allylcyclopropanes (Scheme 3.15), by Toste *et al.* revealed that the stereogenic outcome of the reaction is consistent with a “migration then cyclopropanation” sequence.⁸²

Examples of [3,3]-rearrangement

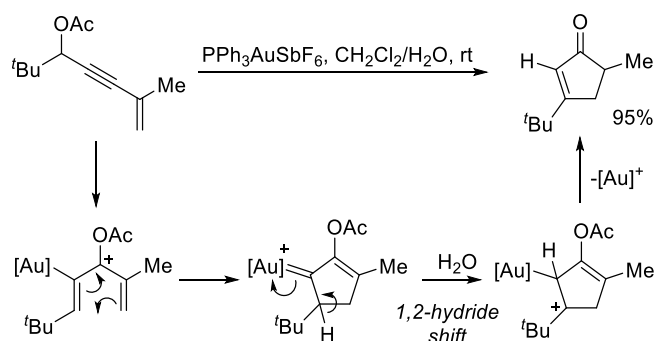
The [3,3] sigmatropic rearrangement allows the transformation of propargylic esters into allenyl esters, which are activated by gold catalysis to undergo also subsequent reactions (Scheme 3.16). For this reason, the expected densely functionalised electron-rich allenyl esters are hardly detected in the reaction mixtures, because they are susceptible to new transformations. The rearrangement outcome depends on which resonance form contributes most (Scheme 3.14) and on the specific structure of the gold-coordinated bent allenes, which, influenced by the substitution, can be η^1 (a bent allene that behaves as a gold-stabilised allylic cation) or η^2 (structure closer to linearity with allene-like behaviour).^{73,83}



Scheme 3.16 Au assisted allene activation and product diversification.

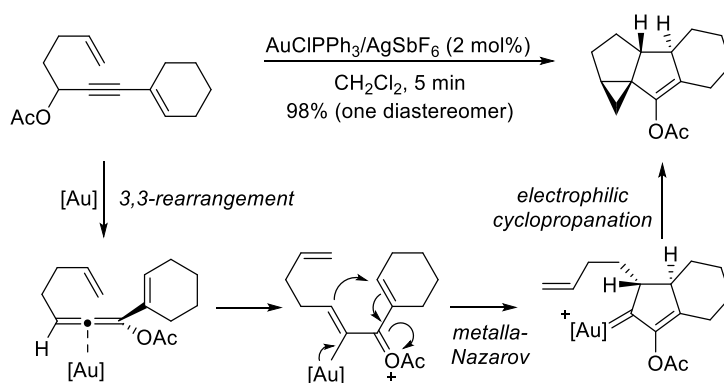
Gold-coordinated allenes generated through a gold-catalysed [3,3]-rearrangement of propargyl esters can react with nucleophilic double bonds. In 2005, Zhang reported the formal [2+2] intramolecular cycloaddition of propargyl esters and nucleophilic indoles,⁸⁴ yielding 2,3-indoline-fused cyclobutanes **a** (Scheme 3.16). This reaction proceeds through an initial [3,3]-rearrangement of the indole-3-acetoxy group leading to the gold-coordinated allenyl ester, which undergoes intramolecular nucleophilic attack by the electron-rich indole ring forming the γ -lactone ring. A subsequent intramolecular trapping of the resulting iminium by the alkenylgold(I) yields the observed cyclobutane. When an aryl group was placed at the propargylic position R' , tandem [3,3]rearrangement/intramolecular hydroarylation of phenylpropargyl acetates afforded indenenes **b** (Scheme 3.16).⁸⁵ When terminal alkynes were used, 1,2-shift of the acetate was observed prior to cyclisation, highlighting the high substrate dependence of the shift. Interestingly, if an alkyne moiety was placed in *ortho* position of the aryl ring, naphthalene derivatives were obtained by means of a Myers–Saito cyclisation.^{86,87} Structural features at the acetylenic position of the cyclisation precursor play also a crucial role. When R'' =vinyl, Nazarov-type cyclisation was observed, yielding cyclopentadienyl esters **c** (Scheme 3.16), which can be hydrolysed *in situ* to give the corresponding conjugated cyclopentenones. This is the work of Zhang and Wang, who reported in 2006 the rearrangement of enynyl acetates forming cyclopentenones *via* a tandem sequence involving a gold(I)-catalysed [3,3]-rearrangement and a Nazarov reaction.⁸⁸ After the 1,3-acyloxy migration, the resulting gold-coordinated allene was conjugated with an alkene, thus becoming a pentadienyl cation (Scheme 3.17). This species is feasible for a Nazarov cyclisation leading to cyclopentenones. From a mechanistic computational analysis,⁸⁹ the [1,2]-hydride shift from intermediate resulted

to be the rate-limiting step, sped up by the presence of water as proton-transport catalyst.



Scheme 3.17 Au-catalysed tandem [3,3]-rearrangement-Nazarov reaction by Zhang *et al.*

One year later, Fensterbank group reported a method for the synthesis of polycyclic compounds from propargyl acetates and vinyl allenes involving three Au(I)-catalysed steps: a 3,3-rearrangement, a metalla-Nazarov reaction and an electrophilic cyclopropanation (Scheme 3.18).⁹⁰



Scheme 3.18 Au-catalysed cyclisation/cyclopropanation by Fensterbank *et al.*

On the other hand, when R'' =allyl, bicyclo[3.1.0]hexenes **d** (Scheme 3.16), isomers of those formed through 1,2-acyl shift, were produced in the presence of gold(I) catalysts.⁹¹ Through modification of the substitution of the alkyne it is possible to synthesise conjugated dienes **e** (Scheme 3.16) by Au-catalysed protodesilylation of intermediate **III**⁹² and for the formation of dihydrofurans **f** (Scheme 3.16) from propargylic alcohols.⁹³

3.2.1.2 Nazarov reaction

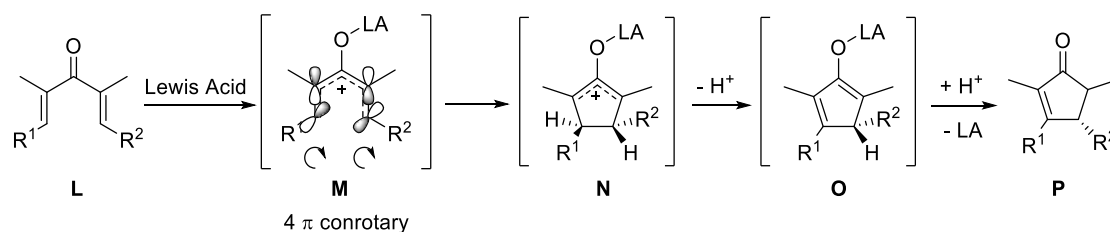
The Nazarov reaction is an acid-catalysed 4 π -electron conrotatory cyclisation of a pentadienyl cation that leads to a five-membered ring, typically a cyclopentenone.^{94–96} The crucial conrotatory electrocycloislation of the pentadienylic cation creates a carbon–carbon bond and two stereocentres. Some or all of the stereochemical information is lost in the subsequent deprotonation.

Besides dienones of type **L** (Scheme 3.19), many species have been used as precursors for the generation of pentadienyl cations suitable to undergo electrocycloislation, *i.e.* α -alkoxy enones, β' -substituted enones, α -vinylcyclobutanones, *gem*-dichloro-homoallyl alcohols, *gem*-dichlorocyclopropylmethanols, vinyl allenes, dienynes, enynol derivatives, and ynediols.

The transformation proceeds through an accepted pathway, as depicted in Scheme 3.19: i) a divinyl ketone (**L**) complexes to the Lewis acid to give a pentadienyl cation (**M**); ii) cyclisation occurs leading to a oxyallyl cation (**N**), which features an anti relationship between R1 and R2 due to the conrotatory ring closure dictated by the principle of conservation of the orbital symmetry during the cyclisation of pentadienyl cation **M**; this intermediate potentially goes through diverse reaction pathways such as carbocationic rearrangements or interception with external nucleophiles. Traditionally, iii) the elimination of a proton occurs giving the Lewis-acid bound enolate (**O**); and finally, the protonation of the enolate providing the cyclopentenone product (**P**). Since disrotatory closure is electronically forbidden, stereospecificity is ensured for the bond formation.⁹⁷ Thus, the Nazarov cyclisation has the potential to transform an achiral molecule into a single stereoisomeric product. Furthermore, the diastereoselectivity of the reaction can be influenced by stereocentres in the substrate ('torquoselectivity').

Despite being a useful strategy, the Nazarov cyclisation process has serious reactivity and selectivity problems that have historically compromised its synthetic utility. In particular, strong Lewis acids are often required to promote cyclisation; ii) multiple equivalents of acid promoter are required; iii) the elimination of the proton is not regioselective (see **N**→**O**); iv) elimination of the proton leads to loss of a stereocentre (see **O**); v) protonation of the enolate is not stereoselective (see **O**→**P**).⁹⁸

The review by Frontier and co-workers discusses the catalytic advances in the Nazarov cyclisation, including the design of new catalysts, formulation of new conditions, variations of the electrocyclicisation, tandem processes, enantioinduction and application to natural product synthesis.⁹⁶ Our interest focuses in the use of Lewis acids including transition metal catalysts, as gold.

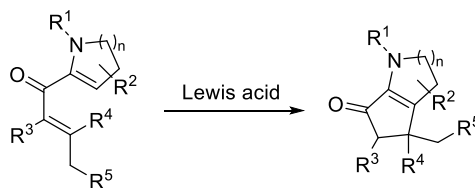


Scheme 3.19 Nazarov reaction mechanism.

In general, the reactivity of divinyl ketones is affected by the Lewis acid promoter and by the features of the substrate such as the conformation of the pentadienyl cation intermediate, and both the position and nature of substituents on the substrate.

A noteworthy case is the one of substituents bearing heteroatoms (Scheme 3.20). The N atom helps the delocalisation of the positive charge from the pentadienyl to the 2-hydroxyallyl cation (rate-limiting step of the Nazarov reaction) stabilising the positive charge and lowering the energy of the transition state, thus accelerating the process. A suitably positioned heteroatom in the cycle is therefore mandatory for electrocyclicisation to occur under mild conditions and at room temperature.⁹⁹

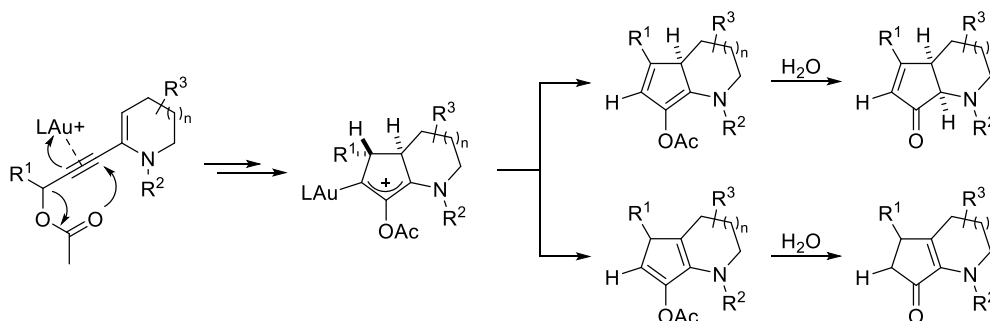
3.2 Tandem gold(I)-catalysed [3,3]-rearrangement/Nazarov reaction



Scheme 3.20 Alternative substrate undergoing Nazarov cyclisation.

3.2.1.3 Tandem 3,3-rearrangement/Nazarov reaction

The employment of the tandem 3,3-rearrangement/Nazarov reaction resulted successful and a valid tool to synthesise cyclo-pentafused heterocycles.⁹⁹ Intrigued by that, Occhiato group wanted to investigate whether the same approach could furnish annulated systems when embodying the same double bond into *N*-heterocycles (Scheme 3.21), in order to provide a new strategy in the field of pentannulation of heterocycles.¹⁰⁰

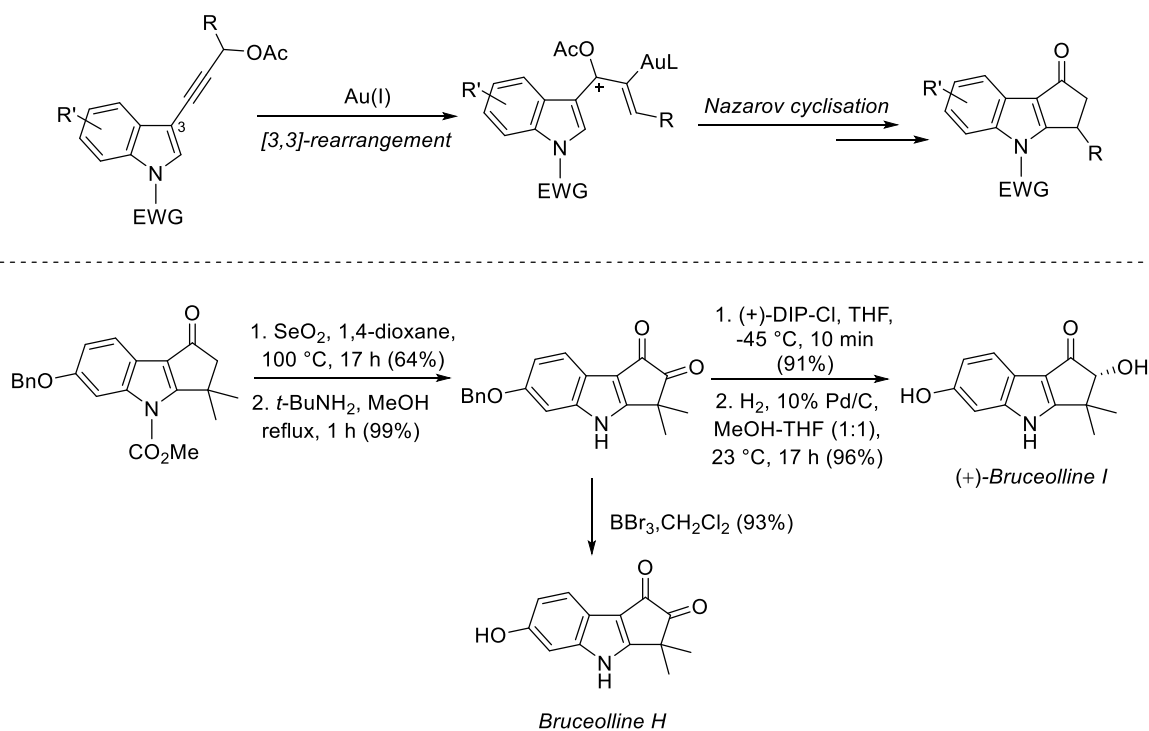


Scheme 3.21 Sequence of gold(I)-catalysed [3,3]-rearrangement/Nazarov reaction for the synthesis of cyclopenta-fused *N*-heterocycles.

They demonstrated that subjecting simple well-designed propargyl ester derivatives to tandem gold(I)-catalysed rearrangement/Nazarov reaction provides cyclopenta-fused *N*-heterocyclic structures present in many natural compounds.¹⁰¹

First, the gold-catalysed rearrangement of enynyl acetates readily occurs when using hexafluoroantimonate as the noncoordinating anion, generating a divinyl cation that undergoes a 4 π electrocycloisomerisation forming the target annulated *N*-heterocyclic compound in good to excellent yield. They found out that the presence of the *N* atom clearly favours the nearly exclusive formation of the Nazarov product having the most substituted double bond. Nevertheless, the synthesis of cyclopenta-fused *N*-heterocycles is more complex than the case of non-heterocyclic systems because several elements, such as the *N*-protecting group, the heterocycle ring size and the gold(I) counterion, influence the reaction rate and regio- and stereo- selectivity.

To expand the applicability of the strategy, Occhiato group started investigating the 5-acyloxy 1,3-enynes, bearing a propargylic moiety in an indole ring at position 3.¹⁰² The tandem gold(I)-catalysed rearrangement/Nazarov reaction of this substrate leads to the formation of cyclopenta[*b*]indoles with a substitution pattern on the five-membered ring. This kind of product is very valuable in total synthesis because it participates in the synthesis of bruceollines and other natural products possessing the cyclopenta[*b*]indol-1-one nucleus. Indeed, the synthetic potential of the methodology is demonstrated by the first total synthesis of bruceolline H and I (Scheme 3.22).^{102,103}



Scheme 3.22 Tandem Au(I)-catalysed [3,3]-rearrangement/Nazarov reaction and application for the synthesis of Bruceolline H and I by Occhiato *et al.*

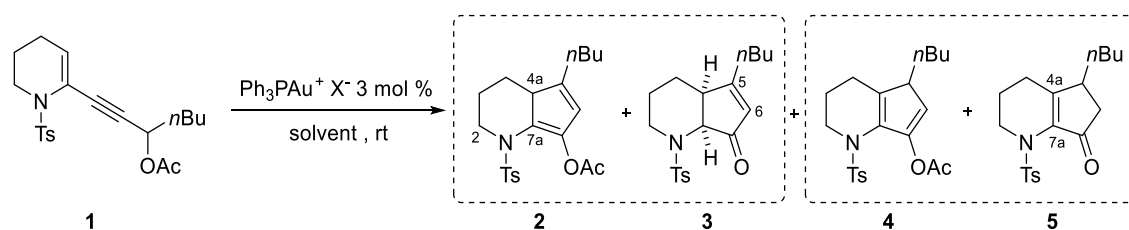
3.2.2 Background

A detailed study of the gold(I)-catalysed tandem [3,3]-rearrangement/Nazarov reaction of propargylic acetate derivatives for the synthesis of cyclopenta-fused *N*-heterocycles was disclosed by the group of Occhiato.¹⁰¹ They started performing the reaction with compound **1**, which proved to be a competent substrate in the screening of the catalytic system (Table 3.2). In all cases, the expected acetate **2** was obtained in mixture with cyclopentenone **5** bearing the more substituted double bond in 4a–7a position and possibly deriving from the hydrolysis *in situ* of its acetate precursor **4** (never isolated). Unexpectedly, in contrast with the behaviour of carbacyclic systems,⁸⁸ only using Ph₃PAuCl/AgOTf compound **2** was the major product and the best result was achieved in toluene affording pure acetate **2** in 61% yield and **5** in 18% yield.

With all of the other silver salts the major product was cyclopentenone **5** (entries 4–5) accompanied by lower amounts of acetate **2** and only traces (less than 5%) of cyclopentenone **3**. The best silver salt was AgSbF₆ (entry 5) providing cyclopentenone **5** in 70% yield together with some residual acetate **2** (14 %).

3.2 Tandem gold(I)-catalysed [3,3]-rearrangement/Nazarov reaction

Table 3.2 Significant reaction of the screening of sequential gold(I)-catalysed rearrangement/Nazarov reaction of acetate **1**.^a



	Catalyst	Conditions	Time (h)	Yield 2	Yield 3	Yield 4	Yield 5
1	Ph ₃ PAuCl/AgOTf	CH ₂ Cl ₂	1.5	51	-	-	35
2	Ph ₃ PAuCl/AgOTf	Toluene	1	61	-	-	18
3	Ph ₃ PAuCl/AgOTf	Toluene, 0°C	5	60	-	-	15
4	Ph ₃ PAuCl/AgBF ₄	CH ₂ Cl ₂	3	18	5	-	62
5	Ph ₃ PAuCl/AgSbF ₆	CH ₂ Cl ₂	2.5	14	3	-	70

^aReactions were carried out on 0.1–0.15 mmol scale, at 25 °C and left standing whilst stirring 16 h after consumption of the starting material. An aqueous work-up was carried out to recover the products from the reaction mixture.

^bCatalysts were prepared by adding the silver salt to a 0.004 M solution of the gold(I) chloride in the reaction solvent.

^cSolvents were not dried before use unless otherwise indicated. ^dTime to reach complete conversion of the starting material. ^eYield after chromatography unless otherwise indicated.

The exclusive isolation of **2** and the impossible isolation of **4**, together with the slower conversion of **2** to corresponding cyclopentenone **3** when under hydrolytic conditions, suggests that acetate **2** only slowly hydrolyses under the reaction conditions, while isomer **4** is quickly converted into the corresponding cyclopentenone **5**, without being isolable. Since cyclopentenone **5** is the major product in the reaction, it is reasonable to hypothesise that the formation of acetate **4** from oxyallyl cation (Scheme 3.23) is more favoured than the formation of isomer **2** and a fast hydrolysis of **4** under the reaction conditions occurs. In the case of the corresponding carbacyclic systems in the work of Zhang group, only the cyclopentenone with the least substituted double bond was observed.⁸⁸

The scope of the reaction ranges from six to seven-membered *N*-heterocyclic rings and various substituents at C3' on the propargyl moiety. Pyrroline derivatives instead resulted unsuitable for this approach. *N*-protecting groups, heterocycle ring size, gold(I) counterion influence the reaction rate and selectivity (regio- and stereoselectivity).

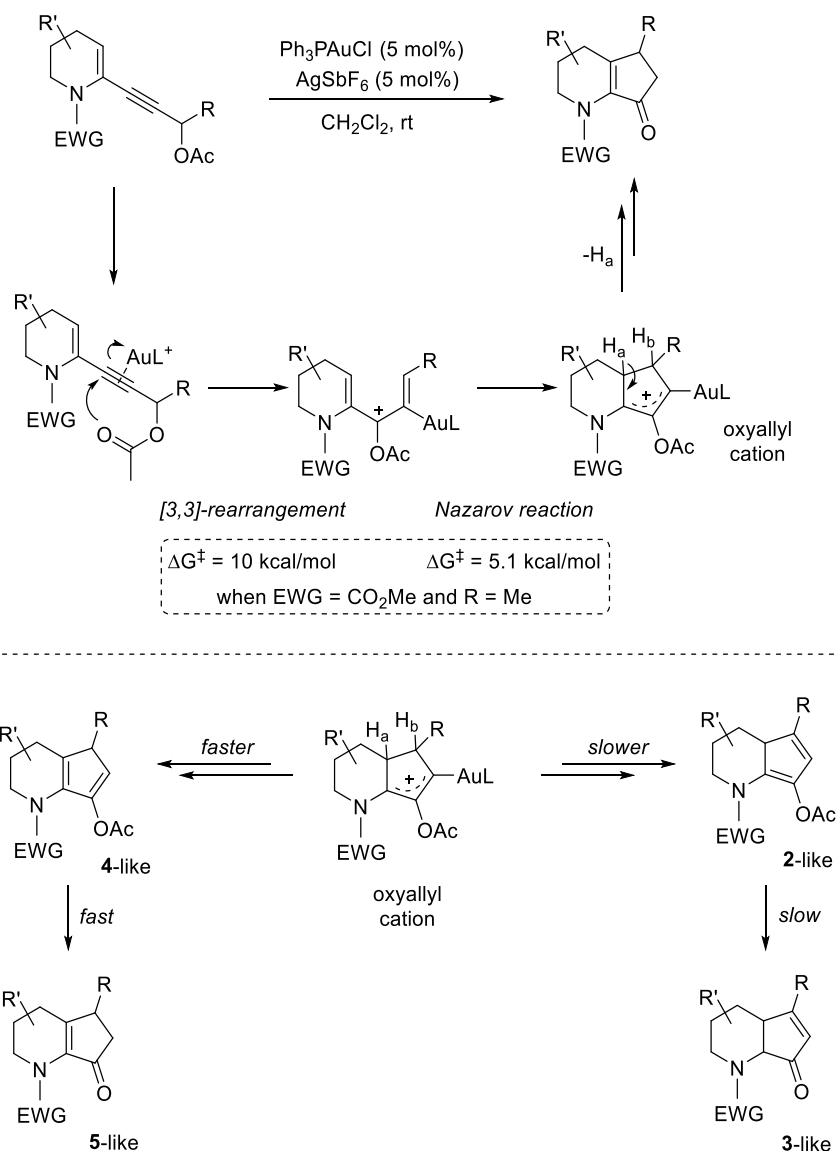
A computational analysis was carried out to clarify the mechanism of the process, using a model complex for sake of simplicity. The model complex bears a methyl substituent in the propargylic position and a *N*-CO₂Me moiety.

Considering as the starting point the alkynyl-gold(I) cationic complex, the reaction proceeds through the [3,3]-rearrangement (energy barrier of 10.0 kcal/mol), followed by the Nazarov cyclisation (energy barrier of 5.1 kcal/mol). The final step is the formation of the diene through proton abstraction. It could occur *via* single-step intramolecular hydride shift with concomitant C-Au bond breaking or *via* deprotonation by an external base. The first pathway was excluded because the calculated energy barrier was too high (30.0 kcal/mol). The second pathway was the most plausible but quite ambiguous because several possible candidates were present in the reaction media: the gold

counterion in the gold(I) salt, the anion of the silver salt^{104,105} or even water molecules.^{88,89,104} The proton abstraction was considered the regiodetermining stage. The triflate-mediated abstraction of H_a or H_b was computed and the results indicated that the process was not highly regioselective. Indeed, the two abstractions resulted to occur overcoming very similar energy barriers (0.8 kcal/mol of difference), with H_b-abstraction being the favoured one. The small energy difference reflects the ratios of regioselectivity found experimentally. The calculations of the hydrolysis step are in agreement with the experimental results and explain why non-hydrolysed **2** and hydrolysed **5** are the final products of the reaction. Indeed, the protonation of **4**-like model compound is predicted to be three or four orders of magnitude faster than the corresponding protonation of the **2**-like model compound. The result can be understood in light of the dienamine structure of compound **2** and the donor character of the nitrogen atom, which can stabilise the structure making it less prone to hydrolysis. It was observed that the protodeauration is substrate-dependent and could be partially controlled by the choice of the counterion and solvent.

To sum up, the computational study showed that the reaction proceeds through an acetate rearrangement, which is the rate-determining step, and a fast Nazarov reaction, accelerated by the stabilising effect of the N atom on the oxyallyl cation intermediate formed upon the ring closure. This was in analogy with that found for the classical Brønsted or Lewis acid catalysed Nazarov reaction involving *N*-heterocycles and in accordance with the polarised Nazarov reaction concept developed by Frontier.^{96,98}

3.2 Tandem gold(I)-catalysed [3,3]-rearrangement/Nazarov reaction



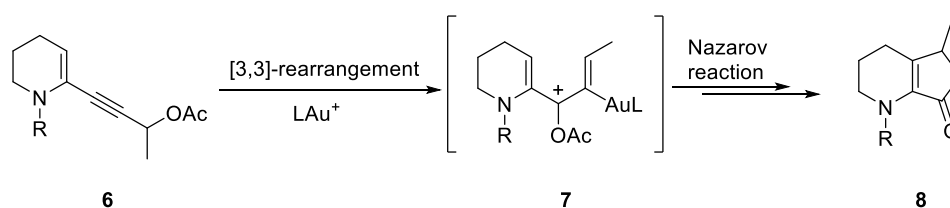
Scheme 3.23 On the top tandem Au(I)-catalysed [3,3]-rearrangement/Nazarov reaction by Occhiato *et al.* and on the bottom the two competing pathways to **3**- and **5**-like compounds.

3.2.3 Abstract

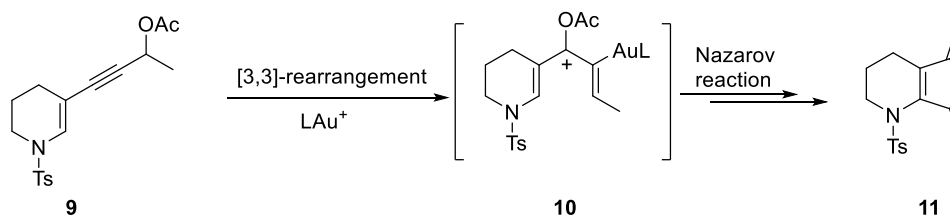
The gold-catalysed rearrangement of suitably substituted propargylic esters provides a platform for cascade processes, which involve a cationic or an allene intermediate generated in the first step. As seen in the previous section, the group of Occhiato reported that the pentannulation of *N*-heterocycles can be efficiently achieved by a cascade gold-catalysed [3,3]-rearrangement/Nazarov reaction of propargyl ester derivatives (Scheme 3.24) and the methodology can be applied for the synthesis of bruceolline H and I from 3-substituted indoles. In an effort to broaden the scope of the reaction and the diversity of products, they assumed that *N*-heterocycles **9** (Scheme 3.24) bearing propargyl side-chain at C3 when treated with gold(I) would deliver a cyclopenta-fused heterocyclic system with alternate position of C=O group on the five-membered ring (**11**, Scheme 3.24). However, an electron donor atom in the wrong position could stabilise the pentadienyl cationic intermediate **10**, thus relenting its 4π-electrocyclisation and causing either degradation of the starting material or the

formation of unwanted side products.¹⁰⁶ For this reason, a computational study could help in evaluating the entire reaction profile and anticipating the reaction outcome, highlighting potential issues before embarking in a total synthesis involving such a process. In this work we computed again with updated methodology the mechanism of the tandem [3,3]-rearrangement/Nazarov reaction for the 2-substituted piperidine derivatives and compared it with the one of 3-substituted piperidine derivatives. The energetic profile of the reactions of the two substrates resulted to be different due to the influence of N atom. In particular, the substitution at position 3 is computed to have a deleterious effect on the electronic properties of the molecules, increasing the activation barriers of the Nazarov reaction. The experimental results corroborate the sluggish reactivity of 3-substituted piperidines predicted by the calculations.

Previous work



This work



Scheme 3.24 Tandem [3,3]-rearrangement/Nazarov reaction for the 2- and 3-substituted piperidine derivatives.

3.2.4 Objectives

Since the effect of N atom in the substrate appears to deeply influence the substrate reactivity, 3-substituted piperidine derivatives are supposed to behave differently from the 2-substituted piperidine ones. Before starting investigating this strategy for application in total synthesis, a computational analysis is required to shed light on the energetic profile of the reaction in every single step. The charge distribution in the intermediate cations could be informative about the influence of the N atom in the stability of the intermediate and justify the proposed reactivity. The proton abstraction step was analysed and different mechanistic hypotheses were elaborated. Finally, some considerations regarding the hydrolysis step are provided in terms of computed energies.

3.2.5 Computational work

3.2.5.1 Methods

In order to identify the structures and the energies of the critical steps of the mechanism, the potential reaction coordinates of the whole tandem [3,3]-

rearrangement/Nazarov cyclisation were studied computationally. A model substrate bearing the p-toluensulfonyl as the *N*-protecting group was chosen owing to its compatibility with such a process. All structures were initially optimised using density functional theory (DFT) with B3LYP and the 6-31G(d,p) basis set for non-metallic atoms and SDD for Au as implemented in Gaussian 16. The alkynyl-gold(I) cationic complexes **I** (Scheme 3.25) and **I'** (Scheme 3.28) were considered as the starting points of the mechanisms ($\Delta G = 0$ kcal/mol), and all reported energies in the following discussion are relative to them. The energy values correspond to ΔG Gibbs energies, computed at M06/def2tzvpp level of theory, in a solvent model (IEFPCM, solvent=dichloromethane). The intrinsic reaction coordinates (IRC) were followed to verify the energy profiles connecting the key transition structures to the correct associated local minima. Ph₃P was chosen as the ligand in analogy with the previous calculation. The calculation of the atomic charges of intermediate **III** and **III'** was carried out through Natural Bond Orbital analysis. For further information, see Chapter 1.

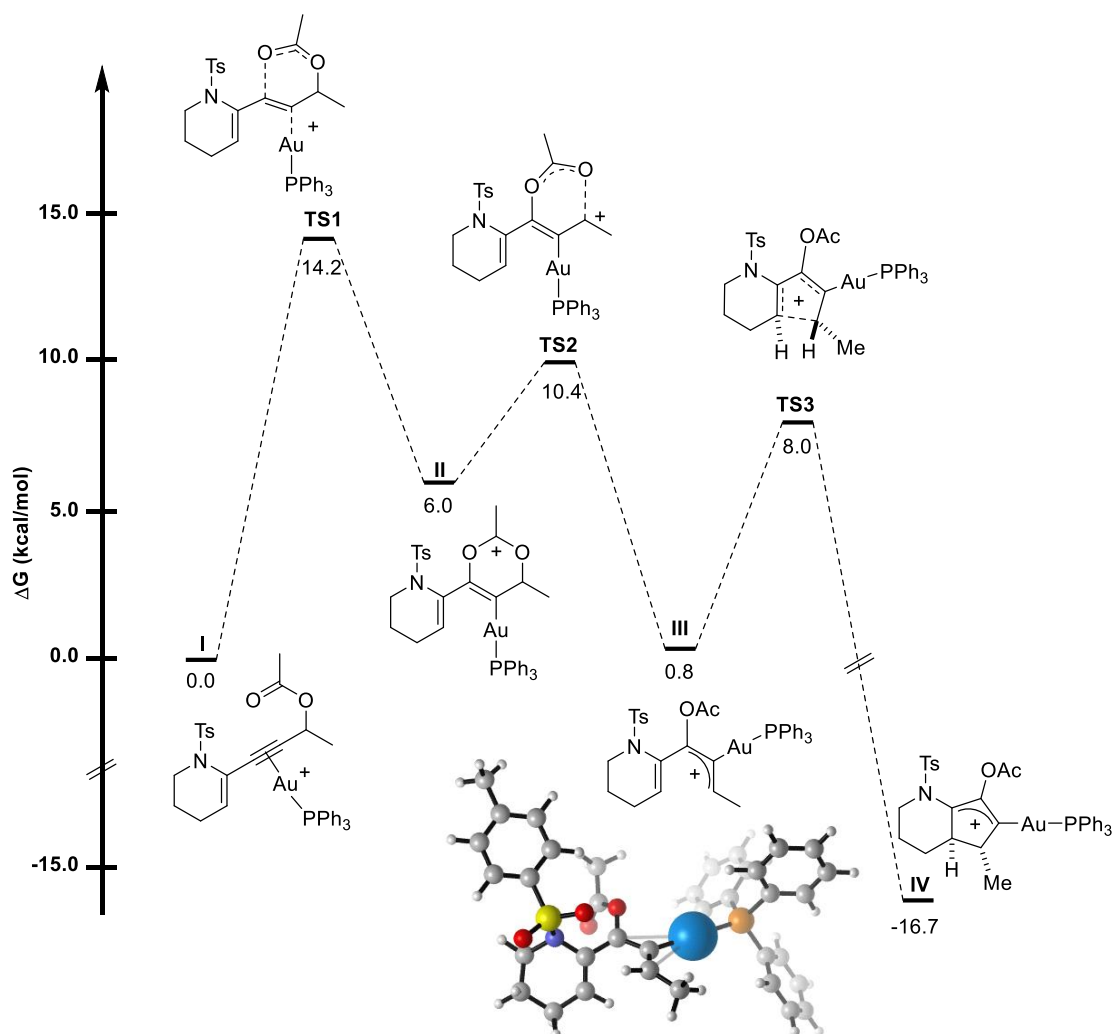
3.2.5.2 Mechanism

2-substituted piperidine derivatives

In the previous work of the group of Occhiato,¹⁰¹ a detailed computational analysis was presented to explain the reaction mechanism and to justify the experimental evidence. The calculations reported in the paper concerned the simplified substrate bearing the *N*-CO₂Me, while in our study we focused on the simple substrate with *N*-tosyl group. Thus, we decided to repeat the calculations with the latter substrate in order to have suitable data to compare with the case of 3-substituted piperidine derivatives, which are the substrates under study in this work. Furthermore, a different computational method was used compared to the previous work.

In Scheme 3.25 the energetic pathway of the tandem [3,3]-rearrangement/Nazarov reaction of 2-substituted piperidine derivatives is represented. All the energies of the structures are calculated taking as a reference the energy of the alkynyl-gold(I) cationic complex **I**, starting point of the mechanism ($\Delta G = 0$ kcal/mol). The coordination with gold in complex **I** catalyses the [3,3]-rearrangement of the acetate group in two steps. First, the oxygen atom of the acetate attacks the activated alkyne forming a cyclic cationic intermediate after overcoming an energy barrier of 14.2 kcal/mol. Intermediate **II** was located at an energy of 6.0 kcal/mol and rapidly proceeds to the formation of the allylic cation **III** stabilised by the gold atom, after the cleavage of the C-O bond. Noteworthy, the energies of **I** and **III** indicate that **I** and **III** are almost isoenergetic (0.8 kcal/mol of difference). The energy required for the second step to occur is lower than the first ($\Delta G^\ddagger = 10.4$ kcal/mol), so it is reasonable to say that the activation energy of the acetate rearrangement is of 14.2 kcal/mol, perfectly feasible at room temperature experimental conditions. In absence of further evolution, **I** and **III** can be considered to be in an almost 1:1 equilibrium. Under gold catalysis, complex **III** evolves through an easy cyclisation to **IV** with a low energy barrier of 8.0 kcal/mol. Complex **IV** is formed in accordance to the conrotatory nature of Nazarov reaction and the diastereoisomer with the two H atoms in a *trans* relationship is the favoured one, as demonstrated and published in the previous paper. The energy barriers of the two steps are low, explaining the fast rate of the

reaction, which gets completed at room temperature in less than two hours. The rate determining step of the reaction results to be the first [3,3]-rearrangement, in accordance with the previous results.



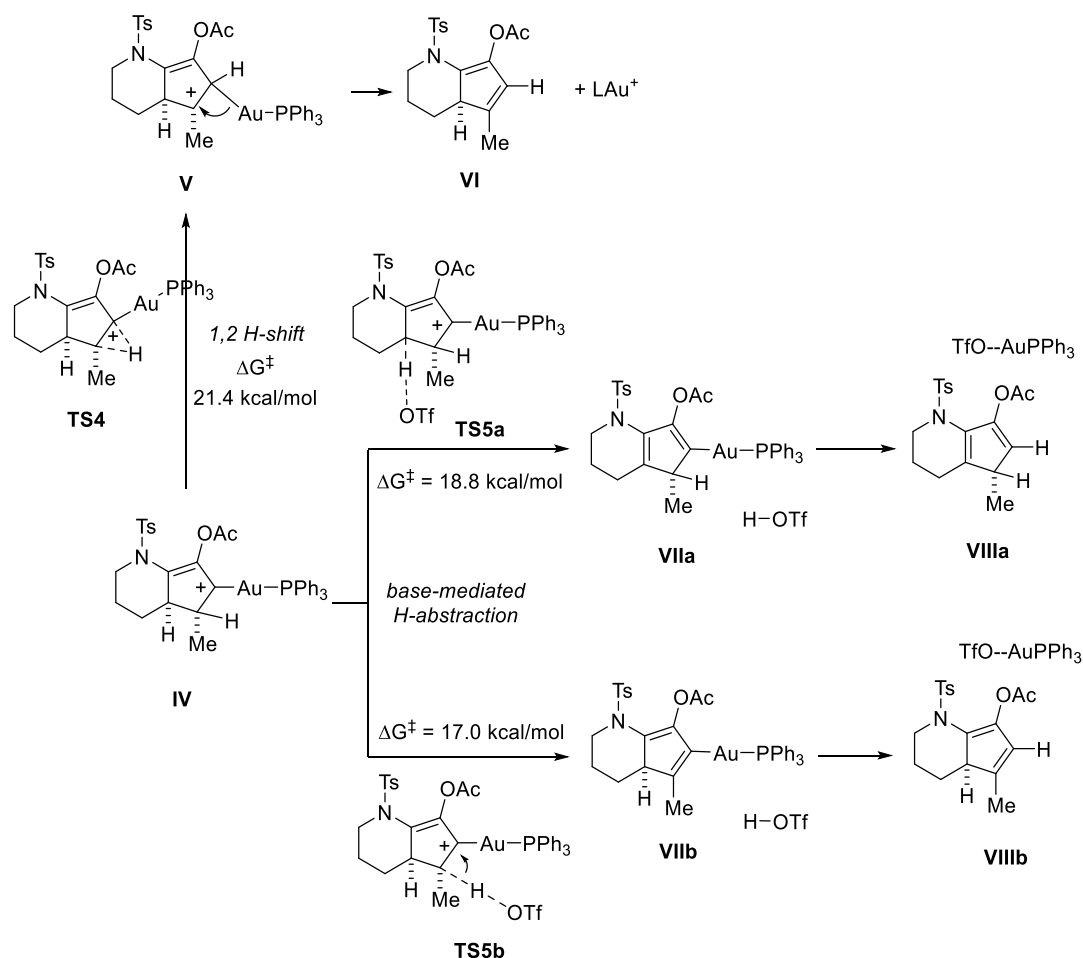
Scheme 3.25 DFT computed energy surface for the tandem Au(I)-catalysed [3,3]-rearrangement/Nazarov reaction of 2-substituted piperidine derivatives.

The following step is the formation of the diene and two regioisomers are possible depending of the hydrogen that is abstracted or moved (Scheme 3.26). The diene formation could be explained as result of a single-step intramolecular hydride shift with concomitant C-Au bond breaking. The energy barrier for this transformation was calculated to be 21.4 kcal/mol, a quite high value. The alternative is the proton abstraction by an external basis. Since many substances are present in the reaction media, it is difficult to identify which component plays that role. The counterion is known to have high importance in gold catalysis, thus we hypothesised it could participate in this step. Although the best catalytic system employs SbF_6^- , we decided to compute the proton abstraction mediated by TfO^- . Indeed, SbF_6^- is a very low coordinating ion and unlikely would bind the proton. In addition, its big size would

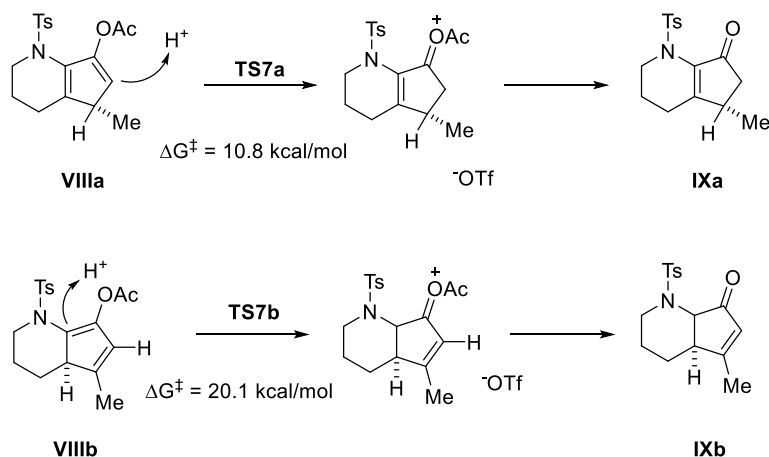
increase the computational cost of the calculations. Triflate instead is supposed to interact more easily with the hydrogen atoms, thus its action was examined.

Two protons, H_a and H_b can be removed, leading to the two different regioisomers, **4**-like and **2**-like respectively. The abstraction of H_a requires 18.8 kcal/mol, while H_b 17.0 kcal/mol. The difference in energy is of 1.8 kcal/mol in favour of the formation of **VIIb**, thus we could conclude that this step is not regioselective. The small energy difference is in agreement with the ratio of products obtained experimentally. However, the base-mediated proton abstraction results to be more plausible than the intramolecular hydride shift.

The final step is the hydrolysis leading to the final pentenone derivative. Since the exact nature of the protonating species is unknown, we simplified this step, computing the protonation of substrates **VIIIa** and **VIIIb** by triflic acid, initial step for the hydrolysis (Scheme 3.27). The protonation of **VIIIa** resulted to occur with an energy barrier of 10.8 kcal/mol, easily affordable at room temperature conditions. This result justifies the experimental evidence of the only hydrolysed product **5** in the reaction mixture and no detection of acetate compound **4**. In contrast, the protonation of **VIIIb** has an energy barrier of 20.0 kcal/mol, the double of the one of **VIIIa**. The reason for this big difference could be the steric hindrance around the protonation sites. Moreover, **VIIIb** bears a dienamine structure and the donating N atom can induce a stabilisation of that structure making it less prone to hydrolysis. The hydrolysis rate for the two substrates differs notably and is in agreement with the experimental outcome.



Scheme 3.26 Diene formation pathways.

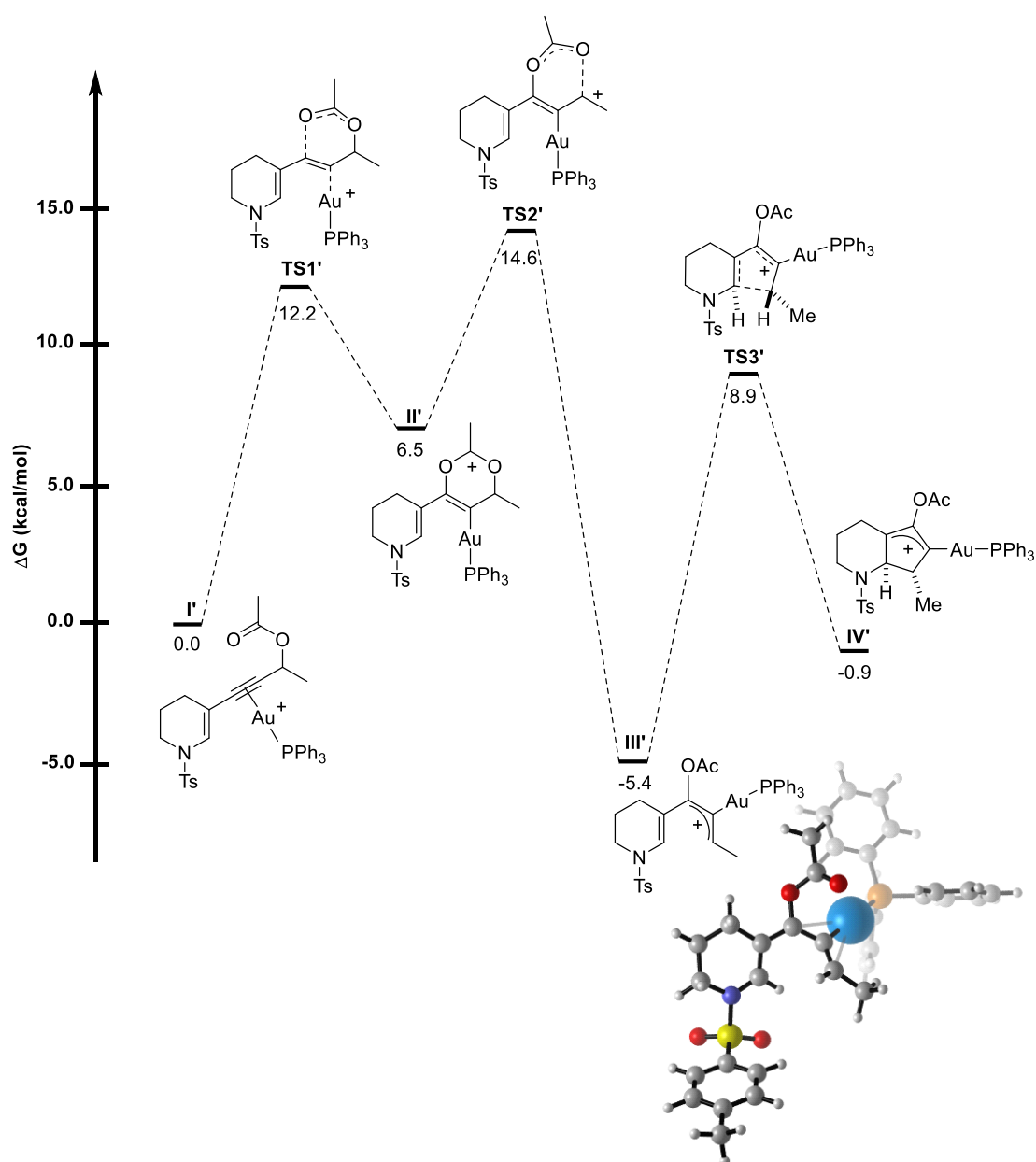


Scheme 3.27 Hydrolysis step.

3-substituted piperidine derivatives

N-heterocycles bearing propargyl side-chain at C3 under gold(I) catalysis are supposed to lead to the formation of cyclopenta-fused heterocyclic systems with alternate position of C=O on the five-membered ring. However, the presence of an electron donor atom in a different position could influence the reactivity of the substrate by stabilising unwanted intermediates that lead to the formation of other unexpected products. In this section, we present the study of the mechanism of 3-piperidine derivatives under

gold(I) catalysis, which proceeds through the same steps of the analogue 2-piperidine derivatives, but with some exceptions, which correctly justify the final complex product mixture found experimentally.



Scheme 3.28 DFT computed energy surface for the tandem Au(I)-catalysed [3,3]-rearrangement/Nazarov reaction of 3-substituted piperidine derivatives.

Scheme 3.28 shows the energetic profile of the reaction. The alkynyl-gold(I) cationic complex **I'** was considered as the starting point of the mechanism ($\Delta G = 0$ kcal/mol), and all reported energies in the following discussion are relative to it. As in the case of 2-piperidine derivatives, at the beginning the substrate undergoes a two-step acetate rearrangement, through the formation of an unstable cyclic cationic intermediate (**II'**), which rapidly reopens through **TS2'** to give the pentadienyl cation **III'**. The total energy required to obtain intermediate **III'** is 14.6 kcal/mol. It is worth to notice that the acetate rearrangement proceeds with a quite high activation barrier, but the formation of intermediate **III'** is an exergonic process ($\Delta G = -5.4$ kcal/mol). The stability of this

intermediate could be attributed to the π -donating ability of the nitrogen atom that stabilises the positive charge. Indeed, the charge of the N atom can be transferred by conjugation through the cationic skeleton, differently from the situation of intermediate **III**, which does not bear a conjugated system and the negative charge of the N atom cannot enter in the allyl system. This phenomenon is evaluated by the calculation of the total charge of the cationic intermediates **III** and **III'**. We calculated the NBO charges on the two intermediates and a significant difference between the two cases was found. The total allyl charge on the 3-substituted intermediate **III'** results to be almost neutral or even slightly negative (-0.056 e) confirming that the negative charge on the nitrogen atom can stabilise by conjugation the positive charge of the allyl system, affecting the following cyclisation reaction. On the other hand, the total allyl charge on the 2-substituted analogue **III** maintains a positive value (+0.115 e) because it cannot be stabilised since the intermediate does not present a conjugated system (Figure 3.8). The high stability of intermediate **III'** affects the following cyclisation step because the π -donating ability of the N atom slows down the 4p-electrocyclisation and causes the formation of unwanted side products. The cyclisation step in this case does not occur as easily as in the case of the 2-piperidine derivatives. Indeed, the activation energy is 14.3 kcal/mol, similar to the energy of the acetate rearrangement. Both energies are affordable at the reaction conditions, but the intermediate **III'** at low energy opens the possibility to have side reactions occurring, if less energy is required.¹⁰⁶ Instead, in the case of 2-piperidine substrates, once the first rearrangement step is overcome, the reaction proceeds easily to the product, limiting other not desired reactions to occur. Indeed, intermediate **III** seems to be much more reactive and its cyclisation much more exergonic than **III'**. The Carbon atoms C1 and C3 are especially more positive in **III** than in **III'**.

The product that is formed is the expected from the Nazarov cyclisation with the H atoms in *trans*. Another important difference between the two energetic pathways in Scheme 3.25 and Scheme 3.28 is the much higher relative stability of the cyclised structure **IV** than its analogue **IV'** (-16.7 vs -0.9 kcal/mol). The π -donating ability of the N atom might have a clear stabilising effect in the case of **IV**, while the nitrogen atom and the cationic allyl system are disconnected in **IV'**. This effect can be probably reflected in the corresponding transition states, being **TS3'** higher than **TS3**.

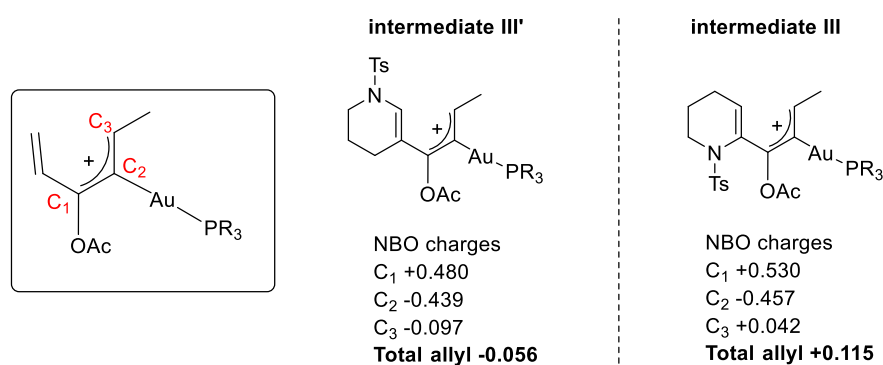
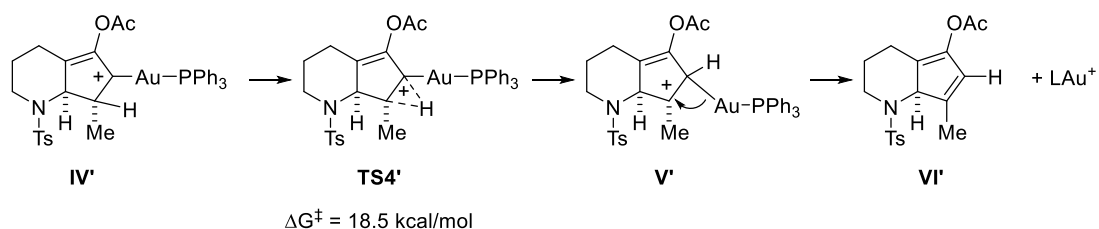


Figure 3.8 NBO charges of the two pentadienyl intermediates **III'** and **III**.

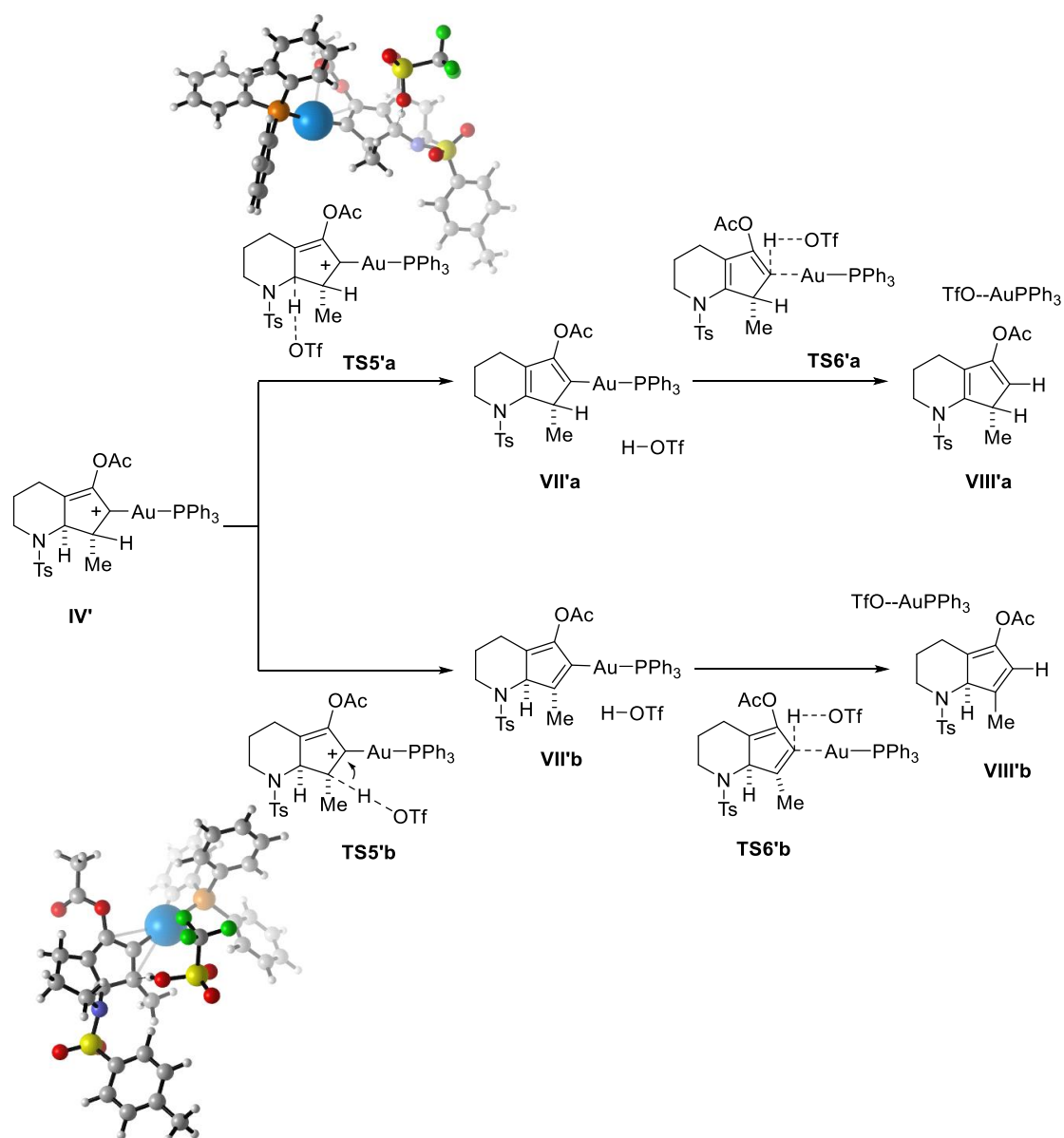
After the slow cyclisation step, we focused our analysis on the diene formation. Basically, the final steps have to include a deprotonation, protodeauration and in some cases the acetate hydrolysis. As in the previous case, we hypothesised that the diene could form through different pathways: i) single-step intramolecular hydride shift with concomitant C-Au bond breaking or ii) base-mediated deprotonation.

In analogy with our previous work, we computed the deprotonation step by using the triflate anion as the base in order to get informative results about the regioselectivity of the process. Computing the different pathways, it emerged that the 1,2 shift is less favoured than the base mediated process, with a difference of activation barrier of 4 kcal/mol. Indeed, the 1,2 shift in dry DCM requires an activation energy of 18.5 kcal/mol (Scheme 3.29), feasible at room temperature, but much higher than the traditional 1,2-hydride shift in carbocations (activation barriers generally less than 10 kcal/mol).⁸⁹ Zhang group demonstrated that the presence of water could catalyse this reaction (proton-transport catalysis strategy) through a two-step deprotonation/protonation process, but in our study, water is not included.



Scheme 3.29 Single-step intramolecular hydride shift pathway.

Therefore, we focused on the proton abstraction step and we also made some considerations about the regioselectivity of the reaction that arises during the deprotonation, due to the presence of two similar H atoms (H_a and H_b) (Scheme 3.30). In both cases depicted in Scheme 3.30, it emerged that the base mediated process is clearly favoured over the 1,2 H-shift. The process occurs in two easy steps, which is remarkable, given the low basicity of the triflate anion, suggesting that other possible anions present in the medium could also play the same role.



Scheme 3.30 Regioselectivity depending of the H-abstraction.

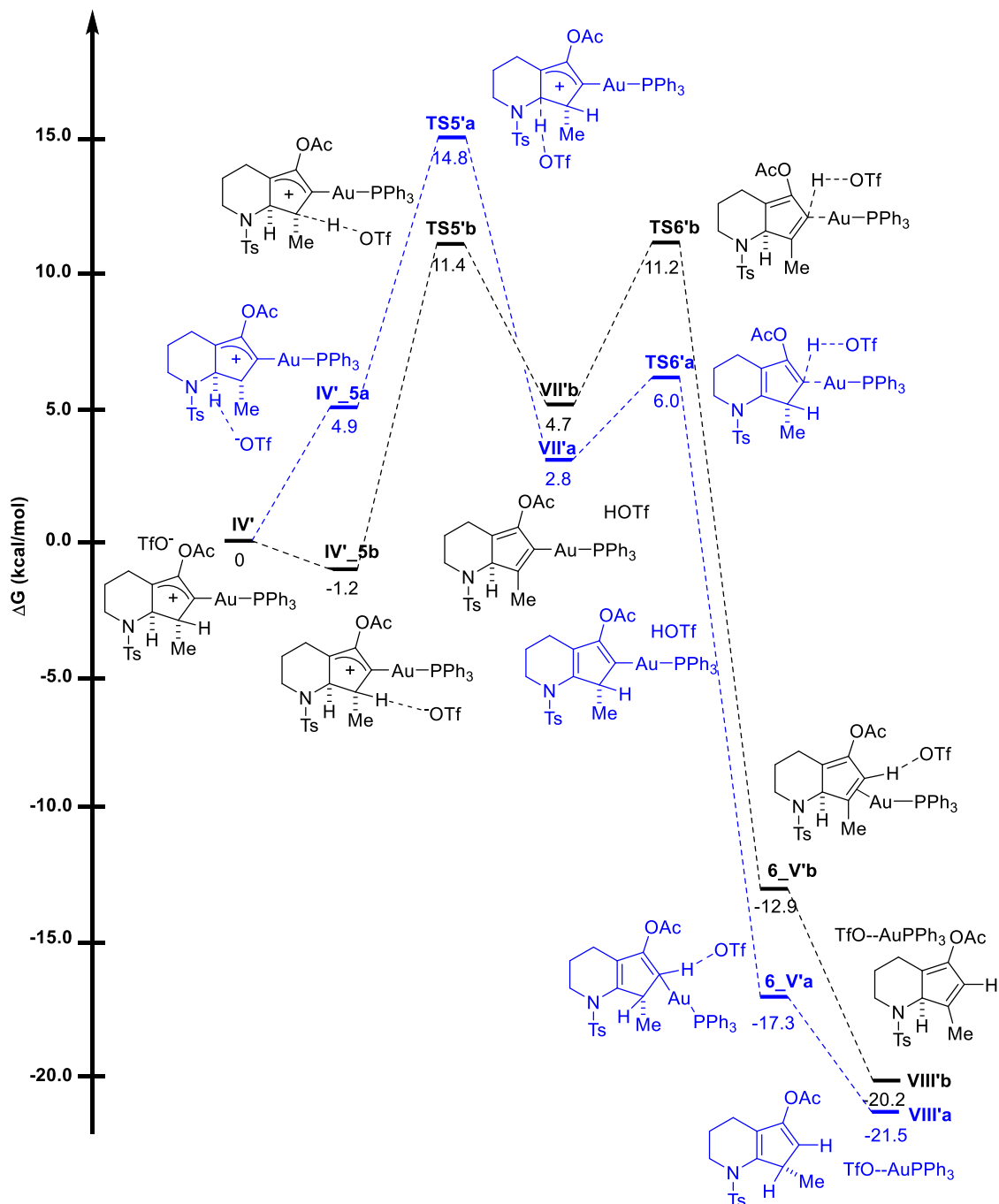
In Scheme 3.31, the energy profiles of the two proton-abstraction pathways are reported. All the energies of the structures are calculated referring to the energy of **IV'** + triflate ($\Delta G = 0$ kcal/mol). We found that the coordination complex of **IV'** with the triflate, which represents a pre-structure of the **TS5'**, is located at lower energy in the case of abstraction of H_b, probably due to the less steric hindrance around the H_b compared to the one of H_a. Indeed, the influence of electronic factors (the most reasonable option) would favour the formation of **VII'a**, driven by the formation of a conjugated system. The difference between the energy barriers for the abstraction of H_a and H_b is 2.2 kcal/mol (14.8 vs 12.6 kcal/mol respectively), which indicates that the triflate abstracts preferably the proton from the carbon bearing the methyl group. Under kinetic control, the reaction would lead to the formation of **VIII'b**. However, as it will be commented later in the experimental section, only the hydrolysed form of the

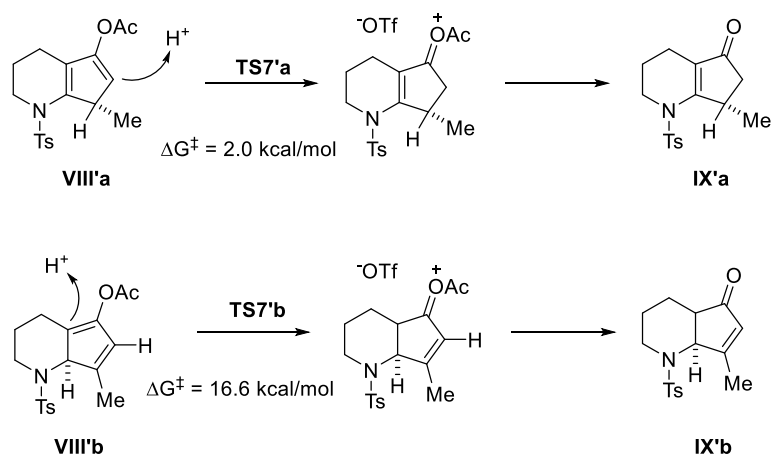
other isomer **VIII'a** was identified in the reaction mixture, in contrast with the computational predictions. The thermodynamics of the process was also analysed to get further insights. Concerning the stability of the intermediates, it cannot be overlooked that intermediate **VII'b** is located at higher energy than intermediate **VII'a**. This means that intermediate **VII'b** is more inclined to the backward reversible reaction that affects its concentration available for the following step. Intermediate **VII'a** instead stands at lower energy and would have to overcome a great barrier to go backward to the starting point, less favourable than proceeding to the following step. Indeed, through a four-member transition state, substrates **VII'** can be converted to the final acetate-bearing product, detaching from the gold complex.

It is noteworthy that **VII'a** has to overcome a lower energy barrier than **VII'b** (6.0 kcal/mol vs 11.2 kcal/mol respectively), which can be determinant for the experimental reaction outcome. The overall reaction is highly exergonic in both cases and intermediate **VIII'a** resulted to stand at 1.3 kcal/mol lower than **VIII'b**, probably due to the conjugation stabilisation in the dienamine system. Thus, we believe that the higher thermodynamic stability of **VIII'a** accounts for its preferential formation. It cannot be overlooked that the formation of intermediates **VIII'a** and **VIII'b** is hardly reversible due to their high exergonic character, and thus, the equilibration of both final isomers through the previous intermediate **IV'** is very unlikely. Our hypothesis is that an isomerisation between **VIII'a** and **VIII'b** must be operative in the reaction conditions, through a non-studied protonation/deprotonation sequence.

We did not study in detail the mechanism of hydrolysis, but we calculated the energy barrier required for the protonation of substrates **VIII'a** and **VIII'b** by triflic acid, as initial step of the hydrolysis (Scheme 3.32). The protonation of **VIII'a** resulted to occur very easily, with a barrier of only 2.0 kcal/mol. In contrast, the protonation of **VIII'b** has an energy barrier of 16.6 kcal/mol, feasible at room temperature, but much higher than the one of **VIII'a**. The reason for this big difference could be the steric hindrance around the protonation sites.

Eventually, we looked at the final hydrolysed products from a thermodynamic point of view. We calculated the energies of the two products and resulted that **IX'a** is located at 6.7 kcal/mol lower than **IX'b**, highlighting that **IX'a** would be the favourable product, probably due to conjugation reasons.

Scheme 3.31 Triflate mediated proton H_a and H_b abstraction pathways.



Scheme 3.32 Hydrolysis step.

3.2.6 Experimental work

The fact that intermediate **III'** is very stable and the activation energy for the cyclisation process is quite high, predicts a slow cyclisation of intermediate **III'**, which could therefore evolve through unwanted side processes. To assess this from the experimental point of view, Dr. Martina Petrović of the group of Ernesto G. Occhiato performed the synthesis of the model compound (**9**) used in the calculation and subjected it to gold-catalysis.

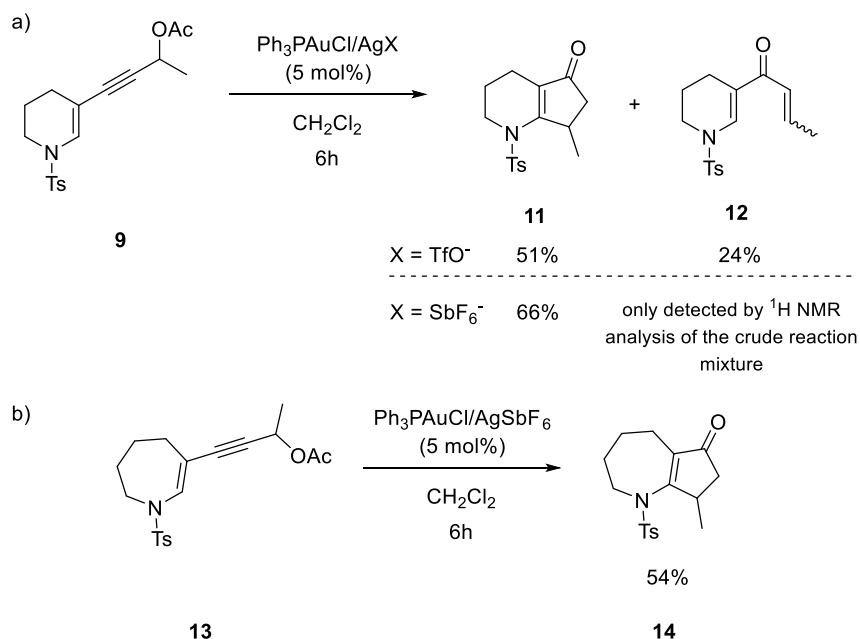
Once synthesised the enynyl acetate, it was treated with 5 mol % $(\text{Ph}_3\text{P})\text{AuCl}/\text{AgOTf}$ in CH_2Cl_2 at room temperature (as considered in the calculations) and 5 mol % $(\text{Ph}_3\text{P})\text{AuCl}/\text{AgSbF}_6$ in the same solvent, which were the best conditions experimented in the rearrangement of 2-substituted piperidine derivatives.¹⁰¹ Under both conditions, the reaction of **9** led to the formation of cyclopentenone **11** in lower yield (51% and 66%, respectively) (Scheme 3.33a) and, in comparison with the gold(I)-catalysed tandem [3,3]-rearrangement/Nazarov reaction of enynyl acetate **6**, it was much slower with both catalytic systems (6-16h vs 1.5-2h for the complete disappearance of the starting material) as predicted by the computational analysis. The slower cyclisation was accompanied by the formation of many unknown compounds, results of side reactions of gold intermediates or degradation of the starting enynyl acetate. The side products could not be isolated due to the complexity of the reaction crude. The other hydrolysed isomer was not found, coherently with the computational predictions, and unexpectedly neither its acetate form was observed. Instead, compound **12** could be identified as byproduct in the reaction with the triflate as the result of the hydrolysis of the pentadienyl cationic intermediate.¹⁰⁷

The occurrence of a [3,2]-rearrangement of **9** as cause of the low reactivity in the tandem reaction under study does not look conceivable because of the inconvenient charge distribution for this process in the initial substrate **9** and the less favourable stabilisation in the potential resulting intermediate, compared to the intermediate formed through the [3,3]-rearrangement.

In order to increase the reaction rate and decrease the amount of side-products, the best reaction conditions (with AgSbF_6) were modified, by using different precatalysts, dry solvent and the reaction was also carried out at higher temperature. However, none

of these attempts met with success, and indeed very sluggish reactivity was recorded in all these cases.

Since the gold(I) catalysed [3,3]-rearrangement/Nazarov reaction of azepane-derived enynyl acetates analogues of **6** was faster than the reaction of corresponding piperidine analogues **6**, enynyl acetate **13** was prepared and subjected to the reaction conditions (5% of $\text{Ph}_3\text{PAuCl}/\text{AgSbF}_6$ in CH_2Cl_2 , 6 h) affording cyclopenta-fused product **14** in 54% yield (Scheme 3.33b). Also with this substrate, the position of N atom influenced the reactivity and the reaction proceeded very slowly compared to the corresponding 2-substituted azepane derivative and provided many unidentified side products.



Scheme 3.33 Gold(I) catalysed [3,3]-rearrangement/Nazarov reactions.

3.2.7 Conclusion

This study on the N atom effect on the gold(I) catalysed tandem [3,3]-rearrangement/Nazarov reaction of 2- and 3-substituted piperidine derivatives came out with interesting information. The two substrates do not behave in the same way due to the different stabilisation of their pentadienyl cationic intermediates (**III** and **III'**) by the N atom.¹⁰⁶ Indeed, the N atom in the intermediate **III'** is able to delocalise its charge through conjugation stabilising the positive charge of the intermediate and decreasing the energy of the substrate, confirmed by the calculation of NBO charges of the two intermediates. While intermediate **III'** has a slightly negative charge, the charge of intermediate **III** keeps a positive value. This implies that the energy required for the second step of the sequence, the Nazarov reaction, is higher than in the case of 2-substituted substrate, opening the possibility that intermediate **III'** undergoes different potential side reactions.

Unfortunately, the complex reaction crude obtained in the experiments did not allow to isolate the side products, thus no investigation on the possible side reactions was carried out.

The calculations performed on the 2-substituted substrates reproduced the same results and trends found and reported in the previous paper.¹⁰¹

Concerning the reaction of 3-substituted piperidine derivatives, it was found that the tandem sequence is affordable at room temperature with similar energy barriers in the two steps. In this case, the Nazarov reaction does not proceed easily straight after the formation of the intermediate **III'**.

The regioselectivity, which depends on which proton is abstracted, was tackled and it came out that the formation of the two isomers required more or less the same energy. Nevertheless, the formation of the conjugated product resulted to be favoured and the detachment from the gold catalyst from this substrate occurred more easily. Furthermore, simplified studies on the hydrolysis step demonstrated that compound **VIII'a** undergoes hydrolysis almost straightforwardly with very small energy barrier, while **VIII'b** requires eight times the energy of the former. Eventually, the conjugated hydrolysed product **IX'a** was located at lower energy than **IX'b** resulting to be the favoured product from a thermodynamic point of view.

The limited experiments that were carried out are in agreement with the computational analysis. Product **11** was the only that could be isolated. Detection of **12** as byproduct could be the evidence of the high stability of the intermediate **III'**, which undergoes hydrolysis rather than proceeding through Nazarov reaction.

3.3 Computational studies on the tandem gold(I)-catalysed Claisen rearrangement/hydroarylation reaction of propargyl vinyl ethers.

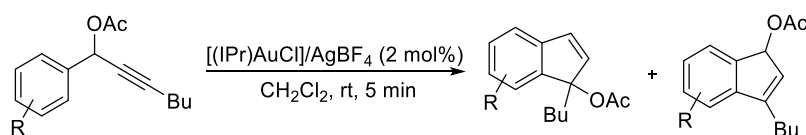
3.3.1 Introduction

3.3.1.1 Indenes

Indenes are interesting molecules that during the years have been attracting the attention of the scientific community due to their versatile applicability.^{108,109} Indeed, the indene scaffold is present in many natural and synthetic bioactive compounds. Natural and synthetic indenes exhibit antitumor, antiallergic, antimicrobial, anti-inflammatory, anti-Alzheimer, fungicidal and many other activities. Moreover, they find application in material science as a result of loosely-held pi-electrons, for example in photovoltaic solar cells and in the preparation of new fluorescent materials and metal complexes with special catalytic activity.¹⁰⁹ The classical approaches for the synthesis of the indene unit include different intramolecular electrophilic substitution reactions, cyclisations induced by a nucleophilic attack to a suitable functional group (such as the carbonyl) and cyclisations involving metal-catalysed processes.^{110,111}

In the category of transition metal catalysis, gold, rhodium and palladium account for most of the examples reported in the last years. The high alkynophilicity of Au(I) was exploited in many examples for the development of interesting catalytic strategies for the synthesis of indenes. These methods include the carbocyclisation of 1-alkynyl-2-(methoxymethyl)benzene derivatives,¹¹² the carbocyclisation of 1,5- and 1,6-enynes embodying an aryl ring,¹¹³ the C_{sp3}-H bond activation in diarylacetylene derivatives,¹¹⁴ the formal (3+2) cycloaddition between allenes and aryl gold(I)-carbenes,¹¹⁵ tandem transformations of 1,5-diynes embodying an aryl ring *via* a gold-vinylidene intermediate,¹¹⁶ and a few other multicomponent processes.¹¹⁷

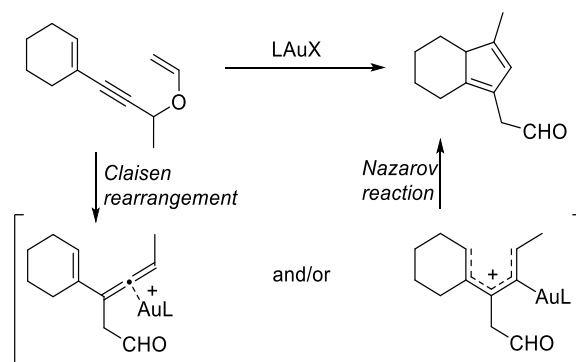
Eventually, also strategies based on [1,2]- or [1,3]-rearrangement and carbocyclisation of propargylic ester derivatives resulted to be efficient tools for the synthesis of indenes.^{85,118} For example, Nolan and co-workers observed that aryl propargyl acetates under gold(I)-catalysis activation could undergo direct nucleophilic attack by the electron-rich phenyl ring or a 1,3-rearrangement of the acetate, producing an allene, which is susceptible to hydroarylation. In both cases, the reactions provided an indene substrate (Scheme 3.34).⁸⁵



Scheme 3.34 Synthesis of indenes by Nolan group.

In 2018, the group of Occhiato reported the synthesis of functionalised cyclopentadienes fused with various *N*-hetero- and carbocycles through a gold(I)-catalysed tandem Claisen rearrangement/Nazarov cyclisation of propargyl vinyl ethers (Scheme 3.35).¹¹⁹ The approach involves a gold-catalysed [3,3]-rearrangement leading to the formation of a gold-allene complex that immediately undergoes a 4π-electrocyclisation plausibly *via* the corresponding pentadienyl cation to form the final

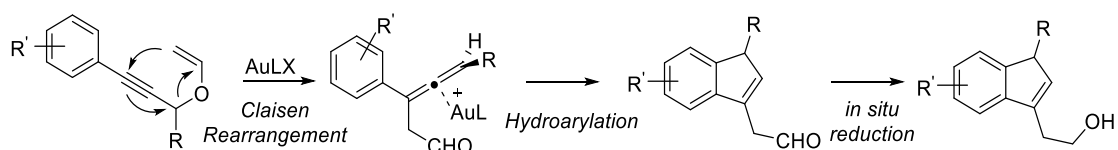
product. The tandem propargyl Claisen rearrangement/Nazarov reaction provides cyclopentadienes bearing, on one side chain, an aldehyde group available for further *in situ* elaboration for chain elongations.



Scheme 3.35 Tandem gold(I)-catalysed Claisen rearrangement/Nazarov reaction.

This methodology represents a useful tool, which can be further elaborated and adapted to the construction of indenenes by exploiting the rearrangement of 3-aryl-substituted propargyl vinyl ethers.

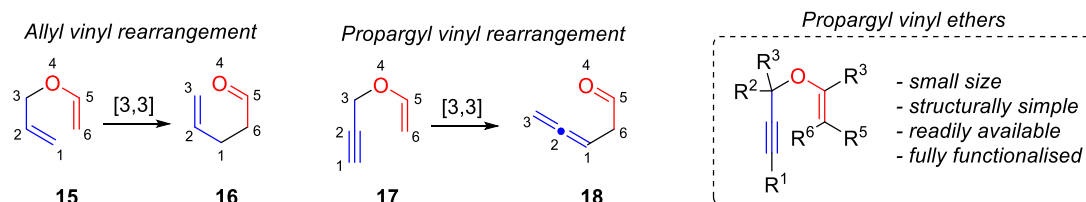
In this section, the synthesis of functionalised indenenes through a tandem gold(I)-catalysed propargyl Claisen rearrangement/hydroarylation reaction of aryl-substituted propargyl vinyl ethers is presented (Scheme 3.36),¹²⁰ and a brief overview of the potential of these substrates and of the reactions involved is provided.



Scheme 3.36 Tandem gold(I)-catalysed Claisen rearrangement/hydroarylation reaction.

3.3.1.2 Propargyl vinyl ethers

Propargyl vinyl ethers (PVEs) are small size, structurally simple, readily available and densely functionalised scaffolds (Scheme 3.37, right). Their key reactivity is known to be the [3,3]-propargylic sigmatropic rearrangement, called *propargyl Claisen rearrangement*, shown in Scheme 3.37,¹²¹ but it is possible also to separately take advantage of each of the different functionalities.



Scheme 3.37 Allyl vinyl rearrangement vs propargyl vinyl rearrangement.

The propargyl Claisen rearrangement gives access to functionalised allenes and the employment of appropriate propargyl vinyl ethers as starting materials coupled with suitable reaction conditions can aid in the development of new domino methodologies for the synthesis of many classes of organic compounds, exploiting the allenes as

valuable intermediates. Classically, the Claisen rearrangement can be described as the [3,3]-sigmatropic transformation of allyl vinyl ethers (**15**) into γ,δ -unsaturated carbonyl compounds (**16**) (Scheme 3.37). When the vinyl group bears a propargyl group, this transformation takes the name of *propargylic Claisen rearrangement*. At the beginning, it was common opinion that a triple bond could not participate in such rearrangement, because propargyl aryl ethers did not rearrange under the studied reaction conditions in the same way that allyl aryl ethers did. Only in the early 1960s the first successful attempts on the rearrangement of a propargyl aryl ether were reported by Rao and co-workers.¹²² Later in 1965, Black and Landor reported the first aliphatic propargylic Claisen rearrangement,¹²³ which became an useful protocol to gain access to functionalised allenes (**18**) through the [3,3]-sigmatropic transformation of propargyl vinyl ethers (**17**).

The propargyl Claisen rearrangement, as any other [3,3]-sigmatropic rearrangement, takes place under thermodynamic control. The cationic nature of the Au(I)-coordinated allenes formed after the rearrangement and the electron-donating abilities of the allene substituents heavily influence their structure-reactivity, determining the η^1 - or η^2 -allene character of Au(I)-coordinated allenes.⁷³

The degree and pattern of substitution in the PVEs have a great impact on the outcome of the reactions. Since the pioneer work of Black and Landor in 1965, it was observed that increased substitution in the PVE enhances the efficiency of the rearrangement at lower temperatures and that steric hindrance in the transition state is not the most relevant factor in terms of energy dependency.¹²³ The inductive or mesomeric effects of electron-withdrawing or electron-donating substituents located at different positions of the carbon skeleton are supposed to be similar to those observed for the better studied Claisen rearrangement of allyl vinyl ethers.¹²⁴ PVEs are usually synthesised as intermediates to obtain the corresponding rearrangement products, the allenes.

In literature, there are several procedures reported and we are going to briefly mention them.

One possibility is the synthesis from propargyl alcohol and aldehydes, which represents an appealing procedure when the desired allenic aldehyde is fully substituted at the α -position to the carbonyl group (R^5 and $R^6 \neq H$).^{125,126}

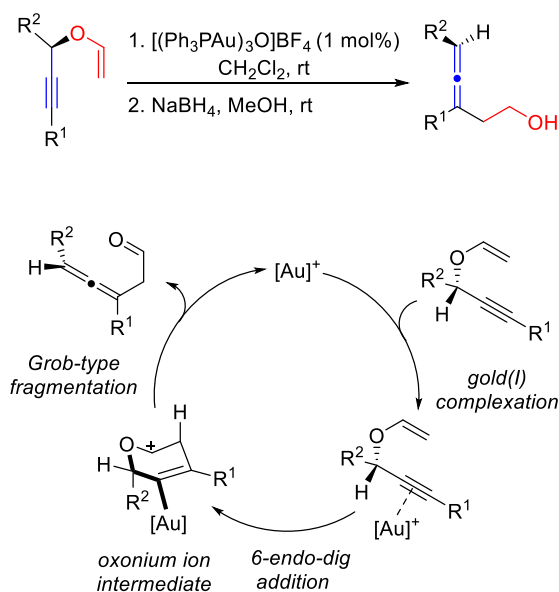
Another way is the synthesis from propargyl alcohol and isopropenyl ethers. In this case the PVE is formed with a substituted vinyl functionality which, upon rearrangement, produces an allenic ketone instead of an allenic aldehyde and, upon treatment with bases, undergo isomerisation to conjugated dienones, leading to important intermediates in the production of fine chemicals.⁶⁷

Then, the synthesis could occur from propargyl alcohols and orthoesters,¹²⁷ from propargyl alcohols and ethyl vinyl ether (R^1 and R^2 or $R^3 \neq H$)¹²⁸ or from propargyl alcohols and conjugated alkynoates.^{129,130} There are many more strategies leading to the PVEs, not exclusively aiming the formation of the allene.¹³¹

Historically, in 1973 Schmid and coworkers reported the first example of a metal-promoted Claisen rearrangement of propargyl vinyl ethers.¹³² In particular, in the presence of stoichiometric amounts of $AgBF_4$ and at high temperatures, propargyl aryl

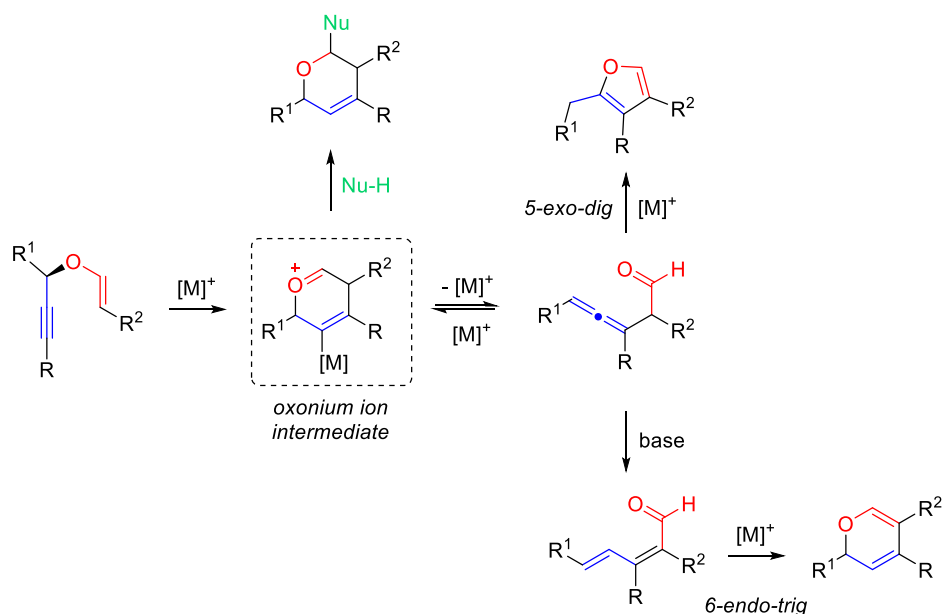
ethers undergo a [3,3]-sigmatropic rearrangement yielding allenyl ketones and rearrangement products derived from them.

Despite the interest of this reaction, only in 1994, Grissom and Huang reported the first catalytic version.¹³³ The great innovation in the Claisen rearrangement was introduced with the development of the gold catalysed version of it, increasing the synthetic potential of this chemistry, available also at milder reaction conditions. In 2004, Toste and co-workers carried out the [3,3]-sigmatropic transformation at room temperature with the gold(I) complex $[(\text{Ph}_3\text{PAu})_3\text{O}]\text{BF}_4$.¹³⁴ The reaction is fairly general in substrate scope and allows the highly stereoselective preparation of allenyl aldehydes, which could be reduced *in situ* to afford allenyl alcohols. The trinuclear gold complex resulted to be more efficient than the mononuclear phosphine-gold(I) catalysts, which afforded very poor levels of chirality transfer (Scheme 3.38). The authors proposed that the rearrangement might proceed through a “cyclisation-induced” mechanism.⁶⁹ Nevertheless, the experimental evidences are most consistent with a mechanism in which the gold catalyst interacts with the carbon–carbon π -bond to promote an intramolecular cyclisation to afford an oxonium ion intermediate, which in turn can afford different products as a function of the reaction conditions (Scheme 3.38 and 3.39).



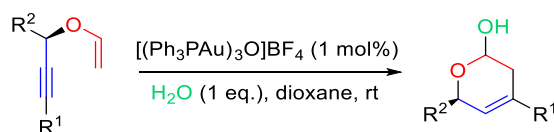
Scheme 3.38 [3,3]-sigmatropic rearrangement of propargyl vinyl ethers by Toste *et al* and proposed mechanism.

In the absence of an external nucleophile, the reaction proceeds through a 5-*exo-dig* cyclisation providing the corresponding furan derivatives. Catalyst modulation is required in the base catalysed rearrangement of the allenal intermediate into the corresponding $\alpha,\beta,\gamma,\delta$ -dial to prevent the otherwise favoured formation of the furan derivative.



Scheme 3.39 Metal-catalysed rearrangement of propargyl vinyl ethers.

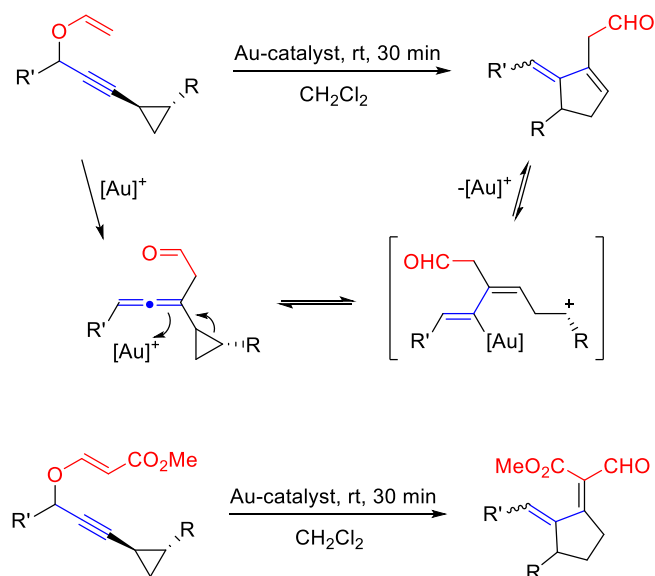
The same group developed a gold-catalysed domino methodology to construct 3,6-dihydro-2H-pyran-2-ol derivatives (Scheme 3.40).¹³⁵ The reaction entails a gold-catalysed *6-endo-trig* cyclisation followed by addition of water.



Scheme 3.40 Gold(I)-catalysed synthesis of 2-hydroxy dihydropyrans.

Inspired by the work of Toste, many contributions were made in the field of metal-catalysed propargyl Claisen rearrangement. Shi *et al.* studied triazole-gold catalysts in the rearrangement of PVEs bearing aromatic and alkyne substituents.¹³⁶ The group of Nevado studied a domino process in which a cyclopropyl group could participate once the propargyl Claisen rearrangement would have taken place (Scheme 3.41).¹³⁷

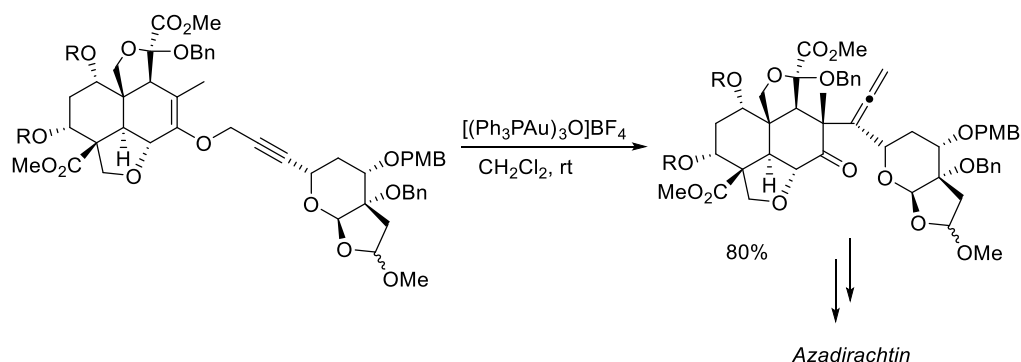
3.3 Tandem gold(I)-catalysed Claisen rearrangement/hydroarylation reaction



Scheme 3.41 Gold(I)-catalysed Claisen rearrangement – cyclopropyl ring opening – cyclisation.

The domino process included a [3,3]-sigmatropic rearrangement, a cyclopropyl ring opening and a cyclisation. The presence of a substituent R aided the delocalisation of the δ^+ generated upon cyclopropyl ring opening.

In general, PVEs can be converted *via* domino processes into furans,¹³⁸⁻¹⁴⁰ 2H-pyrans¹⁴¹ or 3,6-dihydro-2H-pyrans.¹⁴² In a *one pot* manner in the presence of a suitable base and a primary amine they could be converted in pyrroles¹⁴³ and 1,2-dihydropyridines.^{144,145} One interesting example of the synthetic potential of the Claisen rearrangement was shown by Ley and co-workers in their total synthesis of azadirachtin (Scheme 3.42).¹⁴⁶ The reaction took place in 80% yield and with complete transfer of chirality between the substrates shown in Scheme 3.42.

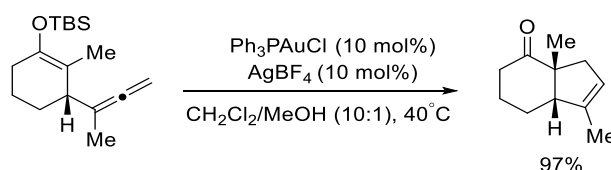


Scheme 3.42 Gold-catalysed transformation towards the total synthesis of azadirachtin.

3.3.1.3 Hydroarylation

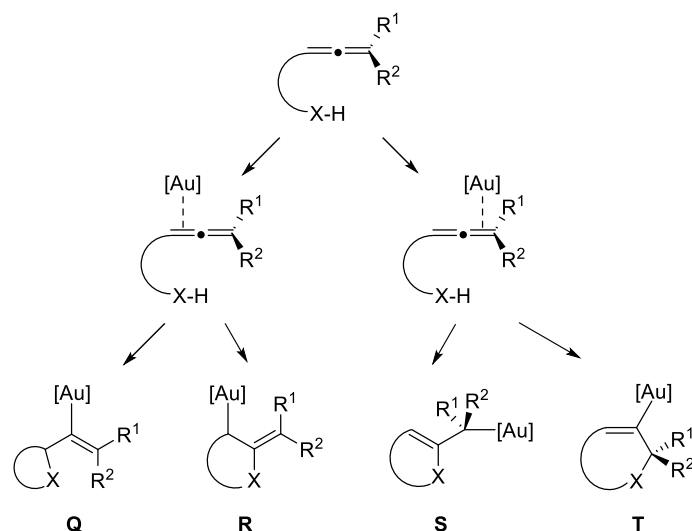
As said previously, allenes are susceptible to many reactions. Among them, the direct addition of aromatic C–H bonds to unsaturated substrates, as the allenes, provides an atom-economical strategy that is complementary to Friedel–Crafts and traditional C–C coupling reactions.

The first transition metal-catalysed hydroarylation of allenes with platinum catalysts was disclosed by Panunzi in 1983,¹⁴⁷ but this area of inquiry was slowly explored only two decades later. In 2006, Widenhoefer and Nelson independently disclosed gold(I)-catalysed methods for the 6-*exo*-hydroarylation of 2-(γ -allenyl)indoles¹⁴⁸ and *N*-(γ -allenyl)pyrroles,¹⁴⁹ respectively, and they ushered in the intense interest in the transition metal-catalysed hydroarylation of allenes as a route to allylic aromatic and heteroaromatic compounds. In the same year, Toste and co-workers used acetylenic and allenic silyl enol ethers for gold-catalysed intramolecular C-C bond formation. They found out that substrate in Scheme 3.43 underwent a 5-*endo-trig* cyclisation to hexahydroindenone derivative when subjected to cationic gold catalysis.



Scheme 3.43 5-*endo-trig* cyclisation to hexahydroindenone derivative.

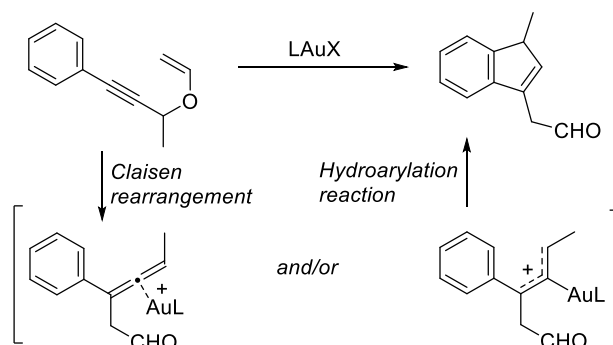
The catalytic allene hydroarylation was studied and many different strategies were reported: *exo*- and *endo*- intramolecular hydroarylation and intermolecular hydroarylation of allenes employing a range of heteroaromatic and heteroatom-substituted arenes. Generally, the metal-catalysed allene hydroarylation protocols lead to the formation of a C-C bond *via* π -activation of the allene followed by the outer-sphere addition of the arene. Thus electron-rich arenes such as indoles and other heteroaromatic compounds and oxygen- and nitrogen-substituted arenes are more indicated for this kind of reaction.¹⁵⁰ Gold cationic catalysts are suitable for this reaction because of their electrophilic and carbophilic character that makes them able to activate unsaturated bonds. The gold catalyst can coordinate both allenic double bonds and the regioselectivity of the subsequent nucleophilic attack depends on the structure of the substrate, in particular on the length of the tether connecting the allene and nucleophile (Scheme 3.44). In theory, four different cyclisation products can be obtained, but the formation of five- or six-membered rings *via* σ -gold species **Q** or **T** is favoured in most cases, while products from intermediates **R** and **S** are rare. Allenes and alkynes react similarly with gold catalysts, but allenes have the advantage of usually bearing an axis of chirality, which allows the chirality transfer to a new stereogenic centre formed in the nucleophilic attack.³⁸



Scheme 3.44 Regioselectivity of the nucleophilic attack.

3.3.2 Abstract

Given the importance of indenenes, together with Occhiato group, as a collaboration, we wanted to evaluate whether their published strategy of tandem Claisen rearrangement/cyclisation of propargyl vinyl ethers¹¹⁹ could be used for the construction of such important ring systems by exploiting the rearrangement of 3-aryl-substituted propargyl vinyl ethers. The achievement of this synthetic objective was not so obvious as the final cyclisation involves the disruption of the aromaticity of the phenyl ring, with the consequence that the optimal conditions (gold ligand, temperature, counterion) for the initial Claisen rearrangement could be unsuitable for the subsequent step of the cascade process and vice versa. This work includes an experimental and computational study of the tandem gold(I)-catalysed Claisen rearrangement/hydroarylation cyclisation of 3-aryl-substituted propargyl vinyl ethers (Scheme 3.45). The reaction occurs at room temperature in dichloromethane in the presence of 3 mol% [IPrAuCl]/AgBF₄ as the best catalytic system. Instead, cyclisation of the allene intermediate either does not take place or is very slow with phosphine ligands. A variety of substituents and functional groups present on the substrate are tolerated. The effect of the aryl ring substituents and the results of a DFT computational study suggest that the final hydroarylation is the rate-determining step of this cascade process. Further *in situ* chain elongation can be performed by Wittig olefination of the aldehyde functionality, thus incrementing the diversity of the products.



Scheme 3.45 Tandem gold(I)-catalysed Claisen rearrangement/hydroarylation reaction

3.3.3 Objectives

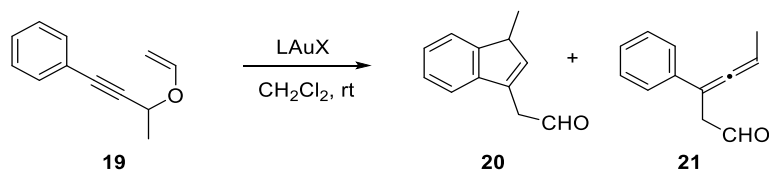
A computational analysis was carried out to define the mechanism of the tandem sequence and to elucidate the effect of the ligands of the gold(I) catalyst on the reaction. Indeed, experimentally, phosphine ligands resulted to slow down or inhibit the cyclisation step. For this purpose, the mechanism of the reaction was computed using two gold(I)-catalysts, one bearing phosphine as ligand and the other bearing carbene.

3.3.4 Experimental work

The experimental work was carried out by Antonia Rinaldi and Vittoria Langé in the laboratory of Prof. Ernesto G. Occhiato, who provided us the data in order to perform a computational analysis of the system.

Substrate **19** was used to screen various gold(I)-catalysts and gold(I)-precatalyst/silver salt combinations to find the best reaction conditions for the gold(I)-catalysed process (Table 3.3). The $[\text{Ph}_3\text{PAu}]^+\text{BF}_4^-$ and $[\text{Ph}_3\text{PAu}]^+\text{TfO}^-$ catalysts (entries 1 and 2) were shown to catalyse the Claisen rearrangement of propargyl vinyl ethers.¹³⁰ With 3 mol% of these catalysts in CH_2Cl_2 , substrate **19** was quickly and quantitatively converted into allene **21** and no presence of **20** was observed. Gold salts with Ph_3P and electron-rich phosphine ligands worked well in the tandem Claisen rearrangement/Nazarov cyclisation of enynyl vinyl ethers,¹¹⁹ but as it is evident from entries 1-2 and 4-5, they do not promote the final hydroarylation step with substrate **19**. Changing ligands to NHC (NHC = *N*-heterocyclic carbene) ligand IPr and various anions (entries 6-10) resulted to be successful for the synthesis of **20**.⁴⁴ The best result was obtained when using the $[\text{IPrAuCl}]/\text{AgBF}_4$ catalytic system (entry 8), as occurred also in the gold(I)-catalysed formation of indene from propargylic acetates.⁸⁵ Also commercial $[\text{IPrAu}(\text{CH}_3\text{CN})]^+\text{BF}_4^-$ (entry 9) catalysed the reaction, ruling out any role of the silver salt in the hydroarylation step. On the other hand, it was found that AgBF_4 alone (entry 16) was able to catalyse the Claisen rearrangement, but not the cyclisation, and similarly IPrAuCl salt alone (entry 15) only provided **20**. Other NHC gold complexes (entries 11-14) were tested and it was found that among them, only the SIPr ligand was effective, although the reaction was slightly slower than with IPr ligand. The reason could be that IPr is a weaker ligand than the corresponding saturated SIPr and therefore could leave the metal centre more electron poor than its saturated congener. Consequently, its metal complexes could be more reactive in activating unsaturated bonds towards nucleophilic attack.¹⁵¹ Other NHC ligands, as ICy, ItBu and IMes, which promote the hydroarylation in the Au(I)-

catalysed tandem [3,3]-rearrangement/hydroarylation of propargylic acetates, were tested but allowed the formation of only allene **21**.⁸⁵

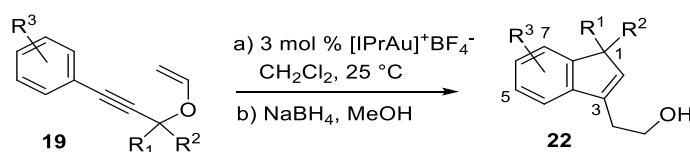
Table 3.3 Optimisation of the reaction conditions.^a

Entry	Catalyst ^b	Time (min)	Yield 19 ^c	Yield 20 ^c	Yield 21 ^c
1	[Ph ₃ PAuCl]/AgBF ₄	30	-	-	100
2	[Ph ₃ PAuCl]/AgOTf	30	-	-	100
3	[(<i>p</i> -CF ₃ C ₆ H ₄) ₃ PAuCl]/AgOTf	30	- ^d	-	-
4	^t Bu ₃ PAuNTf ₂ ^e	30	-	-	100
5	[Cy ₃ PAuCl]/AgOTf	30	-	-	100
6	[IPrAuCl]/AgSbF ₆	30	-	100 ^f	-
7	[IPrAuCl]/AgOTf	40	-	100 ^f	-
8	[IPrAuCl]/AgBF ₄	25	-	100	-
9	IPrAu(CH ₃ CN)BF ₄ ^e	60	-	100	-
10	IPrAuNTf ₂ ^e	120	-	50	50
11	[SIPrAuCl]/AgBF ₄	55	-	100	-
12	[ICyAuCl]/AgBF ₄	55	-	-	100
13	[ItBuAuCl]/AgBF ₄	55	-	-	100
14	[IMesAuCl]/AgBF ₄	55	78	-	22
15	IPrAuCl	55	-	-	100
16	AgBF ₄	60	-	-	100

^aConditions: Reactions carried out on 0.2-0.3 mmol of **19** in CH₂Cl₂ (0.05 M) at 25 °C under N₂ atmosphere. ^bPrepared by mixing the silver salt (3 mol %) and the gold chloride (3 mol %) in CH₂Cl₂ before addition of the substrate unless otherwise noted. IPr = 1,3-bis(diisopropylphenyl)imidazol-2-ylidene, SIPr = 1,3-bis(2,6-diisopropylphenyl)-4,5-dihydroimidazol-2-ylidene, IMes = 1,3-bis(2,4,6-trimethylphenyl)imidazol-2-ylidene, ItBu = 1,3-di-*t*-butylimidazol-2-ylidene, ICy = 1,3-bis(cyclohexyl)imidazol-2-ylidene. ^cRelative amount determined by ¹H NMR of the crude reaction mixture. ^dComplete degradation of the starting material. ^eCommercially available. ^fSome degradation of the starting material occurred.

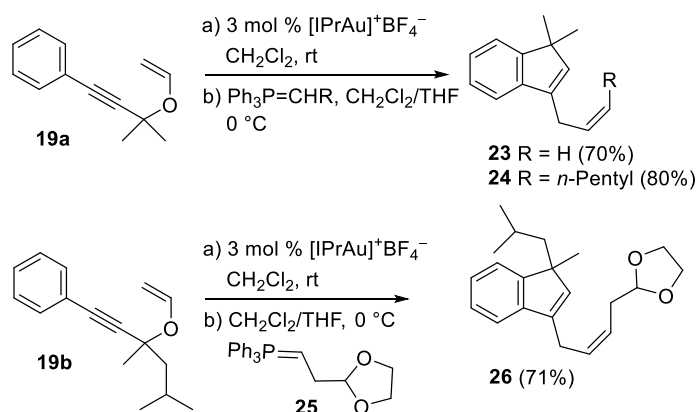
With the optimised conditions in hand, they developed the scope of 3-aryl-substituted propargyl vinyl ethers bearing various groups (R³) on the aromatic ring and substituents (R¹, R²) on the carbinolic position (Scheme 3.46). To avoid both partial degradation of aldehydes **20** and double migration to the exocyclic position during chromatography on silica gel (which generates α,β -unsaturated aldehydes), the reaction products were reduced *in situ* to the corresponding alcohols **22** by NaBH₄ after dilution of the dichloromethane solution with MeOH (method A). Alternatively, upon completion of the reaction, the crude aldehydes were isolated after an aqueous work-up, dissolved in MeOH and then reduced (method B). Summing up the results of the scope, electron-donor groups on the aromatic ring made the reaction faster, while electron-withdrawing groups slowed the hydroarylation of the allene intermediate down. Many groups were tolerated at the carbinolic position, as long as they were not aryl rings. In this case, the reaction provided the allene product, probably because the phenyl ring stabilises the

positively charged gold(I)-complex intermediate (Scheme 3.45), making it less reactive. Another explanation could be the greater stability of the aryl-substituted allene intermediate or the steric hindrance in the ring closure step by the aryl ring.



Scheme 3.46 Model reaction for the scope.

Finally, it was demonstrated that the aldehyde intermediate **20** could be directly employed for further chain elongation without prior work-up of the gold-catalysed step through the Wittig reaction. Substrates **20a** and **20b** were reacted with selected phosphorus ylides (Scheme 3.47). With simple $\text{Ph}_3\text{P}=\text{CH}_2$ the reaction led to the terminal olefin **23** in 70% yield after chromatography. No isomerisation of the double bonds was observed. Similarly, the reaction occurred quantitatively with a substituted ylide prepared from *n*-hexylphosphonium iodide, which provided *cis* olefin **24** in 80% yield. The crude aldehyde **20b** was reacted with ylide **25**, prepared from the corresponding commercial phosphonium bromide, which furnished compound **26** in 71% yield.



Scheme 3.47 Wittig reaction for chain elongation starting from the starting materials.

3.3.5 Computational work

3.3.5.1 Methods

All structures were initially optimised using density functional theory (DFT) with B3LYP and the 6-31G(d,p) basis set and SDD for Au as implemented in Gaussian 16. Final energies were calculated at the M06/def2tzvpp level of theory, in a solvent model (IEFPCM, solvent=dichloromethane). The stationary points were characterised by frequency calculations in order to verify that they have the right number of imaginary frequencies. For additional information, see Chapter 1.

3.3.5.2 Mechanism

We carried out a computational study to elucidate the effect of the catalyst ligands on the reactivity of the substrates. We computed the mechanism of the tandem reaction

using two model gold(I)-catalysts, one bearing phosphine ligand PPh₃ and the other one bearing carbene ligand IPr (Figure 3.9). We compared the energies of every step for the two cases and try to figure out the issues of the hydroarylation step that make phosphine catalysts not suitable for the catalysis of such a process.

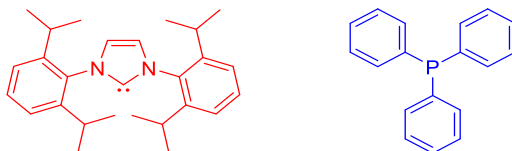
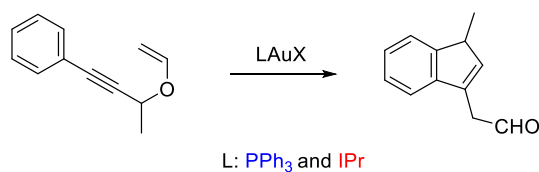
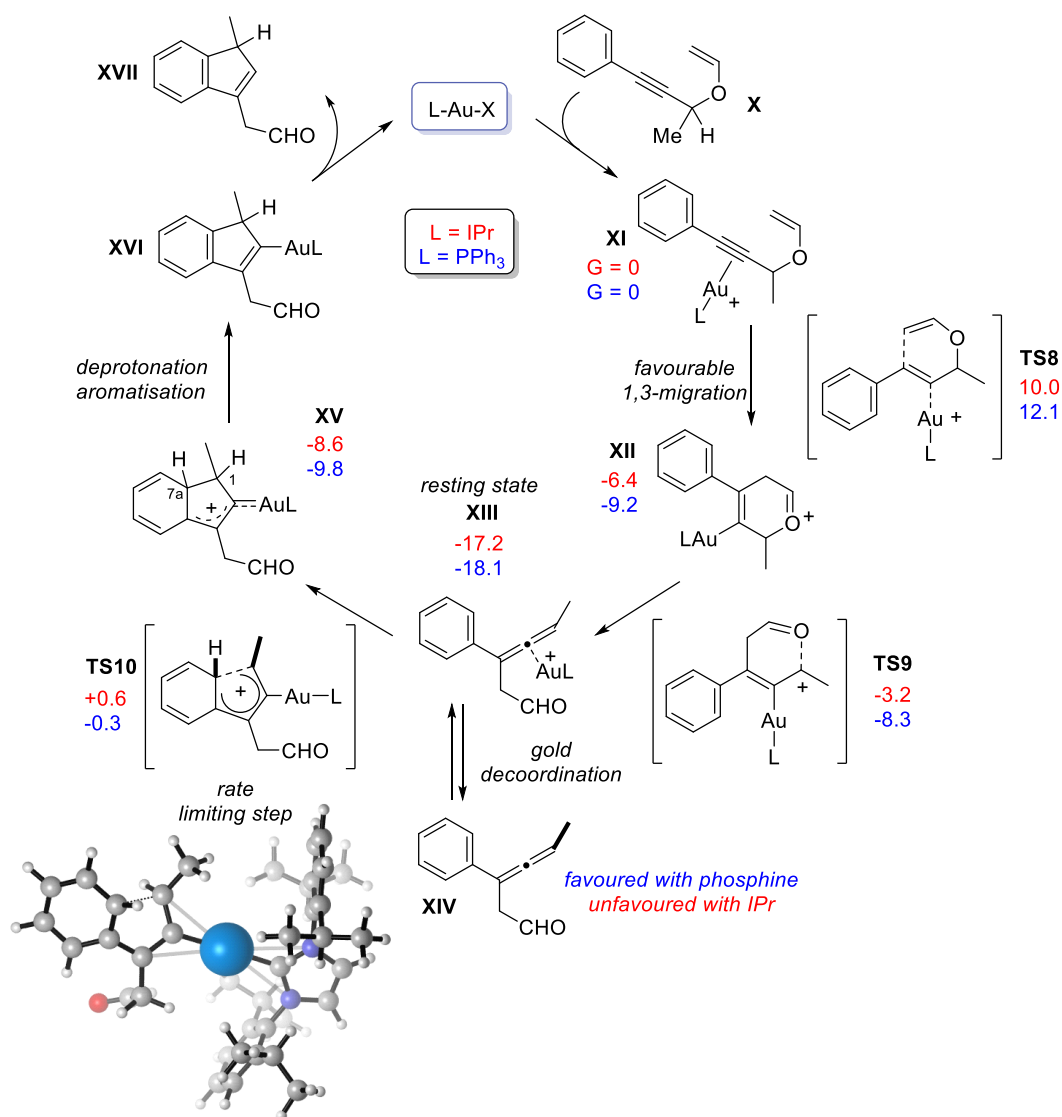


Figure 3.9 Carbene ligand IPr in red and triphenylphosphine ligand PPh₃ in blue.



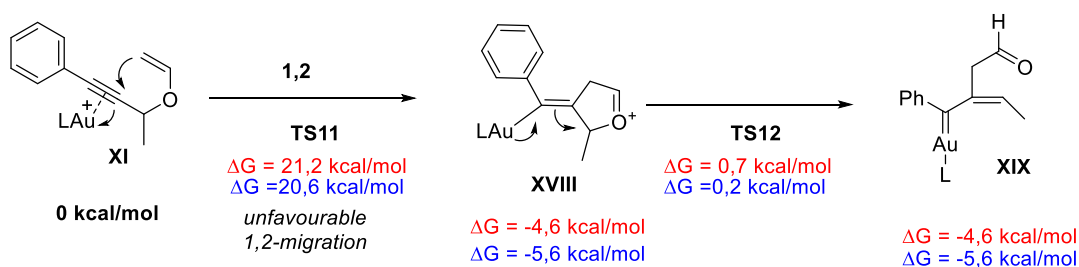
Scheme 3.48 Model reaction studied computationally.

In Scheme 3.49 a plausible mechanism for the tandem Claisen/hydroarylation reaction and the energies calculated relative to complex **XI** ($\Delta G = 0$ kcal/mol) are reported. Upon coordination of the triple bond to the cationic gold(I) complex, intermediate **XI** undergoes a fast two step [3,3]-rearrangement through the formation of the cyclic cationic intermediate **XII**. The energy required for the rearrangement is low with both the catalysts ($\Delta G^\ddagger = 10.0$ kcal/mol for IPr and 12.1 kcal/mol for the phosphine). The conversion of the substrate **XI** into allene **XIV** is immediate. The energy barriers found by calculations are in agreement with the experimental evidence that with any substrate and any catalyst, allene **XIV** is formed. This suggests that the Claisen rearrangement is not the rate determining step of the process.



Scheme 3.49 Schematic representation of the thermodynamics associated with the tandem process. Energies in kcal/mol are calculated relative to XI (in blue for Ph_3P ligand, in red for IPr ligand).

Before proceeding with the cycle, we wanted to confirm that the 1,3-rearrangement was the only one occurring, thus we computed the 1,2-rearrangement from substrate **XI** to **XIX** (Scheme 3.50). Gratifyingly it was found that this reaction requires almost the double of the energy compared to the 1,3-rearrangement ($\Delta G^\ddagger = 21.2$ kcal/mol for IPr and 20.6 kcal/mol for the phosphine), allowing to exclude that this reaction occurs.



Scheme 3.50 Calculation of the energies related to the 1,2-rearrangement of substrate **XI**.

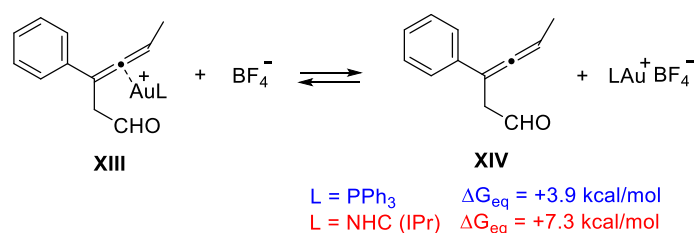
The ring closure of allene-gold(I) complex **XIII**, which is in equilibrium with the free allene **XIV**, presents a higher barrier (17.8 kcal/mol for both the catalysts) than the first step and thus is the rate determining step. When the cyclisation is slow or does not take place, allene **XIV** can be isolated, as when phosphine-catalysts are used.

Instead, in the tandem Claisen/Nazarov process it was not possible to observe (and isolate) the allene intermediate as the cyclisation was a fast step, especially with carbocyclic substrates.

The cyclisation step takes place according to a classic electrophilic aromatic substitution to form **XV** and during this step, a partial positive charge develops on the aromatic ring (**TS10**), which explains the effect of the substituents observed when assessing the scope of the reaction. To restore the aromaticity, a proton elimination from C7a occurs leading to **XVI**, which undergoes protodeauration to provide indene **XVII**.

During the experiments, it was found that IPrAuCl alone (entry 15) could not promote the hydroarylation step and allene **XIV** was isolated. The same was observed with AgBF₄ alone (entry 16). Two important points in the present cascade process are the role of BF₄⁻ counterion and the effect of IPr gold(I)-ligand, which together form the best catalytic system. Looking at the screening in Table 3.3, in particular at entry 9 vs 10, as well as 7 vs 8, it is clear that BF₄⁻ speeds the reaction up, probably acting at the *resting state*. Tetrafluoroborate is a weakly coordinating anion and this could favour the coordination of LAu⁺ cationic complex to allene **XIV** to re-generate the allene-gold complex **XIII**. The calculated energies in Scheme 3.49 are almost the same for both IPr and Ph₃P ligands, thus explaining the efficiency of the NHC gold ligand compared to the phosphine ligand, which instead does not promote the ring closure of the allene **XIV**, results to be challenging.

It is known that in the rearrangement of a model propargyl acetate forming the corresponding allene, the latter is the *resting state* with a NHC ligand (IME) and that the allene coordination to gold is favoured with the IME ligand compared to a phosphine.³⁰ We calculated the energies associated to the dissociation equilibrium of complex **XIII** (Scheme 3.51) and it resulted that the phosphine ligand stabilises more efficiently the LAu⁺ species, as the uphill energy is only +3.9 kcal/mol compared with +7.3 kcal/mol for the NHC carbene. This means that the equilibrium is more shifted to the left with the latter ligand ensuring higher concentration of allene-gold(I) complex **XIII** than of allene **XIV**. Therefore, in this case, intermediate **XIII** can proceed to the following reaction. The reason why, apart from SIPr, the other NHC catalysts are unable to promote cyclisation, remains instead still unclear.



Scheme 3.51 Dissociation equilibrium of complex **XIII** and **XIV**.

3.3.6 Conclusion

The tandem gold(I)-catalysed Claisen rearrangement/hydroarylation cyclisation of 3-aryl-substituted propargyl vinyl ethers was found to be an efficient new strategy for the synthesis of valuable functionalised indenenes. The reaction occurs at room temperature in dichloromethane in the presence of [IPrAuCl]/AgBF₄ as the best catalytic system for both the propargyl Claisen rearrangement and the subsequent allene cyclisation (the hydroarylation step). Instead, it was observed that with phosphine ligands no cyclisation of the allene intermediate occurs and allenes were isolated. Various substituents on the aryl ring and at the carbinolic position of the propargyl vinyl ether are tolerated. Tetrafluoroborate resulted to best perform as counterion probably due to its weak coordinating character, which favours the coordination of LAu⁺ cationic complex to allene **XIV** to regenerate the allene-gold complex **XIII**.

The computational analysis carried out on the mechanism of the reaction using two different catalysts, the one with phosphine as ligand and the other with carbene IPr suggested plausible explanations of the effect of the ligands on the reactivity. The Claisen rearrangement occurs easily with low energy barriers independently of the catalyst used. Indeed, the allene is always formed experimentally.

The hydroarylation was demonstrated to be the rate-determining step with an activation energy of 17.8 kcal/mol in both cases. This result is supported by the effect of the substituents on the aryl ring studied experimentally. Thus, the ligand was supposed to play a determinant role at this level of the cascade process.

We identified compound **XIII** as the *resting state*. As occurs in the work of Cavallo and co-workers,³⁰ the allene coordination to gold is more favoured with the carbene ligand than with phosphine one.

We demonstrated that the equilibrium between the coordinated allene and the free allene is more shifted to the left (to the formation of **XIII**) in the case of carbene than in the case of phosphine. The higher stabilisation of the free cationic gold(I) with phosphine ligands in the equilibrium involving coordination/decoordination of the allene intermediate to gold(I) inhibits the possibility for **XIII** to proceed to the cyclisation step. Finally, further functionalisation can be achieved *in situ* prior final work of the tandem process by a chain elongation carried out by Wittig reaction on the aldehyde functionality, thus incrementing the diversity of the products obtained.

3.4 References

1. Ito, Y., Sawamura, M.; Hayashi, T. *J. Am. Chem. Soc.* **1986**, *108*, 6405–6406.
2. Fukuda, Y., Utimoto, K. *J. Org. Chem.* **1991**, *56*, 3729–3731.
3. Teles, J. H., Brode, S.; Chabanas, M. *Angew. Chem. Int. Ed.* **1998**, *37*, 1415–1418.
4. Mizushima, E., Sato, K., Hayashi, T.; Tanaka, M. *Angew. Chem.* **2002**, *114*, 4563–4565.
5. Hashmi, A. S. K., Frost, T. M.; Bats, J. W. *J. Am. Chem. Soc.* **2000**, *122*, 11553–11554.
6. Hashmi, A. S. K., Schwarz, L., Choi, J.-H.; Frost, T. M. *Angew. Chem. Int. Ed.* **2000**, *39*, 2285–2288.
7. Silva, C., Faza, O. N.; Luna, M. M. *Front. Chem.* **2019**, *7*, 1–22.
8. Garcia, P., Malacria, M., Aubert, C., Gandon, V.; Fensterbank, L. *ChemCatChem* **2010**, *2*, 493–497.
9. Hashmi, A. S. K. *Chem. Rev.* **2007**, *107*, 3180–3211.
10. Fürstner, A.; Davies, P. W. *Angew. Chem. Int. Ed.*, **2007**, *46*, 3410–3449.
11. Fürstner, A. *Chem. Soc. Rev.* **2009**, *38*, 3208–3221.
12. Gorin, D. J.; Toste, F. D. *Nature*, **2007**, *446*, 395–403.
13. Pernpointner, M.; Hashmi, A. S. K. *J. Chem. Theory Comput.* **2009**, *5*, 2717–2725.
14. Dorel, R.; Echavarren, A. M. *Chem. Rev.* **2015**, *115*, 9028–9072.
15. Slaughter, L. M. *Homogenous gold catalysis*; Springer, 2015.
16. Schmidbaur, H. *Gold Bull.* **2000**, *33*, 3–10.
17. Schmidbaur, H.; Schier, A. *Chem. Soc. Rev.* **2012**, *41*, 370–412.
18. Gimeno, M. C.; Laguna, A. *Chem. Rev.*, **1997**, *97*, 511–522.
19. Pyykkö, P. *Angew. Chem. Int. Ed.* **2004**, *43*, 4412–4456.
20. Pyykkoe, P. *Angew. Chem. Int. Ed.* **2002**, *41*, 3573–3578.
21. Schwarz, H. *Angew. Chem. Int. Ed.* **2003**, *42*, 4442–4454.
22. Leyva-Pérez, A.; Corma, A. *Angew. Chem. Int. Ed.* **2012**, *51*, 614–635.
23. Zuccaccia, D., Belpassi, L., Macchioni, A.; Tarantelli, F. *Eur. J. Inorg. Chem.* **2013**, *24*, 4121–4135.
24. Obradors, C.; Echavarren, A. M. *Chem. Commun.* **2014**, *50*, 16–28.
25. Ranieri, B., Escofet, I.; Echavarren, A. M. *Org. Biomol. Chem.* **2015**, *13*, 7103–7118.
26. Dickson, P. N., Wehrli, A.; Geier, G. *Inorg. Chem.* **1988**, *27*, 2921–2925.
27. Brown, T. J.; Widenhofer, R. A. *J. Organomet. Chem.* **2011**, *696*, 1216–1220.
28. Akana, J. A., Bhattacharyya, K. X., Müller, P.; Sadighi, J. P. *J. Am. Chem. Soc.* **2007**, *129*, 7736–7737.

29. a) Marion, N.; Nolan, S. P. *Angew. Chem. Int. Ed.* **2007**, *46*, 2750–2752; b) Wang, S.; Zhang, G.; Zhang, L. *Synlett*, **2010**, 692–706; c) Shiroodi, R. K.; Gevorgyan, V. *Chem. Soc. Rev.*, **2013**, *42*, 4991–5001.
30. Correa, A.; Marion, N.; Fensterbank, L.; Malacria, M.; Nolan, S. P.; Cavallo, L. *Angew. Chem. Int. Ed.* **2008**, *47*, 718–721.
31. De Haro, T., Gómez-Bengoa, E., Cribiú, R., Huang, X.; Nevado, C. *Chem. Eur. J.* **2012**, *18*, 6811–6824.
32. Liu, L. P., Xu, B., Mashuta, M. S.; Hammond, G. B. *J. Am. Chem. Soc.* **2008**, *130*, 17642–17643.
33. Wang, W., Hammond, G. B.; Xu, B. *J. Am. Chem. Soc.* **2012**, *134*, 5697–5705.
34. Ye, L.; Zhang, L. *Org. Lett.* **2009**, *11*, 3646–3649.
35. Lemièrè, G.; Gandon, V.; Cariou, K.; Hours, A.; Fukuyama, T.; Dhimane, A. L.; Fensterbank, L.; Malacria, M. *J. Am. Chem. Soc.* **2009**, *131*, 2993–3006.
36. Dewar, M. J. S. *Bull. Soc. Chim. Fr.* **1951**, *18*, C71–C79.
37. Chat, J.; Duncanson, L. A. *J. Chem. Soc.* **1951**, 2939–2947.
38. Hashmi, A. S. K.; Toste, F. D. *Modern Gold Catalysed Synthesis*; Wiley-VCH, 2012.
39. Kumar, M., Jasinski, J., Hammond, G. B.; Xu, B. *Chem. Eur. J.* **2014**, *20*, 3113–3119.
40. Brown, T. J., Weber, D., Gagné, M. R.; Widenhofer, R. A. *J. Am. Chem. Soc.* **2012**, *134*, 9134–9137.
41. Herrero-Gómez, E., Nieto-Oberhuber, C., López, S., Benet-Buchholz, J.; Echavarren, A. M. *Angew. Chem. Int. Ed.* **2006**, *45*, 5455–5459.
42. Jiménez-Núñez, E.; Echavarren, A. M. *Chem. Rev.* **2008**, *108*, 3326–3350.
43. Jane Wang, Z., Benltez, D., Tkatchouk, E., Goddard, W. A.; Dean Toste, F. *J. Am. Chem. Soc.* **2010**, *132*, 13064–13071.
44. Gatineau, D., Goddard, J. P., Mouriés-Mansuy, V.; Fensterbank, L. *Isr. J. Chem.* **2013**, *53*, 892–900.
45. Jia, M.; Bandini, M. *ACS Catal.* **2015**, *5*, 1638–1652.
46. Schießl, J.; Schulmeister, J.; Doppiu, A.; Wörner, E.; Rudolph, M.; Karch, R.; Hashmi, A. S. K. *Adv. Synth. Catal.* **2018**, *360*, 2493–2502.
47. Schießl, J.; Schulmeister, J.; Doppiu, A.; Wörner, E.; Rudolph, M.; Karch, R.; Hashmi, A. S. K. *Adv. Synth. Catal.* **2018**, *360*, 3949–3959.
48. Zhdanko, A.; Maier, M. E. *ACS Catal.* **2014**, *4*, 2770–2775.
49. Homs, A., Obradors, C., Leboeuf, D.; Echavarren, A. M. *Adv. Synth. Catal.* **2014**, *356*, 221–228.
50. Rocchigiani, L., Jia, M., Bandini, M.; Macchioni, A. *ACS Catal.* **2015**, *5*, 3911–3915.
51. Lu, Z.; Han, J.; Okoromoba, O. E.; Shimizu, N.; Amii, H.; Tormena, C. F.; Hammond, G. B.; Xu, B. *Org. Lett.* **2017**, *19*, 5848–5851.

3.4 References

52. Bandini, M., Bottoni, A., Chiarucci, M., Cera, G.; Miscione, G. P. *J. Am. Chem. Soc.* **2012**, *134*, 20690–20700.
53. Nieto-Oberhuber, C.; Muñoz, M. P.; Buñuel, E.; Nevado, C.; Cárdenas, D. J.; Echavarren, A. M. *Angew. Chem. Int. Ed.* **2004**, *43*, 2402–2406.
54. Hashmi, A. S. K., Weyrauch, J. P., Frey, W.; Bats, J. W. *Org. Lett.* **2004**, *6*, 4391–4394.
55. Davies, P. W.; Martin, N. *Org. Lett.* **2009**, *11*, 2293–2296.
56. Kovács, G., Ujaque, G.; Lledos, A. *J. Am. Chem. Soc.* **2008**, *130*, 853–864.
57. Zhdanko, A., Ströbele, M.; Maier, M. E. *Chem. Eur. J.* **2012**, *18*, 14732–14744.
58. Ciancaleoni, G., Belpassi, L., Zuccaccia, D., Tarantelli, F.; Belanzoni, P. *ACS Catal.* **2015**, *5*, 803–814.
59. a) Bongers, N.; Krause, N. *Angew. Chem. Int. Ed.* **2008**, *47*, 2178–2181; b) Hamilton, G. L.; Kang, E. J.; Mba, M.; Toste, F. D. *Science* **2007**, *307*, 496–499; c) Widenhoefer, R. A. *Chem. Eur. J.* **2008**, *14*, 5382–5391; d) Sengupta, S.; Shi, X. *ChemCatChem* **2010**, *2*, 609–619; e) Pradal, A.; Toullec, P. Y.; Michelet, V. *Synthesis* **2011**, 1501–1514; f) Patil, N. T. *Chem. Asian J.* **2012**, *7*, 2186–2194; g) Cera, G.; Bandini, M. *Isr. J. Chem.* **2013**, *53*, 848–855.
60. Lalonde, R. L., Sherry, B. D., Kang, E. J.; Toste, F. D. *J. Am. Chem. Soc.* **2007**, *129*, 2452–2453; For reviews see: a) Hultsch, K. C. *Adv. Synth. Catal.* **2005**, *347*, 367–391; b) Widenhoefer, R. A.; Han, X. *Eur. J. Org. Chem.* **2006**, 4555–4563.
61. a) Aitken, D. J., Eijsberg, H., Frongia, A., Ollivier, J.; Piras, P. P. *Synthesis* **2014**, *46*, 1–24; b) Simeonov, S. P.; Nunes, J. P. M.; Guerra, K.; Kurteva, V. B.; Afonso, C. A. M. *Chem. Rev.* **2016**, *116*, 5744–5893; Riveira, M. J.; Marsili, L. A.; Mischne, M. P. *Org. Biomol. Chem.* **2017**, *15*, 9255–9274.
62. Nazarov, I. N.; Zaretskaya, I. I. *Izv. Akad. Nauk SSSR Ser. Khim.* **1941**, 211–224.
63. Spencer, W. T., Vaidya, T.; Frontier, A. J. *Eur. J. Org. Chem.* **2013**, 3621–3633.
64. Wenz, D. R.; De Alaniz, J. R. *Eur. J. Org. Chem.* **2015**, *2015*, 23–37.
65. a) Hoffmann, M., Weibel, J. M., De Frémont, P., Pale, P.; Blanc, A. *Org. Lett.* **2014**, *16*, 908–911; b) Rao, W.; Koh, M. J.; Li, D.; Hirao, H.; Chan, P. W. H. *J. Am. Chem. Soc.* **2013**, *135*, 7926–7932; c) Álvarez, E.; Miguel, D.; García-García, P.; Fernández-Rodríguez, M. A.; Rodríguez, F.; Sanz, R. *Synthesis* **2012**, *44*, 1874–1884; d) Sanz, R.; Miguel, D.; Gohain, M.; García-García, P.; Fernández-Rodríguez, M. A.; González-Pérez, A.; Nieto-Faza, O.; de Lera, Á. R.; Rodríguez, F. *Chem. Eur. J.* **2010**, *16*, 9818–9828; e) Oh, C. H.; Karmakar, S. *J. Org. Chem.* **2009**, *74*, 370–374; f) An, S. E.; Jeong, J.; Baskar, B.; Lee, J.; Seo, J.; Rhee, Y. H. *Chem. Eur. J.* **2009**, *15*, 11837–11841; g) Lemièrre, G.; Gandon, V.; Cariou, K.; Hours, A.; Fukuyama, T.; Dhimane, A.-L.; Fensterbank, L.; Malacria, M. *J. Am. Chem. Soc.* **2009**, *131*, 2993–3006; h) Suárez-Pantiga, S.; Rubio, E.; Alvarez-Rúa, C.; González, J. M. *Org. Lett.* **2009**, *11*, 13–16; i) Lin, G. Y.; Li, C. W.; Hung, S. H.; Liu, R. S. *Org. Lett.* **2008**, *10*, 5059–5062; j) Lee, J. H.; Toste, F. D. *Angew. Chem.* **2007**, *119*, 930–932; k) Lee, J. H.; Toste, F. D. *Angew. Chem. Int. Ed.* **2007**, *46*, 912–914; *Angew. Chem.* **2007**, *119*, 930; l) Lin,

- G.-Y.; Yang, C.-Y.; Liu, R.-S. *J. Org. Chem.* **2007**, *72*, 6753–6757; m) Lemière, G.; Gandon, V.; Cariou, K.; Fukuyama, T.; Dhimane, A.-L.; Fensterbank, L.; Malacria, M. *Org. Lett.* **2007**, *9*, 2207–2209; n) Lin, G. Y.; Yang, C. Y.; Liu, R. S. *J. Org. Chem.* **2007**, *72*, 6753–6757; o) Ma, Z.-X.; He, S.; Song, W.; Hsung, R. P. *Org. Lett.* **2002**, *14*, 5736–5739.
66. Saucy, G., Marbet, R., Lindlar, H.; Isler, O. *Helv. Chim. Acta* **1959**, *42*, 1945.
 67. Saucy, G.; Marbet, R. *Helv. Chim. Acta* **1967**, *50*, 1158.
 68. Miki, K., Ohe, K.; Uemura, S. *J. Org. Chem.* **2003**, *68*, 8505–8513.
 69. Overman, L. E. *Angew. Chem. Int. Ed. Engl.* **1984**, *23*, 579.
 70. Closs, G.L.; Moss, R. A. *J. Am. Chem. Soc.* **1964**, *86*, 4042.
 71. Pitzer, K. S. *Acc. Chem. Res.* **1979**, *12*, 271–276.
 72. Soriano, E., Ballesteros, P.; Marco-Contelles, J. *Organometallics* **2005**, *24*, 3182–3191.
 73. Mauleón, P., Krinsky, J. L.; Toste, F. D. *J. Am. Chem. Soc.* **2009**, *131*, 4513–4520.
 74. Moreau, X.; Goddard, J. P.; Bernard, M.; Lemière, G.; López-Romero, J. M.; Mainetti, E.; Marion, N.; Mouriès, V.; Thorimbert, S.; Fensterbank, L.; Malacria, M. *Adv. Synth. Catal.* **2008**, *350*, 43–48.
 75. Soriano, E.; Marco-Contelles, J. *Chem. Eur. J.* **2008**, *14*, 6771–6779.
 76. Soriano, E.; Marco-Contelles, J. *Acc. Chem. Res.* **2009**, *42*, 1026–1036.
 77. Amijs, C. H. M., López-Carrillo, V.; Echavarren, A. M. *Org. Lett.* **2007**, *9*, 4021–4024.
 78. Li, G., Zhang, G.; Zhang, L. *J. Am. Chem. Soc.* **2008**, *130*, 3740–3741.
 79. Huang, X., De Haro, T.; Nevado, C. *Chem. Eur. J.* **2009**, *15*, 5904–5908.
 80. Marion, N.; Lemière, G.; Correa, A.; Costabile, C.; Ramón, R. S.; Moreau, X.; De Frémont, P.; Dahmane, R.; Hours, A.; Lesage, D.; Tabet, J. C.; Goddard, J. P.; Gandon, V.; Cavallo, L.; Fensterbank, L.; Malacria, M.; Nolan, S. P. *Chem. Eur. J.* **2009**, *15*, 3243–3260.
 81. Mamane, V., Gress, T., Krause, H.; Fürstner, A. *J. Am. Chem. Soc.* **2004**, *126*, 8654–8655.
 82. Johansson, M. J., Gorin, D. J., Staben, S. T.; Toste, F. D. *J. Am. Chem. Soc.* **2005**, *127*, 18002–18003.
 83. Gandon, V., Lemière, G., Hours, A., Fensterbank, L.; Malacria, M. *Angew. Chem. Int. Ed.* **2008**, *47*, 7534–7538.
 84. Zhang, L. *J. Am. Chem. Soc.* **2005**, *127*, 16804–16805.
 85. Marion, N., Díez-González, S., De Frémont, P., Noble, A. R.; Nolan, S. P. *Angew. Chem. Int. Ed.* **2006**, *45*, 3647–3650.
 86. Oh, C. H., Kim, A., Park, W., Park, D. I.; Kim, N. *Synlett* **2006**, 2781–2784.
 87. Zhao, J., Hughes, C. O.; Toste, F. D. *J. Am. Chem. Soc.* **2006**, *128*, 7436–7437.
 88. Zhang, L.; Wang, S. *J. Am. Chem. Soc.* **2006**, *128*, 1442–1443.

3.4 References

89. Shi, F. Q., Li, X., Xia, Y., Zhang, L.; Yu, Z. X. *J. Am. Chem. Soc.* **2007**, *129*, 15503–15512.
90. Lemière, G.; Gandon, V.; Cariou, K.; Fukuyama, T.; Dhimane, A. L.; Fensterbank, L.; Malacria, M. *Org. Lett.* **2007**, *9*, 2207–2209.
91. Buzas, A.; Gagosz, F. *J. Am. Chem. Soc.* **2006**, *128*, 12614–12615.
92. Wang, S.; Zhang, L. *Org. Lett.* **2006**, *8*, 4585–4587.
93. Buzas, A., Istrate, F.; Gagosz, F. *Org. Lett.* **2006**, *8*, 1957–1959.
94. Tius, M. A. *Eur. J. Org. Chem.* **2005**, 2193–2206.
95. Pellissier, H. *Tetrahedron* **2005**, *61*, 6479–6517.
96. Vaidya, T., Eisenberg, R.; Frontier, A. J. *ChemCatChem* **2011**, *3*, 1531–1548.
97. Woodward, R. B.; Hoffmann, R. *The Conservation of Orbital Symmetry*; Verlag Chemie: Weinheim, 1970.
98. Frontier, A. J.; Collison, C. *Tetrahedron* **2005**, *61*, 7577–7606.
99. Occhiato, E. G., Prandi, C., Ferrali, A., Guarna, A.; Venturello, P. *J. Org. Chem.* **2003**, *68*, 9728–9741; Frontier, A. J.; Hernandez, J. J. *Acc. Chem. Res.* **2020**, *53*, 1822–1832.
100. Petrović, M.; Occhiato, E. G. *Chem. Asian J.* **2016**, *11*, 642–659.
101. Petrovic, M., Scarpi, D., Fiser, B., Gómez-Bengoia, E.; Occhiato, E. G. *Eur. J. Org. Chem.* **2015**, 3943–3956.
102. Scarpi, D., Petrović, M., Fiser, B., Gómez-Bengoia, E.; Occhiato, E. G. *Org. Lett.* **2016**, *18*, 3922–3925.
103. Scarpi, D., Faggi, C.; Occhiato, E. G. *J. Nat. Prod.* **2017**, *80*, 2384–2388.
104. Krauter, C. M.; Hashmi, A. S. K.; Pernpointner, M. *ChemCatChem* **2010**, *2*, 1226–1230.
105. a) Kovács, G.; Ujaque, G.; Lledós, A. J. *Am. Chem. Soc.* **2008**, *130*, 853; b) Zhang, J.; Shen, W.; Li, L.; Li, M. *Organometallics* **2009**, *28*, 3129.
106. González-Pérez, A. B.; Villar, P.; de Lera, A. R. *Eur. J. Org. Chem.* **2019**, 2539–2551.
107. Compound **12** was easily identified by the α,β -unsaturated ketone moiety $^1\text{H-NMR}$ signals at 6.89 (dq, $J = 15.2, 6.8$ Hz), 6.63 (d, $J = 15.2$ Hz), and 1.94 (d, $J = 6.8$ Hz, CH_3) ppm. The singlet at 5.45 ppm is diagnostic of 2-H in the 2,3-dehydropiperidine ring.
108. Gabriele, B.; Mancuso, R.; Veltri, L. *Chem. Eur. J.* **2016**, *22*, 5056–5094.
109. Rinaldi, A.; Scarpi, D.; Occhiato, E. G. *Eur. J. Org. Chem.* **2019**, 2019, 7401–7419.
110. Ivchenko, N. B.; Ivchenko, P. V.; Nifant'ev, I. E. *Russ. J. Org. Chem.* **2000**, *36*, 609–637.
111. Enders, M.; Baker, R. W. *Curr. Org. Chem.* **2006**, *10*, 937–953.

112. a) Dubé, P.; Toste, F. D. *J. Am. Chem. Soc.* **2006**, *128*, 12062–12063; b) Zi, W.; Toste, F. D. *J. Am. Chem. Soc.* **2013**, *135*, 12600–12603; c) Adcock, H. V.; Langer, T.; Davies, P. W. *Chem. Eur. J.* **2014**, *20*, 7262–7266.
113. a) Virumbrales, C.; Suárez-Pantiga, S.; Solas, M.; Fernández-Rodríguez, M. A.; Sanz, R. *Org. Biomol. Chem.* **2018**, *16*, 2623–2628; b) Sanjuán, A. M.; Virumbrales, C.; García-García, P.; Fernández-Rodríguez, M. A.; Sanz, R. *Org. Lett.* **2016**, *18*, 1072–1075; c) Martínez, A.; García-García, P.; Fernández-Rodríguez, M. A.; Rodríguez, F.; Sanz, R. *Angew. Chem. Int. Ed.* **2010**, *49*, 4633–4637; d) Guo, J.; Peng, X.; Wang, X.; Xie, F.; Zhang, X.; Liang, G.; Sun, Z.; Liu, Y.; Cheng, M.; Liu, Y. *Org. Biomol. Chem.* **2018**, *16*, 9147–9151; e) Álvarez-Pérez, M.; Frutos, M.; Viso, A.; de la Pradilla, R. F.; de la Torre, M. C.; Sierra, M. A.; Gornitzka, H.; Hemmert, C. *J. Org. Chem.* **2017**, *82*, 7546–7554.
114. Nahide, P. D.; Jiménez-Halla, J. O. C.; Wrobel, K.; Solorio-Alvarado, C. R.; Alvarado, R. O.; Yahuaca-Juárez, B. *Org. Biomol. Chem.* **2018**, *16*, 7330–7335.
115. Yin, X.; Mato, M.; Echavarren, A. M. *Angew. Chem. Int. Ed.* **2017**, *56*, 14591–14595.
116. a) Yu, C.; Ma, X.; Chen, B.; Tang, B.; Paton, R. S.; Zhang, G. *Eur. J. Org. Chem.* **2017**, *2017*, 1561–1565; b) Bucher, J.; Stößer, T.; Rudolph, M.; Rominger, F.; Hashmi, A. S. K. *Angew. Chem. Int. Ed.* **2015**, *54*, 1666–1670; c) For a review, see: Raubenheimer, H. G. *ChemCatChem* **2015**, *7*, 1261–1262.
117. a) Ma, B.; Wu, Z.; Huang, B.; Liu, L.; Zhang, J. *Chem. Commun.* **2016**, *52*, 9351–9354; b) Preinfalk, A.; Misale, A.; Maulide, N. *Chem. Eur. J.* **2016**, *22*, 14471–14474; c) Morita, N.; Miyamoto, M.; Yoda, A.; Yamamoto, M.; Ban, S.; Hashimoto, Y.; Tamura, O. *Tetrahedron Letters* **2016**, *57*, 4460–4463.
118. Hueber, D.; Teci, M.; Brenner, E.; Matt, D.; Weibel, J. M.; Pale, P.; Blanc, A. *Adv. Synth. Catal.* **2018**, *360*, 2453–2459.
119. Rinaldi, A.; Petrović, M.; Magnolfi, S.; Scarpi, D.; Occhiato, E. G. *Org. Lett.* **2018**, *20*, 4713–4717.
120. Rinaldi, A.; Langé, V.; Gómez-Bengoña, E.; Zanella, G.; Scarpi, D.; Occhiato, E. G. *J. Org. Chem.* **2019**, *84*, 6298–6311.
121. Claisen, L. *Chem. Ber.* **1912**, *45*, 3157–3167.
122. Thyagarajan, B. S.; Balasubramanian, K. K.; Bhima Rao, R. *Tetrahedron* **1963**, *4*, 1393–1398.
123. Black, D. K.; Landor, S. R. *J. Chem. Soc.* **1965**, 6784–6788.
124. Castro, A. M. M. *Chem. Rev.* **2004**, *104*, 2939–3002.
125. Tsuno, T.; Hoshino, H.; Okuda, R.; Sugiyama, K. *Tetrahedron* **2001**, *57*, 4831–4840.
126. Zachová, H.; Man, S.; Nečas, M.; Potáček, M. *Eur. J. Org. Chem.* **2005**, 2548–2557.
127. Crandall, J. K.; Tindell, G. L. *Chem. Commun.* **1970**, 1411–1412.
128. Nonoshita, K.; Banno, H.; Maruoka, K.; Yamamoto, H. *J. Am. Chem. Soc.* **1990**, *112*, 316–322.

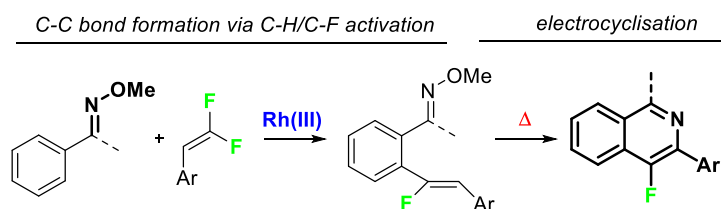
3.4 References

129. Tejedor, D.; Santos-Expósito, A.; Méndez-Abt, G.; Ruiz-Pérez, C.; García-Tellado, F. *Synlett* **2009**, 1223–1226.
130. Inanaga, J.; Baba, Y.; Hanamoto, T. *Chem. Lett.* **1993**, 241–244.
131. Tejedor, D.; Méndez-Abt, G.; Cotos, L.; García-Tellado, F. *Chem. Soc. Rev.* **2013**, *42*, 458–471.
132. Koch-Pomeranz, U.; Hansen, H.-J.; Schmid, H. *Helv. Chim. Acta* **1973**, *56*, 2981.
133. Grissom, J. W.; Huang, D. H. *J. Org. Chem.* **1994**, *59*, 5114.
134. Sherry, B. D.; Toste, F. D. *J. Am. Chem. Soc.* **2004**, *126*, 15978–15979.
135. Sherry, B. D.; Maus, L.; Laforteza, B. N.; Toste, F. D. *J. Am. Chem. Soc.* **2006**, *128*, 8132–8133.
136. Wang, Q.; Aparaj, S.; Akhmedov, N. G.; Petersen, J. L.; Shi, X. *Org. Lett.* **2012**, *14*, 1334–1337.
137. Garayalde, D.; Gómez-Bengoá, E.; Huang, X.; Goeke, A.; Nevado, C. *J. Am. Chem. Soc.* **2010**, *132*, 4720–4730.
138. Cao, H.; Jiang, H. F.; Huang, H. W.; Zhao, J. W. *Org. Biomol. Chem.* **2011**, *9*, 7313–7317.
139. Huang, H.; Jiang, H.; Cao, H.; Zhao, J.; Shi, D. *Tetrahedron* **2012**, *68*, 3135–3144.
140. Suhre, M. H.; Reif, M.; Kirsch, S. F. *Org. Lett.* **2005**, *7*, 3925–3927.
141. Menz, H.; Kirsch, S. F. *Org. Lett.* **2006**, *8*, 4795–4797.
142. Matoušová, E.; Růžička, A.; Kuneš, J.; Králová, J.; Pour, M. *Chem. Commun.* **2011**, *47*, 9390–9392.
143. Binder, J. T.; Kirsch, S. F. *Org. Lett.* **2006**, *8*, 2151–2153.
144. Harschneck, T.; Kirsch, S. F. *J. Org. Chem.* **2011**, *76*, 2145–2156.
145. Wei, H.; Wang, Y.; Yue, B.; Xu, P. F. *Adv. Synth. Catal.* **2010**, *352*, 2450–2454.
146. Veitch, G. E.; Beckmann, E.; Burke, B. J.; Boyer, A.; Maslen, S. L.; Ley, S. V. *Angew. Chem. Int. Ed.* **2007**, *46*, 7629–7632.
147. De Renzi, A.; Panunzi, A.; Saporito, A.; Vitagliano, A. *J. Chem. Soc. Perkin Trans. II* **1983**, 993–996.
148. Zhang, Z.; Liu, C.; Kinder, R. E.; Han, X.; Qian, H.; Widenhofer, R. A. *J. Am. Chem. Soc.* **2006**, *128*, 9066–9073.
149. Liu, Z.; Wasmuth, A. S.; Nelson, S. G. *J. Am. Chem. Soc.* **2006**, *128*, 10352–10353.
150. Ackermann, L.; Gunnoe, T. B.; Habgood, L. G. *Catalytic Hydroarylation of Carbon-Carbon Multiple Bonds*; Wiley-VCH: Weinheim, 2018.
151. Fantasia, S.; Petersen, J. L.; Jacobsen, H.; Cavallo, L.; Nolan, S. P. *Organometallics* **2007**, *26*, 5880–5889.

Chapter 4

Fluorinated isoquinolines

Synthesis of fluorinated heterocycles through C-H activation and following electrocyclisation and computational analysis on synthetic issues.



In this chapter, a new methodology for the synthesis of fluorinated isoquinolines is presented.

It is a two-step reaction that includes a rhodium catalysed C-H activation of an oxime compound with difluoroalkene and following electrocyclisation.

Computational studies were carried out to shed light on the electrocyclisation step and the reaction outcome.

This chapter deals with the work performed at the University of Sheffield in the group of Prof. Harrity during my secondment. The contribution of the author of this thesis is both experimental and computational. A general introduction about isoquinolines and the nature of the chemistry is initially provided. Then, the aim of the work, the experimental and computational procedures and results are described.

4.1 Introduction

4.1.1 Isoquinolines

Isoquinoline is a structural isomer of quinoline that bears a nitrogen-containing heteroaromatic and benzene-ring-fused system. Isoquinolines are commonly found in naturally occurring alkaloids.¹⁻³ They constitute important scaffolds present in pharmaceutical, agricultural and materials sciences because of their bioactivities and useful physical properties. Isoquinoline-related medicines are widely found in worldwide pharmaceutical markets. For example, papaverine hydrochloride, morphine and berberine tannate are prescribed as antispasmodic drug, painkiller and antidiarrheal, respectively.⁴ On the other hand, there are some isoquinolines, as some tetrahydroisoquinoline derivatives, which exhibit severe neurotoxicity leading to Parkinson's disease.⁵

Isoquinoline was first isolated as the sulfate salt from coal tar in 1885 by Hoogewerf and van Dorp.⁶ By 1893, several syntheses of isoquinolinoid compounds were published by Pomeranz,⁷ Fritsch,⁸ Bischler and Napieralski,⁹ through reactions known by their names. Early in the 20th century, Pictet, Gams, and Spengler developed slightly different approaches to prepare isoquinoline derivatives (Figure 4.1).^{10,11} Generally, most early preparations required strong acids and refluxing conditions or dehydrating agents and dehydrogenation catalysts that limited the functional group survival during the reactions. Classic isoquinoline syntheses are still nowadays used to generate dihydro- and tetrahydro-isoquinolines.

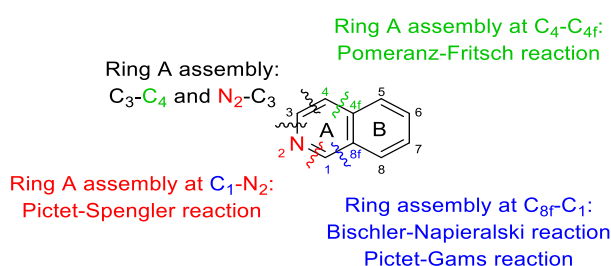
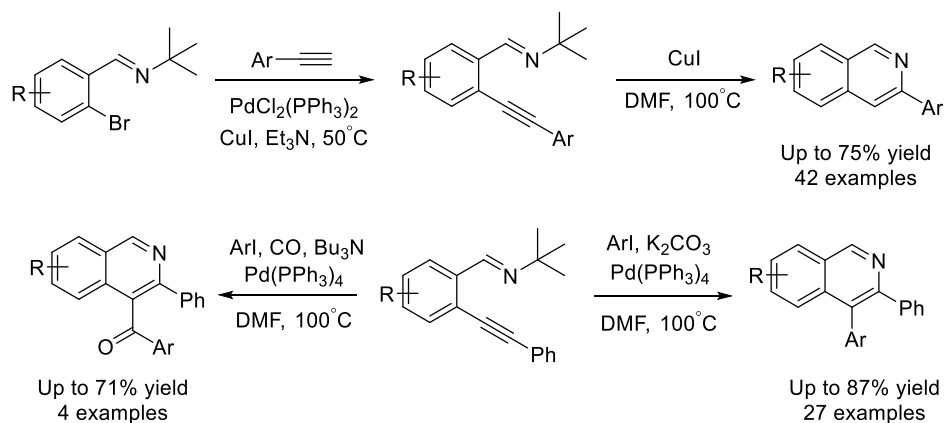


Figure 4.1 Generic representation of synthetic strategies to build the isoquinoline core.

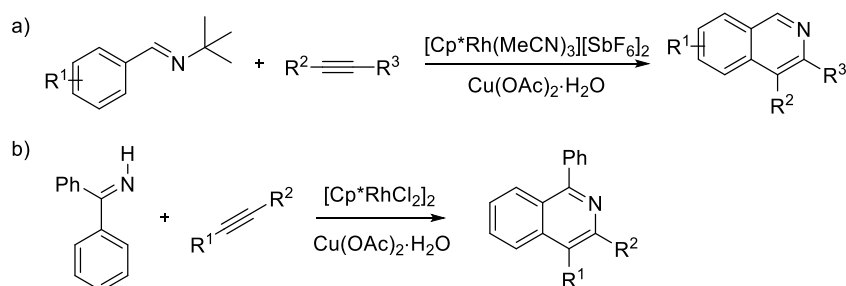
Among the modern strategies for the synthesis of isoquinolines, the Larock synthesis is one of the most versatile (Scheme 4.1).¹²

4.1 Introduction



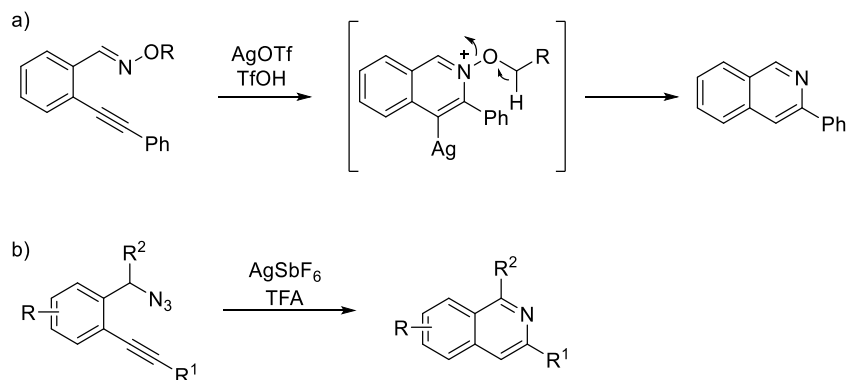
Scheme 4.1 Larock synthesis of isoquinolines.

New modifications and syntheses seek to improve this method. For example, Fagnou group proposed a strategy based on the same disconnections of the Larock synthesis but without the requirement of an *ortho*-halogen. They employed rhodium to induce C–H bond cleavage under mild conditions (Scheme 4.2a).¹³ A very similar transformation was reported by Miura and co-workers, who developed a rhodium-catalysed oxidative coupling of aromatic imines with alkynes to produce quinoline derivatives (Scheme 4.2b).¹⁴



Scheme 4.2 Rh-catalysed synthesis of isoquinolines by a) Fagnou and b) Miura groups.

Several reports illustrated the metal-catalysed cyclisation of *ortho*-alkynylbenzaldoximes. Shin and co-workers developed an isoquinoline synthesis from 2-alkynylbenzaldoximes exploiting the easily oxidised benzyloxy moiety (Scheme 4.3a).¹⁵



Scheme 4.3 a) AgOTf and TfOH co-catalysed isoquinoline synthesis; b) Ag-catalysed cyclisation of *o*-alkynyl-benzylazides.

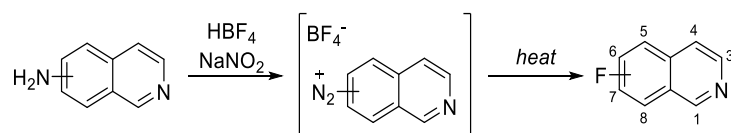
Another approach to isoquinolines involves the cyclisation of *o*-alkynyl-benzylazides. Liang and co-workers reported a silver-catalysed cyclisation to generate 1,3-substituted isoquinolines (Scheme 4.3b).¹⁶

4.1.1.1 Fluorinated isoquinolines

The insertion of fluorine into the isoquinoline scaffold causes dramatic shifts of molecular properties and makes it a more valuable substrate. The inductive effect brought about by the high electronegativity of fluorine and its small van der Waals radius of 1.47Å changes molecular structural and stereoelectronic properties such as conformation, pK_a , polarity, solubility and hydrogen-bonding capacity.¹⁷ Consequently, significant enhancements of bioactivity have been observed in fluorinated isoquinoline derivatives in comparison with the activity of the corresponding fluorine-free compounds. Thus, fluorinated isoquinolines are known to feature biological activities and light-emitting properties, which lead them to be incorporated in many pharmaceuticals and materials. Nowadays, nearly 20% of FDA approved drugs contain fluorine.¹⁸ The very strong σ_{sp^3} C-F bond (110 kcal/mol) increases the metabolic stability of drugs, enabling better bioavailability and binding affinity. Isoquinolines functionalised with fluorine and fluorine containing groups work as important pharmacores with many applications. For instance, isoquinoline carboxamides labelled with ¹⁸F are used in radiolabelling ligands for positron emission tomography.¹⁹ Additionally, the preparation of fluorinated, fluoroalkylated and fluoroarylated isoquinoline variants with antibacterial and antiparasitic properties continues to attract the medicinal chemistry community.

Modern synthetic methodologies for fluorinated isoquinolines have been greatly developed during the last decades. These approaches include (i) the direct introduction of fluorine (or CF₃ group) onto the isoquinoline ring, (ii) the construction of a fused pyridine ring *via* cyclisation of a precursor bearing a pre-fluorinated benzene ring and (iii) the simultaneous installation of an isoquinoline framework and a fluorine substituent.

Many typical synthetic methodologies for the preparation of fluorinated isoquinoline derivatives emerged already in the 1950s and 1960s. In 1951, Roe and Teague reported the first example of synthesis of monofluorinated isoquinolines.²⁰ They successfully prepared 1-, 3-, 4-, and 5-fluoroisoquinolines heating diazonium intermediates derived from the corresponding aminoisoquinolines on treatment with sodium nitrite and fluoroboric acid, known as the Baltz–Schiemann reaction (Scheme 4.4).²¹

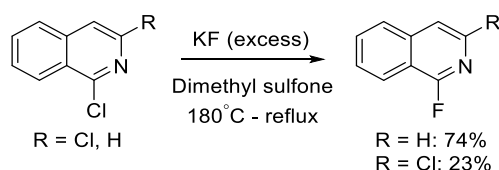


Scheme 4.4 The Baltz-Schiemann reaction.

Additional work involving the Baltz–Schiemann reaction was reported in the 1960s by Belsten and Dyke,²² who synthesised 8-fluoroisoquinoline and by Bellas and Suschitzky, who reported the first synthesis of 6- and 7- fluoroisoquinolines (Scheme 4.4).²³

4.1 Introduction

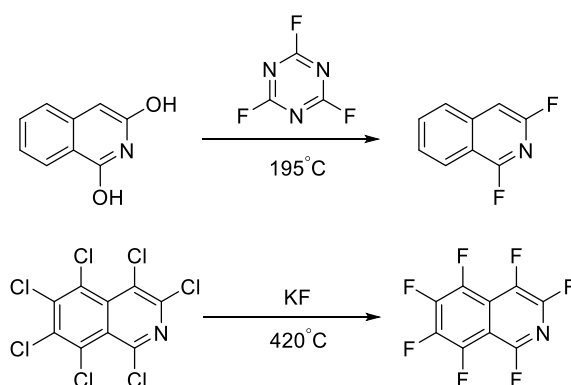
An alternative approach to the synthesis of 1-fluoroisoquinolines was accomplished through nucleophilic aromatic substitution (S_NAr).²³ 1-chloroisoquinolines were subjected to the chlorine–fluorine exchange reaction (Halex reaction)^{24,25} with potassium fluoride affording 1-fluoroisoquinolines in high yields (Scheme 4.5).



Scheme 4.5 The Halex reaction towards 1-fluoroisoquinolines.

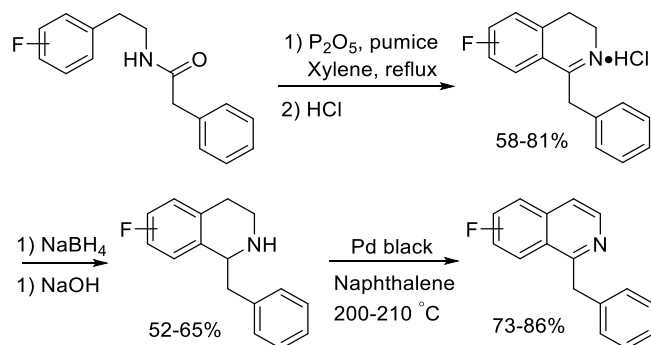
When 1,3-dichloroisoquinoline was used as substrate, 3-chloro-1-fluoroisoquinoline was selectively obtained despite the use of an excess of potassium fluoride. The chemoselectivity was attributed to the lability of the carbon–halogen bond at the 1-position of the isoquinoline ring.

In 1960, the first example of multiple fluorine atoms insertion onto the isoquinoline framework was reported by Bayer (Scheme 4.6), patenting the synthesis of 1,3-difluoroisoquinoline starting from 1,3-dihydroxyisoquinoline and cyanuric fluoride.²⁶ Six years later, Chambers and Musgrave succeeded to replace all the hydrogen atoms of the parent isoquinoline by fluorine atoms *via* a chlorine–fluorine exchange reaction leading to the formation of heptafluoroisoquinoline.²⁷ The mixture of heptachloroisoquinoline and potassium fluoride was heated to 420 °C allowing the global fluorination to provide an excellent yield of heptafluoroisoquinoline, which easily underwent further S_NAr reactions with various nucleophiles (Scheme 4.6).



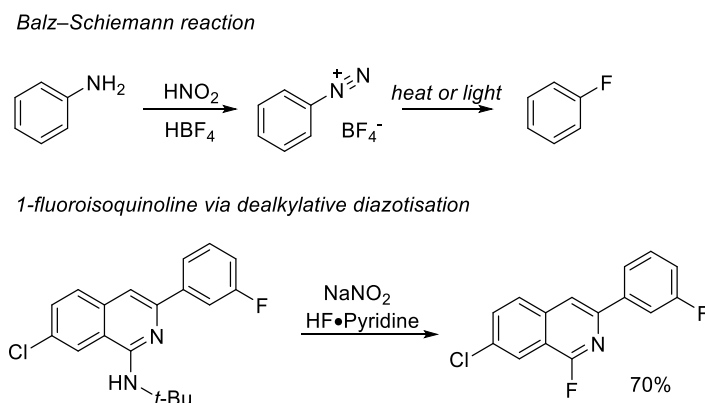
Scheme 4.6 Syntheses of di- and perfluorinated isoquinolines.

Bischler–Napieralski reaction is a useful strategy for the synthesis of functionalised fluoroisoquinolines.⁹ This reaction involves the cyclisation of *N*-[2-(fluorophenyl)ethyl]amides followed by aromatisation. *N*-[2-(fluorophenyl)ethyl]-2-phenylacetamide reacts smoothly, irrespective of the position of fluorine (Scheme 4.7).²²



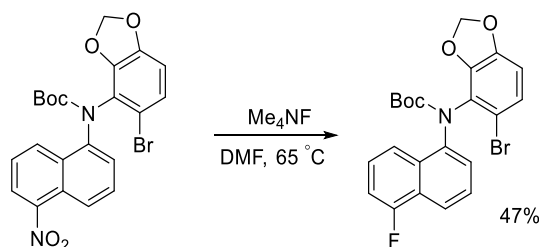
Scheme 4.7 Bischler-Napieralski reaction for the synthesis of fluoroisoquinolines.

Regarding the methods of direct ring fluorination, the Baltz–Schiemann reaction is still one of the most common ones due to the accessibility to aminated isoquinoline derivatives. Originally, the reaction involved the use of tetrafluoroboric acid (fluoroboric acid) and then several modified procedures have been reported.²⁸ For example, Myers and co-workers synthesised 1-fluoroisoquinoline by the dealkylative diazotization of 1-*tert*-butyl-aminoisoquinoline with pyridine hydrofluoride instead of HBF₄ (Scheme 4.8).²⁹



Scheme 4.8 Application of the Balz-Schiemann reaction for the synthesis of fluoroisoquinolines.

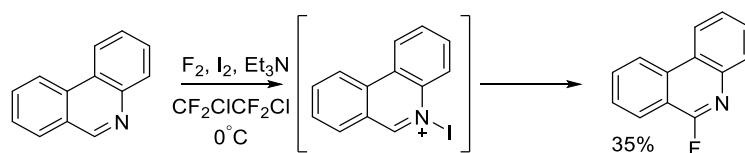
Also a nitro group on an aromatic ring can be directly converted to a fluorine substituent *via* S_NAr mechanism.³⁰ In this fluorodenitration method, tetraalkylammonium fluorides and inorganic fluoride salts have been used as fluorine sources (Scheme 4.9).³¹

Scheme 4.9 Synthesis of 8-fluoroisoquinoline *via* fluorodenitration with Me₄NF.

The direct fluorination of a C–H bond of nitrogen-containing heterocycles was achieved by Chambers and Sandford and co-workers using gaseous fluorine and iodine as sources of both I⁺ and F[−] (Scheme 4.10).³² The heterocycles were activated by *N*-iodination, thus

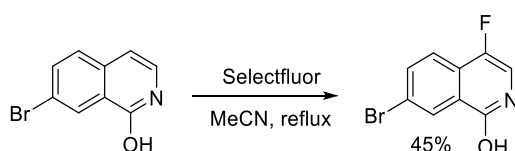
4.1 Introduction

becoming susceptible to fluoride attack at the carbon adjacent to the nitrogen atom. Elimination of hydrogen iodide gave the corresponding ring-fluorinated heterocycles.



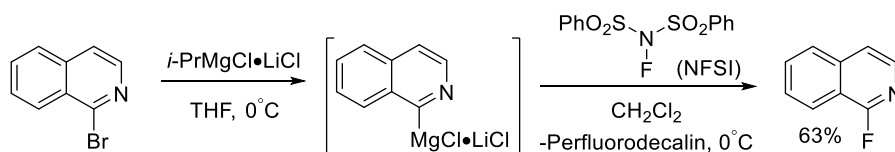
Scheme 4.10 Synthesis of 6-fluorophenanthridine *via* fluorination with F_2 and I_2 .

An alternative to nucleophilic fluorination is the synthesis of fluorinated isoquinolines *via* direct electrophilic fluorination. In 2007, Price group developed the direct electrophilic C–H bond fluorination of an isoquinoline derivative with Selectfluor,³³ which is an efficient electrophilic fluorine source.³⁴ 6-bromo-1-hydroxyisoquinoline and Selectfluor react in acetonitrile at reflux affording 7-bromo-4-fluoro-1-hydroxyisoquinoline as a single isomer in a one-pot reaction (Scheme 4.11).



Scheme 4.11 Electrophilic fluorination with Selectfluor.

In the case of heteroaryl bromides, it is possible to apply the strategy developed in 2010 by Knochel. They reported that heteroaryl bromides undergo a Br–Mg exchange through the addition of an isopropylmagnesium chloride–lithium chloride complex³⁵ and then the heteroarylmagnesium reagents are subjected to electrophilic fluorination using *N*-fluorobenzenesulfonimide (NFSI) as an electrophilic fluorinating agent leading to 1-fluoroisoquinoline (Scheme 4.12). This is an improvement of the electrophilic fluorination of standard aryl Grignard reagents already published by Barnette.³⁶

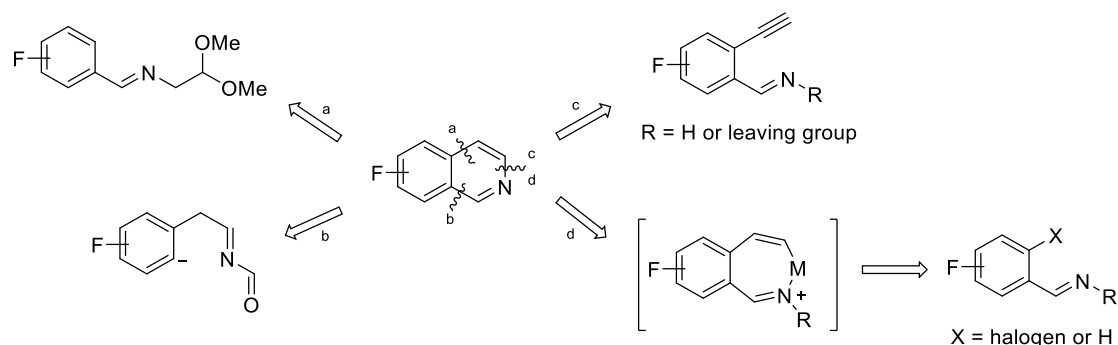


Scheme 4.12 Electrophilic fluorination of 1-isoquinolylmagnesium reagent.

Shifting to the ring construction of pre-fluorinated substrates, fluoroarene substrates could be efficient precursors of ring-fluorinated heterocycles with a fused benzene ring and strategies based on this principle are predominant due to the easy access to fluoroarenes and to the fact that aromatic C–F are bonds robust enough to survive most of the reaction conditions.

For a successful synthesis, the nitrogen atom must be located at appropriate positions and cyclisation accompanied or followed by aromatisation must proceed smoothly. Aryl or benzyl imines have demonstrated to be good precursors of isoquinolines. In Scheme 4.13, different approaches to fluoroisoquinolines starting from *N*-substituted imines bearing a fluoroaryl group are shown. The substituents on the nitrogen atom should be

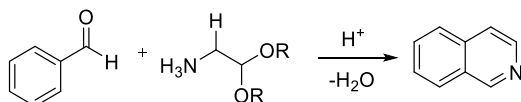
efficiently incorporated or eventually removed. Route d involves simultaneous reductive elimination and removal of *N*-substituents from nitrogen-containing metallacycles. The intermediary metallacycles can be mainly obtained from (*ortho*-haloaryl)methanimines.



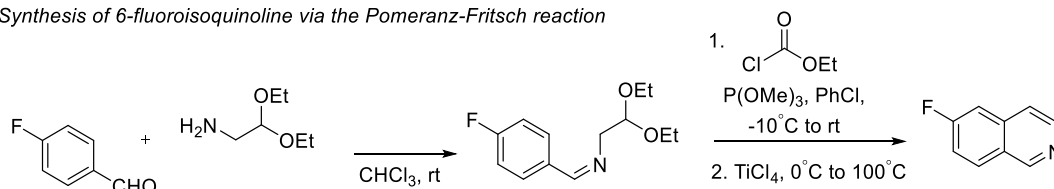
Scheme 4.13 Approaches to fluoroisoquinolines starting from imines bearing a fluoroaryl group.

Route a (Scheme 4.13) is the Pomeranz–Fritsch reaction that allows the synthesis of isoquinolines starting from benzaldehyde and a 2,2-dialkoxyethylamine through the formation of a benzalminoacetal intermediate.^{7,8} The intramolecular cyclisation of this type of imines under acidic conditions provides isoquinolines, where the two-carbon substituent on the nitrogen atom is transformed into a part of the isoquinoline ring. A modified procedure exists using ethyl chloroformate, trimethyl phosphite and titanium tetrachloride for the cyclisation step³⁷ providing 6-fluoroisoquinoline from 4-fluorobenzaldehyde in 34 % overall yield (Scheme 4.14).³¹

General Pomeranz-Fritsch reaction



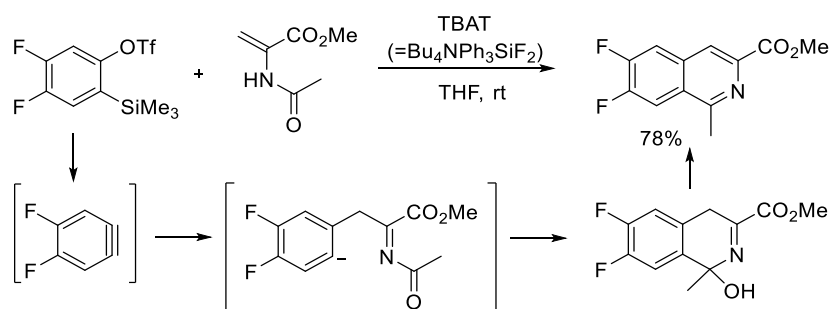
Synthesis of 6-fluoroisoquinoline via the Pomeranz-Fritsch reaction



Scheme 4.14 Application of the Pomeranz-Fritsch reaction for the synthesis of 6-fluoroisoquinoline.

Route b (Scheme 4.13) is relative to the works of the groups of Stoltz³⁸ and Ramtohl,³⁹ who independently reported an isoquinoline synthesis *via* the reaction of *N*-acetylenamines with benzynes (Scheme 4.15). In this strategy, intermediary *N*-acetylimines are subjected to nucleophilic attack by aryl anions providing the corresponding isoquinolines after aromatisation. The carbonyl carbon on the nitrogen atom is incorporated into the 1-position of the resulting isoquinolines.

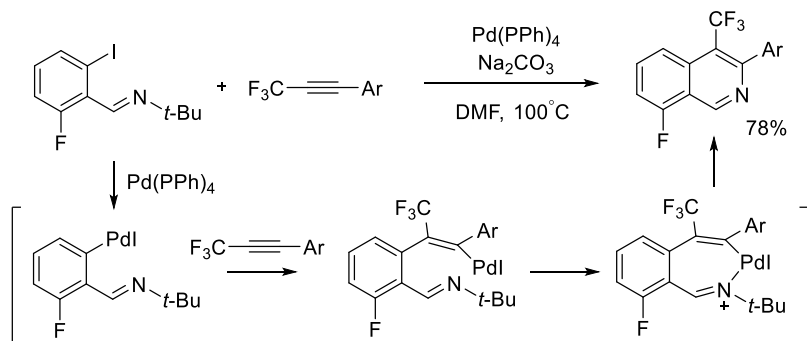
4.1 Introduction



Scheme 4.15 Synthesis of 6,7-difluoroisoquinoline *via* the reaction of *N*-acetylenamine with benzyne.

Route c shows the reaction of 2-alkynylbenzaldehyde *O*-alkyl oxime, which undergoes an intramolecular electrophilic cyclisation, eliminating the *N*-alkoxy group. An example of this strategy was provided by Shin and co-workers, who synthesised 5-fluoro-3-phenylisoquinoline using a AgOTf/TfOH catalytic system (see the F-free analogue in Scheme 4.3a).¹⁵

Route d shows that the reductive elimination from seven-membered nitrogen-containing metallacycles also leads to the construction of the isoquinoline framework. Such metallacycles result from the insertion of alkynes into metal–aryl bonds mainly formed by oxidative addition of aryl–halogen bonds. Following this strategy, Konno and co-workers achieved the synthesis of 8-fluoroisoquinoline *via* the reaction of 2-iodobenzylideneamine with trifluoromethylalkyne under palladium catalysis (Scheme 4.16).⁴⁰ Related synthetic methodologies have been established with nickel⁴¹ and rhodium¹³ catalysis.

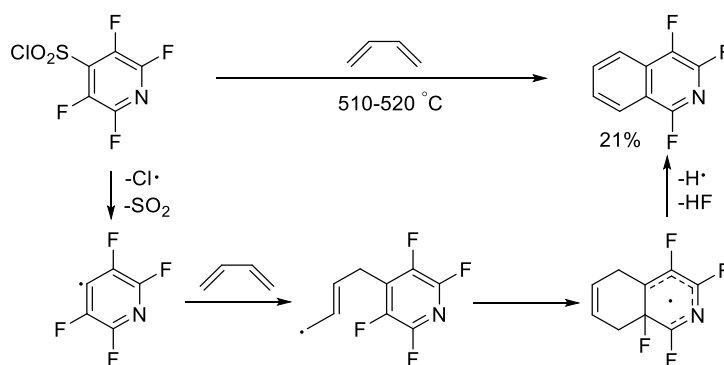


Scheme 4.16 Pd-catalysed domino insertion/cyclisation sequence for 8-fluoroisoquinoline synthesis.

Other nitrogen-containing functional groups can also participate in this type of isoquinoline synthesis, such as nitriles. Fluorinated isoquinolines were prepared *via* intramolecular and intermolecular reactions of nitriles.^{42,43}

Amines, amides, azides, triazoles and enamine-type intermediates are also key precursors for fluorinated isoquinolines.²⁸

It is worth to mention that the use of fluorinated pyridines as starting materials allows to introduce fluorine substitution into the heterocyclic ring carbons. As an example, Platonov group synthesised 1,3,4-trifluoroisoquinoline *via* the copolyolysis of 2,3,5,6-tetrafluoropyridine-4-sulfonyl chloride with butadiene (Scheme 4.17).⁴⁴

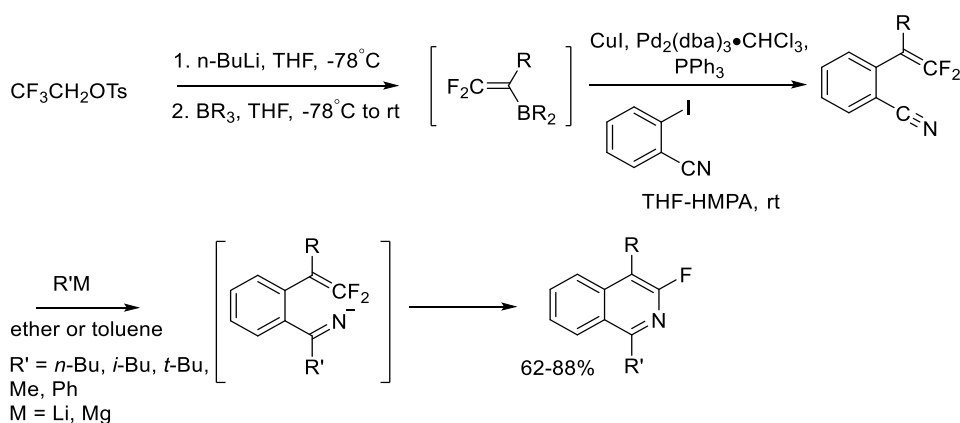


Scheme 4.17 Synthesis of 1,3,4-trifluoroisoquinoline *via* copyrolysis of pyridine-4-sulfonyl chloride with butadiene.

Another strategy for the synthesis of fluorinated isoquinolines is the simultaneous installation of an isoquinoline framework and a fluorine substituent, as for example the intramolecular cyclisation of *ortho*-functionalised β,β -difluorostyrenes. In this methodology, the construction of a heterocyclic nucleus and the introduction of a fluorine substituent occur simultaneously. The difluoromethylene carbon of 1,1-difluoro-1-alkenes features strong electrophilicity due to the electron-deficient and highly polarised carbon-carbon double bond. As a consequence, difluoroalkenes are more keen on reacting with nucleophiles than with electrophiles. Furthermore, the nucleophilic attack to difluoroalkenes followed by fluoride elimination (vinylic nucleophilic substitution; S_NV) provides products bearing a fluorovinyl moiety. An example is the work of the group of Ichikawa, which deals with the construction of 5-membered and 6-membered heterocycles *via* intramolecular S_NV reactions of 1,1-difluoro-1-alkenes.⁴⁵ Differently from direct fluorination methods, this strategy can introduce a fluorine substituent at a prescribed position, without need of regioselective pre-functionalisation. Indeed, this strategy resulted to be successful for the synthesis of 3-fluoroisoquinolines, hard to prepare through pre-existing methods.

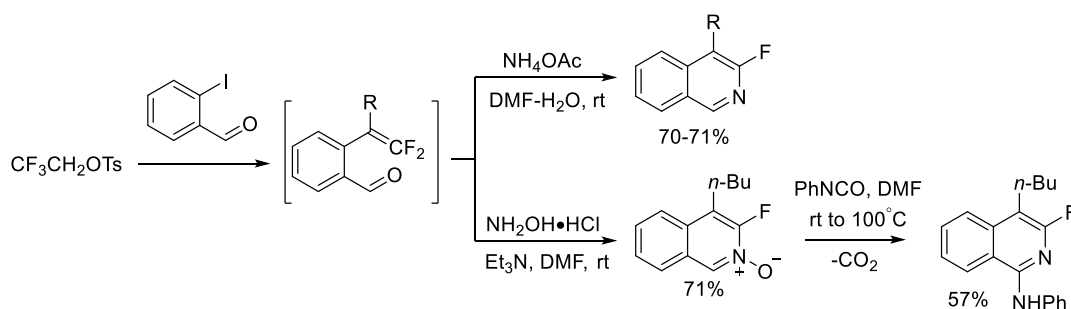
β,β -difluorostyrenes as cyclisation precursors have been mainly prepared *via* palladium-catalysed coupling of *ortho*-functionalised aryl iodides and difluorovinylborans, which were generated from 2,2,2-trifluoroethyl 4-methylbenzenesulfonate.^{46,47} *o*-Cyano- β,β -difluorostyrenes were found to react with organometallics to give the corresponding iminyl metal intermediates, which underwent 6-*endo* cyclisation to give 3-fluoroisoquinolines (Scheme 4.18).⁴⁸ Sulfonamides are other substrates that work as nucleophiles in the reaction with difluorostyrenes under basic conditions.⁴⁹

4.1 Introduction



Scheme 4.18 Synthesis of 3-fluoroisoquinolines *via* intramolecular $\text{S}_{\text{N}}\text{V}$ reaction of iminyl metal intermediates.

Finally, imines and oximes were also employed as nucleophiles to provide 3-fluoroisoquinolines and their *N*-oxides, respectively (Scheme 4.19).⁵⁰ The treatment of the isoquinoline *N*-oxide with isocyanate led to 1,3-dipolar addition and the following elimination of the oxygen atom on the nitrogen affording 1-amino-3-fluoroisoquinoline.



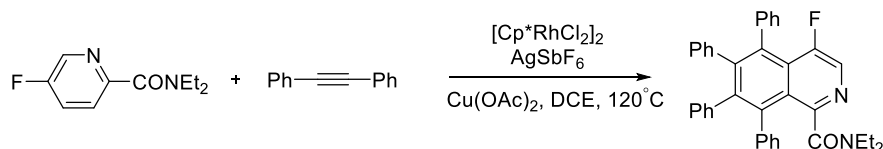
Scheme 4.19 Synthesis of 3-fluoroisoquinolines *via* intramolecular $\text{S}_{\text{N}}\text{V}$ reaction of difluorostyrenes bearing a formyl group.

4.1.1.2 Rhodium catalysis applied in the synthesis of isoquinolines

As seen in some of the above examples, rhodium is capable of catalysing several reactions leading to the formation of isoquinolines as well as fluoroisoquinolines.

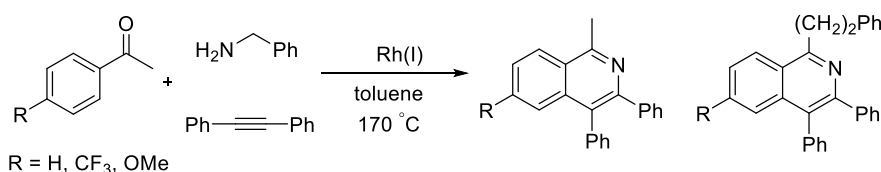
In this section, rhodium-catalysed strategies are presented in addition to the ones shown previously. The aim of this section is to elucidate the potential of rhodium in the synthesis of isoquinolines.

First, the synthesis of Guimond and Fagnou resulted to be successful also for the construction of 6-fluoro- and 6-trifluoromethylisoquinolines (analogues to Scheme 4.2a).¹³ Another noteworthy Rh-catalysed strategy towards isoquinolines bearing fluorine is represented in Scheme 4.20. It was developed by Qian group and consists in a C8f-C8/C4f-C4 annulation of fluoropicolinamide with diphenylacetylene to produce the tetraphenyl 4-fluoroisoquinoline in excellent yield.⁵¹ These catalysed processes are believed to occur *via* a sequence involving Rh(III) insertion followed by reductive elimination/electrocyclisation.⁵²



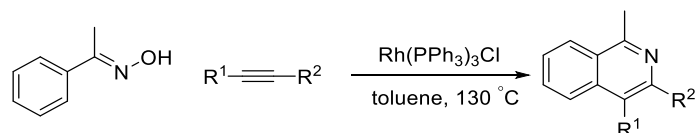
Scheme 4.20 Rh-catalysed synthesis of fluoroisoquinoline.

Concerning rhodium catalysis in isoquinoline synthesis from a general point of view, thus not only related to fluorinated isoquinolines, many examples have been reported. In 2003, the group of Jun developed a Rh(I)-catalysed direct *ortho*-alkenylation of common aromatic ketimines with alkynes providing isoquinoline derivatives. The highly efficient single-step synthesis of isoquinoline derivatives was achieved by the three-component reaction of aromatic ketone with benzylamine and alkyne without any use of *ortho*-functionalised aromatic compounds (Scheme 4.21).⁵³

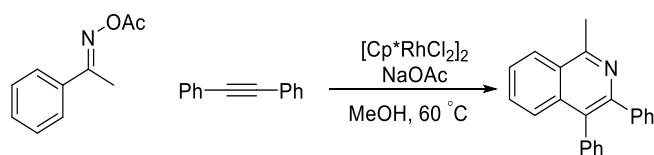


Scheme 4.21 Three-component reaction of aromatic ketone with benzylamine and alkyne affording isoquinolines.

Cheng and co-workers developed a highly regioselective synthesis of substituted isoquinoline derivatives from various aromatic ketoximes and alkynes *via* one pot, rhodium-catalysed C-H bond activation (Scheme 4.22).⁵⁴

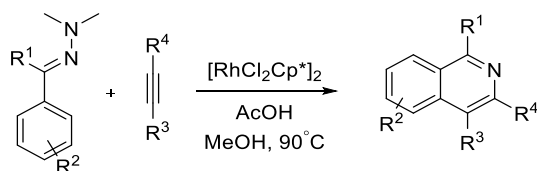
Scheme 4.22 Rh-catalysed synthesis of isoquinoline by Cheng *et al.*

Chiba and co-workers, instead, reported a synthetic method for isoquinolines from aryl ketone O-acyloxime derivatives and internal alkynes using $[\text{Cp}^*\text{RhCl}_2]_2\text{-NaOAc}$ as the potential catalyst system (Scheme 4.23).⁵⁵

Scheme 4.23 Synthesis of isoquinolines from aryl ketone O-acyloxime derivatives and internal alkynes using $[\text{Cp}^*\text{RhCl}_2]_2\text{-NaOAc}$.

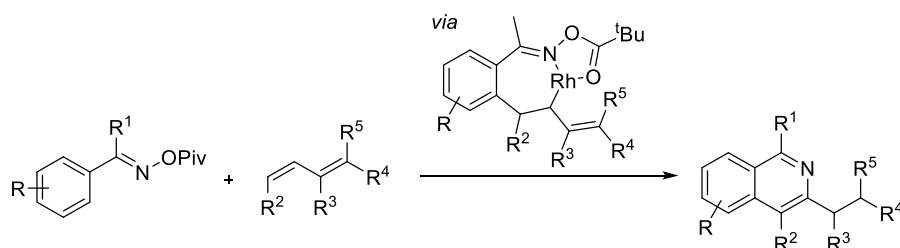
Another interesting work of the same group is the Rh(III)-catalysed synthesis of highly substituted isoquinolines starting from hydrazones. The strategy involves the directed *ortho* C-H bond activation in the hydrazone and annulation without any need of external oxidant. This reaction is accomplished *via* C-C and C-N bond formation along with N-N bond cleavage (Scheme 4.24).⁵⁶

4.1 Introduction



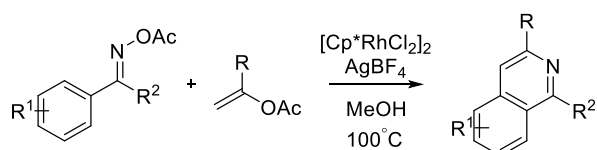
Scheme 4.24 Rh(III)-catalysed synthesis of highly substituted isoquinolines starting from hydrazones.

Trying to abandon the use of alkynes, Glorius and co-workers reported an efficient rhodium(III)-catalysed redox-neutral C–H activation/cyclisation/isomerisation strategy to prepare isoquinolines with complete regioselectivity starting from aromatic oxime esters and diverse 1,3-dienes (Scheme 4.25).⁵⁷



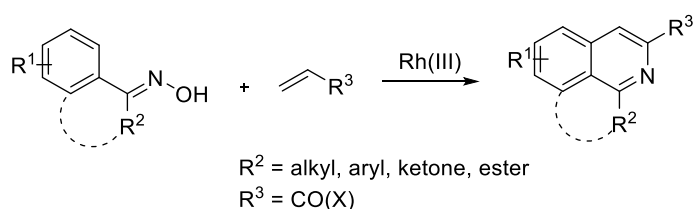
Scheme 4.25 Rh(III)-catalysed isoquinoline synthesis from 1,3-dienes.

Cheng and co-workers employed instead geminal-substituted vinyl acetates to perform a Rh-catalysed sequential oxidative C–H activation/annulation. The protocol was successfully applied to the total synthesis of papaverine (Scheme 4.26).⁵⁸



Scheme 4.26 A Rh-catalysed sequential oxidative C–H activation/annulation.

Transition-metal-catalysed C–H activation/cyclisation of aryl oximes, imines and azides with internal alkynes suffers of poor stereocontrol. Inspired by the work of Glorius⁵⁷ and Cheng⁵⁸ and the Rh(III)-catalysed C–H activation/cyclisation of oxime esters and alkenes affording pyridines by Rovis,⁵⁹ the group of Cui published a Rh(III)-catalysed C–H activation/cyclisation of oximes and alkenes to afford isoquinolines in an easy and regioselective manner. The strategy employs mild reaction conditions and easily accessible starting materials. It found application on the synthesis of moxaverine (Scheme 4.27).⁶⁰

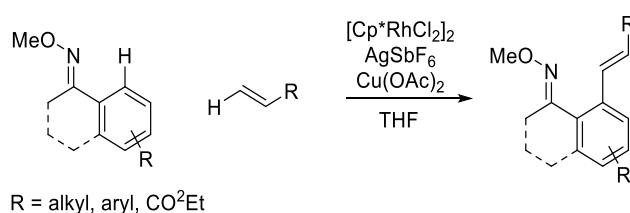


Scheme 4.27 Rh(III)-catalysed C–H activation/cyclisation of oximes and alkenes.

4.1.1.3 Oximes as precursors for the synthesis of isoquinolines

Recently, transition metal-catalysed C-H bond functionalisation reactions have become important for the construction of carbon-carbon and carbon-heteroatom bonds. In particular, Rh- and Ru-catalysed C-H bond activation reactions have displayed a wide scope of applications in the synthesis of heterocyclic and carbocyclic compounds such as isoquinoline derivatives from aromatic imines or oximes with alkynes.

In particular, oximes were found to be useful substrates for the synthesis of isoquinolines. Indeed, oximes work as directing groups for C-H functionalisation, as demonstrated for example by the work of Ellman and co-workers. They reported an oxime directed aromatic C-H bond activation and oxidative coupling to alkenes taking advantage of the cationic Rh(III) catalyst. The method could be used to oxidatively couple unactivated, aliphatic alkenes (Scheme 4.28).⁶¹



Scheme 4.28 Example of C-H activation in oximes under rhodium catalysis.

The synthesis of isoquinolines from oxime derivatives does not require an external oxidant:⁵⁵ The NO bond of oxime acts as an internal oxidant in the reaction.⁶²

Several isoquinoline syntheses starting from oxime derivatives have been reported in recent years, using different metals. The groups of Sundararaju⁶³ and Ackermann⁶⁴ employed [Cp*Co(CO)I₂]-catalysis to perform alkenylation/cyclisation sequences of free OH ketoximes and O-acetylated oximes respectively and diaryl alkynes. Cheng reported an almost identical procedure with the addition that, besides oximes, also N'-hydroxybenzimidamides were used as directing groups which then delivered 1-amino-isoquinolines as products.⁶⁵

Palladium could also be used to promote cyclisation reaction of oximes with vinyl azides or homocoupling of oximes leading to isoquinolines.⁶⁶

Silver was employed by Xu and Liu to develop a silver-catalysed intramolecular oxidative aminofluorination of alkynes using NFSI as a fluorinating reagent leading to the synthesis of various 4-fluoroisoquinolines and 4-fluoropyrrolo[α]isoquinolines.⁶⁷

In general, rhodium,⁶⁸ palladium and ruthenium⁶⁹ are the most employed metals for the synthesis of heterocycles.

4.1.2 Background CH activation in presence of difluoroalkenes

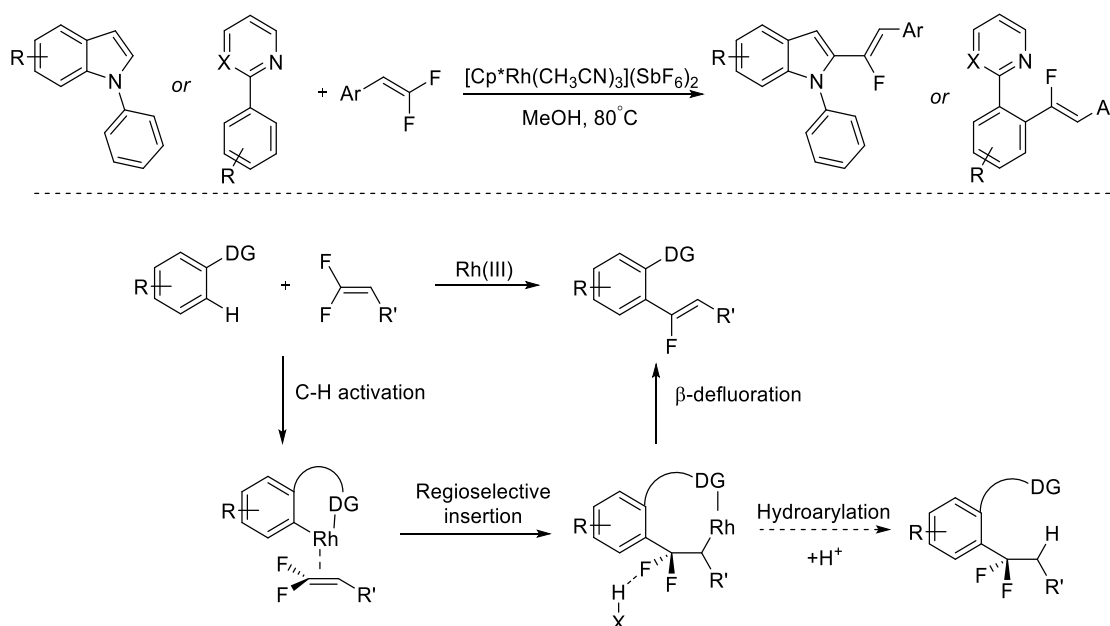
Direct functionalisation of inert C-H bonds is a powerful tool to realise atom- and step-economical synthesis and can be used to initiate a sequence that leads to the formation of isoquinolines.

Fluorine or fluorine-containing small functional groups can be introduced employing various catalysts and reagents.^{70,71} More recently, C-H functionalisation reactions accompanied by selective C-F bond cleavage of multi-fluorinated coupling partners were explored. The use of fluorinated alkenes, as difluorostyrenes, could be strategic

for the construction of fluoroisoquinolines. Nevertheless, difluoroalkenes are peculiar compounds and sometimes their reactivity is not so predictable.

In this section, some interesting works related to C-H functionalisation of arenes with fluoro substituted alkenes are presented.

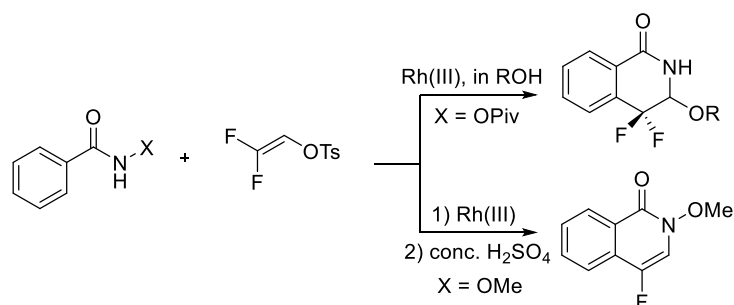
The publication that opened the field of C-H bond activation and C-F bond cleavage was the outstanding work of Tian, Feng and Loh in 2015.⁷² They reported a (hetero)arylated mono-fluoroalkene synthesis using *gem*-difluoroalkenes as electrophiles *via* aromatic C-H activation under Cp*Rh(III) catalysis in oxidant-free conditions. They proposed that β -F elimination after C-H bond cleavage and insertion of C-C double bonds furnishes the product (Scheme 4.29).



Scheme 4.29 Rh(III)-catalysed α -fluoroalkenylation of (hetero)arenes.

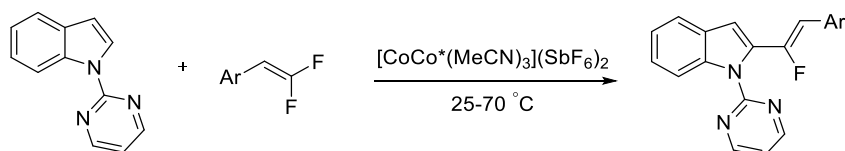
This strategy is based on some considerations, extrapolated from previous knowledge. Rh(III)-catalysed alkenylation constitutes a competent and reliable method for the introduction of olefin segments, although stoichiometric amount of external oxidant was always required to fulfil the redox demand.^{73,74} Moreover, despite its high dissociation energy, the C-F bond could be activated by transition metal or through the formation of hydrogen bonds.⁷⁵ *Gem*-difluoroalkenes are appealing synthetic intermediates with a highly polarised C-C double bond because of the electronegativity of fluorine and also the repulsion effect stemming from its unpaired electrons. Furthermore, it is well-known that hetero-nucleophiles could undergo facile nucleophilic addition or substitution reactions under basic conditions.⁷⁶

In 2017, Li and Wang developed a rhodium(III)-catalysed C-H activation of arenes and versatile coupling with 2,2-difluorovinyl tosylate. With *N*-OMe benzamide being a directing group, the reaction delivered a monofluorinated alkene keeping the tosylate functionality. Subsequent one-pot acid treatment allowed the efficient synthesis of 4-fluoroisoquinolin-1(2H)-ones and 5-fluoropyridin-2(1H)-ones. Instead, when *N*-OPiv benzamides were used, [4+2] cyclisation occurred to provide *gem*-difluorinated dihydroisoquinolin-1(2H)-ones (Scheme 4.30).⁷⁷

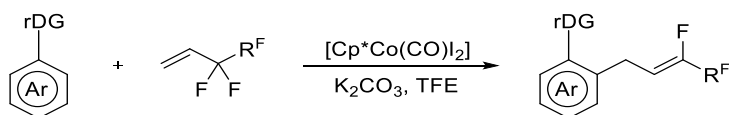


Scheme 4.30 Rh-catalysed coupling of benzamides with 2,2-difluorovinyl tosylate.

Cobalt is a more earth-abundant element and results to work as catalyst for this kind of reactions. Li group reported a cobalt(III)-catalysed α -fluoroalkenylation of different arenes with readily available *gem*-difluorostyrene providing 1,2-diaryl-substituted monofluoroalkenes in excellent *Z* selectivity (Scheme 4.31).⁷⁸

Scheme 4.31 Cobalt(III)-catalysed regio- and stereoselective α -fluoroalkenylation of arenes with *gem*-difluorostyrene.

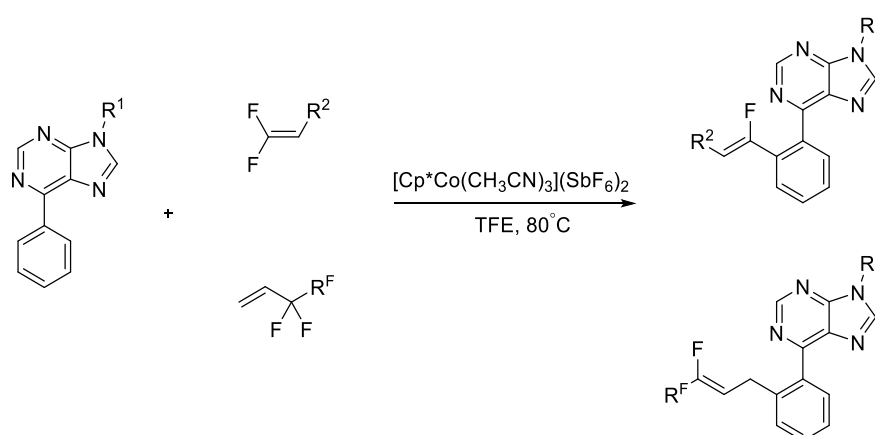
Later, Ackermann and co-workers developed the first efficient C-F/C-H activation at room temperature. A cobalt(III) catalyst enabled fluoroallylations with perfluoroalkyl alkenes under mild reaction conditions with weak base K_2CO_3 . Fluoroalkenylations under mild reaction conditions were also accessible (Scheme 4.32).⁷⁹



Scheme 4.32 Mild Co(III)-catalysed allylative C-F/C-H functionalisation.

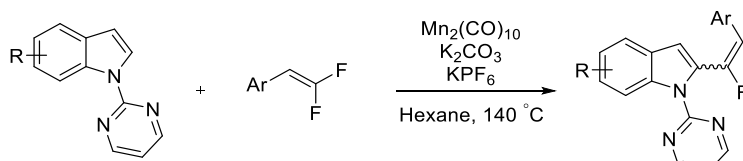
This kind of strategy was also used for the functionalisation of biologically active 6-arylpurines. Yoshino and Matsunaga performed a $Cp^*Co(III)$ -catalysed C-H bond functionalisation of 6-arylpurines using *gem*-difluoroalkenes affording monofluoroalkenes with high (*Z*)-selectivity and allyl fluorides affording C-H allylation in moderate (*Z*)-selectivity (Scheme 4.33).⁸⁰

4.1 Introduction



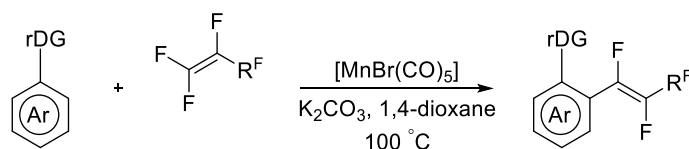
Scheme 4.33 Synthesis of fluorine-containing 6-arylpyridine derivatives *via* Cp*Co(III)-catalysed C–H bond activation.

The group of Feng and Loh expanded the field finding out that manganese could work as catalyst in the synthesis of monofluoroalkenes. Indeed, they developed a Mn-catalysed α -fluoroalkenylation of arenes *via* C–H activation and C–F cleavage leading to monofluoroalkenes with predominant unconventional E-isomer selectivity. Furthermore, manganese is the third most abundant transition metal, it has low toxicity and cost, making it a particularly attractive alternative to the typically used transition-metal catalysts.⁸¹



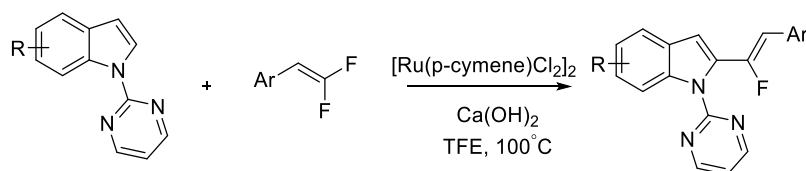
Scheme 4.34 Mn-catalysed synthesis of monofluoroalkenes *via* C–H activation and C–F cleavage.

The group of Ackermann added another example of manganese catalysis. They reported Mn-catalysed C–F/C–H functionalisations, in particular (per)fluoro allylations and alkenylations. Manganese catalysis regime requires rather mild reaction conditions and affords ample substrate scope, including ketimines as well as amino acids and peptides under racemisation-free conditions (Scheme 4.35).⁸²



Scheme 4.35 C–F/C–H functionalisation through Mn(I) Catalysis: (per)fluoro-allylations and alkenylations.

Finally, ruthenium resulted to be effective to catalyse the α -fluoroalkenylation of arenes. Li and co-workers reported a Ru(II)-catalysed α -fluoroalkenylation of *N*-pyrimidinylindoles *via* C–H bond activation and C–F bond cleavage under mild redox-neutral reaction conditions (Scheme 4.36).⁸³

Scheme 4.36 Ru(II)-catalysed α -fluoroalkenylation of arenes.

4.1.3 Electrocyclisation

It is known that thermal electrocyclic reaction of either 6π -electron or aza 6π -electron systems is a successful tool for the synthesis of nitrogen-containing condensed heteroaromatic compounds.⁸⁴

The thermal electrocyclic reaction of 6π -electron systems to form cyclohexadienes occurs as a disrotatory reversible process.⁸⁵ A 6π -electron system with a nitrogen atom is an aza 6π -electron system. The thermal electrocyclic reaction of an aza 6π -electron system to dihydropyridine occurs in a similar process. The thermal electrocyclic reaction of a 6π -electron or an aza 6π -electron system where one member of the double bond is a part of an aromatic or heteroaromatic ring should provide a variety of fused heteroaromatic compounds.

The electrocyclic transformation provides the formation of a single bond between the termini of a linear system containing n π -electrons ($n = 4, 6, 8, 10$). The 6π -electrocyclisation was used for the formulation of the ground-breaking orbital symmetry rules.⁸⁶ The predictability of the stereochemical outcome of these transformations contributed to the acceptability of the Woodward and Hoffmann rules by synthetic chemists.

The transformation is driven by the stabilisation gained by the conversion of the three hexatriene π -bonds into a cycle containing only two π -bonds and a new σ -bond formed at the expense of the remaining π -bond. The new σ -bond is formed between the head and the tail of the triene, through bonding interactions of the molecular orbitals of the hexatriene system, while observing the principle of orbital symmetry conservation.

The reaction looks simple and respects the principles of atom economy, but requires an appropriate geometry of the triene to occur.

If not, the first step is an $E \rightarrow Z$ isomerisation, where triene substituents may play a key role, affecting the outcome of the transformation.

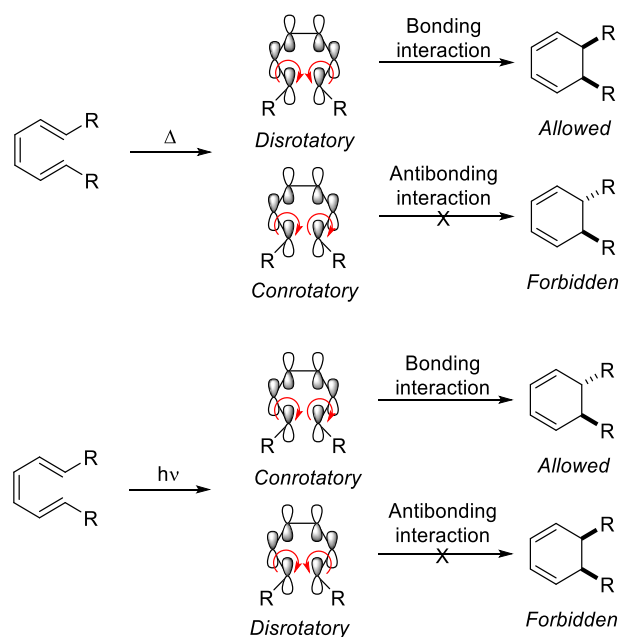


Figure 4.2 Molecular orbital interactions and products distribution for thermal and photochemical 1,3,5-hexatriene cyclisations.

A traditionally accepted picture of this reaction is shown in Figure 4.2, where the starting triene in its reactive *s-cis* conformation proceeds to cyclise. The ring closure occurs driven by heat (Δ) or light ($h\nu$), and only symmetry allowed products will be observed. According to the HOMO (thermal, ground state) and LUMO (photoinitiated, excited state) diagrams, conrotatory or disrotatory motion will produce the allowed interaction between the lobes of these molecular orbitals, creating the final 1,3-cyclohexadiene ring. HOMO–LUMO interactions are influenced and modulated by the nature of the substituents.⁸⁷ Stronger interactions speed up the reaction.

6π -electrocyclisations proceed stereospecifically as a result of the movements, affording *syn*- or *anti*-substitution products, depending on the geometry of the triene backbone and the reaction conditions (promotion by heat or light).⁸⁸ The Woodward and Hoffmann rules predict that the thermal 6π -electrocyclisation is *disrotatory*, while the photochemical process is *conrotatory*.

The high temperature required to initiate the electrocyclicalisation process is the main limitation for its application, because these conditions may also restrict the use of highly functionalised substrates in target-oriented synthesis.⁸⁹

However, these reactions are among the most reliable and powerful and atom-economic synthetic tools available for the rapid generation of complex molecules and many strategies to improve their conditions have been developed.

For instance, the choice of proper substitution of the 6π system or the introduction of a heteroatom can lower the energy barrier towards cyclisation. The presence of oxygen in the starting triene results in an oxatriene which can undergo 6π oxaelectrocyclisation under milder conditions, occurring almost spontaneously at (or even below) room temperature and thus taking place also in nature.⁹⁰

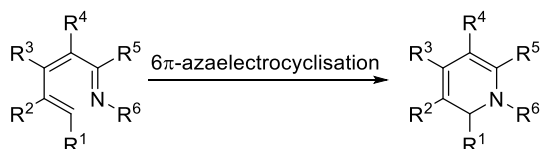
Azatrienes undergo 6π -azaelectrocyclisation, affording dihydropyridines, which can be converted into more stable pyridine through elimination, dehydrogenation or oxidation.

Functionalised six membered nitrogen rings are sought after substrates since they are present in a wide variety of biologically active natural products, pharmaceuticals and agrochemicals.

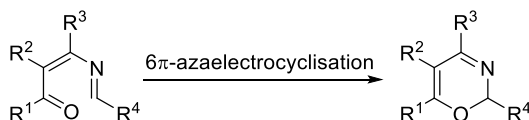
6π -electrocyclisation reactions can be carried out with different starting trienes (Scheme 4.37) to afford 2H-pyridines, 2H-oxazines and 2H-pyridones.

An additional scenario is the use of certain conjugated 1-azadienes for the 6π -electrocyclisation mediated preparation of pyrroles through the intermediacy of 3,4-dihydro-2H-pyrroles.⁹¹

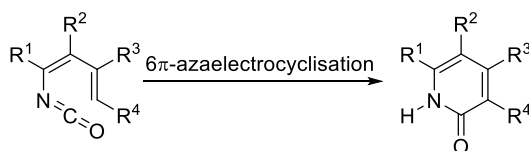
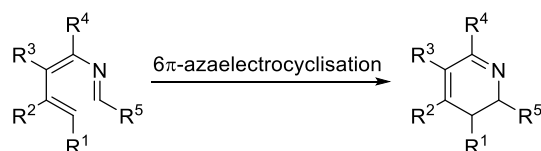
2H-Pyridines



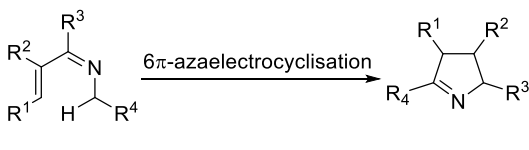
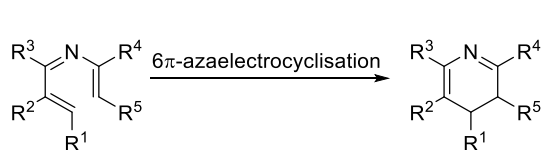
2H-Oxazines



2H-Pyridones



3,4-Dihydro-2H-Pyridones



Scheme 4.37 Different 6π -electrocyclisations and corresponding heterocyclic products.

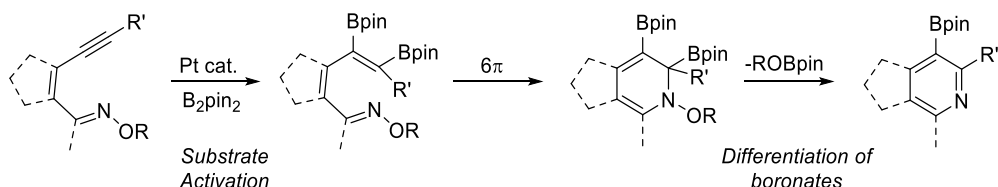
Already in 1972 Schiess, Chia and Ringle reported that oximes and their derivatives undergo thermal reactions leading to the formation of pyridine and isoquinoline derivatives.⁹² In detail, through thermal cyclisation of 1-azatriene, the *cis*-dienone oximes form pyridines at 160 °C in about 25% yield *via* azaelectrocyclisation followed by dehydration of the intermediary 1,2-dihydropyridine derivatives.

Metal-catalysis is a valid strategy for the synthesis of azatrienes, which then under proper conditions can cyclise providing the desired heterocyclic products.⁹³

The first improvements of these sequence reactions were performed in the synthesis of pyridines.

Harrity group focused on the development of new strategies including the reactivity of azatrienes. In particular, they were interested in constructing heterocycles bearing boron groups in order to increase the versatility of these substrates. In 2016, they developed an alkyne diboration/ 6π -electrocyclisation strategy for the synthesis of pyridine boronic acid derivatives. This strategy allows rapid access to bicyclic pyridines, but not to monocyclic heterocycles (Scheme 4.38).⁹⁴

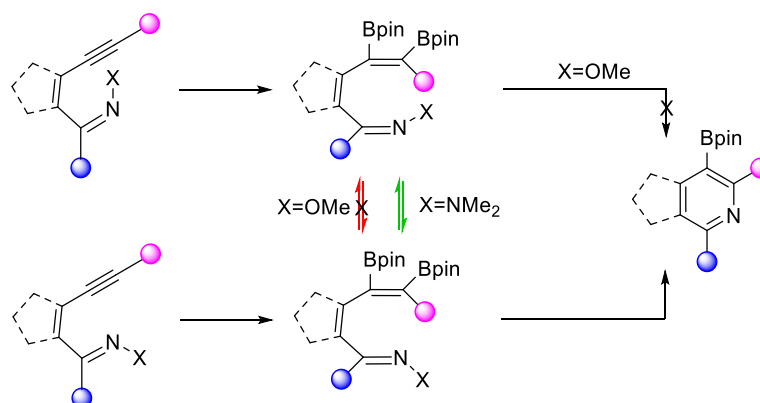
4.1 Introduction



Scheme 4.38 Diboration/ 6π -electrocyclisation strategy.

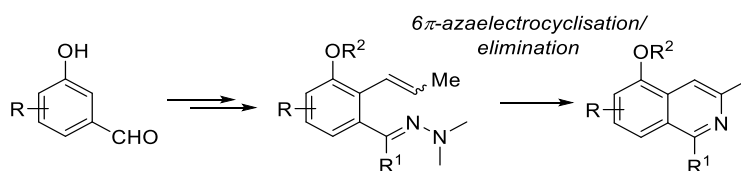
In addition, they observed that there is a direct relationship between oxime ether stereochemistry and reactivity towards electrocyclicisation. Specifically, E-oxime ethers were found to be significantly more reactive than their Z-counterparts (stereochemistry relative to azatriene scaffold). Computational studies proposed that this was due to a $N_{\text{ lone pair}} \rightarrow C=C \pi^*$ orbital interaction, which lowers the energy of the transition state in the electrocyclicisation of E-oxime ethers. However, unreactive Z-oxime ethers can be converted to the corresponding heterocyclic products by a photolytically promoted E \rightarrow Z isomerisation and electrocyclicisation sequence.⁹⁵

Hydrazones were found to be able to overcome the reluctance of Z-oxime ether azatrienes to undergo electrocyclicisation towards the synthesis of borylated (heteroaromatic) pyridines and ring-fused analogues. Hydrazones allowed access to previously inaccessible tri- and tetrasubstituted 3-borylpyridines in high yields (Scheme 4.39).⁹⁶



Scheme 4.39 Synthesis of borylated (heteroaromatic) pyridines and ring-fused analogues from hydrazones.

Hydrazones are also good substrates capable of affording isoquinolines, as reported by Kaufman and co-workers. They developed a synthesis of 3-methylisoquinolines from orthoformyl β -methylstyrenes, through their sequential hydrazone formation with 1,1-dimethylhydrazine in PhCF_3 , followed by a microwave-assisted or thermal cyclisation and final elimination with concomitant aromatisation. This is the first general example involving the 6π -electron cyclisation of 1-azatrienes derived from hydrazones, in which the starting polyene incorporates one double bond belonging to an homocyclic aromatic ring (Scheme 4.40).⁹⁷

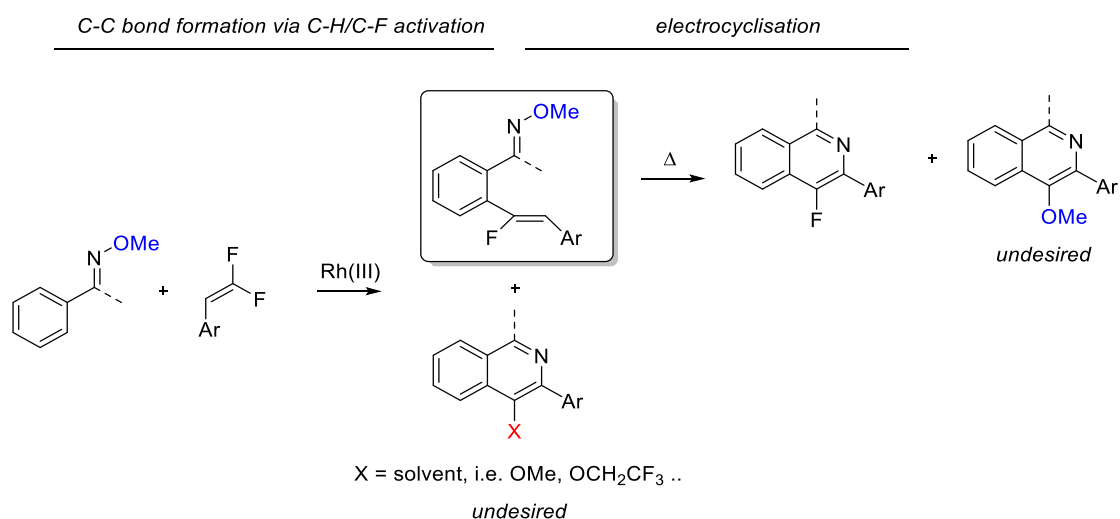


Scheme 4.40 Synthesis of isoquinolines from hydrazones.

Many examples of synthesis of isoquinolines from oximes involving an electrocyclisation step are reported in previous sections.

4.2 Abstract

Due to the importance of isoquinolines in a wide variety of fields and the added value provided by the incorporation of fluorine atom, this work aims to find a new strategy for the synthesis of fluorinated isoquinolines. It is known that oximes are valuable substrates for C-H activation providing azatrienes, Rh(III) is able to catalyse this process and azatrienes at high temperatures can electrocyclise affording heterocycles. Thus, the methodology under study involves a Rh(III)-catalysed C-H activation step of oxime derivative substrates with difluoroalkenes affording azatrienes. Azatrienes are then subjected to high temperatures to undergo electrocyclisation yielding the final isoquinolines. The C-H step works only with protic solvents, but using this kind of solvent causes the formation of an undesired product, the cyclic isoquinoline in which the fluorine is substituted by the deprotonated solvent (Scheme 4.41). Another issue came out in the electrocyclisation step, which did not work for all the substrates. Together with the fluorinated isoquinoline, an unwanted product was formed, whose mechanism is difficult to understand. The undesired product is the isoquinoline that bears the MeO (delivered during the electrocyclisation) at the place of the fluorine. Computational studies were carried out to provide a rationale for the formation of the side product. Once electrocyclisation occurs, different pathways were hypothesised and computed. The fluorinated isoquinoline is theoretically favoured in the presence of additives in the media, as methoxy ions, which help in the H-abstraction step. The methoxy group detaches from the substrates and gets protonated. Free MeOH and protonated bases in the media could take part in the formation of the side-product, mediating the process.



Scheme 4.41 General strategy of our work for the synthesis of fluorinated isoquinolines.

4.3 Objectives

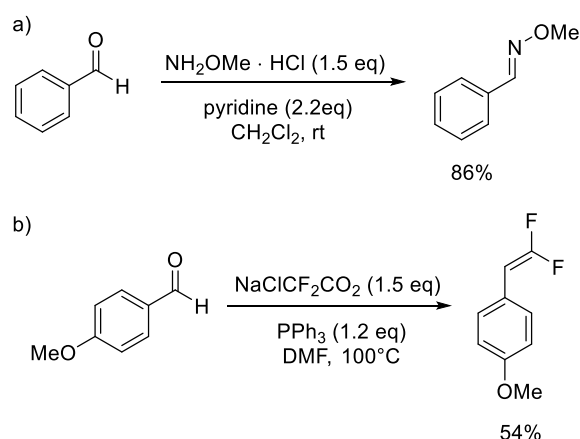
This work is divided in two parts: one experimental and one computational. The experimental work was made during my secondment at the laboratory of Prof. J. Harrity in collaboration with Dr. Matthew Ball-Jones. It aimed to develop a strategy for the synthesis of fluorinated isoquinolines through C-C bond formation *via* C-H/C-F activation and formation of the cycle *via* electrocyclisation. The work includes the optimisation of the C-H activation reaction conditions, the identification of undesired side products, the development of a small scope and finally the submission to electrocyclisation conditions to get fluorinated isoquinolines. A computational analysis was carried out to provide a rationale of the electrocyclisation reaction. In a previous work about electrocyclisation, our group identified a lone-pair(N) to $\pi^*(C=C)$ interaction in related reaction systems.⁹⁵ Thus, theoretically, lowering the energy of the $\pi^*(C=C)$ with an electron withdrawing group should promote the cyclisation. Since the experimental results did not fit with this trend, we computed the electrocyclisation mechanism of fluorine substituted azatrienes. The aim was to identify the rate determining step and to observe the influence of the substitution. The reaction of the fluorinated azatriene was complicated by the formation of 3-methoxyisoquinoline. Different routes were envisioned and computed in order to get an insight into the origin of this side product.

4.4 Experimental work

4.4.1 C-H activation

In the previous sections, it was shown that rhodium(III) catalysts are successful tools to promote the introduction of olefins segments through CH activation and that *gem*-difluoroalkenes represent a class of appealing synthetic intermediates with C-C double bond being highly polarisable.

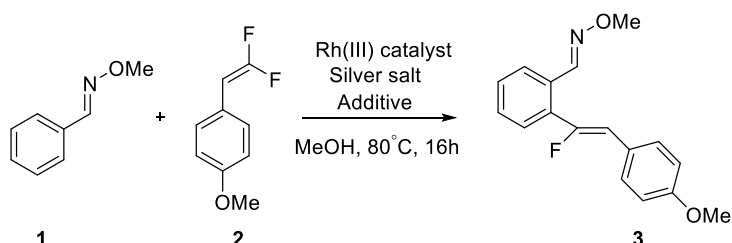
After the synthesis of the starting materials (Scheme 4.42), the work proceeded with the optimisation of the conditions of the Rh-catalysed C-H activation reaction of oxime **1** and difluoroalkene **2** to provide azatriene **3**. Different catalytic systems were tested, screening Rh-catalysts, silver salts, additives, solvents and temperatures. The results are collected in Table 4.1.



Scheme 4.42 Synthesis of the starting materials for the optimisation screening.

Initially, we thought to apply the conditions of the successful strategy of Tian, Feng and Loh⁷² to the reaction of oxime **1** and difluoroalkene **2** (entry 1), but unfortunately it turned out that the conversion to azatriene **3** was very poor (9%). Then, we decided to

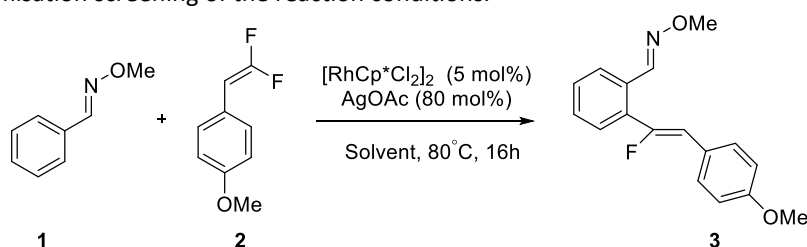
employ the dimer catalyst $[\text{RhCp}^*\text{Cl}_2]_2$ together with AgOAc , which is supposed to ensure the anion exchange with the rhodium catalyst (entry 2). This catalytic system resulted to work better, even if still provided low conversion. The use of AgSbF_6 as silver salt (entry 3) and the addition of $\text{Cu}(\text{OAc})_2$ (entry 4) did not improve the efficiency of the reaction.

Table 4.1 Optimisation screening of the reaction conditions.^a

Entry	Rh(III) catalyst (%)	Silver Salt	Additive	Conversion ^b
1	$[\text{Cp}^*\text{Rh}(\text{CN})_3](\text{SbF}_6)$ (4 mol%)	-	-	9
2	$[\text{RhCp}^*\text{Cl}_2]_2$ (5 mol%)	AgOAc (80 mol%)	-	18
3	$[\text{RhCp}^*\text{Cl}_2]_2$ (5 mol%)	AgSbF_6 (20 mol%)	-	9
4	$[\text{RhCp}^*\text{Cl}_2]_2$ (5 mol%)	AgSbF_6 (1eq)	$\text{Cu}(\text{OAc})_2$ (2.1 eq)	17

^aReactions were carried out on 0.2 mmol scale under inert atmosphere in sealed tubes at 80 °C, using 1.5 eq. of **2** in MeOH (0.12M) and left standing whilst stirring 16 h. After removal of the solvent, the crude was purified by silica-gel chromatography to give the pure compound. ^bConversion calculated by ¹H-NMR.

The conditions of entry 2 were chosen to carry out further optimisation screening of the solvents. One evidence that emerges from Table 4.2 is that the reaction works only with protic solvents. Indeed, DMF and THF inhibited the reaction. Trifluoroethanol and hexafluoroisopropanol demonstrated to be the best candidates. In particular, the reaction in TFE reached 70% conversion and azatriene **3** could be isolated in 35% yield.

Table 4.2 Optimisation screening of the reaction conditions.^a

Entry	Solvent	Conversion ^b
1	MeOH (dry)	18
2	MeOH (not dry)	12
3	HFIP	35 (45) ^c
4	TFE	70 (55) ^c
5	DMF	-
6	THF	1

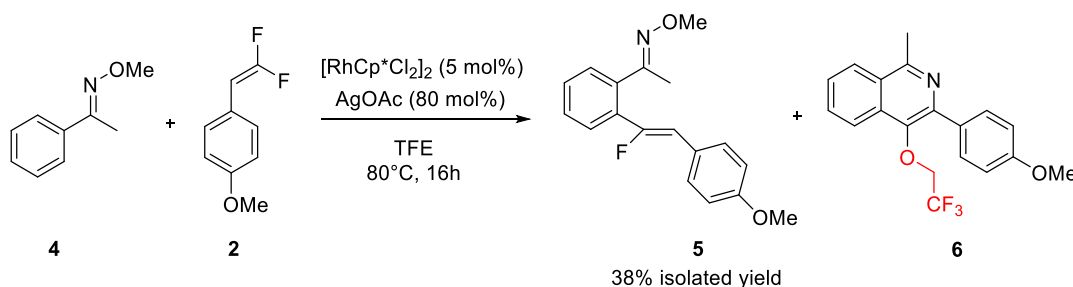
^aReactions were carried out on 0.2 mmol scale under inert atmosphere in sealed tubes at 80 °C, using 1.5 eq. of **2** in solvent (0.12M) and left standing whilst stirring 16 h. After removal of the solvent, the crude was purified by silica-

4.4 Experimental work

gel chromatography to give the pure compound. ^bConversion calculated by ¹H-NMR. ^cIn brackets the conversion when the reactions were carried out on 0.5 mmol scale.

Taking TFE as best solvent, we screened also other silver salts (AgOAc, AgSF₆, AgOTf, Ag₂CO₃, AgCO₂CF₃, AgBF₄), but no one behaved better than AgOAc, which was set as the best silver salt for this strategy. Neither the addition of additives to the reaction mixture helped in increasing the yield of the reaction. Pivalic acid, cesium acetate and sodium acetate did not affect the reaction.

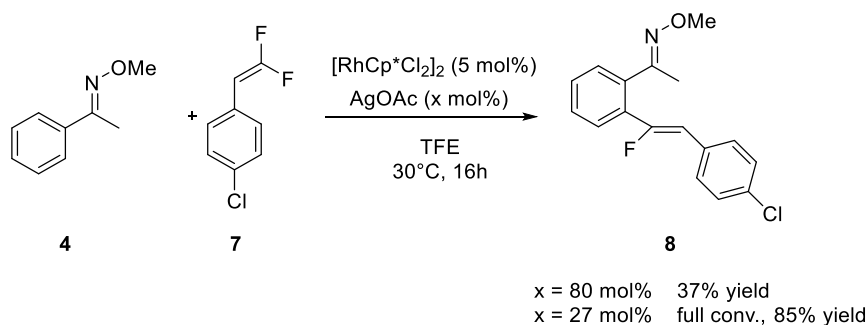
At this point, we decided to change the oxime substrate and use the analogue **4**, which bears a methyl group at the C_{sp2} carbon instead of the proton in **1**. The result was similar in yield (38%), but the final reaction mixture was cleaner and it could be possible to identify only some residues of starting materials, the product and a side product. Meanwhile, in the reaction with substrate **1**, the ¹H-NMR of the final reaction revealed the presence of a complex mixture of compounds.



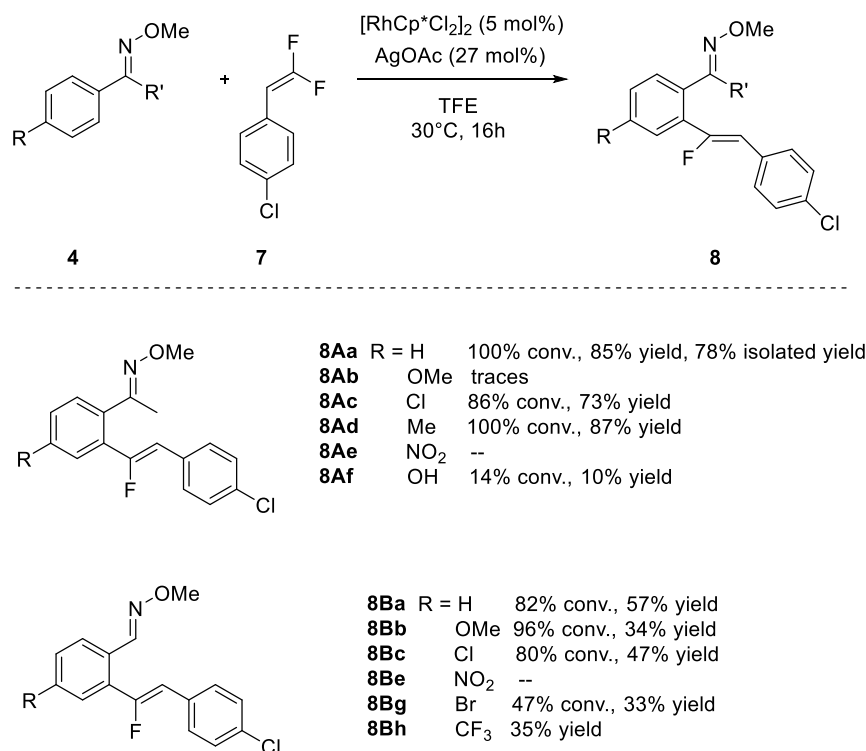
Scheme 4.43 Rh-catalysed reaction of oxime **4** with difluoroalkene **2**.

The main side product was identified as compound **6**, which is the result of the cyclisation and substitution of the fluorine by a molecule of trifluoroethanol. When the reaction was performed at lower temperatures, azatriene **5** was formed in similar yield and a reduction of undesired product **6** was observed.

However, the reaction conditions were not satisfactory yet and since *p*-chloro substituted difluoroalkene was easier to synthesise and purify we decided to work with the reaction in Scheme 4.44, adjusting the silver salt load. Thus, the reduction of the AgOAc load to 27 mol% (that is the same ratio of using 15 mol% of Rh catalyst and 80 mol% of AgOAc) allowed to reach full conversion and the desired product was isolated in 85% yield. Disappointingly, when these conditions were applied to the reaction in Scheme 4.43, we did not observe any improvement, rendering 75 % of conversion and only 21% yield of **5**. The presence of an electron withdrawing substituent on the aryl group of the alkene resulted to increase the reactivity.

Scheme 4.44 Rh-catalysed reaction of oxime **4** with difluoroalkene **7**.

Taking in mind this evidence and with these conditions in hand, we decided to develop a small scope in order to explore the versatility of the strategy (Table 4.3). The results were quite unpredictable and not all the substrates underwent the reaction completely after 16 hours. We observed that substrates with $R' = \text{Me}$, provided the product in moderate yields, better than those with $R' = \text{H}$ (**8Aa** vs **8Ba** and **8Ac** vs **8Bc**). Weak electron donating and electron withdrawing groups were tolerated, while products bearing strong EWD groups were difficult to obtain (**8Ab** and **8Ae**). Even if the yields with $R' = \text{H}$ were lower, the reactions worked with a wider range of substituents with different electronic properties.

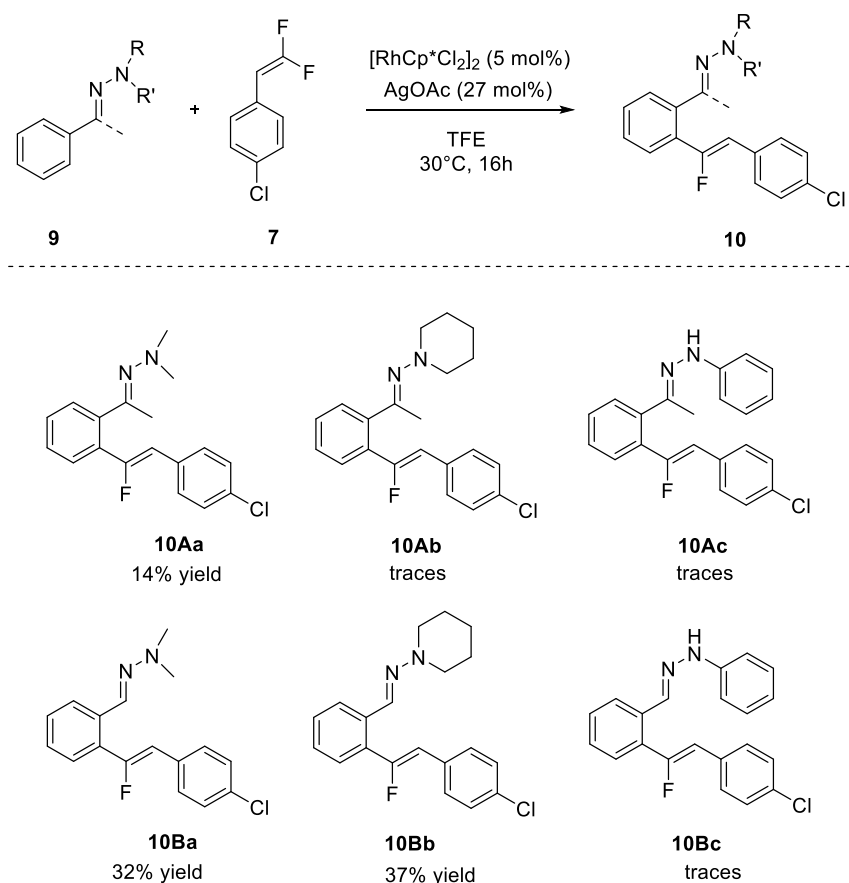
Table 4.3 Substrate scope with oximes.^a

^aReactions were carried out on 0.2 mmol scale under inert atmosphere in sealed tubes at 30 °C, using 1.5 eq. of **7** in TFE (0.12M) and left standing whilst stirring 16 h. After removal of the solvent, when feasible, the crude was purified by silica-gel chromatography to give the pure compound. ^bYields calculated using trimethoxybenzene as internal standard, except when differently reported.

4.4 Experimental work

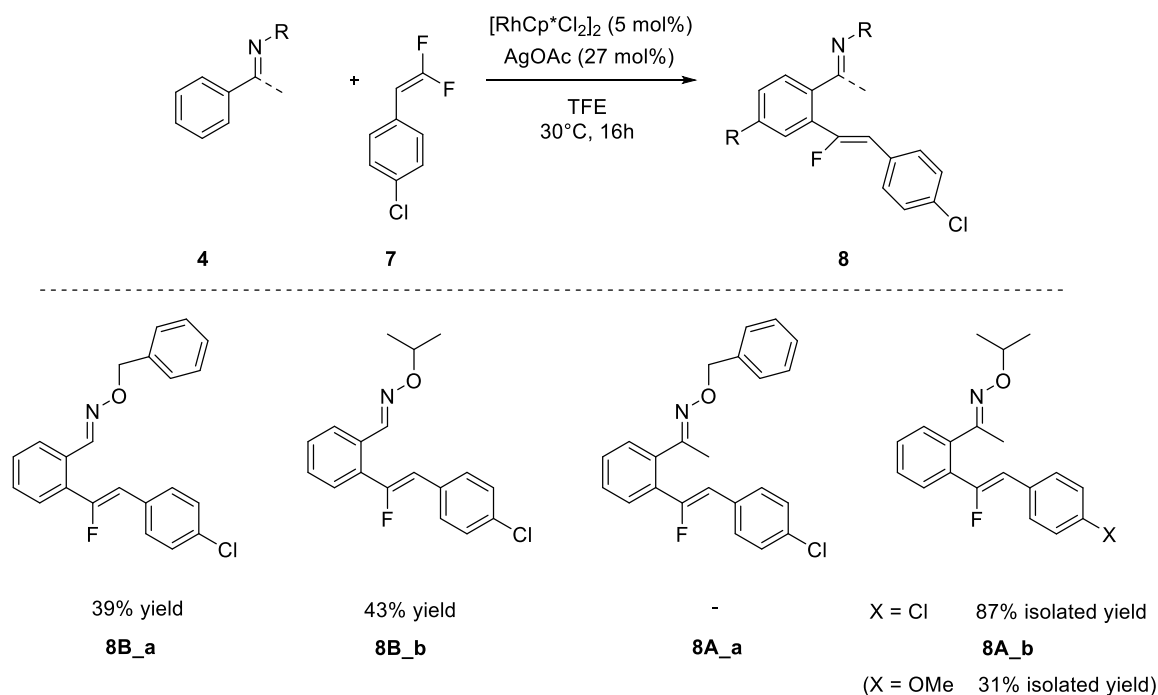
An alternative to oximes for the synthesis of fluorinated isoquinolines through electrocycloisatation is the use of hydrazones. Thus, we first checked whether hydrazones could undergo Rh(III)-catalysed C-H activation providing the corresponding azatrienes (Table 4.4). However, it was found that hydrazones had limited reactivity towards the formation of azatrienes under the chosen reaction conditions, and thus, were discarded from our investigation.

Table 4.4 Substrates scope with hydrazones.^a



^aReactions were carried out on 0.2 mmol scale under inert atmosphere in sealed tubes at 30 °C, using 1.5 eq. of **7** in TFE (0.12M) and left standing whilst stirring 16 h. After removal of the solvent, when feasible, the crude was purified by silica-gel chromatography to give the pure compound. ^bYields calculated using trimethoxybenzene as internal standard.

As we will see in the following section, electrocycloisatation reaction, when occurred, led to the formation of fluorinated isoquinoline together with a side product, in which the methoxy group attached to the N-atom is displaced during the process and substitutes the fluorine. In order to avoid this undesired outcome, we decided to synthesise azatrienes bearing a different substitution at the N position avoiding the migration of the methoxy. For this purpose, other oximes were synthesised and subjected to Rh(III) catalysis (Table 4.5). The oximes were functionalised at the N position with benzyl and isopropyl groups. The substrates bearing the isopropyl group worked properly providing **8B_b** and **8A_b**. **8A_b** could be obtained in moderate yield, up to 87%. On the other hand, substrates bearing the benzyl group only afforded **8B_a** in poor yield and not **8A_a**.

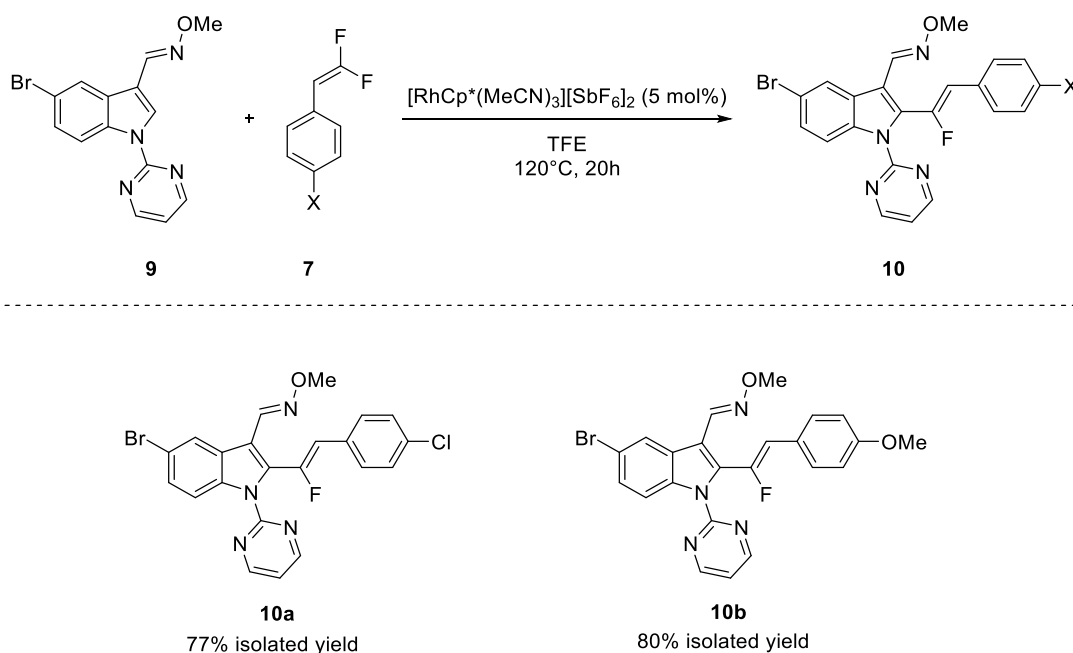
Table 4.5 Substrate scope of *N*-substituted oximes.^a

^aReactions were carried out on 0.2 mmol scale under inert atmosphere in sealed tubes at 30 °C, using 1.5 eq. of **7** in TFE (0.12M) and left standing whilst stirring 16 h. After removal of the solvent, when feasible, the crude was purified by silica-gel chromatography to give the pure compound. ^bYields calculated using trimethoxybenzene as internal standard, except when stated otherwise.

Despite several attempts, this strategy still performed poorly and was limited to a narrow range of substrates, preventing its potential general applicability. The last substrate modification was made taking inspiration from the work of Tian, Feng and Loh,⁷² who used indole derivatives as good substrates in the Rh(III)-catalysed tandem C-H/C-F activation for the synthesis of (hetero)arylated monofluoroalkenes. The idea was to construct a substrate bearing two directing groups to facilitate the C-H activation reaction. In particular, we envisioned a substrate based on the indole scaffold bearing the oxime and the pyrimidine moieties, both of them acting as directing groups. Substrate **9** was synthesised through a three step sequence and subjected to the same catalyst of the strategy of Tian, Feng and Loh⁷², $[\text{RhCp}^*(\text{MeCN})_3][\text{SbF}_6]_2$. The result was positive and compounds **10a** and **10b** were obtained in good yields. The effect of two directing groups helped to the purpose.

4.4 Experimental work

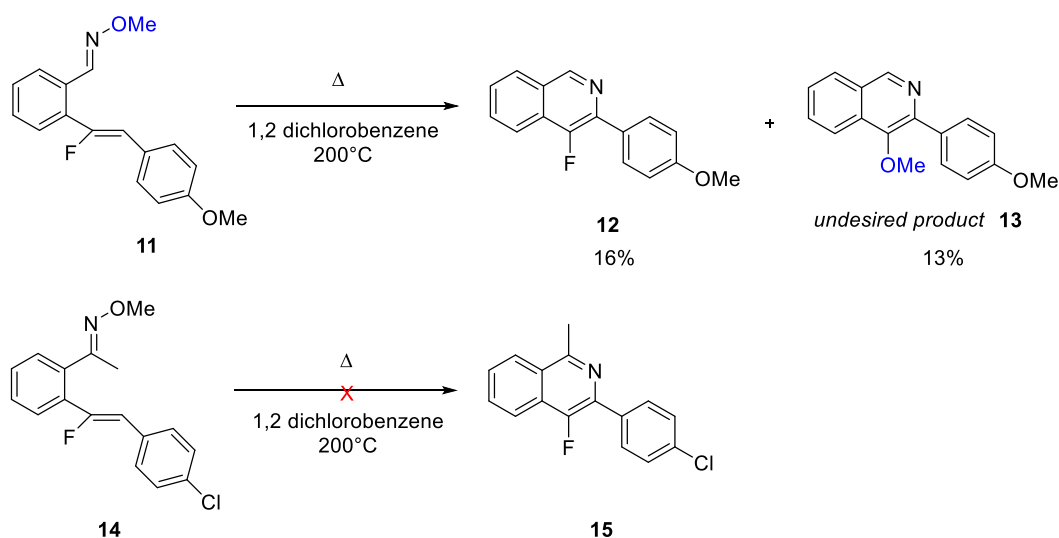
Table 4.6 Substrate scope with indole derivatives bearing an oxime moiety.^a



^aReactions were carried out on 0.4 mmol scale under inert atmosphere in sealed tubes at 120 °C, using 1.5 eq. of **7** in TFE (0.12M) and left standing whilst stirring 20 h. After removal of the solvent, the crude was purified by silica-gel chromatography to give the pure compound.

4.4.2 Electrocyclisation

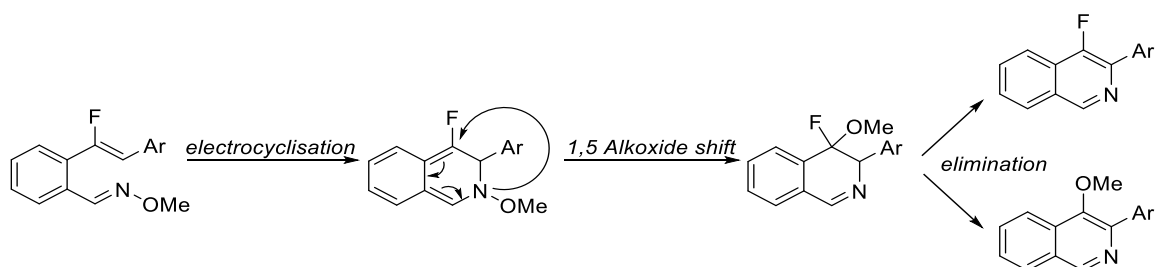
Once azatrienes were formed, their electrocyclisation reactions were attempted at high temperature (200 °C) in dichlorobenzene. Despite the several examples of azatrienes undergoing electrocyclisation, we observed that in our case the reaction did not proceed smoothly as expected. Indeed, as represented in Scheme 4.45, we succeeded to run the reaction to full conversion with compound **11**. Unfortunately, the results were very poor and we obtained only 16% of desired product together with 13% of compound **13**, in which the fluorine is substituted by the MeO⁻ delivered during the cyclisation. Substrate **14** did not show any reactivity towards electrocyclisation and the starting material could be recovered.



Scheme 4.45 Electrocyclisation reactions of azatrienes obtained through Rh(III)-catalysed C-H activation.

Regarding the mechanism of formation of the side product **13**, the main hypothesis was a S_NAr mechanism. To prove it, some experiments were carried out, in which large excesses of good S_NAr substrates were added to the reaction mixture. In particular, monofluoropyridine and pentafluoropyridine were employed. In both cases, these substrates had no effect on avoiding the formation of compound **13** and the ratio between **12** and **13** remained unchanged. Moreover, an attempt to trap the free methanol was done by adding molecular sieves to the reaction medium, but it did not change the outcome. In addition, compound **12** was subjected to high temperatures (200°C) in presence of free methanol and no reaction occurred, recovering the starting material.

These evidences let us discard the S_NAr mechanism. A second hypothesis concerned the occurrence of a 1,5-alkoxy shift, which would have re-established the aromaticity of the heterocycle (Scheme 4.46). As we did not find any experimental evidence for this mechanism, it was investigated computationally and explained in the following section.



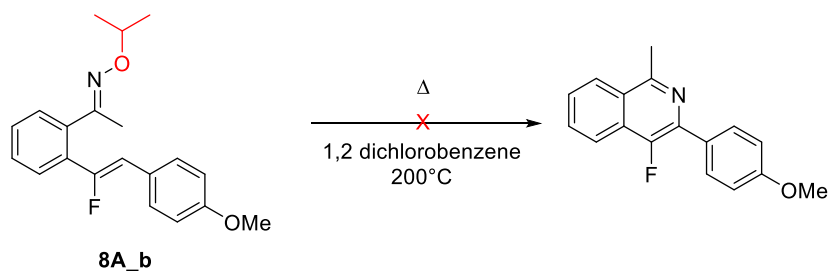
Scheme 4.46 1,5 Alkoxy-shift mechanism.

To avoid the formation of the side product, the idea of synthesising azatrienes starting from hydrazones was taken in consideration. Unfortunately, the first Rh(III) catalysed step provided scarce results, leading us to abandon the hydrazones as substrates for this sequence strategy.

In another attempt, substrates **8** were synthesised as candidates to undergo electrocyclisation preventing the formation of **13**-like side product. Indeed, the presence of larger groups as benzyl or isopropyl, instead of the methoxy, aimed to avoid the shift of the *N*-group. Compound **8A_b** (with X = OMe) was used to perform the reaction. The compound bearing the MeO group and not the chloride in the aryl group was chosen because compounds with the chloride resulted to be also less reactive towards electrocyclisation (i.e. compound **14** in Scheme 4.45).

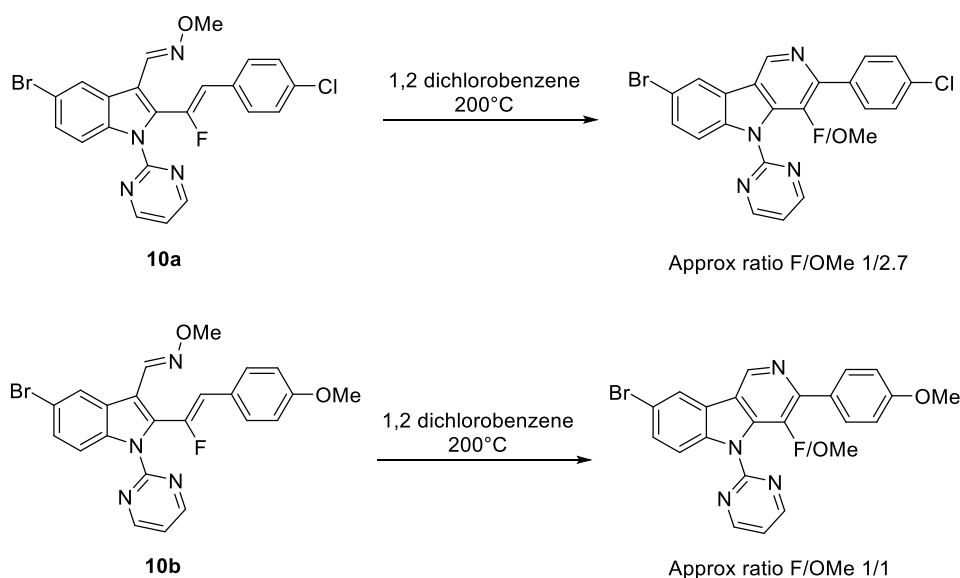
As Scheme 4.47 shows, substrate **8A_b** resulted to be unreactive towards cyclisation. This result could be attributed to the steric hindrance of the isopropyl group or to the presence of the methyl in the oxime moiety, as *R'* group. Indeed, as shown in Scheme 4.45, compound **14** is not reactive. Unfortunately, this result points to a limitation of this strategy, since the substrates that are easier to obtain and purified from the CH activation step are those that work worse in the electrocyclisation. This is the reason why we could not test the **8A_b** analogue with *R'* = H.

4.5 Computational work



Scheme 4.47 Electrocyclisation of compound **8A_b**.

Finally, **10**-type substrates were tested in the electrocyclisation step and they revealed to be susceptible to this reaction, although providing significant amount of undesired side product. Indeed, compound **10a** cyclises to afford the products with a ratio F/OMe 1/2.7, while in the case of **10b** the ratio obtained was 1/1. The mixture of these two products did not permit to isolate properly the fluorinated isoquinolines.



Scheme 4.48 Electrocyclisation for substrates **10a** and **10b**.

4.5 Computational work

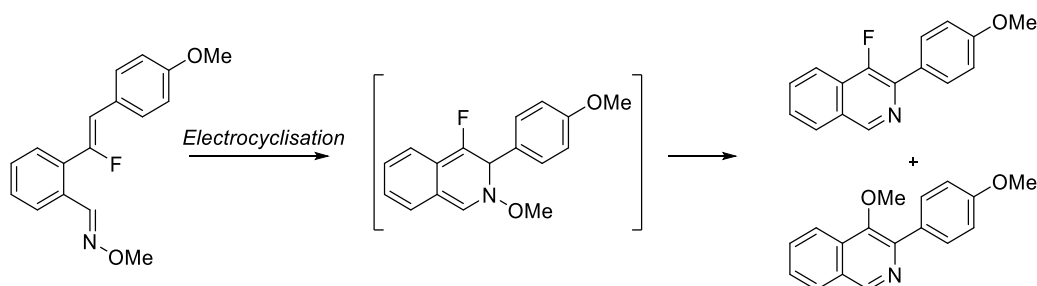
4.5.1 Methods

All structures were initially optimised using density functional theory (DFT) with B3LYP and the 6-311+G(d,p) basis set as implemented in Gaussian 16. Final energies were calculated at M06-2X/6-311+G(d,p) level of theory, in a solvent model (IEFPCM, solvent= *o*-DiChloroBenzene). The stationary points were characterised by frequency calculations in order to verify that they have the right number of imaginary frequencies. For further information, please see Chapter 1.

4.5.2 Electrocyclisation studies

Our computational analysis focused on the second step of the sequence presented above: the electrocyclisation step and following elimination to afford the fluoroisoquinoline of interest. The need of a computational study raised from the evidence of the formation of 3-methoxyisoquinoline, as a side product, together with

the desired fluorinated isoquinoline (Scheme 4.49). The experiments performed to justify the side product formation did not provide a valid rationale, but were useful to exclude that an aromatic nucleophilic substitution (S_NAr) takes place. Indeed, the addition of a better S_NAr substrate as fluoropyridine had no effect on the reaction outcome. Furthermore, adding molecular sieves to trap the freed methanol was ineffective. The most reasonable hypothesis is that after electrocycloisisation, a 1,5-alkoxyshift operates and then, the elimination of either HF or MeOH leads to the two products (Scheme 4.49).



Scheme 4.49 Products formed after subjecting azatrienes to electrocycloisisation conditions.

Our work started with a small computational study of the starting material of the electrocycloisisation reaction, the fluorinated azatriene substrate, derived from the C-H activation step. The structures of the four possible conformers were computed and optimised. Structure **11_III** resulted to be the most stable conformation and was taken as reference point for the calculation of the energies of all the intermediates and transition states. It is worth to notice that conformers **11_III** and **11_IV** are almost isoenergetic and their stability can be associated with the less steric hindrance due to the position of the oxime moiety. The higher energy of conformer **11_II**, which features the most significant steric hindrance, confirms it. Only E-conformers were considered because previous calculations by our group demonstrated that Z-oximes are unreactive to electrocycloisisation.⁹⁵

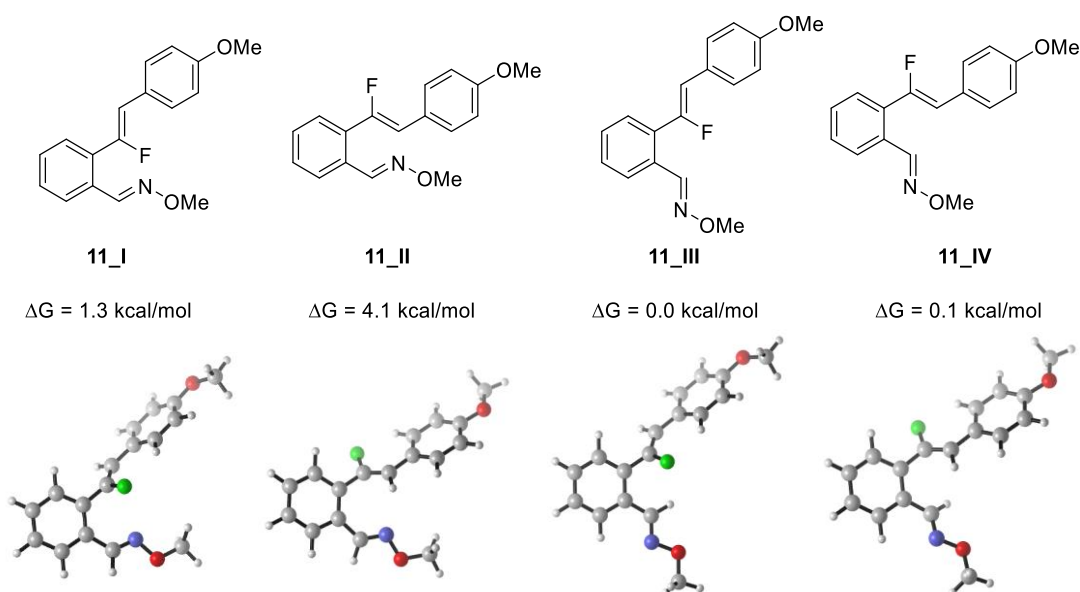


Figure 4.3 Conformers of azatriene **11** and relative energies. Energies (ΔG) referred to the lowest energy conformation, $\Delta G=0.0$ kcal/mol.

Once the most stable conformation of the azatriene was determined, we proceeded to

study the mechanism of the sequence of electrocyclisation, 1,5-shift and elimination. In the evaluation of the energy barriers, it is important to take into consideration that the reaction is performed at 200 °C, allowing to overcome higher barriers than those we were used to see in the previous chapters.

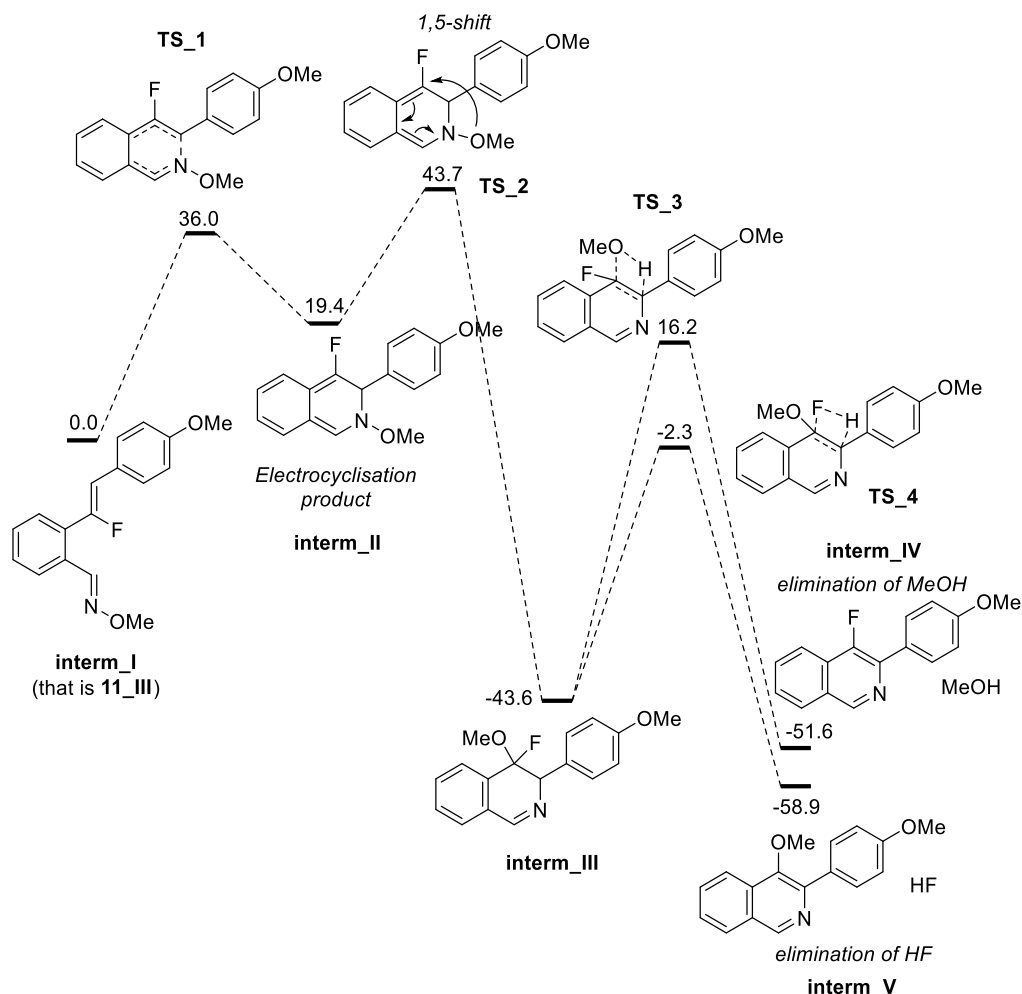
Initially, we were mainly interested in understanding the mechanism of formation of the undesired product, considering the formation of the fluorinated isoquinoline an easy and spontaneous process, constituted by the electrocyclisation and following elimination of the proton and methoxy, as methanol. Anyway, some calculations related to it are also presented later in the section.

In Scheme 4.50 the energetic pathways that lead to 3-fluoroisoquinoline and 3-methoxyisoquinoline are represented. The energy of the fluorinated azatriene (**11_III** in Figure 4.3 \equiv **interm_I** in Scheme 4.50) is taken as reference with $\Delta G = 0$ kcal/mol.

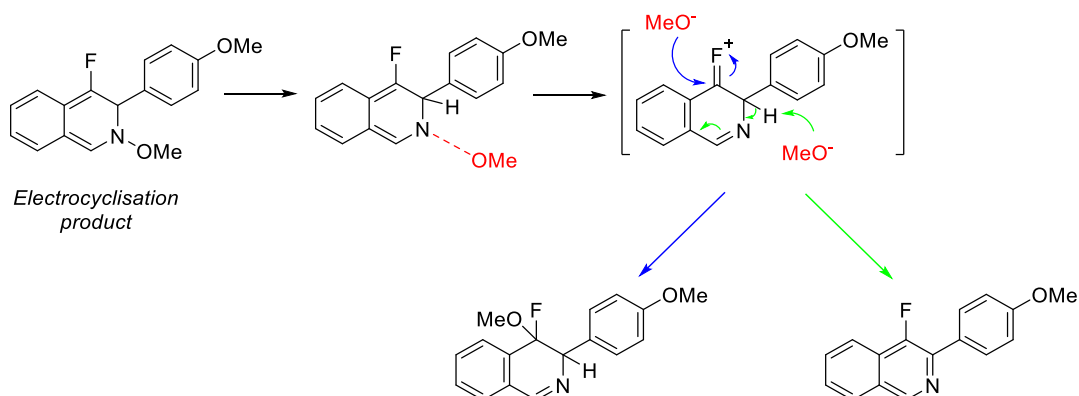
At the reaction conditions, the azatriene substrate undergoes easily electrocyclisation in a disrotatory fashion after overcoming a feasible energetic barrier ($\Delta G^\ddagger = 36.0$ kcal/mol). The intermediate (**interm_II**) that is formed (named *electrocyclisation intermediate or product* throughout this chapter) was located at relatively high energy ($\Delta G = 19.4$ kcal/mol) but the energy required for the 1,5-methoxyshift resulted to be too high to make this process feasible at the reaction conditions ($\Delta G^\ddagger = 43.7$ kcal/mol). Although the formation of **interm_III** through a 1,5-shift looks improbable, its geometry was optimised and the intermediate was located at low energy ($\Delta G = -43.6$ kcal/mol). The low energy of this intermediate is meaningful because it indicates the stability of this intermediate, due to the formation of a fully aromatic benzene ring, that can exist but probably forms through an alternative pathway. At this point, either MeOH or HF are available to be eliminated. Thus, the two elimination processes were computed, but in both cases, the energies required were too high (> 40 kcal/mol). It is of key importance to observe that the difference in energy for the two pathways is very significant. Indeed, HF is much easier to eliminate, it requires 18.5 kcal/mol less than the elimination of MeOH. This result supports the formation of the methoxy-substituted isoquinoline over the formation of the fluorinated one through this pathway.

After this initial study, it was clear that the electrocyclisation occurred easily but the following steps required a different approach and we started hypothesising possible pathways starting from the electrocyclisation product (**interm_II** in Scheme 4.50).

Since **interm_II** stands at relatively high energy ($\Delta G = 19.4$ kcal/mol), we thought that it could somehow lose spontaneously the methoxy group (Scheme 4.51). Thus, the freed methoxy (in red) could either abstract the proton at the C_{sp^3} (green arrow) or attack the carbon bound to the fluorine leading in this way to **interm_III** (blue arrow). We computed the two alternative pathways but unfortunately, the transition state for the spontaneous displacement of the methoxy group could not be located, showing the limit of our hypothesis.



Scheme 4.50 Energetic pathways that lead to 3-fluoroisoquinoline and 3-methoxyisoquinoline. The energy of the fluorinated azatriene (**interm_I**) is taken as reference with $\Delta G = 0$ kcal/mol. All the energies are Gibbs energies in kcal/mol.



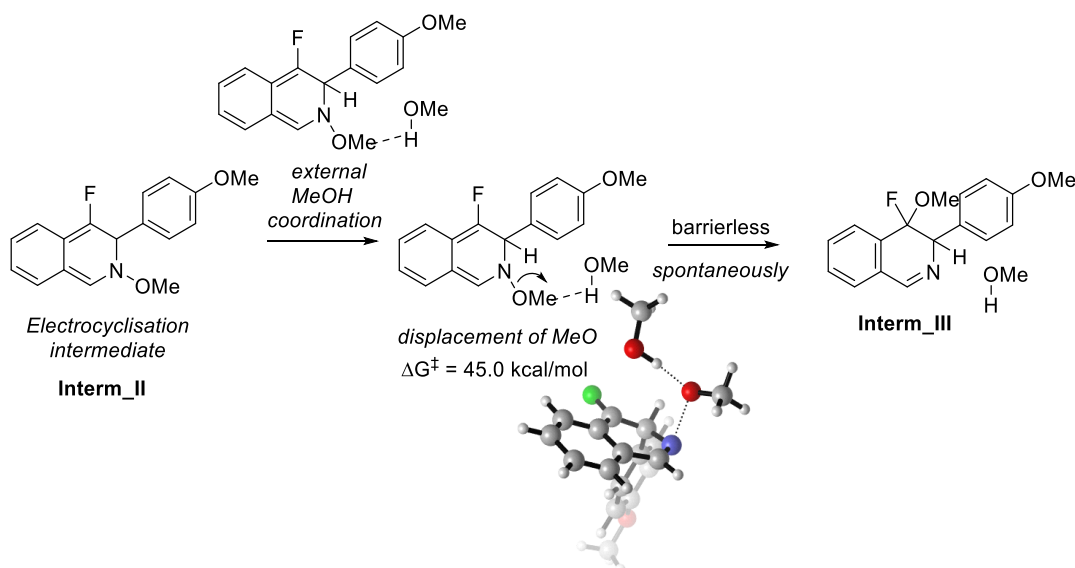
Scheme 4.51 Mechanism for the spontaneous displacement of the methoxy group and following possible routes.

During our experiments, we observed that the final fluorinated isoquinoline remains unreactive if subjected to high temperature in presence of methanol, meaning that the side product (**interm V**) originates from a precedent step. Thus, it is reasonable to assume that **interm_III** is formed and we tried to investigate how.

In the reaction media, reagent, forming intermediates and freed molecules are present during the reaction. We assumed that all these molecules could interact with the

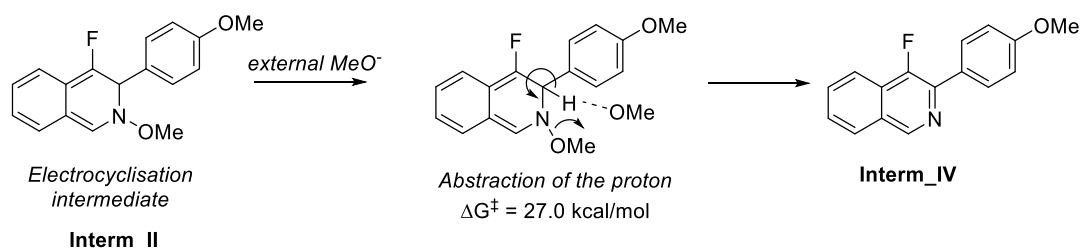
electrocyclisation intermediate and help in mediating the shift of the methoxy group from the nitrogen atom to the carbon bound to fluorine.

The first hypothesis was the mediation by an external MeOH molecule. We computed the mechanism (Scheme 4.52) and we observed that the external methanol could help the abstraction of the methoxy group, which spontaneously moved to bind the C adjacent to fluorine during the calculation. Unfortunately, the intervention of the extra molecule of methanol was not effective in decreasing the energy barrier required for the formation of the intermediate, which resulted to be 45.0 kcal/mol.



Scheme 4.52 Mechanism mediated by an external molecule of MeOH present in the reaction media. All the energies are Gibbs energies in kcal/mol using as reference **interm_I** (Scheme 4.50) with $\Delta G = 0$ kcal/mol.

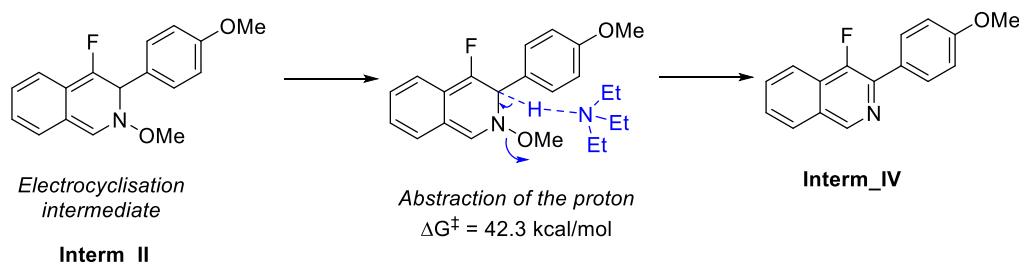
Then, as depicted in Scheme 4.53, we considered that a freed methoxy ion could act as external mediator molecule. We observed that it easily abstracts the proton ($\Delta G^\ddagger = 27.0$ kcal/mol) and facilitates the displacement of the methoxy from the nitrogen atom, leading to the formation of the desired fluorinated isoquinoline. In this case, the freed methoxy does not migrate to the fluorinated carbon, but interacts with the ion, which stabilises it.



Scheme 4.53 Mechanism mediated by an external methoxy ion present in the reaction media. All the energies are Gibbs energies in kcal/mol using as reference **interm_I** (Scheme 4.50) with $\Delta G = 0$ kcal/mol.

The second approach was assuming that in the reaction media, the azatriene, the *electrocyclisation product* and the formed isoquinoline could work as weak bases to abstract the proton in the molecule of the electrocyclisation intermediate. The removal of the proton could induce the displacement of the methoxy group, which then could be stabilised as in the case of the external methoxy group or can migrate to form

intermediate III. To validate this hypothesis, we computed this mechanism using a molecule of triethylamine as a model base (Scheme 4.54).

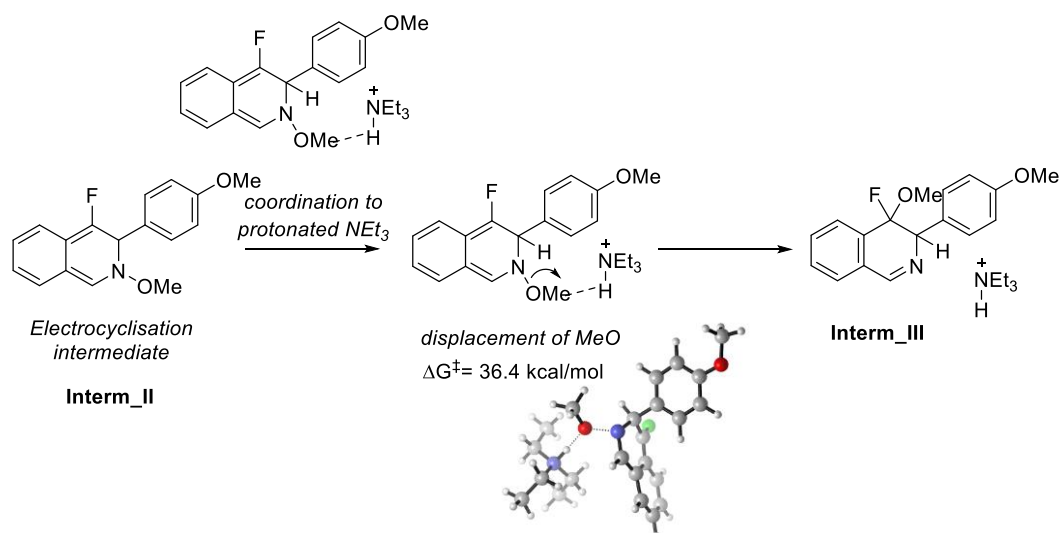


Scheme 4.54 Mechanism mediated by a molecule of Et_3N as model base present in the reaction media. All the energies are Gibbs energies in kcal/mol using as reference **interm_I** (Scheme 4.50) with $\Delta G = 0$ kcal/mol.

As in the previous case with the methoxy ion (Scheme 4.53), the triethylamine abstracts the proton and causes the displacement of the methoxy from the nitrogen atom. The energy cost in this case, differently from the use of an external methoxy ion, is high and not affordable at the reaction conditions ($\Delta G^\ddagger = 42.3$ kcal/mol). Anyway, the methoxy, after detachment from N atom, abstracts the proton from the protonated base leading to the formation of methanol. The methoxy shift was not observed.

Apparently, the migration of the methoxy group occurred when an external group interacts with it without first abstracting the proton. We assumed that in the media there could be a protonated base, described in our case by a model protonated triethylamine. We computed the mechanism of the migration of the methoxy group mediated by a molecule of protonated base (Scheme 4.55). The protonated base mediates the displacement of the methoxy group from the nitrogen atom in the **intermediate II** contributing in decreasing the energy cost of the process. The energy barrier is feasible at the reaction conditions (36.4 kcal/mol). The freed methoxy spontaneously migrates during convergence to the carbon adjacent to the fluorine, forming the stable **intermediate III**. At this point, two alternatives are possible: the displacement of MeOH forming the fluorinated isoquinoline or the displacement of HF affording the undesired side product. The two processes were computed adding the mediator action of the model protonated base. It was found that the steric hindrance of the protonated triethylamine did not allow the molecule to interact with both the H atom and the OMe or the F to help their removal. Indeed, the calculations did not converge. The re-establishment of the aromaticity, which might be a spontaneous mechanism, hides in this case several issues, probably due to the high stability of **intermediate III**. Nevertheless, it is worth to notice from Scheme 4.50 that the removal of HF from **intermediate III** is much more favoured than the removal of MeOH. This qualitative analysis justifies the formation of the side product, which is probably mediated by additives in the media.

4.6 Conclusion



Scheme 4.55 Mechanism mediated by a molecule of protonated Et_3N as model protonated base present in the reaction media. All the energies are Gibbs energies in kcal/mol using as reference **interm_I** (Scheme 4.50) with $\Delta G = 0$ kcal/mol.

4.6 Conclusion

Fluorinated isoquinolines are valuable compounds in the pharmaceutical field. Indeed, they are common scaffolds in several bioactive compounds. In this work, we aimed to synthesise fluorinated isoquinolines through a two-step synthesis involving Rh(III)-catalysed C-H activation of oxime derivatives with difluoroalkenes followed by electrocyclicalisation. This methodology resulted to be challenging because of the limitation on the choice of the substrates. In general, it was observed that substrates that smoothly undergo CH activation provide azatrienes that are not keen on electrocyclicalising. Oximes and hydrazones in presence of difluoroalkenes, $[RhCp^*(Cl)_2]$ as catalyst and $AgOAc$ as anion exchange agent in protic solvent, as TFE, afford azatrienes, although not always in good yields. The employment of protic solvents is necessary for the reaction, but implies the formation of a sideproduct, in which the fluorine atom is substituted by the solvent. The electrocyclicalisation step occurred only in few cases affording the corresponding fluorinated isoquinolines, together with an undesired product, in which the fluorine is substituted by the methoxy delivered after the cyclisation to restore the aromaticity in the heterocycle. The formation of this latter compound cannot be controlled and the mechanism appears to be difficult to explain. The addition of good methoxy traps in the reaction mixture was ineffective and the result allowed to exclude the nucleophilic aromatic substitution as mechanism of formation. The hypothesis of a 1,5-methoxy shift looked plausible but no experimental evidence could prove it.

It is worth to say that the mechanism for the formation of fluorinated isoquinolines looks obvious, mainly if we think that in the reaction media there are many compounds that can help in the abstraction of the proton inducing the displacement of the methoxy group to restore the aromaticity, and does not need further investigation.

On the other hand, the formation of the methoxy substituted isoquinoline remains unknown and deserves a different approach. A computational study was conducted on the second step of the methodology, from azatrienes to isoquinoline products, with a particular focus on the formation of the sideproduct. We observed that the electrocyclicalisation occurs easily overcoming a feasible energy barrier and affording a cyclic not aromatic product. The 1,5-methoxy shift was computed and resulted to be

unaccessible at the reaction conditions because the computed energy barrier was too high. Taking in consideration that in the reaction media there are many components that can mediate and help the shift, we computed the shift mechanism mediated by a free methanol molecule, a methoxy anion, a model base like Et_3N (representing a generic weak base in the media, such as isoquinoline or azatriene molecules) and the protonated base model. The presence of ions in the system to compute could affect the accuracy of the calculations and lead to results that are counterintuitive. The action of an external molecule of methanol did not help in decreasing the shift energy barrier. The methoxy ion and the base instead removed the proton leading to the formation of the fluorinated isoquinoline and could not justify the formation of the side product. Only computing the action of a protonated base as Et_3N provided an energy barrier feasible at the reaction conditions.

Due to the variety of species in the reaction media, it is difficult to understand and predict what really causes the shift. The methoxy is shifted to form an intermediate bearing a methoxy group and a fluorine atom bound at the same atom, located computationally at low energy, indicating high stability. The issue is determining how it is formed. All the calculations we performed concerning the participation of external species in the process converged, meaning that these mechanisms are plausible, thus we can draw the conclusion in a qualitative way, focusing on the trend of the energetic profiles. After the shift of the methoxy, the intermediate that is formed is stable and either the methoxy or the fluorine could leave together with the adjacent proton forming respectively either the fluorinated isoquinoline and methanol or the methoxy-substituted isoquinoline and hydrofluoric acid. The latter process resulted to be less energetic than the former. This evidence could justify the formation of the sideproduct: if the methoxy shift occurs in some way, then the detachment of the hydrofluoric acid is more favourable than the removal of methanol.

4.7 References

1. Kametani, T. *The chemistry of the isoquinoline alkaloids*; Hirokawa Publishing Company: Tokyo, 1968.
2. Kitamura, M.; Hsiao, Y.; Ohta, M.; Tsukamoto, M.; Ohta, T.; Takaya, H.; Noyori, R. *J. Org. Chem.* **1994**, *59*, 297–310.
3. Chrzanowska, M.; Rozwadowska, M. *Chem. Rev.* **2004**, *104*, 3341–3370.
4. Shamma, M. *The isoquinoline alkaloids: chemistry and pharmacology*; Academic: New York, 1972.
5. Nagatsu, T. *Neurosci. Res.* **1997**, *229*, 99–111.
6. Hoogewerf, S.; van Dorp, W. *Recl. des Trav. Chimiques des Pays-Bas* **1885**, *4*, 125–129.
7. Pomeranz, C. *Monatshefte fur Chemie* **1893**, *14*, 116–119.
8. Fritsch, P. *Berichte der Dtsch. Chem. Gesellschaft* **1893**, *26*, 419–422.
9. Bischler, A.; Napieralski, B. *Berichte der Dtsch. Chem. Gesellschaft* **1893**, *26*, 1903–1908.
10. Pictet, A.; Gams, A. *Dtsch. Berichte der Gesellschaft, Chem.* **1910**, *43*, 2384–2391.
11. Pictet, A.; Spengler, T. *Berichte der Dtsch. Chem. Gesellschaft* **1911**, *44*, 2030–2036.
12. Roy, S.; Roy, S.; Neuenswander, B.; Hill, D.; Larock, R. C. *J. Comb. Chem.* **2009**, *11*, 1061–1065.
13. Guimond, N.; Fagnou, K. *J. Am. Chem. Soc.* **2009**, *131*, 12050–12051.
14. Fukutani, T.; Umeda, N.; Hirano, K.; Satoh, T.; Miura, M. *Chem. Commun.* **2009**, 5141–5143.
15. Hwang, S.; Lee, Y.; Lee, P. H.; Shin, S. *Tetrahedron Lett.* **2009**, *50*, 2305–2308.
16. Niu, Y. N.; Yan, Z. Y.; Gao, G. L.; Wang, H. L.; Shu, X. Z.; Ji, K. G.; Liang, Y. M. *J. Org. Chem.* **2009**, *74*, 2893–2896.
17. a) O'Hagan, D. *Chem. Soc. Rev.* **2008**, *37*, 308–319; b) Purser, S.; Moore, P. R.; Swallow, S.; Gouverneur, V. *Chem. Soc. Rev.* **2008**, *37*, 320–330; c) Hagmann, W. K. *J. Med. Chem.* **2008**, *51*, 4359–4369; d) Lee, S.; Park, J.-S.; Lee, T.-R. *Bulletin of the Korean Chemical Society*, **2011**, *32*, 1, 41–48; Yun, J. H.; Park, S.; Heo, J. H.; Lee, H.-S.; Yoon, S.; Kang, J.; Im, S. H.; Kim, H.; Lee, W.; Kim, B.S.; Ko, M. J.; Chung, D. S.; Son, H. J. *Chem. Sci.* **2016**, *7*, 6649–6661; Fujita, T.; Ichikawa, J. *Fluorinated isoquinolines: synthesis, properties and applications in Fluorine in Heterocyclic Chemistry Volume 2: 6-Membered Heterocycles*, V. Nenajdenko, Ed., 181–210, Springer International Publishing: Switzerland, 2014.
18. Zhang, H.; Li, Y.; Jiang, Z.-X. *J. Biomol. Res. Ther.* **2012**, *1*:e107.
19. Yu, W.; Wang, E.; Voll, R. J.; Miller, H.; Goodman, M. M. *Bioorg. Med. Chem.* **2008**, *16*, 6145–6155.
20. Roe, A.; Teague, C. *J. Am. Chem. Soc.* **1951**, *73*, 687–688.

21. Balz, G.; Schiemann, G. *Berichte der Dtsch. Chem. Gesellschaft* **1927**, *5*, 1186–1190.
22. Belsten, J.; Dyke, S. *J. Chem. Soc.* **1964**, 22–26.
23. Bellas, M.; Suschitzky, H. *J. Chem. Soc.* **1964**, 4561–4564.
24. Bunnet, J. F.; Zahler, R. E. *Chem. Rev.* **1951**, *49*, 273–412.
25. Fuller, G. J. *J. Chem. Soc.* **1965**, 6264–6267.
26. Bayer, A. G. Nuclearly fluorinated *N*-heterocyclic compounds and a process for their production. GB Patent 845,062, 17 Aug 1960.
27. Chambers, R. D.; Hole, M.; Iddon, B.; Musgrave, W. K. R.; Storey, R. A. *J. Chem. Soc. C* **1966**, 2328–2331.
28. Nenajdenko, V. *Fluorine in heterocyclic chemistry: Volume 2: 6-Membered heterocycles*; Springer: 2014.
29. Si, C.; Myers, A. G. *Angew. Chem. Int. Ed.* **2011**, *50*, 10409–10413.
30. Finger, G. C.; Kruse, C. W. *J. Am. Chem. Soc.* **1956**, *78*, 6034–6037.
31. Sit, S.-Y.; Xie, K.; Jacutin-Porte, S.; Boy, K. M.; Seanz, J.; Taber, M. T.; Gulwadi, A. G.; Korpinen, C. D.; Burris, K. D.; Molski, T. F.; Ryan, E.; Xu, C.; Verdoorn, T.; Johnson, G.; Nichols, D. E.; Mailman, R. B. *Bioorganic Med. Chem.* **2004**, *12*, 715–734.
32. Chambers, R. D.; Parson, M.; Sandford, G.; Skinner, C. J.; Atherton, M. J.; Moilliet, J.S. *J. Chem. Soc. Perkin Trans. I* **1999**, *1*, 803–810.
33. Price, D. A.; James, K.; Osborne, S.; Harbottle, G. W. *Tetrahedron Lett.* **2007**, *48*, 7371–7373.
34. a) Nyffeler, P. T.; Durón, S. G.; Burkart, M. D.; Vincent, S. P.; Wong, C. H. *Angew. Chem. Int. Ed.* **2004**, *44*, 192–212; b) Banks, R.E.; Mohialdin-Khaffaf, S.N., Lal, G. S., Sharif I., Syvret, R.G. *J Chem. Soc. Chem. Commu.n* **1992**, 595–596; c) Singh, R.P., Shreeve, J.M. *Acc. Chem. Res.* **2004**, *37*, 31–44.
35. a) Krasovskiy, A.; Knochel, P. *Angew. Chem. Int. Ed.* **2004**, *43*, 3333–3336; b) Ila, H., Baron, O., Wagner, A.J., Knochel, P. *Chem. Commun.* **2006**, 583–593; c) Krasovskiy, A., Straub, B.F., Knochel, P. *Angew. Chem. Int. Ed.* **2006**, *45*, 159–162.
36. Barnette, W. E. *J. Am. Chem. Soc.* **1984**, *106*, 452–454.
37. Hendrickson, J. B.; Rodríguez, C. *J. Org. Chem.* **1983**, *48*, 3344–3346.
38. Gilmore, C. D.; Allan, K. M.; Stoltz, B. M. *J. Am. Chem. Soc.* **2008**, *130*, 1558–1559.
39. Blackburn, T.; Ramtohul, Y. K. *Synlett* **2008**, 1159–1164.
40. Konno, T.; Chae, J.; Miyabe, T.; Ishihara, T. *J. Org. Chem.* **2005**, *70*, 10172–10174.
41. Shih, W. C.; Teng, C. C.; Parthasarathy, K.; Cheng, C. H. *Chem. Asian J.* **2012**, *7*, 306–313.
42. Booth, B. L. & Collis, A. *J. Chem. Res. Synop.* **1989**, 304–305.
43. Churruca, F.; SanMartin, R.; Carril, M.; Urriaga, M. K.; Solans, X.; Tellitu, I.; Domínguez, E. *J. Org. Chem.* **2005**, *70*, 3178–3187.

4.7 References

44. Kolechkina, V. G.; Maksimov, A. M.; Platonov, V. E.; Osina, O. I. *Russ. Chem. Bull. Int. Ed.* **2001**, *50*, 322–323.
45. Ichikawa, J. *Synthetic Methods for the Preparation of Ring-Fluorinated Heterocycles via Intramolecular Vinylic Substitution of gem-Difluoroalkenes*. in *Fluorine-Containing Synthons - Vol. 911*; ed. Soloshonok, V. A.; 262–275, ACS Symposium Series: Washington, DC, 2005.
46. Ichikawa, J. *J. Fluor. Chem.* **2000**, *105*, 257–263.
47. Ichikawa, J.; Wada, Y.; Fujiwara, M.; Sakoda, K. *Synthesis-Stuttgart* **2002**, 1917–1936.
48. Ichikawa, J.; Wada, Y.; Miyazaki, H.; Mori, T.; Kuroki, H. *Org. Lett.* **2003**, *5*, 1455–1458.
49. Ichikawa, J.; Sakoda, K.; Moriyama, H.; Wada, Y. *Synthesis-Stuttgart* **2006**, 1590–1598.
50. Ichikawa, J.; Wada, Y.; Kuroki, H.; Mihara, J.; Nadano, R. *Org. Biomol. Chem.* **2007**, *5*, 3956–3962.
51. Qian, Z.-C.; Zhou, J.; Li, B.; Shi, B.-F. *Synlett* **2014**, *25*, 1036–1040.
52. Sloop, J. C. *J. Chem.* **2017**, 2017.
53. Lim, S. G.; Lee, J. H.; Moon, C. W.; Hong, J. B.; Jun, C. H. *Org. Lett.* **2003**, *5*, 2759–2761.
54. Parthasarathy, K.; Cheng, C. H. *J. Org. Chem.* **2009**, *74*, 9359–9364.
55. a) Too, P. C.; Wang, Y. F.; Chiba, S. *Org. Lett.* **2010**, *12*, 5688–5691; b) Too, P. C.; Chua, S. H.; Wong, S. H.; Chiba, S. *J. Org. Chem.* **2011**, *76*, 6159; c) Guimond, N.; Gorelsky, S. I.; Fagnou, K. *J. Am. Chem. Soc.* **2011**, *133*, 6449; d) Hyster, T. K.; Rovis, T. *Chem. Commun.* **2011**, *47*, 11846; e) Zhang, S.; Chen, D.; Zhao, M.; Zhao, J.; Jia, A.; Li, X. *Adv. Synth. Catal.* **2011**, *353*, 719.
56. Chuang, S. C.; Gandeepan, P.; Cheng, C. H. *Org. Lett.* **2013**, *15*, 5750–5753.
57. Zhao, D.; Lied, F.; Glorius, F. *Chem. Sci.* **2014**, *5*, 2869–2873.
58. Chu, H.; Sun, S.; Yu, J. T.; Cheng, J. *Chem. Commun.* **2015**, *51*, 13327–13329.
59. a) Neely, J. M.; Rovis, T. *J. Am. Chem. Soc.* **2013**, *135*, 66–69; b) Neely, J. M.; Rovis, T. *J. Am. Chem. Soc.* **2014**, *136*, 2735; c) Romanov-Michailidis, F.; Sedillo, K. F.; Neely, J. M.; Rovis, T. *J. Am. Chem. Soc.* **2015**, *137*, 8892; d) Hyster, T. K.; Rovis, T. *Chem. Commun.* **2011**, *47*, 11846.
60. Chen, R.; Qi, J.; Mao, Z.; Cui, S. *Org. Biomol. Chem.* **2016**, *14*, 6201–6204.
61. Tsai, A. S.; Brasse, M.; Bergman, R. G.; Ellman, J. A. *Org. Lett.* **2011**, *13*, 540–542.
62. Sambaglio, C.; Schönbauer, D.; Blicke, R.; Dao-Huy, T.; Pototschnig, G.; Schaaf, P.; Wiesinger, T.; Zia, M. F.; Wencel-Delord, J.; Besset, T.; Maes, B. U. W.; Schnürch, M. *Chem. Soc. Rev.* **2018**, *47*, 6603–6743.
63. Sen, M.; Kalsi, D.; Sundararaju, B. *Chem. Eur. J.* **2015**, *21*, 15529–15533.
64. Wang, H.; Koeller, J.; Liu, W.; Ackermann, L. *Chem. Eur. J.* **2015**, *21*, 15525–15528.

65. Muralirajan, K.; Kuppusamy, R.; Prakash, S.; Cheng, C. H. *Adv. Synth. Catal.* **2016**, *358*, 774–783.
66. Zhu, Z.; Tang, X.; Li, X.; Wu, W.; Deng, G.; Jiang, H. *J. Org. Chem.* **2016**, *81*, 1401–1409.
67. Xu, T.; Liu, G. *Org. Lett.* **2012**, *14*, 5416–5419.
68. a) Han, W.; Zhang, G.; Li, G.; Huang, H. *Org. Lett.* **2014**, *16*, 3532–3535; b) Shi, Z.; Koester, D. C.; Boultadakis-Arapinis, M.; Glorius, F. *J. Am. Chem. Soc.* **2013**, *135*, 12204–12207; c) Lian, Y.; Hummel, J. R.; Bergman, R. G.; Ellman, J. *J. Am. Chem. Soc.* **2013**, *135*, 12548–12551; d) Wang, Y.-F.; Toh, K. K.; Lee, J.-Y.; Chiba, S. *Angew. Chem., Int. Ed.* **2011**, *50*, 5927–5931; e) Sun, Z.-M.; Chen, S.-P.; Zhao, P. *Chem. Eur. J.* **2010**, *16*, 2619–2627; f) Guimond, N.; Fagnou, K. *J. Am. Chem. Soc.* **2009**, *131*, 12050–12051; g) Parthasarathy, K.; Cheng, C.-H. *J. Org. Chem.* **2009**, *74*, 9359–9364.
69. a) Rouchet, J. B. E. Y.; Schneider, C.; Fruit, C.; Hoarau, C. *J. Org. Chem.* **2015**, *80*, 5919–5927; b) Villuendas, P.; Urriolabeitia, E. P. *J. Org. Chem.* **2013**, *78*, 5254–5263; c) Donohoe, T. J.; Pilgrim, B. S.; Jones, G. R.; Bassuto, J. R. *Proc. Natl. Acad. Sci. U.S.A.* **2012**, *109*, 11605–11608; d) Chinnagolla, R. K.; Pimparkar, S.; Jeganmohan, M. *Org. Lett.* **2012**, *14*, 3032–3035; e) Kornhaaf, C.; Li, J.; Ackermann, L. *J. Org. Chem.* **2012**, *77*, 9190–9198; f) Gerfaud, T.; Neuville, L.; Zhu, J. *Angew. Chem. Int. Ed.* **2009**, *48*, 572–577; g) Fischer, D.; Tomeba, H.; Pahadi, N. K.; Patil, N. T.; Huo, Z.; Yamamoto, Y. *J. Am. Chem. Soc.* **2008**, *130*, 15720–15725.
70. Furuya, T.; Kamlet, A. S.; Ritter, T. *Nature* **2011**, *473*, 470–477.
71. Campbell, M. G.; Ritter, T. *Chem. Rev.* **2015**, *115*, 612–633.
72. Tian, P.; Feng, C.; Loh, T. P. *Nat. Commun.* **2015**, *6*, 1–7.
73. Ueura, K.; Satoh, T.; Miura, M. *Org. Lett.* **2007**, *9*, 1407–1409.
74. Patureau, F. W.; Glorius, F. *J. Am. Chem. Soc.* **2010**, *132*, 9982–9983.
75. Amii, H. & Uneyama, K. *Chem. Rev.* **2009**, *109*, 2119–2183.
76. Yang, E.; Reese, M. R.; Humphrey, J. M. *Org. Lett.* **2012**, *14*, 3944–3947.
77. Wu, J. Q.; Zhang, S. S.; Gao, H.; Qi, Z.; Zhou, C. J.; Ji, W. W.; Liu, Y.; Chen, Y.; Li, Q.; Li, X.; Wang, H. *J. Am. Chem. Soc.* **2017**, *139*, 3537–3545.
78. Kong, L.; Zhou, X.; Li, X. *Org. Lett.* **2016**, *18*, 6320–6323.
79. Zell, D.; Müller, V.; Dhawa, U.; Bursch, M.; Presa, R. R.; Grimme, S.; Ackermann, L. *Chem. Eur. J.* **2017**, *23*, 12145–12148.
80. Murakami, N.; Yoshida, M.; Yoshino, T.; Matsunaga, S. *Chem. Pharm. Bull.* **2018**, *66*, 51–54.
81. Cai, S. H.; Ye, L.; Wang, D. X.; Wang, Y. Q.; Lai, L. J.; Zhu, C.; Feng, C.; Loh, T. P. *Chem. Commun.* **2017**, *53*, 8731–8734.
82. Zell, D.; Dhawa, U.; Müller, V.; Bursch, M.; Grimme, S.; Ackermann, L. *ACS Catal.* **2017**, *7*, 4209–4213.

4.7 References

83. Li, N.; Chang, J.; Kong, L.; Li, X. *Org. Chem. Front.* **2018**, *5*, 1978–1982.
84. Choshi, T.; Hibino, S. *Heterocycles* **2011**, *83*, 1205–1239.
85. a) Marvel, E. N. *Thermal Electrocyclic Reactions*; Academic Press: New York, 1980; b) Mallory, F. B.; Mallory, C. W. *Org. React.* **1984**, *30*, 1; c) Okamura, W. H.; de Lera, A. R. in *Comprehensive Organic Synthesis*, ed. by Trost, B. M.; Fleming, I.; Paquette, L. A., Pergamon Press: New York, 1991, Vol. 5, p. 699.
86. a) Woodward, R. B.; Hoffmann, R. *J. Am. Chem. Soc.* **1965**, *87*, 395–397; b) Woodward, R. B.; Hoffmann, R. *Angew. Chem. Int. Ed.* **1969**, *8*, 781–932; c) Fleming, I. *Molecular Orbitals and Organic Chemical Reactions*, Wiley: Chichester, UK, 2009.
87. Tanaka, K.; Mori, H.; Yamamoto, M.; Katsumura, S. *J. Org. Chem.* **2001**, *66*, 3099–3110.
88. Sünnemann, H. W.; Banwell, M. G.; De Meijere, A. *Eur. J. Org. Chem.* **2007**, 3879–3893.
89. a) Beaudry, C. M.; Malerich, J. P.; Trauner, D. *Chem. Rev.* **2005**, *105*, 4757–4778; b) Thompson, S.; Coyne, A. G.; Knipe, P. C.; Smith, M. D. *Chem. Soc. Rev.* **2011**, *40*, 4217–4231.
90. a) Chen, D. Y. K.; Tseng, C. C. *Org. Biomol. Chem.* **2010**, *8*, 2900–2911; b) Fotiadou, A. D.; Zografos, A. L. *Org. Lett.* **2012**, *14*, 5664–5667; c) Sloman, D. L.; Bacon, J. W.; Porco Jr, J. A. *J. Am. Chem. Soc.*, **2011**, *133*, 9952–9955; d) Pavan Kumar, V.; Gruner, K. K.; Kataeva, O.; Knölker, H.-J. *Angew. Chem. Int. Ed.* **2013**, *52*, 11073–11077; e) Volgraf, M.; Lumb, J.-P.; Brastianos, H. C.; Carr, G.; Chung, M. K. W.; Münzel, M.; Mauk, A. G.; Andersen, R. J.; Trauner, D. *Nat. Chem. Biol.*, **2008**, *4*, 535–537.
91. Vargas, D. F.; Larghi, E. L.; Kaufman, T. S. *Nat. Prod. Rep.* **2019**, *36*, 354–401.
92. Schiess, P.; Chia, H. L.; Ringlele, P. *Tetrahedron Lett.* **1972**, *4*, 313–316.
93. Trost, B. M.; Gutierrez, A. C. *Org. Lett.* **2007**, *9*, 1473–1476.
94. Mora-Radó, H.; Bialy, L.; Czechtizky, W.; Méndez, M.; Harrity, J. P. A. *Angew. Chem. Int. Ed.* **2016**, *55*, 5834–5836.
95. Mora-Radó, H.; Sotorríos, L.; Ball-Jones, M. P.; Bialy, L.; Czechtizky, W.; Méndez, M.; Gómez-Bengoa, E.; Harrity, J. P. A. *Chem. Eur. J.* **2018**, *24*, 9530–9534.
96. Ball-Jones, M. P.; Tyler, J.; Mora-Radó, H.; Czechtizky, W.; Méndez, M.; Harrity, J. P. A. *Org. Lett.* **2019**, *21*, 6821–6824.
97. Vargas, D. F.; Larghi, E. L.; Kaufman, T. S. *Eur. J. Org. Chem.* **2018**, 5605–5614.

Chapter 5

Experimental section



In this chapter, the experimental part concerning the work explained in Chapter 4 is presented.

It regards all the experiments performed by the author of this thesis at the University of Sheffield in the group of Prof. Harrity. Experimental procedures, as well as materials and techniques are described in detail.

5.1 Materials and techniques

5.1.1 Reagents and solvents

Reagents were purchased from common commercial suppliers such as Aldrich, Across, Alfa Aesar, Fluka, TCI, Merck, Fluorochem, etc., stored as specified by the manufacturer and used without previous purification.

Anhydrous solvents were dispensed by a “Grubbs apparatus”. The untreated solvent is contained within a lined metal reservoir and forced by nitrogen flow through a pair of metal columns each containing either activated alumina or molecular sieves. The dried solvent is then collected under vacuum *via* a Schlenk line system.

5.1.2 General experimental

All reactions were conducted under an inert atmosphere of dry nitrogen or argon unless otherwise stated using oven-dried glassware and were magnetically stirred.

Heat requiring reactions were performed using a hotplate with a sand bath and condenser. Organic layers washed with aqueous phases were dried over MgSO_4 and filtered through celite.

Organic solvents were evaporated under reduced pressure using rotavapors. For the complete removal of solvents vacuum pump was employed. Flash chromatography was performed on silica gel (Fluorochem Davisil silica gel 43-60). The solvent system used is specified in every single example. Thin layer chromatography (TLC) was performed on aluminium backed plates pre-coated with silica (0.2 mm, Merck DC-ALUFOLIEN Kieselgel 60 F₂₅₄), which were developed using ultraviolet light or potassium permanganate. Yields refer to chromatographically purified and spectroscopically pure compounds, unless otherwise stated.

5.1.3 NMR spectra

NMR spectra were recorded using either a Bruker Avance III HD 400 spectrometer (400 MHz for ^1H , 100 MHz for ^{13}C , 377 MHz for ^{19}F) or Bruker Avance 400 (400 MHz for ^1H , 100 MHz for ^{13}C) on solutions at room temperature. Chemical shifts (δ) are quoted in parts per million (ppm, δ), downfield from tetramethylsilane (TMS) and referenced to the residual solvent peak, chloroform CDCl_3 , ^1H ($\delta = 7.26$ ppm) and ^{13}C ($\delta = 77.0$ ppm) as internal standard. The spectra were analysed according to first order and the multiplicity of each signal is designated using the following abbreviations: s, singlet; d, doublet; t, triplet; q, quartet; m, multiplet. Coupling constants (J) are reported in Hertz (Hz).

MestrReNova Mnova 11.0.4 program was used to process and edit the registered spectra.

5.1.4 Mass spectra

High-resolution mass spectroscopy (HRMS) spectra, for accurate mass analysis, were recorded on a MicroMass LCT operating in Electrospray mode (TOF ES⁺).

5.1.5 Infrared Spectra

Infrared spectra were recorded on a Perkin Elmer Paragon 100 FTIR spectrophotometer. Samples were recorded neat. ν_{\max} in cm^{-1} .

5.2 Experimental procedures of Chapter 4

5.2.1 Synthesis of O-alkyl oximes

General procedure A (GPA)

Aldehyde (1 eq.) was dissolved in CH_2Cl_2 to a final concentration of 0.45 M. To this, 1.5 eq. of the O-methylhydroxylamine hydrochloride salt and 2.2 eq. of pyridine were added. The mixture was stirred for 2 hours at room temperature under inert atmosphere. The reaction mixture was subsequently washed with 5% aqueous HCl (3 times) and saturated NaCl (2 times). The resulting organic layer was dried over MgSO_4 and concentrated under reduced pressure to provide the crude oxime. The compound was purified by silica-gel chromatography (petroleum ether/ethyl acetate) to give the pure compound.

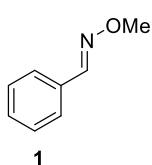
Nat Chem Biol. **2011**, 7(10):685-91

General procedure B (GPB)

Aldehyde oxime (1 eq.) and KOH (6 eq.) were dissolved in DMSO/ H_2O (2.5/1) to a final concentration of benzaldehyde oxime of 0.43 M. The mixture was let stirring for 15 minutes and then 1.2 eq. of alkyl bromide were added. After 2h the reaction was completed and brine was added to it, followed by extraction with ethyl acetate. The organic layer was washed with brine 3 times, dried over MgSO_4 and concentrated under reduced pressure. The residue was purified through silica-gel chromatography (petroleum ether/ethyl acetate) to give the pure compound.

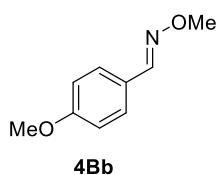
Chinese Chemical Letters, **2002**, 13 (2), 95-96.

Benzaldehyde O-methyl oxime (1)



Following GPA using benzaldehyde (2.87 ml, 28.2 mmol), 60ml of CH_2Cl_2 , 2.82 g (42.2 mmol) of O-methylhydroxylamine hydrochloride salt and 5.01mL (62.04 mmol) of pyridine. Work-up with 5% aqueous HCl (3x50mL) and saturated NaCl (2x50mL). Purification by silica-gel chromatography (petroleum ether/ethyl acetate 20/1) to give the pure compound as a pale yellow oil in 86% yield (3.28 g).

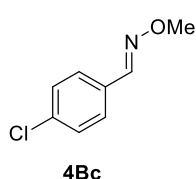
$^1\text{H NMR}$ (CDCl_3 , 400 MHz): δ 8.12 (s, 1H), 7.65 – 7.62 (m, 2H), 7.42 – 7.39 (m, 3H), 4.03 (s, 3H). $^{13}\text{C NMR}$ (CDCl_3 , 100.6 MHz): δ 148.6, 132.3, 129.8, 128.7, 127.0, 62.0.

4-methoxybenzaldehyde O-methyl oxime (4Bb)

Following GPA using 4-methoxybenzaldehyde (2.00 ml, 16.4 mmol), 37ml of CH₂Cl₂, 2.05 g (24.6 mmol) of O-methylhydroxylamine hydrochloride salt and 2.9mL (36.08 mmol) of pyridine. Work-up with 5% aqueous HCl (3x40mL) and saturated NaCl (2x40mL).

Purification by silica-gel chromatography (petroleum ether/ethyl acetate 20/1) to give the pure compound as a colourless oil in 98% yield (2.65g).

¹H NMR (CDCl₃, 400 MHz): δ 8.04 (s, 1H), 7.54 (d, *J* = 8.8 Hz, 2H), 6.92 (d, *J* = 8.8 Hz, 2H), 3.97 (s, 3H), 3.85 (s, 3H). **¹³C NMR (CDCl₃, 100.6 MHz):** δ 160.9, 148.2, 128.5, 124.8, 114.2, 61.8, 55.3.

4-chlorobenzaldehyde O-methyl oxime (4Bc)

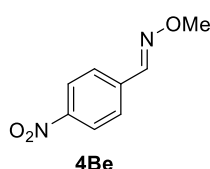
Following GPA using 4-chlorobenzaldehyde (2.30 g, 16.4 mmol), 37ml of CH₂Cl₂, 2.05 g (24.6 mmol) of O-methylhydroxylamine hydrochloride salt and 2.9 mL (36.08 mmol) of pyridine. Work-up with 5% aqueous HCl (3x40mL) and saturated NaCl (2x40mL). Purification by silica-gel chromatography (petroleum ether/ethyl acetate 20/1) to give the pure compound as a white solid in 41% yield (1.14g).

¹H NMR (CDCl₃, 400 MHz): δ 8.03 (s, 1H), 7.53 (d, *J* = 8.5 Hz, 2H), 7.36 (d, *J* = 8.5 Hz, 2H), 4.00 (s, 3H). **¹³C NMR (CDCl₃, 100.6 MHz):** δ 147.3, 135.6, 130.7, 129.0, 128.2, 62.1.

4-bromobenzaldehyde O-methyl oxime (4Bg)

Following GPA using 4-bromobenzaldehyde (1.02 g, 5.5 mmol), 13ml of CH₂Cl₂, 0.69 g (8.3 mmol) of O-methylhydroxylamine hydrochloride salt and 0.98 mL (12.2 mmol) of pyridine. Work-up with 5% aqueous HCl (3x20mL) and saturated NaCl (2x20mL). Purification by silica-gel chromatography (petroleum ether/ethyl acetate 20/1) to give the pure compound as a colourless oil in 94% yield (1.11 g).

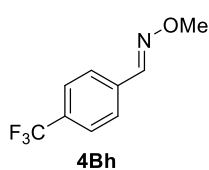
¹H NMR (CDCl₃, 400 MHz): δ 8.02 (s, 1H), 7.53 (d, *J* = 8.5 Hz, 2H), 7.47 (d, *J* = 8.5 Hz, 2H), 3.99 (s, 3H). **¹³C NMR (CDCl₃, 100.6 MHz):** δ 147.4, 131.9, 131.1, 128.4, 123.9, 62.2.

4-nitrobenzaldehyde O-methyl oxime (4Be)

Following GPA using 4-bromobenzaldehyde (2.48 g, 16.4 mmol), 37ml of CH₂Cl₂, 2.05 g (24.6 mmol) of O-methylhydroxylamine hydrochloride salt and 2.9 mL (36.08 mmol) of pyridine. Work-up with 5% aqueous HCl (3x40mL) and saturated NaCl (2x40mL).

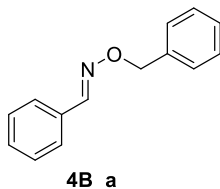
Purification by silica-gel chromatography (petroleum ether/ethyl acetate 20/1) to give the pure compound as a beige/white solid in 82% yield (2.42 g).

¹H NMR (CDCl₃, 400 MHz): δ 8.26 (d, *J* = 8.9 Hz, 2H), 8.13 (s, 1H), 7.77 (d, *J* = 8.9 Hz, 2H), 4.06 (s, 3H). **¹³C NMR (CDCl₃, 100.6 MHz):** δ 148.3, 146.3, 138.4, 127.5, 124.0, 62.7.

4-(trifluoromethyl)benzaldehyde O-methyl oxime (4Bh)

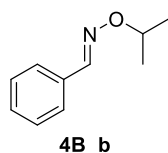
Following GPA using 4-bromobenzaldehyde (2.24 mL, 16.4 mmol), 37ml of CH₂Cl₂, 2.05 g (24.6 mmol) of O-methylhydroxylamine hydrochloride salt and 2.9 mL (36.08 mmol) of pyridine. Work-up with 5% aqueous HCl (3x40mL) and saturated NaCl (2x40mL). Purification by silica-gel chromatography (petroleum ether/ethyl acetate 20/1) to give the pure compound as a colourless oil in 98% yield (3.27 g).

¹H NMR (CDCl₃, 400 MHz): δ 8.10 (s, 1H), 7.71 (d, *J* = 8.3 Hz, 2H), 7.64 (d, *J* = 8.3 Hz, 2H), 4.03 (s, 3H). **¹³C NMR (CDCl₃, 100.6 MHz):** δ 147.1, 135.6, 131.4 (q, ²*J*_{C-F} = 32.5, 1C), 127.1, 125.6 (q, ³*J*_{C-F} = 3.7 Hz, 2C), 123.9 (q, ¹*J*_{C-F} = 272.3 Hz, 1C), 62.3. **¹⁹F NMR (CDCl₃, 377 MHz):** δ -62.9.

Benzaldehyde O-benzyl oxime (4B_a)

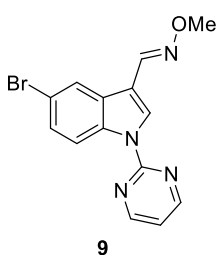
Following GPB using benzaldehyde oxime (0.36 g, 3 mmol), KOH (1g, 18 mmol) in 5 mL of DMSO and 2 mL of H₂O, then 0.43 mL of benzyl bromide. Work-up adding 4 mL of brine, followed by extraction with EtOAc (10 mL). The organic layer was washed with brine (3x10mL). Purification through silica-gel chromatography (petroleum ether/ethyl acetate 30/1) to give the pure compound as a colourless oil in 85% yield (0.54 g).

¹H NMR (CDCl₃, 400 MHz): δ 8.19 (s, 1H), 7.59 – 7.66 (m, 2H), 7.32 – 7.50 (m, 8H), 5.27 (s, 2H). **¹³C NMR (CDCl₃, 100.6 MHz):** δ 149.1, 137.5, 132.3, 129.9, 128.7, 128.5, 128.4, 128.0, 127.1, 77.4.

Benzaldehyde O-isopropyl oxime (4B_b)

Following GPB using benzaldehyde oxime (0.36 g, 3 mmol), KOH (1g, 18 mmol) in 5 mL of DMSO and 2 mL of H₂O, then 0.34 mL of *i*-propyl bromide. Work-up adding 4 mL of brine, followed by extraction with EtOAc (10 mL). The organic layer was washed with brine (3x10mL). Purification through silica-gel chromatography (petroleum ether/ethyl acetate 30/1) to give the pure compound as a colourless oil in 75% yield (0.37 g).

¹H NMR (CDCl₃, 400 MHz): δ 8.10 (s, 1H), 7.58 – 7.64 (m, 2H), 7.35 – 7.42 (m, 3H), 4.44-4.56 (m, 1H), 1.32-1.38 (m, 6H). **¹³C NMR (CDCl₃, 100.6 MHz):** δ 147.9, 132.7, 129.5, 128.6, 126.9, 75.8, 21.7.

5-bromo-1-(pyrimidin-2-yl)-1H-indole-3-carbaldehyde O-methyl oxime (9)

9

Following GPA using 5-bromo-1-(pyrimidin-2-yl)-1H-indole-3-carbaldehyde (0.18 g, 0.6 mmol), 6 ml of CH₂Cl₂, 0.75 g (0.9 mmol) of O-methylhydroxylamine hydrochloride salt and 0.11 mL (1.32 mmol) of pyridine. Work-up with 5% aqueous HCl (3x10mL) and saturated NaCl (2x10mL). Purification by silica-gel chromatography (petroleum

ether/ethyl acetate 6/4) to give the compound as a white solid in 81% yield (0.16 g) as a mixture of *Z*- and *E*- isomers (ratio *Z/E* 3.5/1).

Z-only: $^1\text{H NMR}$ (CDCl_3 , 400 MHz): δ 8.73-8.77 (m, 3H), 8.46 (s, 1H), 8.43 (d, $J = 2.0$ Hz, 1H), 8.30 (s, 1H), 7.52 (dd, $J = 8.9, 2.1$ Hz, 1H), 7.16 (t, $J = 4.8$ Hz, 1H), 4.07 (s, 3H). $^{13}\text{C NMR}$ (CDCl_3 , 100.6 MHz): δ 158.2, 157.0, 143.2, 134.9, 131.9, 129.3, 128.9, 127.7, 125.2, 117.7, 117.0, 116.6, 113.1. HRMS m/z $[\text{M}+\text{H}]^+$ $\text{C}_{14}\text{H}_{12}^{79}\text{BrN}_4\text{O}$ calcd. 331.0189, found 331.0178. IR: $\nu_{\text{max}}/\text{cm}^{-1}$ (neat) 2934, 1617, 1573, 1542, 1455, 1427, 1293, 1229, 1136, 1153, 1058.

General procedure C (GPC)

A round bottom flask equipped with a stir bar was charged with acetophenone (1 eq.), $\text{MeONH}_2\cdot\text{HCl}$ (2.7 eq.), NaOAc (4.4 eq.), $\text{H}_2\text{O}/\text{EtOH}$ 3/1. The flask was equipped with a reflux condenser and heated at 70°C for 2 hours. After cooling to room temperature, the mixture was extracted with EtOAc (3 times). The organic layers were dried with MgSO_4 and the filtrate was concentrated under reduced pressure. The residue was purified by silica-gel column chromatography (eluent petroleum ether/ethyl acetate) to give the corresponding product.

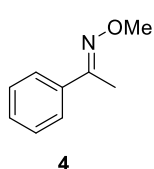
Org. Lett. **2017**, *19*, 11, 2905-2908.

General procedure D (GPD)

Acetophenone oxime (1 eq.) and KOH (6 eq.) were dissolved in $\text{DMSO}/\text{H}_2\text{O}$ (2.5/1) to a final concentration of acetophenone oxime of 0.43 M. The mixture was let stirring for 15 minutes and then 1.2 eq. of alkyl bromide were added. After 2h the reaction was completed and brine was added to it, followed by extraction with ethyl acetate. The organic layer was washed with brine 3 times, dried over MgSO_4 and concentrated under reduced pressure. The residue was purified through silica-gel chromatography (petroleum ether/ethyl acetate) to give the pure compound.

Chinese Chemical Letters, **2002**, *13* (2), 95-96.

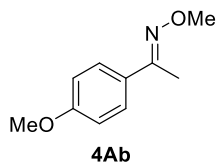
1-phenylethan-1-one *O*-methyl oxime (4)



Following GPC using acetophenone (0.5 ml, 4.27 mmol), $\text{MeONH}_2\cdot\text{HCl}$ (0.97 g, 11.5 mmol), NaOAc (1.55 g, 18.8 mmol), H_2O (39 mL) and EtOH (13 mL). Work-up with EtOAc (3x50mL). Purification by silica-gel column chromatography (eluent petroleum ether/ethyl acetate 20/1) to give the corresponding product in 85% yield (0.54 g) as a colourless oil.

$^1\text{H NMR}$ (CDCl_3 , 400 MHz): δ 7.68 – 7.71 (m, 2H), 7.38 – 7.43 (m, 3H), 4.05 (s, 3H), 2.27 (s, 3H). $^{13}\text{C NMR}$ (CDCl_3 , 100.6 MHz): δ 154.7, 136.7, 129.0, 128.4, 126.1, 61.9, 12.7.

1-(4-methoxyphenyl)ethan-1-one *O*-methyl oxime (4Ab)

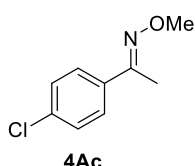


Following GPC using 4-methoxyacetophenone (0.64 ml, 4.27 mmol), $\text{MeONH}_2\cdot\text{HCl}$ (0.97 g, 11.5 mmol), NaOAc (1.55 g, 18.8 mmol), H_2O (39 mL) and EtOH (13 mL). Work-up with EtOAc (3x50mL).

Purification by silica-gel column chromatography (eluent petroleum ether/ethyl acetate 20/1) to give the corresponding product in 33% yield (0.25 g) as a white solid.

¹H NMR (CDCl₃, 400 MHz): δ 7.62 (d, *J* = 8.9 Hz, 2H), 6.91 (d, *J* = 8.9 Hz, 2H), 4.00 (s, 3H), 3.85 (s, 3H), 2.23 (s, 3H). **¹³C NMR (CDCl₃, 100.6 MHz):** δ 160.4, 154.2, 129.2, 127.3, 113.8, 61.8, 55.3, 12.5.

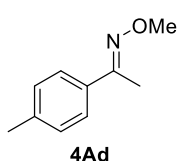
1-(4-chlorophenyl)ethan-1-one O-methyl oxime (4Ac)



Following GPC using 4-chloroacetophenone (0.55 ml, 4.27 mmol), MeONH₂·HCl (0.97 g, 11.5 mmol), NaOAc (1.55 g, 18.8 mmol), H₂O (39 mL) and EtOH (13 mL). Work-up with EtOAc (3x50mL). Purification by silica-gel column chromatography (eluent petroleum ether/ethyl acetate 20/1) to give the corresponding product in 82% yield (0.64 g) as a colourless oil.

¹H NMR (CDCl₃, 400 MHz): δ 7.61 (d, *J* = 8.6 Hz, 2H), 7.36 (d, *J* = 8.6 Hz, 2H), 4.02 (s, 3H), 2.22 (s, 3H). **¹³C NMR (CDCl₃, 100.6 MHz):** δ 153.5, 135.0 (two peaks, s, 1C+1C), 128.6, 127.3, 62.0, 12.5.

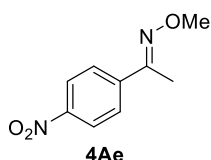
1-(*p*-tolyl)ethan-1-one O-methyl oxime (4Ad)



Following GPC using 4-methylacetophenone (0.57 ml, 4.27 mmol), MeONH₂·HCl (0.97 g, 11.5 mmol), NaOAc (1.55 g, 18.8 mmol), H₂O (39 mL) and EtOH (13 mL). Work-up with EtOAc (3x50mL). Purification by silica-gel column chromatography (eluent petroleum ether/ethyl acetate 20/1) to give the corresponding product in 80% yield (0.56 g) as a colourless oil.

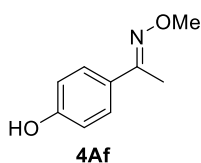
¹H NMR (CDCl₃, 400 MHz): δ 7.59 (d, *J* = 8.0 Hz, 2H), 7.22 (d, *J* = 8.0 Hz, 2H), 4.04 (s, 3H), 2.41 (s, 3H), 2.26 (s, 3H). **¹³C NMR (CDCl₃, 100.6 MHz):** δ 154.6, 139.0, 133.8, 129.1, 126.0, 61.8, 21.3, 12.6.

1-(4-nitrophenyl)ethan-1-one O-methyl oxime (4Ae)



Following GPC using 4-nitroacetophenone (0.71 g, 4.27 mmol), MeONH₂·HCl (0.97 g, 11.5 mmol), NaOAc (1.55 g, 18.8 mmol), H₂O (39 mL) and EtOH (13 mL). Work-up with EtOAc (3x50mL). Purification by silica-gel column chromatography (eluent petroleum ether/ethyl acetate 20/1) to give the corresponding product in 78% yield (0.65g) as a white solid.

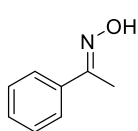
¹H NMR (CDCl₃, 400 MHz): δ 8.24 (d, *J* = 9.0 Hz, 2H), 7.85 (d, *J* = 9.0 Hz, 2H), 4.07 (s, 3H), 2.28 (s, 3H). **¹³C NMR (CDCl₃, 100.6 MHz):** δ 152.5, 148.0, 142.6, 126.7, 123.6, 62.4, 12.3.

1-(4-hydroxyphenyl)ethan-1-one O-methyl oxime (4Af)

Following GPC using 4-hydroxyacetophenone (0.58 g, 4.27 mmol), MeONH₂·HCl (0.97 g, 11.5 mmol), NaOAc (1.55 g, 18.8 mmol), H₂O (39 mL) and EtOH (13 mL). Work-up with EtOAc (3x50mL). Purification by silica-gel column chromatography (eluent petroleum ether/ethyl acetate 20/1) to give the corresponding product in 66% yield (0.47 g)

as a white solid.

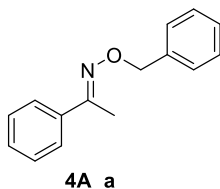
¹H NMR (CDCl₃, 400 MHz): δ 7.53 (d, *J* = 8.7 Hz, 2H), 6.84 (d, *J* = 8.7 Hz, 2H), 4.00 (s, 3H), 2.22 (s, 3H). **¹³C NMR (CDCl₃, 100.6 MHz):** δ 156.8 (s, 1C), 155.4 (s, 1C), 128.8 (s, 1C), 127.7 (s, 2C), 115.4 (s, 2C), 61.7 (s, 1C), 13.1 (s, 1C).

Acetophenone oxime

A 100mL round-bottom flask was charged with acetophenone (0.5 ml, 4.27 mmol), HONH₂·HCl (0.80 g, 11.5 mmol), NaOAc (1.55 g, 18.8 mmol), H₂O (10 mL) and EtOH (15 mL). The flask was equipped with a reflux condenser and the mixture was let stirring at reflux for 3h. after cooling down to room

temperature, the mixture was extracted with ethyl acetate (3x20mL). The organic layers were collected and dried over MgSO₄ and the filtrate was concentrated under reduced pressure. The crude product (white solid) was used directly for the synthesis of acetophenone O-isopropyl oxime without further purification.

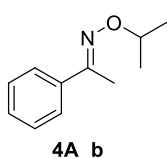
Chem. Commun. **2017**, 53, 12189-12192.

Acetophenone O-benzyl oxime (4A_a)

Following GPD using acetophenone oxime (0.15 g, 1.12 mmol), KOH (0.38 g, 6.72 mmol) DMSO (2 mL), H₂O (0.7 mL), then benzylbromide (0.16 mL, 1.34 mmol). Work-up adding 2 mL of brine, followed by extraction with EtOAc (7 mL). The organic layer was washed with

brine (3x7mL). Purification through silica-gel chromatography (petroleum ether/ethyl acetate 30/1) to give the pure compound as a colourless oil in 82% yield (0.21 g).

¹H NMR (CDCl₃, 400 MHz): δ 7.74-7.78 (m, 2H), 7.52 – 7.56 (m, 2H), 7.41 – 7.50 (m, 6H), 5.37 (s, 2H), 2.38 (s, 3H). **¹³C NMR (CDCl₃, 100.6 MHz):** δ 138.2, 136.7, 129.1, 128.5 (two signals), 128.2, 127.9, 127.8, 126.2, 76.3, 13.0.

Acetophenone O-isopropyl oxime (4A_b)

Following GPD using acetophenone oxime (0.15 g, 1.12 mmol), KOH (0.38 g, 6.72 mmol) DMSO (2 mL), H₂O (0.7 mL), then isopropylbromide (0.13 mL, 1.34 mmol). Work-up adding 2 mL of brine, followed by extraction with EtOAc (7 mL). The organic layer was washed with brine (3x7mL).

Purification through silica-gel chromatography (petroleum ether/ethyl acetate 30/1) to give the pure compound as a colourless oil in 79% yield (0.16 g).

¹H NMR (CDCl₃, 400 MHz): δ 7.68 – 7.71 (m, 2H), 7.36-7.42 (m, 3H), 4.70 (hept, *J* = 6.2 Hz, 1H), 2.26 (s, 3H), 1.35 (d, *J* = 6.2 Hz, 6H). **¹³C NMR (CDCl₃, 100.6 MHz):** δ 153.6, 137.2, 128.7, 128.3, 126.0, 75.6, 21.9, 12.7.

5.2.2 Synthesis of Hydrazones

General Procedure E

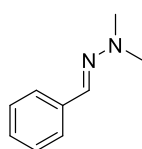
A round bottom flask was charged with benzaldehyde (1 eq.), hydrazine (1.2 eq.), acetic acid (1.2 eq.) and dry dichloromethane to a concentration of 0.1 M. The mixture was stirred for 2 hours at room temperature and then extracted with water 3 times. The organic layer was dried over MgSO₄ and the filtrate was concentrated under reduced pressure. The residue was purified by silica-gel column chromatography (eluent petroleum ether/ethyl acetate) to give the corresponding product.

General Procedure F

A flame dried round bottom flask equipped with a condenser was charged with acetophenone (1 eq.), hydrazine (2 eq.), acetic acid (0.1 eq.) and ethanol to a concentration of 0.5 M. The mixture was stirred for 12 hours under reflux in inert atmosphere. Then, the solvent was removed under reduced pressure and the mixture was extracted with ethyl acetate and water (3 times). The organic layer was dried over MgSO₄ and the filtrate was concentrated under reduced pressure. The residue was purified by silica-gel column chromatography (eluent petroleum ether/ethyl acetate) to give the corresponding product.

Org. Lett., **2013**, *15* (22).

2-benzylidene-1,1-dimethylhydrazine (9Ba)

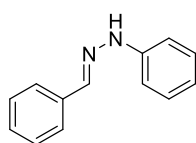


9Ba

Following the GPE using benzaldehyde (0.96 mL, 9.4 mmol), 1,1-dimethylhydrazine (0.86 mL, 11.28 mmol), acetic acid (0.65 mL, 11.28 mmol), dichloromethane (94mL). Work-up with 3x70mL of water. Purification by silica-gel column chromatography (eluent petroleum ether/ethyl acetate 9/1) to give 2-benzylidene-1,1-dimethylhydrazine in 92% yield (1.28 g) as a pale yellow oil.

¹H NMR (CDCl₃, 400 MHz): δ 7.59-7.63 (m, 2H), 7.33-7.38 (m, 2H), 7.23-7.29 (m, 2H), 3.00 (s, 6H). **¹³C NMR (CDCl₃, 100.6 MHz):** δ 136.8, 132.9, 128.5, 127.4, 125.6, 42.9.

1-benzylidene-2-phenylhydrazine (9Bc)



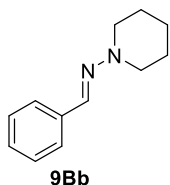
9Bc

Following the GPE using benzaldehyde (0.96 mL, 9.4 mmol), phenylhydrazine (1.11 mL, 11.28 mmol), acetic acid (0.65 mL, 11.28 mmol), dichloromethane (94mL). Work-up with 3x70mL of water. Purification by silica-gel column chromatography (eluent petroleum ether/ethyl acetate 9/1) to give 1-benzylidene-2-phenylhydrazine in

96% yield (1.77 g) as a light orange solid.

^1H NMR (CDCl₃, 400 MHz): δ 7.66-7.76 (m, 3H), 7.36-7.45 (m, 2H), 7.28-7.36 (m, 3H), 7.12-7.19 (m, 2H), 6.87-6.94 (m, 1H). **^{13}C NMR (CDCl₃, 100.6 MHz):** δ 144.6, 137.3, 135.3, 129.3, 128.6, 128.4, 126.2, 120.1, 112.7.

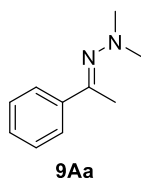
1-phenyl-*N*-(piperidin-1-yl)methanimine (9Bb)



Following the GPE using benzaldehyde (0.96 mL, 9.4 mmol), piperidin-1-amine (1.22 mL, 11.28 mmol), acetic acid (0.65 mL, 11.28 mmol), dichloromethane (94mL). Work-up with 3x70mL of water. Purification by silica-gel column chromatography (eluent petroleum ether/ethyl acetate 9/1) to give 1-phenyl-*N*-(piperidin-1-yl)methanimine in 98% yield (1.76g) as a pink solid.

^1H NMR (CDCl₃, 400 MHz): δ 7.59-7.64 (m, 2H), 7.57 (s, 1H), 7.32-7.39 (m, 2H), 7.24 – 7.30 (m, 1H), 3.16-3.22 (m, 4H), 1.74-1.82 (m, 4H), 1.53-1.61 (m, 2H). **^{13}C NMR (CDCl₃, 100.6 MHz):** δ 136.7, 134.6, 128.5, 127.8, 126.0, 52.1, 25.2, 24.2.

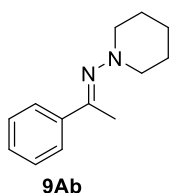
1,1-dimethyl-2-(1-phenylethylidene)hydrazine (9Aa)



Following the GPF using acetophenone (1.17 mL, 10.0 mmol), 1,1-dimethylhydrazine (1.52 mL, 20.0 mmol), acetic acid (0.06 mL, 1.00 mmol), ethanol (20 mL). Work-up 30 mL of ethyl acetate and washing with 3 x 30mL of water. Purification by silica-gel column chromatography (eluent petroleum ether/ethyl acetate 95/5) to give the product in 98% yield (1.59 g) as a yellow oil.

^1H NMR (CDCl₃, 400 MHz): δ 7.73-7.78 (m, 2H), 7.36-7.40 (m, 3H), 2.63 (s, 6H), 2.38 (s, 3H). **^{13}C NMR (CDCl₃, 100.6 MHz):** δ 162.2, 139.1, 129.2, 128.3, 126.4, 47.3, 15.6.

1-phenyl-*N*-(piperidin-1-yl)ethan-1-imine (9Ab)



Following the GPF using acetophenone (0.47 mL, 4.00 mmol), piperidin-1-amine (0.86 mL, 8.00 mmol), acetic acid (0.02 mL, 0.40 mmol), ethanol (8 mL). Work-up 10 mL of ethyl acetate and washing with 3 x 10mL of water. Purification by silica-gel column chromatography (eluent petroleum ether/ethyl acetate 95/5) to give the product in 80% yield (0.65g) as a yellow oil.

^1H NMR (CDCl₃, 400 MHz): δ 7.75-7.79 (m, 2H), 7.36-7.40 (m, 3H), 2.80-2.84 (m, 4H), 2.38 (s, 3H), 1.73-1.80 (m, 4H), 1.49-1.56 (m, 2H). **^{13}C NMR (CDCl₃, 100.6 MHz):** δ 162.2, 139.3, 129.2, 128.2, 126.4, 56.2, 25.5, 24.0, 15.7.

5.2.3 Synthesis of difluoroalkenes

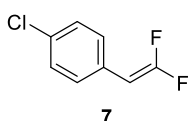
General procedure (GP)

To a dried round-bottom flask equipped with a magnetic stir bar and charged with benzaldehyde (1 eq.), triphenylphosphine (1.2 eq.), and DMF (0.5 mol/L for aldehyde) was added a solution of sodium chlorodifluoroacetate (1.5 eq.) in DMF (2 mol/L)

dropwise at 100 °C over 30 min. After the addition was completed, the reaction mixture was heated additionally at the same temperature for 1 hour. After cooling to 0 °C, to the reaction mixture was added water and the mixture was extracted with Et₂O (3 times). The organic extract was washed with water and brine, and then dried over anhydrous magnesium sulfate. After filtration, the filtrate was concentrated under reduced pressure. The residue was purified by silica-gel column chromatography (eluent petroleum ether/ethyl acetate) to give the corresponding gem-difluoroalkene, if not differently reported.

J. Am. Chem. Soc. **2017**, *139*, 36, 12855-12862.

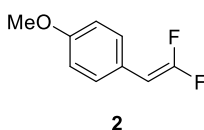
1-chloro-4-(2,2-difluorovinyl)benzene (7)



Following GP using 4-chlorobenzaldehyde (2g, 14.2 mmol), PPh₃ (4.48 g, 17.1 mmol), 28.4 ml of DMF, 10.7 ml of solution of sodium chlorodifluoroacetate (3.25 g, 21.3 mmol) in DMF with silica-gel column chromatography (eluent petroleum ether/ethyl acetate 50/1) to give 1-chloro-4-(2,2-difluorovinyl)benzene as a colourless oil in 54% yield (1.34g).

¹H NMR (CDCl₃, 400 MHz): δ 7.27 – 7.35 (m, 4H), 5.27 (dd, *J*_{H-F} = 26.0, 3.6 Hz, 1H). **¹³C NMR (CDCl₃, 100.6 MHz):** δ 156.3 (dd, ¹*J*_{C-F} = 298.4, 288.9 Hz), 132.8, 128.7-129.0 (three signals overlapped), 81.4 (dd, ²*J*_{C-F} = 29.8, 13.7 Hz). **¹⁹F NMR (CDCl₃, 377 MHz):** δ -81.6 (d, *J*_{F-F} = 29.9 Hz), -83.4 (d, *J*_{F-F} = 29.9 Hz).

1-(2,2-difluorovinyl)-4-methoxybenzene (2)



Following GP using 4-methoxybenzaldehyde (3.57 ml, 29.4 mmol), PPh₃ (9.23 g, 35.3 mmol), 60 ml of DMF, 22ml of solution of sodium chlorodifluoroacetate (6.72 g, 44.1 mmol) in DMF with silica-gel column chromatography (eluent petroleum ether/ethyl acetate 20/1)

to give the product contaminated by residue of PPh₃. The mixture was treated with CuCl (2 g) in acetone (40ml) and stirred for 30 min. After filtration with celite, the acetone was removed in vacuum and the product was further purified by silica-gel column chromatography to give the pure 1-(2,2-difluorovinyl)-4-methoxybenzene, as a colourless oil in 54% yield (2.70 g).

¹H NMR (CDCl₃, 400 MHz): δ 7.28 – 7.32 (d, *J* = 7.0 Hz, 2H), 6.90 – 6.93 (d, *J* = 7.0 Hz, 2H), 5.26 (dd, *J*_{H-F} = 26.3, 2.2 Hz, 1H), 3.84 (s, 3H). **¹³C NMR (CDCl₃, 100.6 MHz):** δ 158.6, 155.9 (dd, ¹*J*_{C-F} = 296.4, 286.4 Hz), 128.8 (dd, ⁴*J*_{C-F} = 6.4, 3.4 Hz), 122.7 (t, ³*J*_{C-F} = 6.1 Hz), 114.2, 81.5 (dd, ²*J*_{C-F} = 29.2, 14.2 Hz), 55.2. **¹⁹F NMR (CDCl₃, 377 MHz):** δ -84.8 (d, *J*_{F-F} = 37.1 Hz), -86.6 (d, *J*_{F-F} = 37.1 Hz).

5.2.4 Synthesis of azatrienes through Rh-catalysed CH activation

General procedure G (GPG)

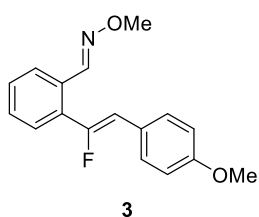
In a flame dried flask, oxime (1 eq.), difluoroalkene (1.5 eq.), [RhCp*Cl₂]₂ (5 mol%), AgOAc (27 mol%) and TFE were added. The reaction was let stirring at 30 °C for 16h

under inert atmosphere. After removal of the solvent, the crude was purified by silica-gel chromatography to give the pure compound.

General procedure H (GPH)

In a flame dried flask, oxime (1 eq.), difluoroalkene (1.5 eq.), $[\text{RhCp}^*(\text{MeCN})_3][\text{SbF}_6]_2$ (5 mol%), and TFE were added. The reaction was let stirring at 120 °C for 20h under inert atmosphere. After removal of the solvent, the crude was purified by silica-gel chromatography to give the pure compound.

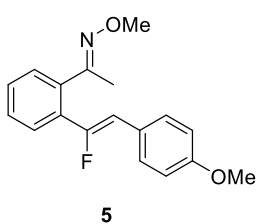
2-((Z)-1-fluoro-2-(4-methoxyphenyl)vinyl)benzaldehyde O-methyl oxime (3)



Following GPG (with different solvent), using benzaldehyde O-methyl oxime (54.2 mg, 0.40 mmol), 1-(2,2-difluorovinyl)-4-methoxybenzene (82.2 mg, 0.48 mmol), $[\text{RhCp}^*\text{Cl}_2]_2$ (12.7 mg, 5 mol%), AgOAc (16.8 mg, 25 mol%) in HFIP (2.0 mL). Following silica gel flash column chromatography (petrol-Et₂O [95:5]), the azatriene was isolated as a colourless oil (26.3 mg, 23%). (If performed in TFE, yield of 35%).

¹H-NMR (CDCl₃, 400 MHz): δ 8.43 (d, *J* = 3.5 Hz, 1H), 7.93-7.91 (m, 1H), 7.57 (d, *J* = 9.0 Hz, 2H), 7.54-7.52 (m, 1H), 7.43-7.38 (m, 2H), 6.92 (d, *J* = 9.0 Hz, 2H), 5.87 (d, *J* = 38.5 Hz, 1H), 4.00 (s, 3H), 3.84 (s, 3H); **¹³C-NMR (CDCl₃, 101 MHz)** δ 159.2, 155.1 (d, *J*_{C-F} = 260.5 Hz, C), 147.6, 133.3 (d, *J*_{C-F} = 26.0 Hz, C), 130.4 (d, *J*_{C-F} = 8.0 Hz, 2CH), 130.3, 129.7, 129.4, 128.8 (d, *J*_{C-F} = 4.5 Hz, CH), 126.9, 126.1 (d, *J*_{C-F} = 3.5 Hz, C), 114.1 (overlap of two signals), 111.6 (d, *J*_{C-F} = 11.0 Hz, CH), 62.2, 55.4; **¹⁹F-NMR (CDCl₃, 377 MHz)** δ -99.4 (dd, *J* = 38.5 Hz, 3.5 Hz, 1F); **HRMS** *m/z* [M+H]⁺ C₁₇H₁₇FNO₂ calcd. 286.1238, found 286.1238; **IR:** *v*_{max}/cm⁻¹ (neat) 2936, 1606, 1592, 1301, 1249, 1178, 1056, 1043.

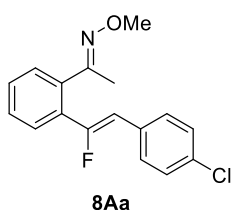
1-(2-((Z)-1-fluoro-2-(4-methoxyphenyl)vinyl)phenyl)ethan-1-one O-methyl oxime (5)



mg).

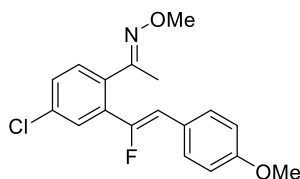
Following GPG using 1-phenylethan-1-one O-methyl oxime (60.0 mg, 0.4 mmol), 1-(2,2-difluorovinyl)-4-methoxybenzene (102.0 mg, 0.6 mmol), $[\text{RhCp}^*\text{Cl}_2]_2$ (12.4 mg, 0.02 mmol), AgOAc (18.0 mg, 0.108 mmol) and TFE (2.5mL). Purification by silica-gel chromatography (eluent petroleum ether/ethyl acetate 20/1) to give the pure compound as a green/yellow oil in 21% yield (25.1 mg).

¹H NMR (CDCl₃, 400 MHz): δ 7.55 – 7.60 (m, 3H), 7.41-7.45 (m, 3H), 6.94 (d, *J* = 8.7 Hz, 2H), 6.04 (d, *J*_{H-F} = 38.9 Hz, 1H), 4.01 (s, 3H), 3.86 (s, 3H), 2.18 (s, 3H). **¹³C NMR (CDCl₃, 100.6 MHz):** δ 158.9 (d, ⁴*J*_{C-F} = 2.9 Hz, 1C), 157.5, 155.6 (d, ¹*J*_{C-F} = 259.0 Hz, 1C), 136.0, 132.1 (d, ²*J*_{C-F} = 25.8 Hz, 1C, 130.2 (d, ³*J*_{C-F} = 7.9 Hz, 1C), 129.5, 129.1, 128.7, 128.2 (d, ⁴*J*_{C-F} = 5.1 Hz, 2C), 126.4 (d, ³*J*_{C-F} = 3.3 Hz, 1C, 114.0, 109.9 (d, ²*J*_{C-F} = 10.4 Hz, 1C), 61.9, 55.3, 15.9. **¹⁹F NMR (CDCl₃, 377 MHz):** δ -102.9 (d, *J*_{F-H} = 38.9 Hz, 1F). **HRMS** *m/z* [M+H]⁺ C₁₈H₁₉FNO₂ calcd. 300.1394, found 300.1387. **IR:** *v*_{max}/cm⁻¹ (neat) 2935, 1607, 1573, 1512, 1464, 1365, 1250, 1178, 1050, 1037.

1-(2-((Z)-2-(4-chlorophenyl)-1-fluorovinyl)phenyl)ethan-1-one O-methyl oxime (8Aa)

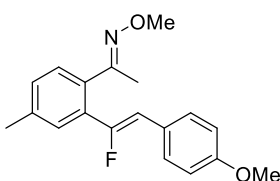
Following GPG using 1-phenylethan-1-one O-methyl oxime (74.6 mg, 0.5 mmol), 1-chloro-4-(2,2-difluorovinyl)benzene (130.6 mg, 0.75 mmol), [RhCp*Cl₂]₂ (15.4 mg, 0.025 mmol), AgOAc (22.5 mg, 0.135 mmol) and TFE (3.5 mL). Purification by silica-gel chromatography (eluent petroleum ether/ethyl acetate 50/1) to give the pure compound as a pale yellow oil in 78% yield (118.9 mg).

¹H NMR (CDCl₃, 400 MHz): δ 7.57 – 7.61 (m, 1H), 7.55 (d, *J* = 8.6 Hz, 2H), 7.42-7.46 (m, 3H), 7.36 (d, *J* = 8.6 Hz, 2H), 6.05 (d, *J*_{H-F} = 38.0 Hz, 1H), 4.01 (s, 3H), 2.19 (s, 3H). **¹³C NMR (CDCl₃, 100.6 MHz):** δ 157.5 (d, ¹*J*_{C-F} = 262.8 Hz, 1C), 157.1, 136.3, 133.1 (d, ³*J*_{C-F} = 3.5 Hz, 1C), 132.1 (d, ³*J*_{C-F} = 3.3 Hz, 1C), 131.6 (d, ²*J*_{C-F} = 25.6 Hz, 1C), 130.1 (d, ³*J*_{C-F} = 8.1 Hz, 1C), 129.6 (s, 1C), 129.5 (s, 1C), 128.8 (overlap of two signals, 2C+1C), 128.5 (d, ⁴*J*_{C-F} = 5.1 Hz, 2C), 109.1 (d, ²*J*_{C-F} = 10.1 Hz, 1C), 61.9, 15.9. **¹⁹F NMR (CDCl₃, 377 MHz):** δ -98.7 (d, *J*_{F-H} = 38.0 Hz, 1F). **HRMS** *m/z* [M+H]⁺ C₁₇H₁₆³⁵ClFNO calcd. 304.0899, found 304.0908. **IR:** *v*_{max}/cm⁻¹ (neat) 2936, 1661, 1592, 1493, 1366, 1310, 1194, 1093, 1050.

1-(4-chloro-2-((Z)-1-fluoro-2-(4-methoxyphenyl)vinyl)phenyl)ethan-1-one O-methyl oxime (8Ac analogue, not included in the thesis)

Following GPG using 1-(4-chlorophenyl)ethan-1-one O-methyl oxime (126 mg, 0.69 mmol), 1-(2,2-difluorovinyl)-4-methoxybenzene (175 mg, 1.03 mmol), [RhCp*Cl₂]₂ (21.6 mg, 0.035 mmol), AgOAc (30.9 mg, 0.186 mmol) and TFE (4 mL). Purification by silica-gel chromatography (eluent petroleum ether/ethyl acetate 50/1) to give the pure compound as a yellow oil in 28% yield (64.7 mg).

¹H NMR (CDCl₃, 400 MHz): δ 7.53 – 7.58 (m, 3H), 7.33-7.39 (m, 2H), 6.94 (d, *J* = 8.8 Hz, 2H), 6.05 (d, *J*_{H-F} = 38.7 Hz, 1H), 4.00 (s, 3H), 3.86 (s, 3H), 2.15 (s, 3H). **¹³C NMR (CDCl₃, 100.6 MHz):** δ 159.2 (d, ⁴*J*_{C-F} = 2.9 Hz, 1C), 156.5, 154.2 (d, ¹*J*_{C-F} = 258.9 Hz, 1C), 134.6, 134.4, 133.7 (d, ²*J*_{C-F} = 26.5 Hz, 1C), 130.9, 130.4 (d, ³*J*_{C-F} = 7.9 Hz, 1C), 129.0, 128.1 (d, ⁴*J*_{C-F} = 5.4 Hz, 2C), 125.9 (d, ³*J*_{C-F} = 3.3 Hz, 1C), 114.1, 110.8 (d, ²*J*_{C-F} = 10.0 Hz, 1C), 62.0, 55.3, 15.7. **¹⁹F NMR (CDCl₃, 377 MHz):** δ -104.4 (d, *J*_{F-H} = 38.7 Hz, 1F). **HRMS** *m/z* [M+H]⁺ C₁₈H₁₈³⁵ClFNO₂ calcd. 334.1005, found 334.0996. **IR:** *v*_{max}/cm⁻¹ (neat) 2935, 1663, 1606, 1511, 1463, 1366, 1298, 1253, 1178, 1103, 1044.

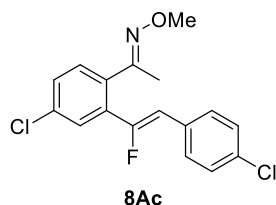
1-(2-((Z)-1-fluoro-2-(4-methoxyphenyl)vinyl)-4-methylphenyl)ethan-1-one O-methyl oxime (8Ad analogue, not included in the thesis)

Following GPG using 1-(4-methylphenyl)ethan-1-one O-methyl oxime (41 mg, 0.25 mmol), 1-(2,2-difluorovinyl)-4-methoxybenzene (65 mg, 0.38 mmol), [RhCp*Cl₂]₂ (7.7 mg, 0.013 mmol), AgOAc (11.2 mg, 0.068 mmol) and TFE (2.5 mL). Purification by silica-gel chromatography (eluent petroleum ether/ethyl acetate 50/1) to give the pure compound as a yellow oil in 28% yield (64.7 mg).

ether/ethyl acetate 50/1) to give the pure compound as a yellow oil in 49% yield (38.3 mg).

¹H NMR (CDCl₃, 400 MHz): δ 7.56 (d, *J* = 8.8 Hz, 2H), 7.39 (s, 1H), 7.30 (d, *J* = 7.7 Hz, 1H), 7.21 (d, *J* = 7.7 Hz, 1H), 6.93 (d, *J* = 8.8 Hz, 2H), 6.01 (d, *J*_{H-F} = 38.9 Hz, 1H), 4.00 (s, 3H), 3.86 (s, 3H), 2.41 (s, 3H), 2.16 (s, 3H). **¹³C NMR (CDCl₃, 100.6 MHz):** δ 158.9 (d, ⁴*J*_{C-F} = 2.9 Hz, 1C), 157.5, 155.9 (d, ¹*J*_{C-F} = 259.2 Hz, 1C), 138.6, 133.3, 131.9 (d, ²*J*_{C-F} = 25.7 Hz, 1C), 130.2 (d, ³*J*_{C-F} = 7.9 Hz, 1C), 129.8, 129.4, 128.8 (d, ⁴*J*_{C-F} = 5.0 Hz, 2C), 126.5 (d, ³*J*_{C-F} = 3.3 Hz, 1C), 114.0, 109.6 (d, ²*J*_{C-F} = 10.5 Hz, 1C), 61.8, 55.3, 21.2, 15.9. **¹⁹F NMR (CDCl₃, 377 MHz):** δ -102.7 (d, *J*_{F-H} = 38.9 Hz, 1F). **HRMS** *m/z* [M+H]⁺ C₁₉H₂₁FNO₂ calcd. 314.1551, found 314.1543. **IR:** *v*_{max}/cm⁻¹ (neat) 2936, 1607, 1513, 1464, 1257, 1179, 1080, 1048.

1-(2-((Z)-2-(4-chlorophenyl)-1-fluorovinyl)-4-chlorophenyl)ethan-1-one O-methyl oxime (8Ac)

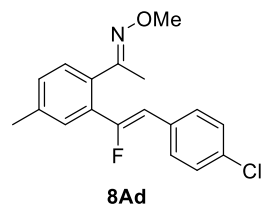


Following GPG using 1-(4-chlorophenyl)ethan-1-one O-methyl oxime (71.6 mg, 0.4 mmol), 1-chloro-4-(2,2-difluorovinyl)benzene (104.4 mg, 0.6 mmol), [RhCp*Cl₂]₂ (12.4 mg, 0.02 mmol), AgOAc (18 mg, 0.108 mmol) and TFE (3.5 mL). Purification by silica-gel chromatography (eluent petroleum ether/diethyl ether 95/5) to give the pure compound as a yellow

oil in 30% yield (40.6 mg).

¹H NMR (CDCl₃, 400 MHz): δ 7.58 (d, *J* = 2.0 Hz, 1H), 7.54 (d, *J* = 8.6 Hz, 2H), 7.35-7.42 (m, 4H), 6.05 (d, *J*_{H-F} = 37.7 Hz, 1H), 3.99 (s, 3H), 2.16 (s, 3H). **¹³C NMR (CDCl₃, 100.6 MHz):** δ 156.1, 156.0 (d, ¹*J*_{C-F} = 262.8 Hz, 1C), 134.7, 134.6, 133.5 (d, ³*J*_{C-F} = 3.5 Hz, 1C), 133.2 (d, ²*J*_{C-F} = 26.5 Hz, 1C), 131.6 (d, ³*J*_{C-F} = 3.5 Hz, 1C), 130.9, 130.2 (d, ⁴*J*_{C-F} = 8.1 Hz, 2C), 129.5, 128.8, 128.3 (d, ³*J*_{C-F} = 5.5 Hz, 1C), 110.0 (d, ²*J*_{C-F} = 9.6 Hz, 1C), 62.0, 15.8. **¹⁹F NMR (CDCl₃, 377 MHz):** δ -100.1 (d, *J*_{F-H} = 37.7 Hz, 1F). **HRMS** *m/z* [M+H]⁺ C₁₇H₁₅³⁵Cl₂FNO calcd. 338.0509, found 338.0516. **IR:** *v*_{max}/cm⁻¹ (neat) 2935, 1663, 1589, 1492, 1366, 1311, 1261, 1195, 1096, 1045.

1-(2-((Z)-2-(4-chlorophenyl)-1-fluorovinyl)-4-methylphenyl)ethan-1-one O-methyl oxime (8Ad)

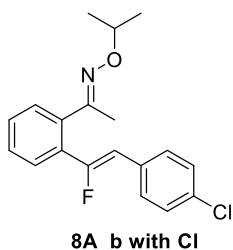


Following GPG using 1-(4-methylphenyl)ethan-1-one O-methyl oxime (48.9 mg, 0.3 mmol), 1-chloro-4-(2,2-difluorovinyl)benzene (78.3 mg, 0.45 mmol), [RhCp*Cl₂]₂ (9.3 mg, 0.015 mmol), AgOAc (13.5 mg, 0.081 mmol) and TFE (3 mL). Purification by silica-gel chromatography (eluent petroleum ether/diethyl ether 95/5) to give the pure compound as a light yellow oil in 87% yield (83.6 mg).

¹H NMR (CDCl₃, 400 MHz): δ 7.54 (d, *J* = 8.6 Hz, 2H), 7.40 (s, 1H), 7.36 (d, *J* = 8.6 Hz, 2H), 7.32 (d, *J* = 7.6 Hz, 1H), 7.25 (d, *J* = 7.8 Hz, 1H), 6.03 (d, *J*_{H-F} = 38.0 Hz, 1H), 4.00 (s, 3H), 2.42 (s, 3H), 2.17 (s, 3H). **¹³C NMR (CDCl₃, 100.6 MHz):** δ 157.7 (d, ¹*J*_{C-F} = 262.9 Hz, 1C), 157.0, 138.7, 133.6, 133.0 (d, ³*J*_{C-F} = 3.4 Hz, 1C), 132.2 (d, ³*J*_{C-F} = 3.2 Hz, 1C), 131.5 (d, ²*J*_{C-F} = 25.6 Hz, 1C), 130.3, 130.0 (d, ⁴*J*_{C-F} = 8.0 Hz, 2C), 129.4, 129.0 (d, ³*J*_{C-F} = 4.9 Hz,

1C), 128.7, 108.9 (d, $^2J_{C-F}$ = 10.1 Hz, 1C), 61.8, 21.1, 15.9. **^{19}F NMR (CDCl₃, 377 MHz):** δ -98.5 (d, J_{F-H} = 37.8 Hz, 1F). **HRMS** m/z [M+H]⁺ C₁₈H₁₈³⁵ClFNO calcd. 318.1055, found 318.1060. **IR:** $\nu_{\text{max}}/\text{cm}^{-1}$ (neat) 2935, 1661, 1491, 1365, 1310, 1180, 1093, 1081, 1046, 1013.

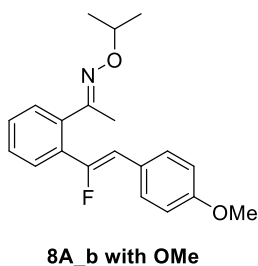
1-(2-((Z)-2-(4-chlorophenyl)-1-fluorovinyl)phenyl)ethan-1-one O-isopropyl oxime (8A_b with Cl)



Following GPG using acetophenone O-isopropyl oxime (53.2 mg, 0.3 mmol), 1-chloro-4-(2,2-difluorovinyl)benzene (78.3 mg, 0.45 mmol), [RhCp*Cl₂]₂ (9.3 mg, 0.015 mmol), AgOAc (13.5 mg, 0.081 mmol) and TFE (2.5 mL). Purification by silica-gel chromatography (eluent petroleum ether/diethyl ether 95/5) to give the pure compound as a green/yellow oil in 87% yield (86.4 mg).

^1H NMR (CDCl₃, 400 MHz): δ 7.58-7.61 (m, 1H), 7.55 (d, J = 8.6 Hz, 2H), 7.41-7.45 (m, 3H), 7.36 (d, J = 8.6 Hz, 2H), 6.05 (d, J_{H-F} = 38.0 Hz, 1H), 4.47 (hpt, J = 6.2 Hz, 1H), 2.20 (s, 3H), 1.31 (d, J = 6.2 Hz, 6H). **^{13}C NMR (CDCl₃, 100.6 MHz):** δ 157.7 (d, $^1J_{C-F}$ = 262.9 Hz, 1C), 156.0, 136.9, 133.0 (d, $^3J_{C-F}$ = 3.5 Hz, 1C), 132.2 (d, $^3J_{C-F}$ = 3.4 Hz, 1C), 131.7 (d, $^2J_{C-F}$ = 25.5 Hz, 1C), 130.0 (d, $^4J_{C-F}$ = 8.1 Hz, 2C), 129.6, 129.4, 128.7, 128.6, 128.5, 109.0 (d, $^2J_{C-F}$ = 10.0 Hz, 1C), 75.5, 21.9, 16.0. **^{19}F NMR (CDCl₃, 377 MHz):** δ -98.8 (d, J_{F-H} = 30.0 Hz, 1F). **HRMS** m/z [M+H]⁺ C₁₉H₂₀³⁵ClFNO calcd. 332.1212, found 332.1218. **IR:** $\nu_{\text{max}}/\text{cm}^{-1}$ (neat) 2925, 1663, 1607, 1511, 1494, 1368, 1309, 1151, 1119, 1093, 1012.

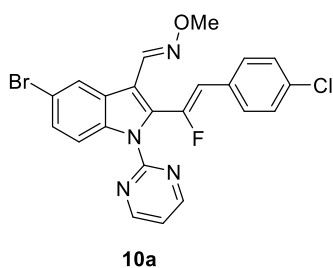
1-(2-((Z)-1-fluoro-2-(4-methoxyphenyl)vinyl)phenyl)ethan-1-one O-isopropyl oxime (8A_b with OMe)



Following GPG using acetophenone O-isopropyl oxime (53.2 mg, 0.3 mmol), 1-(2,2-difluorovinyl)-4-methoxybenzene (76.6 mg, 0.45 mmol), [RhCp*Cl₂]₂ (9.3 mg, 0.015 mmol), AgOAc (13.5 mg, 0.081 mmol) and TFE (2.5 mL). Purification by silica-gel chromatography (eluent petroleum ether/diethyl ether 95/5) to give the pure compound as a yellow oil in 31% yield (30.6 mg).

^1H NMR (CDCl₃, 400 MHz): δ 7.55-7.61 (m, 3H), 7.39-7.43 (m, 3H), 6.94 (d, J = 8.8 Hz, 2H), 6.03 (d, J_{H-F} = 38.9 Hz, 1H), 4.48 (hpt, J = 6.2 Hz, 1H), 3.86 (s, 3H), 2.19 (s, 3H), 1.31 (d, J = 6.2 Hz, 6H). **^{13}C NMR (CDCl₃, 100.6 MHz):** δ 158.8 (d, $^4J_{C-F}$ = 2.9 Hz, 1C), 156.6, 155.7 (d, $^1J_{C-F}$ = 259.1 Hz, 1C), 136.6, 132.1 (d, $^2J_{C-F}$ = 25.8 Hz, 1C), 130.2 (d, $^3J_{C-F}$ = 7.9 Hz, 1C), 129.4, 129.1, 128.5, 128.2 (d, $^4J_{C-F}$ = 5.1 Hz, 2C), 126.5 (d, $^3J_{C-F}$ = 3.3 Hz, 1C), 114.0, 109.8 (d, $^2J_{C-F}$ = 10.3 Hz, 1C), 75.4, 55.3, 21.9, 16.1. **^{19}F NMR (CDCl₃, 377 MHz):** δ -103.1 (d, J_{F-H} = 39.0 Hz, 1F). **HRMS** m/z [M+H]⁺ C₂₀H₂₃FNO₂ calcd. 328.1707, found 328.1698. **IR:** $\nu_{\text{max}}/\text{cm}^{-1}$ (neat) 2931, 1664, 1607, 1511, 1464, 1368, 1249, 1178, 1117, 1078, 1034.

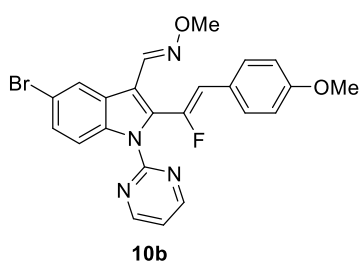
5-bromo-2-((Z)-2-(4-chlorophenyl)-1-fluorovinyl)-1-(pyrimidin-2-yl)-1H-indole-3-carbaldehyde O-methyl oxime (10a)



Following GPH using 5-bromo-1-(pyrimidin-2-yl)-1H-indole-3-carbaldehyde O-methyl oxime (99.0 mg, 0.3 mmol), 1-chloro-4-(2,2-difluorovinyl)benzene (78.4 mg, 0.45 mmol), [RhCp*(MeCN)₃][SbF₆]₂ (12.5 mg, 0.015 mmol) and TFE (1.5 mL). Purification by silica-gel chromatography (eluent petroleum ether/ethyl acetate 9/1) to give the pure compound as a white solid in 77% yield (111.4 mg).

¹H NMR (CDCl₃, 400 MHz): δ 8.81 (s, 1H), 8.80 (s, 1H), 8.56 (d, J = 2.1 Hz, 1H), 8.45 (s, 1H), 8.36 (d, J = 8.9 Hz, 1H), 7.57 (d, J = 8.5 Hz, 2H), 7.54 (d, J = 2.2 Hz, 1H), 7.38 (d, J = 8.5 Hz, 2H), 7.25 (t, J = 4.8 Hz, 1H), 6.10 (d, J = 35.4 Hz, 1H), 4.11 (s, 3H). **¹³C NMR (CDCl₃, 100.6 MHz):** δ 158.3, 156.9, 148.4 (d, J = 259.8 Hz, 1C), 143.2, 135.6, 133.7 (d, J = 3.1 Hz, 1C), 132.8 (d, J = 25.0 Hz, 1C), 131.5 (d, J = 4.5 Hz, 1C), 130.3 (d, J = 7.8 Hz, 2C), 129.0, 128.8, 127.3, 126.0, 118.1, 116.8, 115.9, 114.6 (d, J = 5.3 Hz, 1C), 113.1 (d, J = 10.2 Hz, 1C), 62.4. **¹⁹F NMR (CDCl₃, 377 MHz):** δ -96.2 (d, J_{F-H} = 35.3 Hz, 1F). **HRMS** m/z [M+H]⁺ C₂₂H₁₆⁷⁹Br³⁵ClFN₄O calcd. 485.0175, found 485.0181. **IR:** ν_{max}/cm⁻¹ (neat) 2935, 1671, 1571, 1492, 1448, 1440, 1417, 1395, 1291, 1228, 1155, 1098, 1082, 1046.

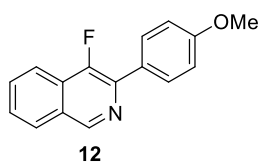
5-bromo-2-((Z)-1-fluoro-2-(4-methoxyphenyl)vinyl)-1-(pyrimidin-2-yl)-1H-indole-3-carbaldehyde O-methyl oxime (10b)



Following GPH using 5-bromo-1-(pyrimidin-2-yl)-1H-indole-3-carbaldehyde O-methyl oxime (67.0 mg, 0.2 mmol), 1-(2,2-difluorovinyl)-4-methoxybenzene (51.6 mg, 0.3 mmol), [RhCp*(MeCN)₃][SbF₆]₂ (8.4 mg, 0.01 mmol) and TFE (1.5 mL). Purification by silica-gel chromatography (eluent petroleum ether/ethyl acetate 9/1) to give the pure compound as a beige solid in 80% yield (77.0 mg).

¹H NMR (CDCl₃, 400 MHz): δ 8.80 (s, 1H), 8.79 (s, 1H), 8.55 (d, J = 2.1 Hz, 1H), 8.47 (s, 1H), 8.31 (d, J = 9.0 Hz, 1H), 7.59 (d, J = 8.8 Hz, 2H), 7.53 (dd, J = 8.9, 2.1 Hz, 1H), 7.23 (t, J = 4.8 Hz, 1H), 6.94 (d, J = 8.8 Hz, 2H), 6.10 (d, J = 36.4 Hz, 1H), 4.10 (s, 3H), 3.87 (s, 3H). **¹³C NMR (CDCl₃, 100.6 MHz):** δ 159.4, 158.3, 157.0, 146.6 (d, J = 256.1 Hz, 1C), 143.5, 135.5, 133.6 (d, J = 25.5 Hz, 1C), 130.6 (d, J = 7.8 Hz, 2C), 128.8, 127.4, 125.9, 125.8 (d, J = 4.6 Hz, 1C), 118.1, 116.7, 115.7, 114.1, 114.0 (d, J = 10.6 Hz, 1C), 62.3, 55.3. **¹⁹F NMR (CDCl₃, 377 MHz):** δ -100.6 (d, J_{F-H} = 36.4 Hz, 1F). **HRMS** m/z [M+H]⁺ C₂₃H₁₉⁷⁹BrFN₄O₂ calcd. 481.0670, found 481.0670. **IR:** ν_{max}/cm⁻¹ (neat) 2935, 1606, 1571, 1511, 1449, 1440, 1418, 1398, 1291, 1252, 1179, 1155, 1081, 1045.

5.2.5 Synthesis of fluorinated isoquinoline (12)



2-((Z)-1-fluoro-2-(4-methoxyphenyl)vinyl)benzaldehyde O-methyl oxime (61.7 mg, 0.22 mmol) was dissolved in *o*-dichlorobenzene (2.0 mL) and heated to 200 °C for 72 h and then allowed to cool to r.t. The mixture was filtered through silica with petrol (removing *o*-dichlorobenzene) and then EtOAc. The crude material was subjected to silica gel flash column chromatography to give the the fluoroisoquinoline as a colourless oil (8.9 mg, 16%) and 2-(4-methoxybenzene)-3-methoxyisoquinoline (7.6 mg, 13%).

¹H-NMR (CDCl₃, 400 MHz) δ 9.14 (s, 1H), 8.15 (d, *J* = 8.5 Hz, 1H), 8.09 (d, *J* = 9.0 Hz, 2H), 8.00 (d, *J* = 8.5 Hz, 1H), 7.77 (app. t, *J* = 8.5 Hz, 1H), 7.63 (app. t, *J* = 8.5 Hz, 1H), 7.06 (d, *J* = 9.0 Hz, 2H), 3.89 (s, 3H); **¹³C-NMR (CDCl₃, 101 MHz)**: δ 160.1, 152.8 (d, *J*_{C-F} = 264.0 Hz, C), 147.7 (d, *J*_{C-F} = 6.0 Hz, CH), 136.6 (d, *J*_{C-F} = 10.5 Hz, C), 130.8, 130.4 (d, *J*_{C-F} = 6.5 Hz, 2CH), 129.3 (d, *J*_{C-F} = 2.5 Hz, C), 128.5 (d, *J*_{C-F} = 5.5 Hz, C), 127.7, 127.5, 127.1 (d, *J*_{C-F} = 2.0 Hz, CH), 120.0 (d, *J*_{C-F} = 6.0 Hz, CH), 114.1, 55.5; **¹⁹F-NMR (CDCl₃, 377 MHz)**: δ -138.3; **IR**: *v*_{max}/cm⁻¹ (neat) 2925, 1630, 1608, 1539, 1515, 1452, 1375, 1254, 1177, 1028.

